



**HAL**  
open science

# Impact of the catecholaminergic polymorphic ventricular tachycardia (CPVT) mutation RyR2R420Q in cell function

Liheng Yin

► **To cite this version:**

Liheng Yin. Impact of the catecholaminergic polymorphic ventricular tachycardia (CPVT) mutation RyR2R420Q in cell function. Tissues and Organs [q-bio.TO]. Université Paris-Saclay, 2020. English. NNT : 2020UPASS068 . tel-02984146

**HAL Id: tel-02984146**

**<https://theses.hal.science/tel-02984146>**

Submitted on 30 Oct 2020

**HAL** is a multi-disciplinary open access archive for the deposit and dissemination of scientific research documents, whether they are published or not. The documents may come from teaching and research institutions in France or abroad, or from public or private research centers.

L'archive ouverte pluridisciplinaire **HAL**, est destinée au dépôt et à la diffusion de documents scientifiques de niveau recherche, publiés ou non, émanant des établissements d'enseignement et de recherche français ou étrangers, des laboratoires publics ou privés.

# Impact of the catecholaminergic polymorphic ventricular tachycardia (CPVT) mutation RyR2<sup>R420Q</sup> on cell function

**Thèse de doctorat de l'université Paris-Saclay**

École doctorale n° n°569 : innovation thérapeutique : du fondamental à  
l'appliqué (ITFA)

Spécialité de doctorat : physiologie, physiopathologie

Unité de recherche : Université Paris-Saclay, Inserm, UMR-S 1180, 92296, Châtenay-  
Malabry, France

Référent : Faculté de pharmacie

**Thèse présentée et soutenue à Châtenay-Malabry, le 29  
Juin 2020, par**

**Liheng YIN**

## Composition du Jury

<b>Denis DAVID</b> Professeur, Université Paris-Saclay, Paris	Président
<b>Vincent JACQUEMOND</b> Directeur de recherche, CNRS, Lyon	Rapporteur & Examineur
<b>María FERNANDEZ VELASCO</b> Chargée de recherche, Hospital Universitario La Paz, Madrid	Rapporteur & Examinatrice
<b>Jose-Manuel CANCELA</b> Chargée de recherche (HDR), CNRS, Orsay	Examineur
<b>Nathalie GABORIT</b> Chargée de recherche, Inserm, Nantes	Examinatrice
<b>Pierre JOANNE</b> Maître de conférence, Sorbonne Université	Examineur
<b>Ana-Maria GOMEZ</b> Directeur de recherche, Inserm	Directrice de thèse
<b>Jean-Pierre BENITAH</b> Directeur de recherche, Inserm	Co-Directeur de thèse

# Acknowledgements

*I would like to express my deep and sincere gratitude to all the persons who helped me during my Ph.D studies.*

*My deepest gratitude goes first and foremost to Dr. Ana-Maria Gomez, my supervisor and Dr. Jean-Pierre Benitah, my co-supervisor. They are the most lovable couple that I ever met, who just like the parents of a big family. Ana is very gentle and considerate, who always keeps the eyes on one's merits. Her patience, optimism, enthusiasm, professional advice and unwavering support are invaluable to me. Even when I made mistakes during experiments due to carelessness, she didn't blame me but tried to pick up my good points to encourage me, which makes her like a gracious mother. Jean-Pierre takes a scientific and rigorous attitude towards research, who always fast and accurately finds the problems in experiment procedures or results and provides many valuable comments and suggestions, which makes him like a strict father. They, together, make our team like a harmonious and warm family.*

*My sincere gratitude is reserved for all the members of the jury. I am thankful to Professor Denis David for kindly accepting to chair this thesis committee. I would like to thank the reviewers of this thesis: Dr. Vincent Jacquemond and Dr. María Fernández Velasco, for taking time to carefully review this thesis. I am grateful to Dr. Jose-Manuel Cancela, Dr. Nathalie Gaborit and Dr. Pierre Joanne for accepting to evaluate my work and participating in this jury as examiners.*

*Very special thanks to China Scholarship Council for their financial support for my Ph.D studies in France.*

*I warmly thank and appreciate all the members of UMR-S1180. It is really a very warm big family with all the nice people who make me feel happy and relaxed in the lab.*

*I would like to express my heartfelt gratitude to Pascale Gerbaud and Florence Lefebvre, who prepared the cells for my experiments, to Julio L Álvarez, who taught me microelectrode technique, and to Patrick Lechene who repaired all the setup for work for me.*

*Many thanks to Dr. Pascale Guicheney and Malorie Blancard for the nice collaboration with them.*

*I am also thankful to secretary Mrs Gladys.Rene-Corail for her efficient help in facilitating my travels and accommodations for the international conferences and preparing contracts with Inserm.*

*I would like to thank my Chinese friends who made my life enjoyable in France especially in the first two years. Great thanks go to Xiaoyan Zhu, Hui Chen and Liang Zhang. It is you who helped me a lot when I first came here and made me not lonely in France. Thanks to Yuxiang Song, Lin Lei, Wenwen Gao, Yueyi Wang, Yongchao Xu, Jiao Feng, Guangkuan Zhao, Dawei Liu, Jianbin Xue, for the interesting moment and delicious food we shared.*

*I want to express my great gratitude and deepest appreciation to my beloved husband Xiaolin Cheng and my lovely son Lucas. They are my strong backing and my dynamic source of learning, the inexhaustible power on the road of my life.*

*Last but definitely not least, I would like to give my most sincere gratitude to my father, my mother, my younger brother and parents-in-law. Thanks for their support and encouragement. I hope my parents and my parents-in-law will always be healthy and happy.*

# Table of contents

<b>ACKNOWLEDGEMENTS</b> .....	<b>0</b>
<b>TABLE OF CONTENTS</b> .....	<b>2</b>
<b>RESUME</b> .....	<b>5</b>
<b>ABSTRACT</b> .....	<b>7</b>
<b>LIST OF ABBREVIATIONS</b> .....	<b>9</b>
<b>PREAMBLE</b> .....	<b>12</b>
<b>INTRODUCTION</b> .....	<b>14</b>
<b>I THE HEART</b> .....	<b>15</b>
<b>II HEART RHYTHM</b> .....	<b>16</b>
II.1 NORMAL HEART RHYTHM—SINUS RHYTHM.....	17
II.2 MOLECULAR MECHANISMS OF HEART BEAT .....	18
II.2.1 Action potential.....	18
II.2.2 excitation-contraction coupling (ECC) .....	21
<b>III THE RYANODINE RECEPTORS (RYRS)</b> .....	<b>22</b>
III.1 GENERAL INTRODUCTION OF RYRS .....	22
III.1.1 Location and distribution of RyRs.....	23
III.1.2 General structure of RyRs.....	24
III.2 SPECIAL ARCHITECTURE OF RYR2 .....	28
<b>IV ARRHYTHMIA</b> .....	<b>30</b>
IV.1 WHAT IS ARRHYTHMIA? .....	30
IV.2 VENTRICULAR ARRHYTHMIAS .....	31
IV.2.1 The mechanism of ventricular arrhythmias.....	31
IV.2.2 Acquired ventricular arrhythmias .....	39
IV.2.3 Genetic ventricular arrhythmias.....	41

<b>V CPVT1.....</b>	<b>54</b>
V.1 CPVT MUTATIONS ON RYR2.....	54
V.2 EXPERIMENTAL MODELS USING IN CPVT STUDY.....	57
V.2.1 Expression systems .....	57
V.2.2 Animal model .....	58
V.2.3 New breakthrough: hiPSC line.....	59
V.3 PATHOLOGIC MECHANISM OF CPVT1.....	59
V.3.1 Increased RyR2 channel sensitivity to Ca <sup>2+</sup> .....	60
V.3.2 Store-overload-induced Ca <sup>2+</sup> release (SOICR).....	60
V.3.3 Altered domain zipping-unzipping .....	61
V.3.4 Defective FKBP Binding .....	63
<b>VI TREATMENT OF CPVT.....</b>	<b>74</b>
VI.1 TRADITIONAL TREATMENTS.....	74
VI.2 NOVEL EXPLORING TREATMENTS.....	74
VI.2.1 Venlafaxine .....	75
VI.2.1 Pregabalin .....	77
<b>VII OBJECTIVES.....</b>	<b>78</b>
<b><u>METHODS AND MATERIALS .....</u></b>	<b><u>80</u></b>
<b>I. CPVT (RYR2<sup>R420Q</sup>) PATIENT SPECIFIC IPS CELL CULTURE AND DIFFERENTIATION INTO CARDIOMYOCYTES.....</b>	<b>81</b>
I.1 HIPSCS CULTURE.....	82
I.1.1 Thaw the hiPSCs .....	83
I.1.2 Passage of hiPSCs .....	84
I.1.3 Freeze hiPSCs .....	85
I.2 HIIPS CELL DIFFERENTIATION INTO CARDIOMYOCYTES .....	85
I. 3 RECOVERY AND MATURATION OF HIIPS-CMS.....	87
<b>II DISSOCIATION OF VENTRICULAR CARDIOMYOCYTES FROM RYR2<sup>R420Q</sup> KNOCK-IN MICE.....</b>	<b>88</b>
II.1 SOLUTION PREPARATION.....	88
II.2 ETHICS STATEMENT .....	89
II.3 DISSOCIATION PROCESS .....	89
<b>III HEK293 CELL LINE CULTURE AND TRANSFECTION BY RYR2<sup>D3291V</sup> PLASMID .....</b>	<b>89</b>
III.1 HEK293 CELL LINE CULTURE .....	90
III.2 TRANSFECT HEK293 CELL BY RYRD3291V PLASMID.....	90

<b>IV CONFOCAL MICROSCOPY TECHNIQUE .....</b>	<b>90</b>
IV.1 THE APPLICATION OF CONFOCAL MICROSCOPY ON HIPSC-CMs .....	92
IV.1.1 preparation .....	92
IV.1.2 record.....	92
IV.1.3 Perfusions .....	92
IV.2 THE APPLICATION OF CONFOCAL MICROSCOPY ON MICE VENTRICULAR CARDIOMYOCYTES .....	93
IV.2.1 Solutions .....	93
IV.2.2 Process of experiment.....	93
IV.2.3 Perfusions .....	95
IV.3 THE APPLICATION OF CONFOCAL MICROSCOPY ON HEK293 CELLS .....	95
IV.3.1 Preparation .....	95
IV.3.2 recording.....	95
<b>V MICRO-ELECTRODE TECHNIQUE .....</b>	<b>96</b>
V.1 THE MAIN PRINCIPLES OF MICRO-ELECTRODE TECHNIQUE .....	96
V.2 THE APPLICATION OF MICRO-ELECTRODE ON HIPSC-CM .....	97
V.2.1 Solutions: .....	97
V.2.2 Pipettes: .....	97
V.2.3 Recording .....	97
<b>VI IMMUNOLABELING OF HIPSC-CMs (PERFORMED BY PASCALE GERBAUD AND PIERRE JAONNE) .....</b>	<b>98</b>
<b>VII PROTEIN MEASUREMENT (PERFORMED BY PASCALE GERBAUD).....</b>	<b>99</b>
<b>VIII MATERIALS AND REAGENTS.....</b>	<b>99</b>
<b>IX STATISTICS.....</b>	<b>101</b>
<b><u>RESULTS.....</u></b>	<b><u>102</u></b>
<b>I MANUSCRIPT 1: RYR2<sup>R420Q</sup> MUTATION IN THE CALCIUM RELEASE CHANNEL INDUCES ULTRASTRUCTURAL NANOSCALE ALTERATIONS INVOLVED IN ARRHYTHMIA AND CARDIAC SUDDEN DEATH .....</b>	<b>103</b>
<b>II MANUSCRIPT 2: A FUNCTIONAL STUDY OF A N-TERMINAL CPVT MUTATION RYR2<sup>R420Q</sup> IN PATIENT SPECIFIC HIPSC-CMs MODEL .....</b>	<b>158</b>
<b><u>DISCUSSION .....</u></b>	<b><u>187</u></b>
<b><u>REFERENCES.....</u></b>	<b><u>197</u></b>
<b><u>ANNEXES.....</u></b>	<b><u>228</u></b>

# Résumé

La tachycardie ventriculaire polymorphe catécholergique (CPVT) est une arythmie génétique létale qui se manifeste par une syncope ou une mort subite chez les enfants et les jeunes adultes dans des conditions de stress sans anomalie structurelle cardiaque évidente. Plusieurs mécanismes ont été proposés pour expliquer les altérations fonctionnelles sous-jacentes de la libération de  $\text{Ca}^{2+}$  dues aux mutations de RyR2 ou de ses protéines accessoires. Une nouvelle mutation CPVT située sur la partie N terminale de RyR2 a été identifiée dans une famille espagnole (RyR2<sup>R420Q</sup>). Ici, nous avons utilisé un modèle de souris KI exprimant le canal RyR2<sup>R420Q</sup> et des cardiomyocytes différenciés de cellules souches pluripotentes induites (hiPSC-CM) générées à partir de deux patients frères (l'un avec mutation, l'autre sans mutation utilisé comme témoin). L'analyse des cardiomyocytes ventriculaires exprimant le RyR2<sup>R420Q</sup> humain et de souris étudiées par imagerie  $\text{Ca}^{2+}$  confocale montre une augmentation des libérations de  $\text{Ca}^{2+}$  spontanée durant la diastole (visualisé par les Sparks  $\text{Ca}^{2+}$ ), une libération fractionnelle plus élevée et une fréquence de vagues  $\text{Ca}^{2+}$  proarythmogènes augmentée après stimulation à l'isoprotérénol. L'analyse électrophysiologique, étudiée en enregistrant les potentiels d'action (AP) en utilisant les techniques de micro-électrodes sur les hiPSC-CM et de patch-clamp sur les cellules ventriculaires de souris KI, a montré des post-dépolarisations retardées dépendants du  $\text{Ca}^{2+}$  (DAD). L'amplitude des transitoires  $[\text{Ca}^{2+}]_i$  des cellules stimulées à 1 Hz étaient plus faible chez le groupe muté. La charge en  $\text{Ca}^{2+}$  du réticulum sarcoplasmique (SR), estimée par application rapide de caféine (10 mM), était aussi plus réduite dans les hiPSC-CM exprimant RyR2<sup>R420Q</sup>, avant et après l'application ISO (1  $\mu\text{M}$ ). Cependant, le RyR2<sup>R420Q</sup> semble plus enclin à libérer du  $\text{Ca}^{2+}$ , car le transitoire  $[\text{Ca}^{2+}]_i$  normalisé par la quantité de  $\text{Ca}^{2+}$  stockée dans le SR, la libération fractionnaire, était plus élevée dans les cellules mutées. Même si la charge  $\text{Ca}^{2+}$  du SR était plus petite dans les cellules RyR2<sup>R420Q</sup>, elles présentaient souvent un comportement pro-arythmogène tel que les vagues  $\text{Ca}^{2+}$  pendant les périodes diastoliques. Ce comportement est encore augmentée lors de la stimulation  $\beta$ -adrénergique. Des résultats similaires ont été observés chez les souris KI, montrant ce modèle comme un outil précieux pour étudier la maladie CPVT. Nous avons ensuite étudié l'effet antiarythmique potentiel de la venlafaxine et

de la prégabaline dans les cardiomyocytes de souris KI et le hiPS-CM, deux médicaments parmi d'autres prescrits à un membre porteur de la famille et qui a montré une réversion des symptômes du CPVT après le traitement. Nous avons constaté que ces deux médicaments atténuent les événements arythmogènes de libération du  $\text{Ca}^{2+}$  induits par l'ISO dans les cardiomyocytes de souris KI. La venlafaxine a montré un effet antiarythmique dans hiPS-CM à la fois en traitements aigus et chroniques.

Ainsi 1) le RyR2<sup>R420Q</sup> montre une augmentation de la libération diastolique du  $\text{Ca}^{2+}$ , encore plus augmentée par la stimulation à l'isoproterenol, induisant des événements proarythmogènes. 2) les effets sont retrouvés chez des cardiomyocytes ventriculaires des souris KI et chez des cellules hiPSC-CM, montrant que ces dernières sont un outil valable pour étudier les mécanismes pathologiques ; et 3) que la Venlafaxine peut protéger des arythmies chez les patients CPVT, bien que d'avantage d'expériences sont nécessaires afin de conclure quant à son utilité antiarythmique.

# Abstract

Catecholaminergic polymorphic ventricular tachycardia (CPVT) is a lethal genetic arrhythmia that manifests by syncope or sudden death in children and young adults under stress conditions without obvious cardiac structural abnormality. Several mechanisms have been proposed to explain the underlying  $\text{Ca}^{2+}$  release functional alterations due to mutations of RyR2 or of its accessory proteins. A novel CPVT mutation located on RyR2 N terminal portion has been identified in a Spanish family (RyR2<sup>R420Q</sup>). Here we used a KI mice model expressing the RyR2<sup>R420Q</sup> channel, and differentiated cardiomyocytes from induced pluripotent stem cells (hiPS-CM) generated from two brother patients (one with mutation, the other without mutation used as control). Confocal  $\text{Ca}^{2+}$  imaging analysis showed that human and mouse RyR2<sup>R420Q</sup> expressing ventricular cardiomyocytes have higher occurrence of  $\text{Ca}^{2+}$  sparks, enhanced fractional release, and significantly more proarrhythmogenic  $\text{Ca}^{2+}$  waves after isoproterenol stimulation. The action potential (AP) analysis, recorded using the micro-electrode technique in hiPSC-CMs and patch-clamp in KI mouse ventricular cells, showed  $\text{Ca}^{2+}$ -dependent delayed after depolarizations (DADs). The  $[\text{Ca}^{2+}]_i$  transient amplitudes of 1-Hz paced CPVT hiPSC-CMs was similar to control hiPSC-CMs. Whereas sarcoplasmic reticulum (SR)  $\text{Ca}^{2+}$  load, estimated by rapid caffeine (10 mM) application, was smaller in hiPS-CM from the RyR2<sup>R420Q</sup> carrier, both before and after 1  $\mu\text{M}$  ISO application. However, the RyR2<sup>R420Q</sup> seems more prone to release  $\text{Ca}^{2+}$ , as the  $[\text{Ca}^{2+}]_i$  transient normalized by the amount of  $\text{Ca}^{2+}$  stored in the SR, the fractional release, was higher in CPVT hiPSC-CMs. Even if SR  $\text{Ca}^{2+}$  load was smaller in CPVT hiPSC-CMs, they often presented proarrhythmogenic behavior such as  $\text{Ca}^{2+}$  waves during diastolic periods. This behavior was further enhanced during  $\beta$ -adrenergic stimulation. Similar results were observed in KI mice, pointing to this model as a valuable tool to study the CPVT disease. We then studied the potential antiarrhythmic effect of venlafaxine and pregabalin in KI mouse cardiomyocytes and hiPS-CMs, two drugs among other medications that have been prescribed to one family carrier member and devoted of CPVT symptoms. We found that both of those drugs blunted ISO induced arrhythmogenic events in KI mouse cardiomyocytes. Venlafaxine showed antiarrhythmic effect in hiPS-CMs both by acute and chronic treatments.

On overall, 1) the RyR2<sup>R420Q</sup> mutation shows enhanced diastolic  $\text{Ca}^{2+}$  release, which is further enhanced by isoproterenol inducing proarrhythmogenic events. 2) The effects were

similar in hiPSC-CM and RyR2<sup>R420Q</sup> KI mice cardiomyocytes, pointing to hiPSC-CM as a valuable model to analyze pathological mechanisms; and 3) Venlafaxine may protect from arrhythmic CPVT patients, although more experiments are needed for *in vivo* test and to determine the mechanism of this antiarrhythmic effect.

# List of abbreviations

**ACM:** arrhythmogenic cardiomyopathy

**ANS:** autonomic nervous system

**AP:** action potential

**APD:** action potential duration

**ASIC:** acid-sensitive ionic currents

**ATP:** adenosine triphosphate

**Brs:** brugada syndrome

**BSA:** bovine serum albumin

**CaM:** calmodulin

**CASQ:** calsequestrin

**CRUs:** Ca<sup>2+</sup> release units

**CICR:** Ca<sup>2+</sup> -induced Ca<sup>2+</sup> -release

**CaMKII:** Ca<sup>2+</sup>/CaM-dependent protein kinase II

**CPVT:** polymorphic ventricular tachycardia

**D50:** duration at 50% amplitude

**DAD:** delayed depolarizations

**DMEM:** dulbecco's modified eagle medium

**DHPR:** dihydropyridine receptor

**DMSO:** dimethyl sulfoxide

**DAPI:** 4',6-diamidino-2-phenylindole

**EAD:** early depolarizations

**EBs:** embryoid bodies

**ECC:** excitation-contraction coupling

**ECG:** electrocardiography

**EDTA:** ethylenediaminetetraacetic acid

**EM:** electron microscopy

**ER:** endoplasmic reticulum

**ESCs:** embryonic stem cells

**FDHM:** full duration at half maximum amplitude

**FGFs:** fibroblast growth factors

**FKBP:** FK-binding protein

**FRET:** fluorescence resonance energy transfer

**FWHM:** full width at half maximum amplitude

**F/F<sub>0</sub>:** peak fluorescence/ basal fluorescence

**HEK293:** human embryonic kidney 293 cell line

**HF:** heart failure

**hiPSCs:** human induced pluripotent stem cells

**hiPSC-CMs:** human induced pluripotent stem cells derived cardiomyocytes

**ICD:** implantable cardioverter defibrillator

**ISO:** isoproterenol

**jSR:** junctional sarcoplasmic reticulum

**JPH2:** junctophilin-2

**KO:** knock out

**KI:** knock in

**LA:** left atrium

**LTCC:** L-type calcium channel

**LQTS:** congenital long QT syndrome

**MDP:** maximal diastolic potential

**NCX:** Na<sup>+</sup> - Ca<sup>2+</sup> exchanger

**NKA:** Na<sup>+</sup> /K<sup>+</sup> -ATPase pump

**PMCA:** plasma membrane  $\text{Ca}^{2+}$  ATPase

**PLB:** phospholamban

**PKA:** protein kinase A

**PBS:** phosphate-buffered saline

**RA:** right atrium

**RyR:** ryanodine receptor

**ROCK:** Rho-Associated Coil Kinase

**SAN:** sinoatrial node

**SCD:** sudden cardiac death

**SERCA:** sarco/endoplasmic reticulum  $\text{Ca}^{2+}$ -ATPase

**SR:** sarcoplasmic reticulum

**SOICR:** store overload-induced  $\text{Ca}^{2+}$  release

**TA:** tricuspid valve

**TWA:** T-Wave alternans

**VHD:** valvular Heart Diseases

**WT:** wild type

**WNTs:** Wiggless/INT proteins

# Preamble



Catecholaminergic polymorphic ventricular tachycardia (CPVT) is a genetic disease that manifests by syncope or sudden death in children and young adults under stress conditions without obvious cardiac structural abnormality. It is caused by the mutations in ryanodine receptor 2 (RyR2) or other 4 genes that code for proteins of RyR2 complexes. CPVT1, which is caused by RyR2 mutations, is the most common type contributing to around 60% of CPVT identified cases. So far, more than 150 of RyR2 mutations have been identified (Bezzarides *et al.*, 2019), most of which are located at 3 “hot-spots” including the N-terminal domain, the central domain and the C-terminal domain (Bezzina, Lahrouchi and Priori, 2015)(Medeiros-Domingo *et al.*, 2009). Numerous researches have studied the mechanism of CPVT1 in cell models or animal models, but a big controversy still exists, and the locations of mutations seem to play an important role. In this thesis, we were trying to gain the knowledge of an N-terminal mutation (RyR2<sup>R420Q</sup>) in human induced pluripotent stem cells derived cardiomyocytes (hiPSC-CMs) model. Thus, in the first three parts of the Introduction, we will mainly explain the normal heart function, generation of normal heart rhythm and the structure of RyR, which will help to know how the arrhythmias generate and how the mutations can affect the structure and stability of RyR. In the following part, we address arrhythmias and the common triggers of ventricular arrhythmias, as well as a short introduction of some genetic ventricular arrhythmias and acquired ventricular arrhythmias. Then we will focus on CPVT1, and introduce the analyzed CPVT1 mutations, the different experimental models used for CPVT1 functional study and main reported pathologic mechanism of CPVT1. We will also summarize all the reported functional researches of CPVT1 according to the mutations. Finally, we will introduce the traditional and novel exploring treatments of CPVT.

# Introduction



## I The heart

The heart is a very important organ located in thoracic cavity, playing a vital role in blood circulation. It is divided into 4 compartments, left atrium (LA) and left ventricle (LV) and right atrial (RA) and right ventricle (RV) that were separated by septum (Fig 1). The LA and LV take in charge of oxygen-rich blood as shown in red in Fig 1, and RA and RV take in charge of oxygen-poor blood as shown in blue in Fig 1. In each heartbeat, the oxygen-rich blood from lung flows into LA through pulmonary veins, then enter into LV through automatically opened mitral valve which separate LA and LV (Fig 1). While in the right side, the oxygen-poor blood return from the body enter RA through superior and inferior vena cava (SCV and ICV), which in turn flow into RV by passing the tricuspid valve (TV). Then, with atrial contraction, the blood pass from atria to ventricles, and with ventricles contraction, the LV pumps the oxygen-rich blood to the body through aorta, and RV pump oxygen-poor blood into lungs where it gets oxygen through pulmonary arteries. The blood flowing from atriums to ventricles happens during diastole, while the blood exiting the heart from ventricles happens during systole. During this process, all valves depicted in Fig 1 play an important role to prevent blood backflow. In the RA, near the entrance of the SCV, there is a location of heart pacemaker as shown by yellow circle in Fig 1, the Sinoatrial node (SAN, see next session). The other yellow circle in Fig 1 close to TV in RA depict the position of atrioventricular valve node (AV node), which is also a key component in cardiac electrophysiology.

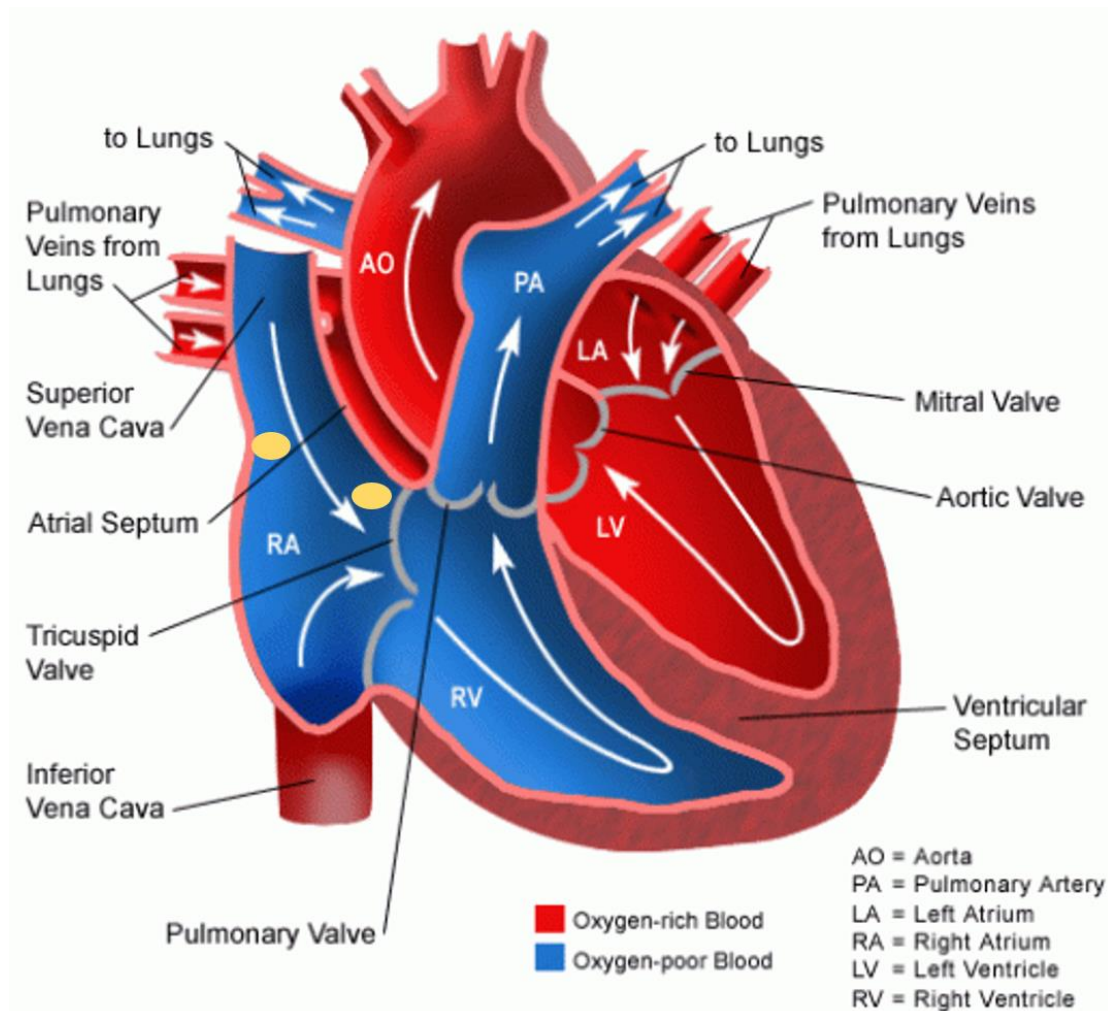


**Figure 1. Anatomy of the heart.** Section through the human heart showing the structures of heart and circulatory system. (Adapted from <http://colvincuriosity.com/2017/06/27/how-does-the-heart-work/>)

## II Heart rhythm

The heart beats regularly and consistently pump oxygen-rich blood to the body and send oxygen-poor blood into lungs, completing the blood circulation. This regular and consistent heartbeat, we call heart rhythm. The heart rhythm can be read on the electrocardiogram (ECG) as a series of consecutive heart beats displaying identical waveforms as shown in Fig 2B. The similarity of the waveforms indicates that the origin of the impulse is the same. The SAN is the heart's pacemaker under normal circumstances and the rhythm is referred to as sinus rhythm.

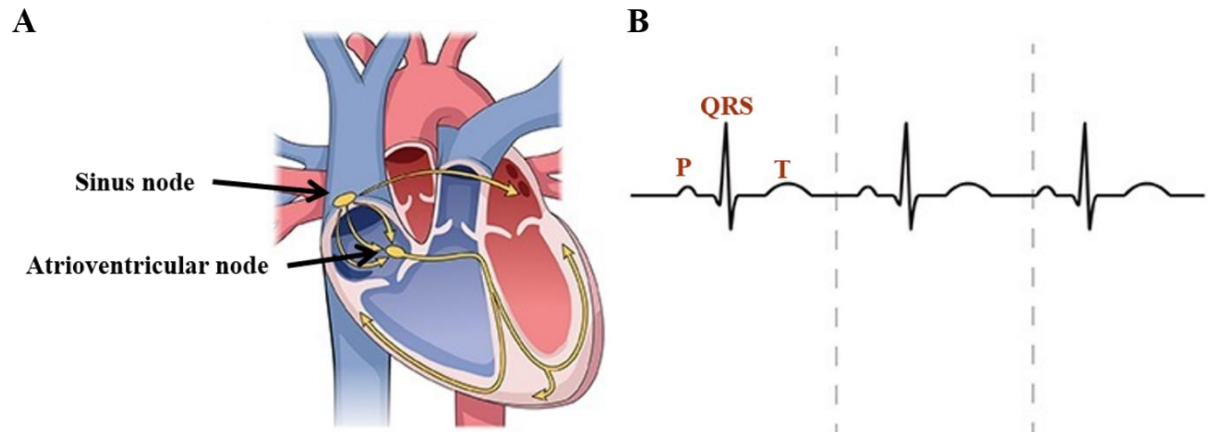


**Figure 2. Generation of normal heart rhythm.** A. Schematic diagram of conduction of impulse generated from sinus node. B. Schematic diagram of ECG with P, QRS and T waves. (Adapted from U.S. National Library of Medicine)

## II.1 Normal heart rhythm—sinus rhythm

Normal heart rhythm is often called normal sinus rhythm because the SAN fires regularly. The electrical stimulus generated by the SAN sets the rate and rhythm of the heart beats, since all cardiomyocytes are electrically linked to one another, by structures known as gap junctions which allow the action potential to pass from one cell to the next. This spontaneous electrical activity of the SAN spreads through the walls of the atria and causes them to contract, which forces blood into the ventricles. As Fig 2B shows, the contraction of atria depicts P wave (~0.08s in humans) on ECG. The electrical activity goes then through the atrioventricular (AV) node (Fig 2A) which connect the atria and ventricles. Thanks to the much slower conduction of AV node, the electrical activity will be delayed for about 20 milliseconds in human, giving the atria time to pump blood into the ventricles (Keating and Sanguinetti, 2001). After AV node, the electrical activity will be conveyed to specialized fibers known as bundle His branches, leading to rapid depolarization of all ventricular myocytes and coordinated contraction of the ventricles. During ventricular activation, impulses are first conducted down the left and right bundle branches on either side the septum. This causes the septum to depolarize from left-to-right and record as a small negative deflection on the ECG (Q wave of the QRS). About 20 milliseconds later, the mean electrical activity points downward toward the apex producing a very tall positive deflection (R wave of the QRS). After another 20 milliseconds, the electrical pulse is pointing toward the left arm and anterior chest as the free wall of the ventricle depolarizes from the endocardial to the epicardial surface (S wave of the QRS). Then ventricles repolarize slowly (T wave), leading to cardiac relaxation and completed heart beat (Keating and

Sanguinetti, 2001). At rest, a normal human heart beats around 50 to 99 times per minute. Exercise, emotions, fever and some medications can cause heart to beat faster, sometimes to well over 100 beats per minute.

## II.2 Molecular mechanisms of heart beat

### II.2.1 Action potential

Action potential (AP) is the membrane potential ( $E_m$ ) waveform generated by the cell membrane upon valid stimulation. In human cardiomyocytes, there are several different morphologies of AP according to different cell types as shown in Figure 3A.

AP is the basic unit of electrophysiological signal that is determined by a complex interplay of many ion channels (Fig 3B). Here we take ventricular myocyte as example (Fig 3B). Before the stimulation, ventricular myocytes are in resting potential (approximately -85 mV) maintained by  $I_{K1}$  generated by Kir2.1 channels. (Bers, no date)(Amin, Tan and Wilde, 2010)(Landstrom, Dobrev and Wehrens, 2017)(Sorensen, Søndergaard and Overgaard, 2013). Then, after received an electrical stimulation which depolarizes their membrane above threshold, the AP is triggered by the fast inward sodium current ( $I_{Na}$ ) through the voltage-gated sodium channels (Nav1.5), inducing fast depolarization and composing the upstroke (phase 0) of AP. Then the membrane starts to repolarize due to the rapid inactivation of Nav1.5 and the activation of repolarizing (outward) currents. The repolarization is divided into 4 phases according to the repolarized velocity. Phase 1 (early repolarization) is a fast process accomplished by the transient outward potassium current  $I_{to}$  generated by Kv 4.2/4.3 and rapid inactivation of Nav1.5. The existence and amplitude of  $I_{to}$  vary from different animal species, for example, in dogs, the  $I_{to}$  is very important for the repolarization and even form a peak down before the plateau, but in Guinea pigs, no clear  $I_{to}$  exists, so it's hard to see phase 1 in their repolarization. Phase 2 is a plateau that is generated by the balance between the depolarizing L-type inward  $Ca^{2+}$  current ( $I_{Ca,L}$ ) generated by Cav1.2 (LTCC) and the repolarizing ultra-rapidly ( $I_{Kur}$  by Kv 1.5/3.1), rapidly ( $I_{Kr}$  by HERG), and slowly ( $I_{Ks}$  by KVLQT1) activating delayed outward rectifying currents. LTCC is a voltage gated channel on sarcolemmal membrane expressed all over the heart (Mangoni and Nargeot, 2008)(Benitah, Alvarez and Gómez, 2010). It is activated when membrane potential reaches  $\sim -50mV$ (Mesirca et al 2015), and generates  $I_{Ca,L}$ , the main trigger of excitation-contraction coupling (ECC) that we will explain latter. Repolarization in phase 3 turns to be faster due to the inactivation (closing) of the LTCCs while

the delayed rectifying  $K^+$  channels remain active. In phase 4,  $I_{K1}$  helps cells to regain resting potential and get ready for next stimulus. There is an inward current during the whole repolarization, which is  $I_{NCX}$ , generated by  $Na^+$ - $Ca^{2+}$  exchanger (NCX) as shown in Fig 3B. NCX is a high-capacity, voltage-dependent,  $Ca^{2+}$ -dependent and time-independent electrogenic protein. It catalyses the countertransport of three  $Na^+$  by one  $Ca^{2+}$  using the energy of the  $Na^+$  gradient as driving force (Shattock *et al.*, 2015) and always tend to bring cytoplasmic free  $Ca^{2+}$  to its thermodynamic equilibrium (Reuter *et al.*, 2005). Another persistent current is an outward current  $I_{NaK}$  (Fig 3B) generated by  $Na^+/K^+$ -ATPase (NKA, or  $Na^+$  pump). NKA, moving  $Na^+$  ions from the cytoplasm to the extracellular space against their gradient by utilizing the energy released from ATP hydrolysis, is essential for re-establishing and maintaining the trans-sarcolemmal  $Na^+$  gradient for many membrane trans-porters like NCX to move ions, substrates, amino acids and metabolites into or out of the cell (Shattock *et al.*, 2015).

The human induced pluripotent stem cells derived cardiomyocytes (hiPSC-CM) is engineering human cardiomyocytes, which present some special characteristics such as lack of t-tubular network, their polygonal shapes, disorganized sarcomeric myofilament, and their rhythmic automaticity comparing to native human cardiomyocytes due to their immaturity (X. Zhang and Morad 2020). While with further research, multiple ionic currents verified in native human cardiomyocytes have been characterized in single hiPSC-CMs (Figure 3C), including Sodium current ( $I_{Na}$ ), L-type and T-type inward  $Ca^{2+}$  current ( $I_{Ca,L}$ ) ( $I_{Ca,T}$ ) (Protze *et al.*, 2016), sodium calcium exchanger current ( $I_{NCX}$ ) (X. Zhang and Morad 2020), transient outward potassium current ( $I_{to1}$ ), rapidly ( $I_{Kr}$ ), and slowly ( $I_{Ks}$ ) activating delayed outward rectifying potassium currents, the inward rectifier potassium ( $I_{K1}$ ), hyperpolarization-activated pacemaker( $I_r$ ) (Protze *et al.*, 2016)(Karakikes *et al.*, 2015)(Prajapati, Pölönen and Aalto-Setälä, 2018) (Figure 3C). All these described ionic currents in hiPSC-CMs and their channel gating properties are similar to those reported for human cardiac myocytes (Ma *et al.*, 2011). Moreover, acetylcholine-activated  $K^+$  current ( $I_{K,ACh}$ ), the atrial-selective ion current (Devalla *et al.*, 2015), and acidic solutions activated acid-sensitive ionic currents (ASIC), the proton-gated cation channels (Zhang *et al.*, 2019), have recently been reported in hiPSC-CM.

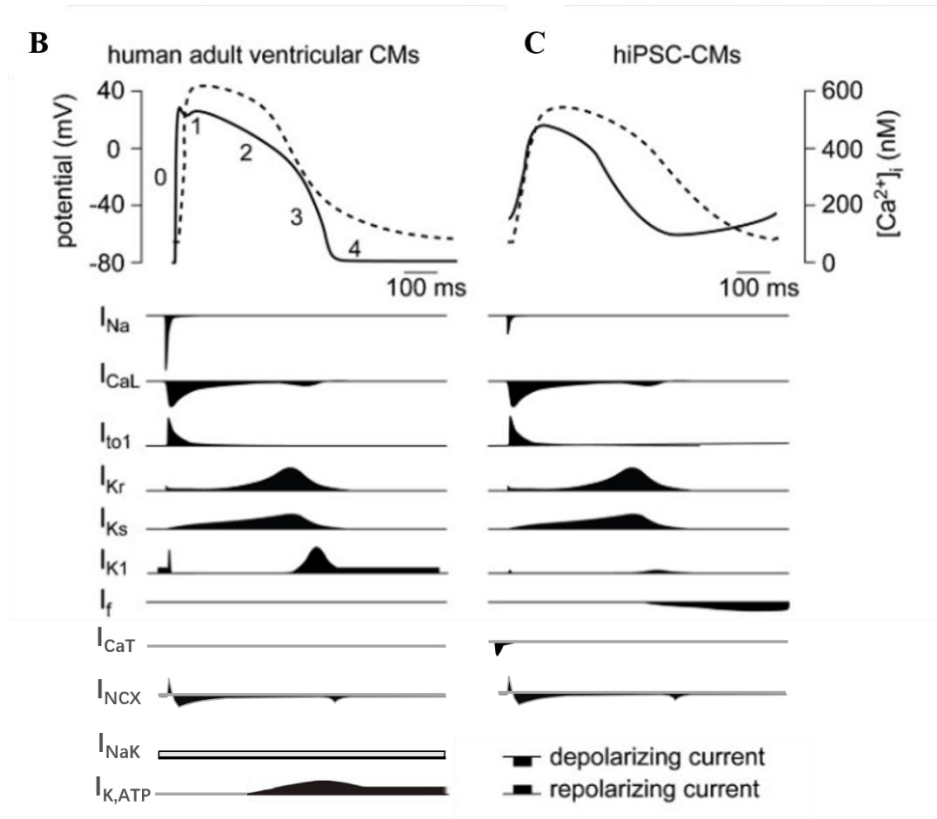
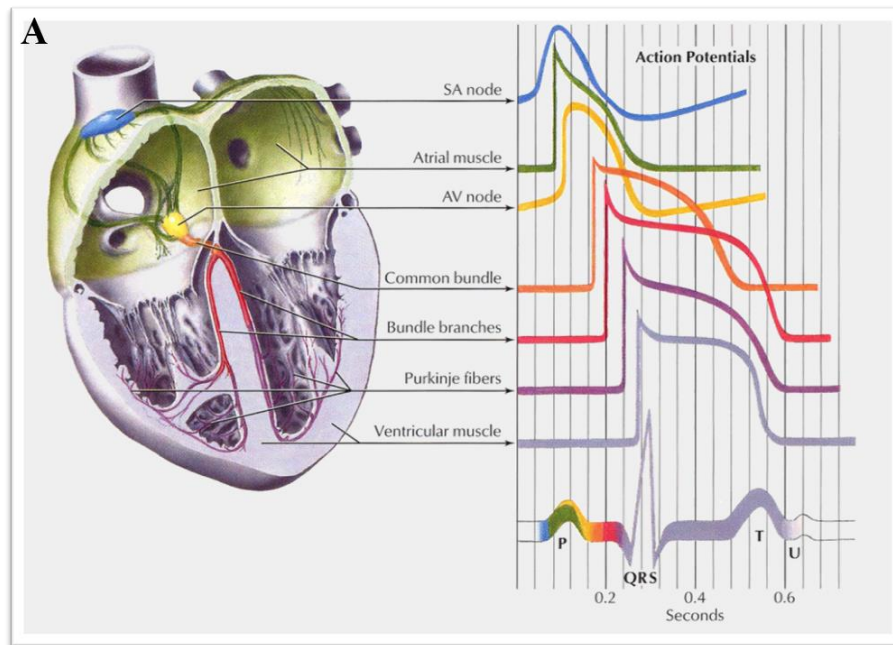


**Figure 3. The different morphologies of AP generated by different tissues and the corresponding ECG diagram. A) and currents involved in AP of human adult ventricular myocytes and hiPSC-CM B). Sodium current ( $I_{Na}$ ), L-type inward  $Ca^{2+}$  current ( $I_{Ca,L}$ ), transient outward potassium current ( $I_{to1}$ ), T-type inward  $Ca^{2+}$  current ( $I_{Ca,T}$ ), rapidly ( $I_{Kr}$ ), and slowly ( $I_{Ks}$ ) activating delayed outward rectifying potassium currents, the inward rectifier potassium ( $I_{K1}$ )  $I_{NCX}$  generated by Sodium-calcium exchanger,  $I_{NaK}$  generated by  $Na^+/K^+$ -ATPase, hyperpolarization-activated pacemaker( $I_f$ ). The dash lines in B and C panels represent  $Ca^{2+}$  transients. (Adapted from <https://www.creative-bioarray.com/acrosscell/ipsc-derived-cardiomyocytes.html>)**

### II.2.2 excitation-contraction coupling (ECC)

Here we mainly take ventricular cells as example. ECC is an important process which transfers the electricity of action potential (AP) to the contraction of the heart. The cation  $\text{Ca}^{2+}$  is the most important messenger during this process. Figure 4 designed by Donald M. Bers shows the movements of ions during ECC and relationship with AP,  $[\text{Ca}^{2+}]_i$  and contraction. With the development of AP, the depolarization of the membrane potential activates LTCC which bring a small amount of  $\text{Ca}^{2+}$  into cytosol and generate an inward current ( $I_{\text{Ca,L}}$ ). The amount of  $\text{Ca}^{2+}$  influx by  $I_{\text{Ca}}$  varies among cell types and animal species as well as with the AP configuration and SR  $\text{Ca}^{2+}$  release (Bers, 2008). This small amount of  $\text{Ca}^{2+}$  then triggers the large amount of  $\text{Ca}^{2+}$  release from sarcoplasmic reticulum (SR) through ryanodine receptors (RyR) by  $\text{Ca}^{2+}$  - induced  $\text{Ca}^{2+}$  -release (CICR) process which has been firstly demonstrated by Fabiato and Fabiato (Fabiato and Fabiato, 1975). With the  $\text{Ca}^{2+}$  concentration increasing, L-type calcium channels are turned off by  $\text{Ca}^{2+}$ - dependent inactivation. This process is mediated by calmodulin bound to the carboxy terminus of the  $\text{Ca}^{2+}$  channel (Peterson *et al.*, 1999)(Zuhlke *et al.*, 1999)(Alseikhan *et al.*, 2002)(Avila *et al.*, 2020). The increased intracellular  $\text{Ca}^{2+}$  ( $[\text{Ca}^{2+}]_i$ ) binds to myofilaments leading to contraction. In order to be ready for next contraction, the cell needs to return to relaxation condition which demands  $[\text{Ca}^{2+}]_i$  concentration decrease to previous level. There are mainly 4 ways for  $[\text{Ca}^{2+}]_i$  removal from the cytosol: pumped back into SR by SERCA pump, extruded out of cell by sodium calcium exchanger (NCX), pumped out of cell by sarcolemmal  $\text{Ca}^{2+}$  pump and transferred into mitochondria by mitochondrial  $\text{Ca}^{2+}$  uniporter (Bers, 2002). In rabbits, about 74% of  $\text{Ca}^{2+}$  is removed by SERCA pump and restored in SR to maintain the dynamic balance of the SR content, which is very important for the continuation of normal heartbeat. About 24%  $\text{Ca}^{2+}$  is removed by NCX and the rest is removed by the other two ways. In physiological condition, whether mitochondria take part in the regulation of  $[\text{Ca}^{2+}]_i$  concentration during ECC remains to be determined (Gambardella *et al.*, 2018), but in pathological condition, they can increase the storage to compensate the  $[\text{Ca}^{2+}]_i$  (Brandes and Bers, 1997) (Walsh *et al.*, 2009) (Gunter and Sheu 2009) (Drago *et al.*, 2012) (Morciano *et al.*, 2017). However, in rats, the SERCA pump contribute 93% and NCX only contribute 6% for  $[\text{Ca}^{2+}]_i$  removal (Bers, 2014). Observations in mouse ventricle is more like rat (Li *et al.*, 1998), whereas in human is more like rabbit, which, may be due to the different heart rate since the efficiency of SERCA pump is much higher than NCX which can fulfill fast clearance of  $[\text{Ca}^{2+}]_i$  for preparation of next contraction, because, in order to keep the steady state, the quantity of  $\text{Ca}^{2+}$  efflux should be equal to  $\text{Ca}^{2+}$ influx (Eisner *et al.*, 2017).

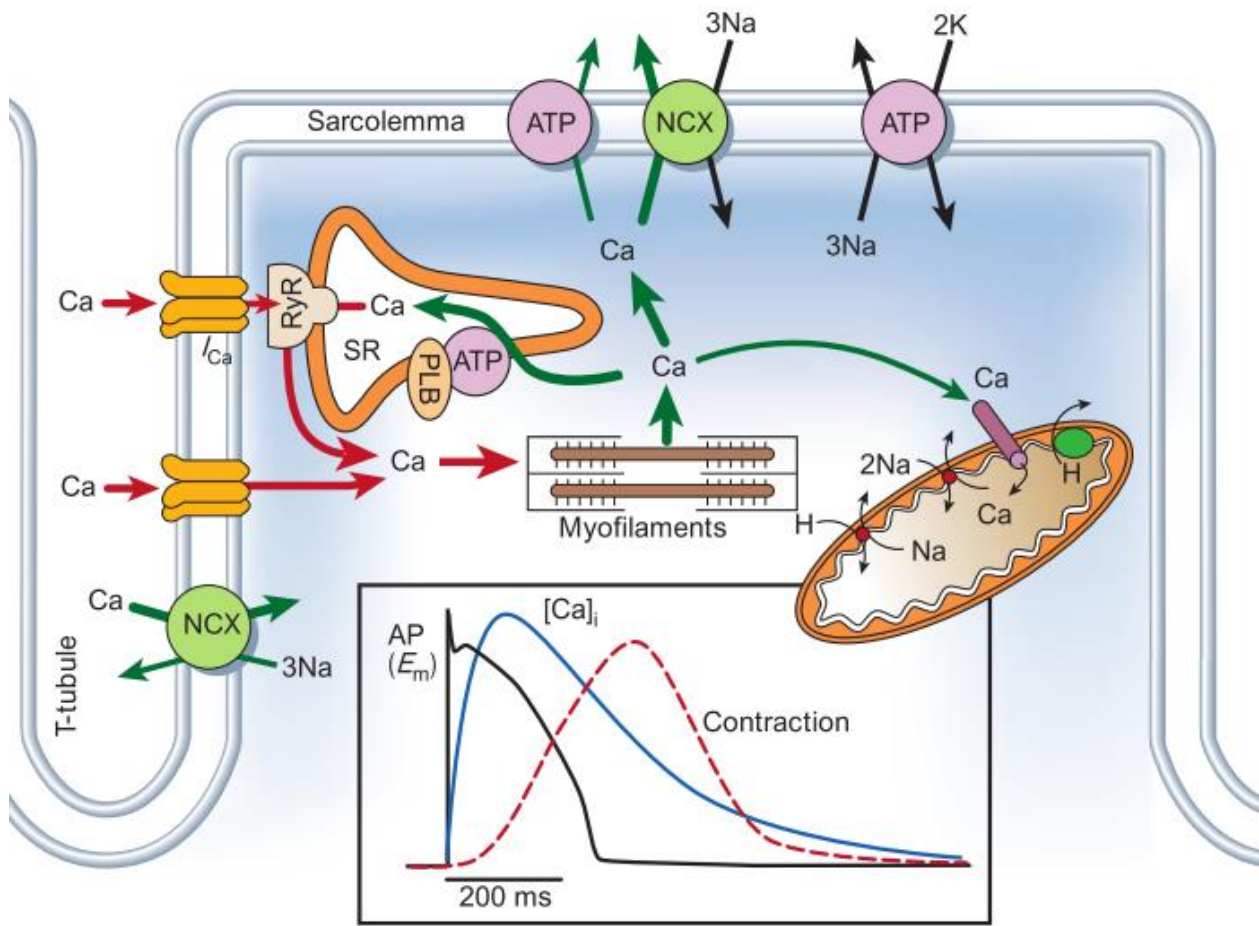


**Figure 4. Ca<sup>2+</sup> transport in ventricular myocytes.** Inset shows the time course of an action potential, Ca<sup>2+</sup> transient and contraction measured in a rabbit ventricular myocyte at 37 °C. NCX, Na<sup>+</sup>/ Ca<sup>2+</sup> exchange; ATP, ATPase; PLB, phospholamban; SR, sarcoplasmic reticulum. (Adapted from (Bers, 2002))

### III The ryanodine receptors (RyRs)

We already said, during E-C coupling and heart contraction, Ca<sup>2+</sup> is a very important second messenger, the majority of intracellular Ca<sup>2+</sup> being released from SR by RyRs. Thus, in order to study the Ca<sup>2+</sup> handling during ECC coupling, we need to gain the knowledge of RyRs firstly.

#### III.1 General introduction of RyRs

Ca<sup>2+</sup> is a key mediator during E-C coupling as we mentioned above, but Ca<sup>2+</sup> may be toxic to the cells. In resting period, extracellular concentration and intracellular concentration are 1.2 mM and 50-100 nM respectively (Bronner, 2001). The very low resting cytosolic [Ca<sup>2+</sup>]<sub>i</sub> is maintained by plasmalemmal NCX and Ca<sup>2+</sup>-ATPase pump, SERCA, and the mitochondrial Ca<sup>2+</sup> uniporter. The 4 ways for removing the Ca<sup>2+</sup> from cytosol, as well as by Ca<sup>2+</sup> buffering

molecules of differing capacity and kinetics (Cheng and Lederer, 2008)(Bers, 2002) avoid the toxicity of sustained high  $[Ca^{2+}]_i$ , as well as bestows on the  $Ca^{2+}$  signaling system a wide dynamic range and a high signal-to-background ratio (Cheng and Lederer, 2008). However, as  $Ca^{2+}$  rises in each twitch, the local cytosolic  $[Ca^{2+}]_i$  may maximally reach to around 1  $\mu$ M within 200 ms (Bers, 2002), more than 10 fold increase. This so considerable amount and efficient  $[Ca^{2+}]_i$  change relies on the large-conductance of  $Ca^{2+}$  release channels located in the membrane of SR in cardiac myocytes. There are two families of  $Ca^{2+}$  release channels, the RyRs and inositol 1,4,5-triphosphate receptors (IP3Rs) (Mackenzie *et al.*, 2002)(Berridge, 2012)(Berridge, 2016). In physiological condition, RyR is the main  $Ca^{2+}$  release channel which is expressed much more abundantly than IP3Rs, whereas during cardiac hypertrophy, IP3R expression and function is increased, which is thought to contribute to cardiac remodeling (Garcia and Boehning, 2017). In the following section, we will look into RyRs.

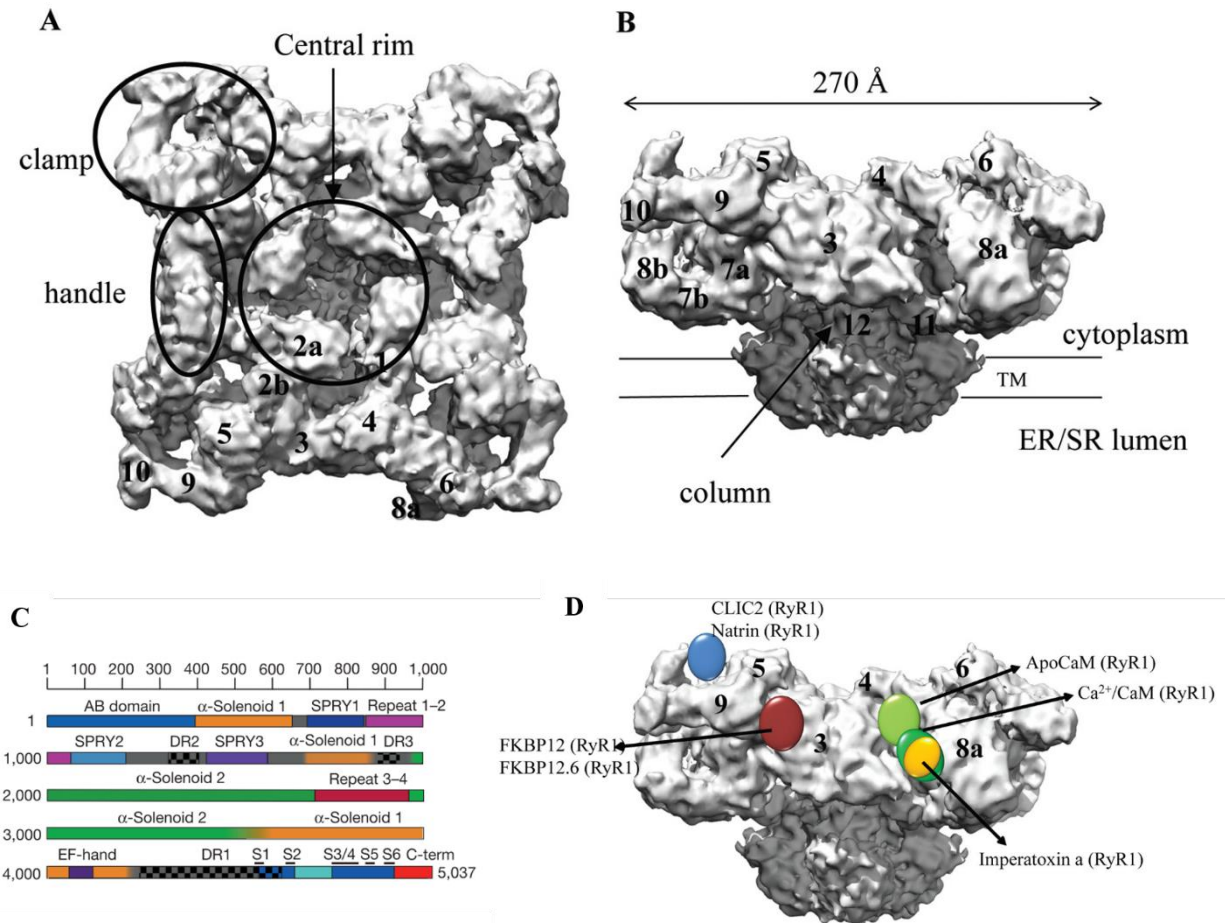
### III.1.1 Location and distribution of RyRs

RyRs are large-conductance  $Ca^{2+}$  release channels located on the membrane of endoplasmic reticulum (ER) in skeletal muscle cells and SR in cardiac myocytes. RyR is named for its high affinity binding to and regulation by ryanodine. Three isoforms, RyR1, RyR2 and RyR3, have been found in mammalian species (Yuchi and Van Petegem, 2016)(Meissner, 2017). The human gene encoding RyR1 is located on chromosome 19q13.2 and contains 104 exons; the gene encoding RyR2 is located on chromosome 1q43 with 102 exons; the gene encoding RyR3 is located on chromosome 15q13.3-14 with 103 exons (Lanner *et al.*, 2010b). In mice, they are separately located in chromosomes 7A3, 13A2, and 2E4, respectively (Mattei MG, Giannini G, Moscatelli F, 1994). The RyR1 isoform is primarily expressed in skeletal muscles, which also appears to be expressed at low levels in cardiac muscle, smooth muscle (McPherson and Campbell, 1993), stomach, kidney, thymus (Nakai *et al.*, 1990)(Giannini *et al.*, 1995), cerebellum, Purkinje cells, adrenal glands, ovaries, and testis (Furuichi *et al.*, 1994)(Ottini *et al.*, 1996). RyR2 is the cardiac isoform (Otsu *et al.*, 1990)(Nakai *et al.*, 1990)(Coussin *et al.*, 2000), but also expresses at high levels in Purkinje cells of cerebellum and cerebral cortex, and at low levels in stomach, kidney, adrenal glands, ovaries, thymus, and lungs (Lanner *et al.*, 2010b). RyR3 is sometimes referred to as the brain isoform, but it's not exact since RyR2 is more abundantly expressed in the brain relative to RyR3 (McPherson and Campbell, 1993). RyR3 also has been found to express at low level in various cell types, including hippocampal neurons, thalamus, Purkinje cells, corpus striatum, skeletal muscles, the smooth muscle cells of

many organs such as lung, kidney, spleen (Lanner *et al.*, 2010b). In skeletal muscle, RyR3 is preferentially expressed in slow-twitch type muscles (Ottini *et al.*, 1996), whereas RyR1 is selectively expressed in muscle attributing to rapid contractions (O'Brien, Meissner and Block, 1993). The distribution in different tissues to some extent reflects the function mechanism and capacity of each isoform, which in turn decide their special structure.

### III.1.2 General structure of RyRs

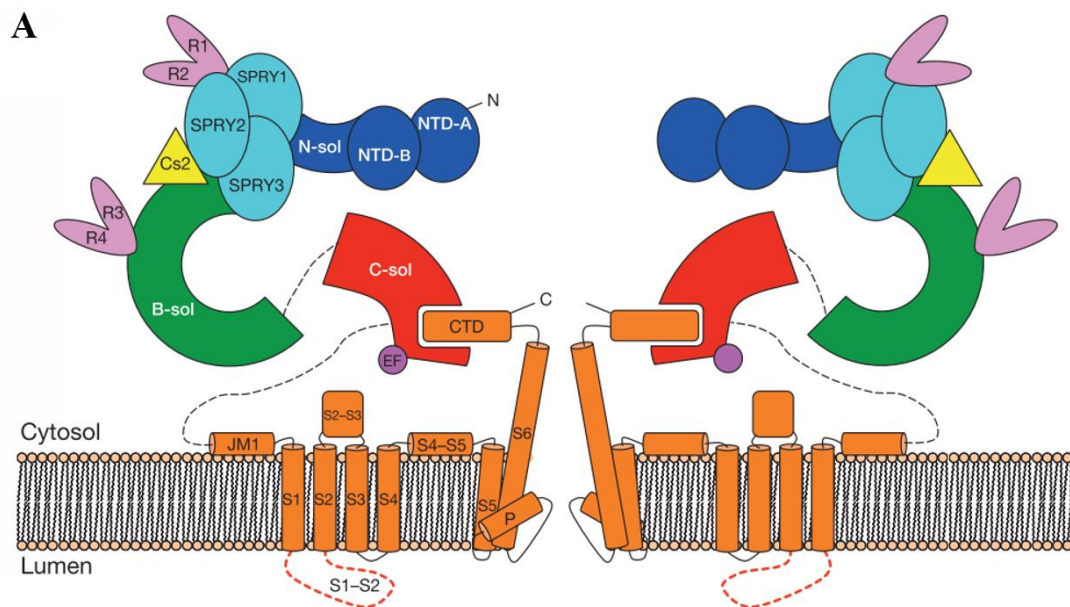
RyRs are the largest ion channels to date (~2.2MDa), consisting of four homologous subunits with approximately 5000 amino acids in each subunit (Anthony Lai *et al.*, 1988)(Van Petegem, 2012). The huge molecular body makes it more difficult to study its structure, but with the developing of cryo-electron microscopy (cryo-EM), more than two thirds of the molecular mass of RyRs was resolved nowadays (Meissner, 2017). The basic architecture of RyR can be described as a mushroom, with a large cap representing around 80% of the volume located in the cytoplasm and the stalk crossing the membrane into the SR/ER lumen (Fig 5). The transmembrane region measures 120x120x60 Å, whereas the cytoplasmic area measures around 270x270x100 Å (Fig. 5B). Terms of “clamps,” “handles,” and a “central rim” are used to facilitate the description of the structure, and they surround a central cavity as shown in Fig. 5A. The overall shape is very similar for all RyR isoforms (Sharma *et al.*, 1998)(Sharma *et al.*, 2000). Beside the similar shapes, the 3 isoforms share 65-70% sequence identity, and the difference mainly comes from three “divergent regions” throughout the sequence, known as D1 (residues 4254–4631 in RyR1), D2 (residues 1342–1403), and D3 (residues 1872–1923) (Figure 5C), which are likely to be responsible for the functional differences between isoforms (Sharma *et al.*, 1998). Along with revealing the global structure, cryo-EM in combination with fluorescence resonance energy transfer (FRET) measurements identified regulatory sites on RyR1 and RyR2 such as the FKBP binding site and sites of the Ca<sup>2+</sup>-free and Ca<sup>2+</sup>- bound forms of CaM (Fig 5C.)



**Figure 5. Overall structure of RyRs.** Shown is a cryo-EM reconstruction of RyR1 at 9.6 Å. A, top view from the cytoplasm, looking toward the SR/ER. B, side view showing the large cytoplasmic head. Labels show the structural elements and the numbered subregions. TM, transmembrane domain. C, consequence of all the domains within RyR1. D, Locations of several protein-binding partners based on difference cryo-EM. (panel A, B, D adapted from (Van Petegem, 2012), panel C adapted from (Efremov *et al.*, 2015))

Due to the abundant expression and ease for purification, RyR1 became the first one to be seen through electron microscopy (Anthony Lai *et al.*, 1988) and also the most thoroughly examined isoform until now (Meissner, 2017). An interesting feature of the RyRs is that they can form regular arrays at the SR-plasma membrane junctions as observed in electron-microscopy images (Van Petegem, 2012). The closed and open pore structures of RyR1 and RyR2 were determined at 3.6~6 Å resolution by single-particle electron cryomicroscopy recently (Efremov *et al.*, 2015)(Zalk *et al.*, 2015)(Yan *et al.*, 2015)(Bai *et al.*, 2016)(des Georges *et al.*, 2016)(Peng *et al.*, 2016)(Wei *et al.*, 2016). Determination of the high-resolution closed- and open-channel structures provides a better understanding of the mechanisms of channel gating and ion permeation and how they are altered in RyRs-associated diseases. Each

RyR subunit has been subdivided into ~10 domains. As Figure 6A shows, these include (1) the N-terminal domain, consisting of three domains: A (residues 10–223), B (224–408) and C (409–544)(Borko *et al.*, 2014), is often considered zipping with central domain to regulate channel gating, which is a hotspot of RyR1 and RyR2 disease mutations, (2) the SPRY1 domain that is part of the binding site for FKPB12, (3) bridging solenoid (B-sol), containing PKA and Ca<sup>2+</sup>/CaM-dependent protein kinase II (CaMKII) phosphorylation sites, (4) the central solenoid (C-sol) domain that contains two EF hand Ca<sup>2+</sup> binding motifs, (5) the transmembrane domain that forms the conductance pathway for Ca<sup>2+</sup>, and (6) the intra-SR luminal C-terminal domain (CTD) that forms part of the Ca<sup>2+</sup>, ATP, and caffeine activation sites. As for the number of transmembrane helices, there has once been much debate (Van Petegem, 2012), but the overall consensus now is that there are six segments per subunit, which was identified as one of the best-resolved regions of the cryo-EM maps (Fig. 6B-C ). The transmembrane region could be separated into two domains: the pore domain, formed by two transmembrane helices (S5, S6) and the extended peptide (P-segment); and the interfacing domain formed by S1-S4 that is connected with the pore domain (Fig 6A) (Zalk *et al.*, 2015). Due to the inhomogeneous resolution of cryo-EM maps, ambiguity still persists in certain regions at the periphery of the cytosolic cap (Yuchi and Van Petegem, 2016)(Pancaroglu and Van Petegem, 2018).



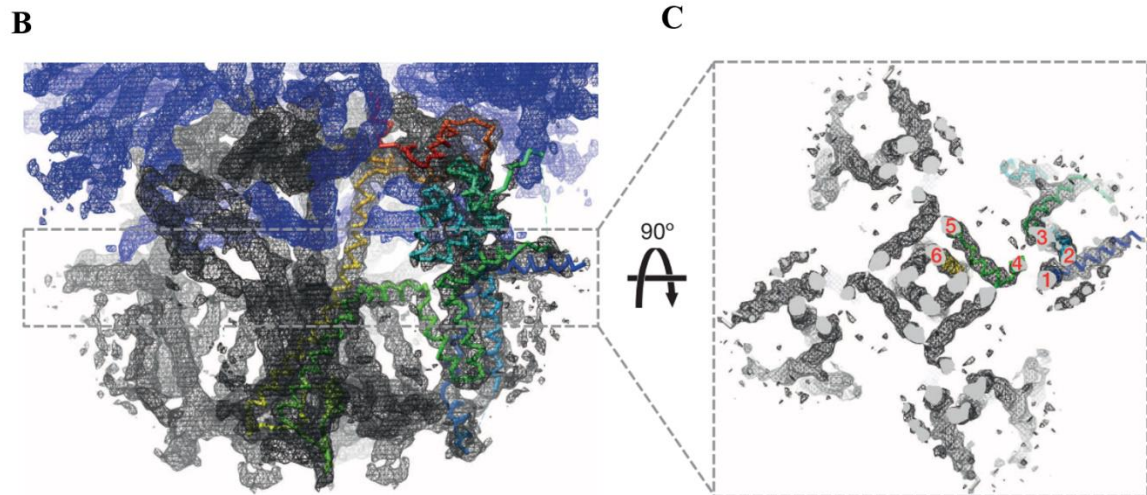


**Figure 6. General structure of RyR1.** A. Color-coded schematic representation of the RyR1. B-sol, bridge solenoid; C-sol, core solenoid; N-sol, N-terminus solenoid. B. RyR1 transmembrane pore and CTD. Density map of the pore region (black mesh) and the core solenoid (blue mesh), displayed with the transmembrane region of one protomer in spectral coloring (N terminus is blue, C terminus is red). C. A906 slab through the plane of the membrane, with numbering indicating the positions of the six transmembrane helices. (Adapted from (Zalk *et al.*, 2015))

The state of channel is directly determined by S6, the straighter S6 forming the open state and the bent S6 forming the closed state (Pancaroglu and Van Petegem, 2018). However, conformational landscape of RyRs is such large that the simple open-closed model is not sufficient to describe. An important of recent finding is the establishment of an intermediate state between open- and closed-state, which named “primed” (Fig. 7) (des Georges *et al.*, 2016). They found that either ATP or  $\text{Ca}^{2+}$  alone can induce conformational changes in the cytoplasmic assembly (“priming”) of RyR1, but not induce pore dilation (Fig. 7). The channel can be further adjusted to open state in presence of 3 activated ligands (ATP,  $\text{Ca}^{2+}$ , caffeine), or completely closed by high concentration of ryanodine (Fig. 7) (des Georges *et al.*, 2016).

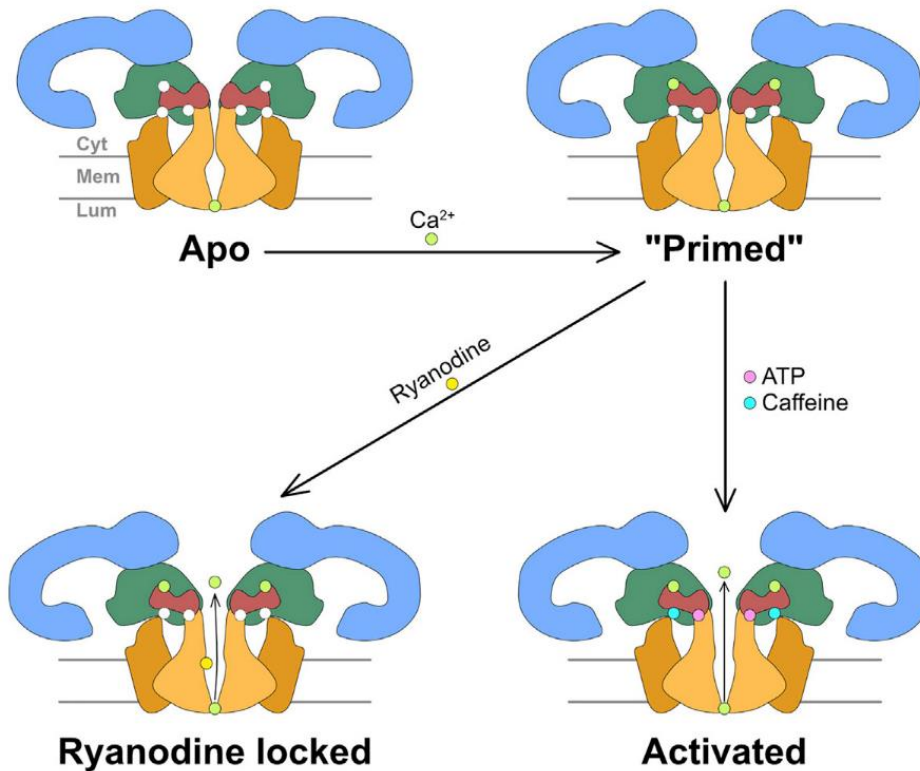


**Figure 7. Schematic diagram of RyR transition between different states.** Small circles indicate the molecule binding sites: green, Ca<sup>2+</sup>; purple, Adenosine triphosphate (ATP); blue, caffeine; yellow, ryanodine. (adapted from (des Georges *et al.*, 2016))

### III.2 Special architecture of RyR2

The study on the structure of RyR2 is lagged behind that on RyR1 for many years, which is the consequence of the difficulty for purification and more harsh condition for maintenance of RyR2 (Pancaroglu and Van Petegem, 2018)(Sharma *et al.*, 1998). The highest resolution for RyR2 currently reported is at 4.2 Å (Fig 8.) (Peng *et al.*, 2016). The closed and open states were separately reconstructed at 4.4- and 4.2-Å resolutions (Fig. 8). Moreover, they depicted the conformational changes between the open and closed states of RyR2 (Fig. 8B). However, limited to the low resolution, the Ca<sup>2+</sup> binding site wasn't unveiled, hampering the understanding of the role of the Central domain in cytosolic Ca<sup>2+</sup> activation of RyR2 (Peng *et al.*, 2016). Thus, the cryo-EM maps did not readily show differences between RyR1 and RyR2 (Pancaroglu and Van Petegem, 2018). Another recent study on ultrastructural analysis of RyR2 (Cabra, Murayama and Samsó, 2016) shows that RyR2s can interact in two rigids with two RyR2s alongside each other forming an angle of 12°. They further demonstrated that the adjoining interaction of two RyR2s involves contacts between the SPRY1 domains (domains 9)

and P1 domains (domains 10), yet not through domain 6 as previously thought (Cabra, Murayama and Samsó, 2016). In addition, the N-terminal domain is the most solved region of RyR2 to date, and several special structures have been identified. For example, Van Petegem's group solved the crystal structure of the N-terminal region of mice RyR2 and found that the A, B and C domains in this region are held together via a central chloride anion that shields repulsive positive charges (Kimlicka, Tung, *et al.*, 2013). The N-terminal region mutation RyR2<sup>R420Q</sup> was demonstrated to ablate chloride binding which could be the underlying mechanism of the RyR2<sup>R420Q</sup> mutation causing CPVT (Kimlicka, Tung, *et al.*, 2013). However, No Cl<sup>-</sup> anion was found and the structure did not show any evidence of a chloride-binding site in N-terminal region of human RyR2 according to Borko's investigation (Borko *et al.*, 2014). Moreover, a unique and dynamic  $\alpha$ -Helix within the first  $\beta$ -trefoil in domain A of RyR2, which can rescue the  $\beta$ -strand lost in RyR2A, was revealed by nuclear magnetic resonance (NMR) spectroscopy and X-ray crystallography (Amador *et al.*, 2013) (Lobo *et al.*, 2011).

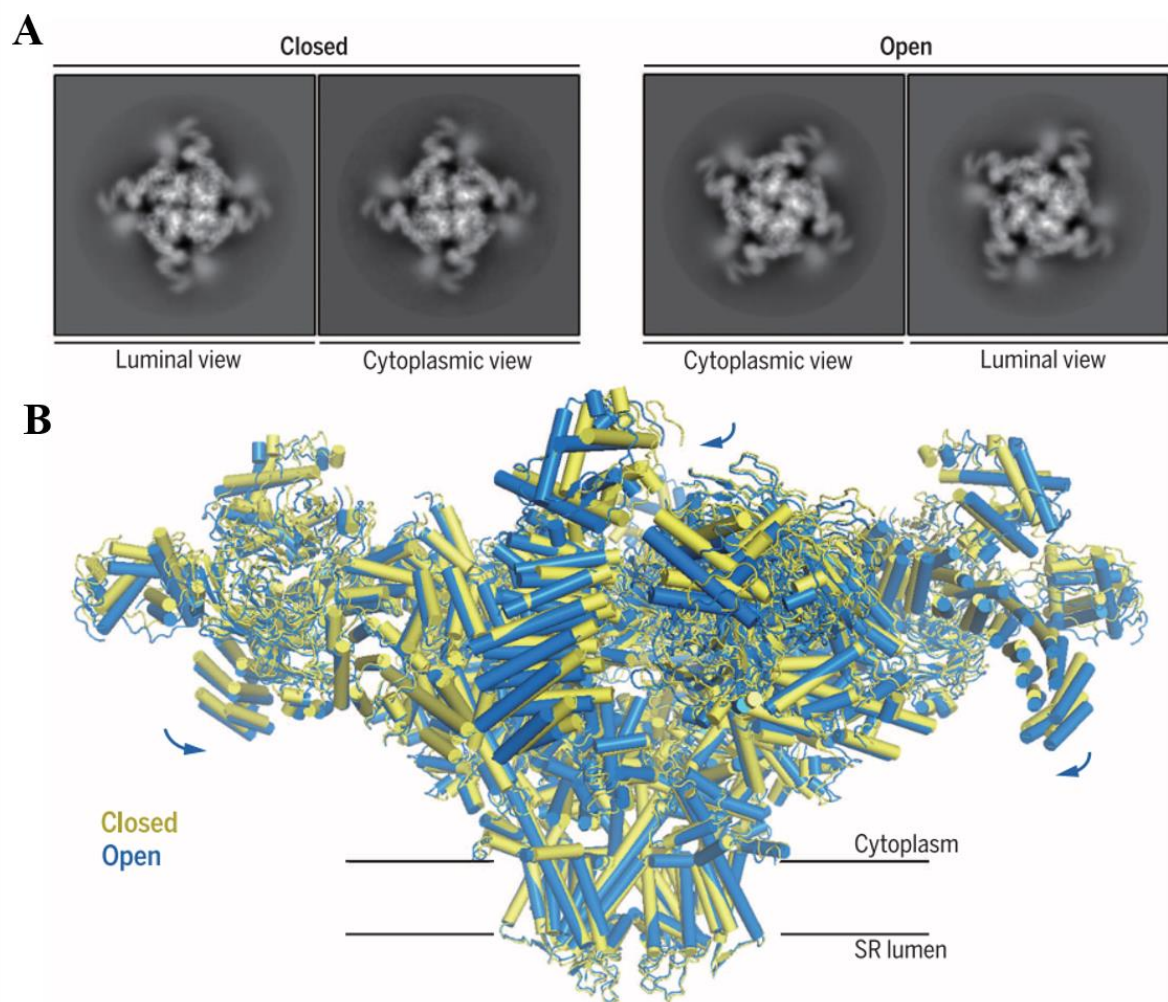


**Fig 8. Cryogenic EM structures of RyR2 from porcine heart in both the closed and open states at near-atomic resolutions.** (Top) Representative two-dimensional class averages of electron micrographs of the closed and open RyR2. (Bottom) The two structures are superimposed relative to the transmembrane domain. The blue arrows indicate the overall shifts of the cytoplasmic region from the closed state to the open state. (adapted from (Peng *et al.*, 2016))

## IV Arrhythmia

### IV.1 What is arrhythmia?

Arrhythmia is a wide conception covering all the conditions with unnormal heart rate (lower than 50/min has been considered as bradycardia and higher than 100/min has been considered as tachycardia in human), but the rhythms which are physiologically justified, such as sinus bradycardia in athletes and during sleep, should not be considered abnormal. A simple pro-arrhythmic activity excluding the genetic reasons usually doesn't present symptoms. However, with aging, overwork, or other diseases factors, it may deteriorate and present symptoms, such as palpitations, chest pain and even sudden cardiac death (SCD). Though rarely happen, the genetic arrhythmias, such as catecholaminergic polymorphic ventricular tachycardia (CPVT), often present severe symptoms and even cause SCD without proper treatment in early age. Arrhythmia is also a common complication appearing in many cardiac diseases (Janse and Rosen, 2006)(Words, 2000), such as Valvular Heart Disease and heart failure (HF).(Landstrom, Dobrev and Wehrens, 2017)(Austin *et al.*, 2019)

Depending on the original site, arrhythmias were divided into atrial arrhythmia, junctional arrhythmia and ventricular arrhythmia. Due to the different functions of these three parts, arrhythmias generated in different sites usually present different symptoms and severity. Left ventricle as the part directly drives fresh blood to the whole body and maintains systemic blood pressure at approximately 120 max and 80 min millimeters of mercury and right ventricle as the part directly drive blood to lungs to be refresh, both play vital role for life. Once ventricles work failed, even very short, it may damage the sensitive cells such as neurons. So ventricular arrhythmias are apt to result in severe consequences (Keating and Sanguinetti, 2001). Fig 9 is showing the generation of ventricular arrhythmia and corresponding schematic ECG diagram presenting disorder heart rhythm.

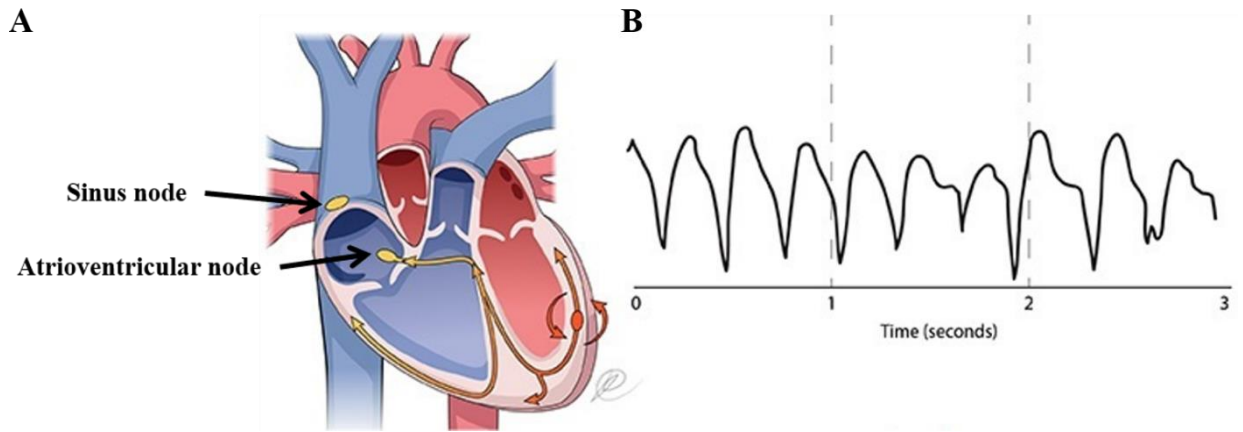


**Figure 9. Formation of ventricular tachycardia.** A. Schematic diagram of abnormal impulse generation and disorder conduction. B. Schematic diagram of ECG presenting disorder heart rhythm. (Adapted from U.S. National Library of Medicine)

## IV.2 Ventricular arrhythmias

Ventricular arrhythmias are important causes of morbidity and mortality in almost all forms of heart disease, which come in a variety of forms from single premature ventricular complexes to sustained ventricular tachycardia and fibrillation (Cronin *et al.*, 2019). In the past few decades, with the developing of a variety of techniques, including molecular and cellular electrophysiology and optical mapping of electrical excitation, we have come to better understand the underlying mechanisms of cardiac arrhythmias (Anumonwo and Pandit, 2015). These abnormalities in cardiac rhythm may occur as a result of inherited genetic disorders (Cerrone and Priori, 2011), acquired cardiac disease conditions such as HF (Tomaselli and Zipes, 2004), or may be due to side effects of drugs (Behr and Roden, 2013) or strenuous physical exercise (Behr and Roden, 2013). In this section, we will summarize the characteristics of different types of ventricular arrhythmias as well as the underlying mechanisms.

### IV.2.1 The mechanism of ventricular arrhythmias

The occurrence of a ventricular tachyarrhythmia is linked to the interactions between three arrhythmogenic factors that Coumel and Thomas (Coumel and Thomas, 1997) schematized in the form of a triangle, each vertex of which represents one of the factors as shown in Figure 10: the substrate, the trigger factors and the modulation factors that the most common is the autonomic nervous system (ANS). The substrate are the anatomical and electrophysiological supports allowing the maintenance of the arrhythmia, such as a scar of infarction, an ischemic zone (sequelae of necrosis) or even a structural or functional cardiomyopathy (Rubart and Zipes,

2005). The triggers such as trigger activities, automaticity and reentry could initiate arrhythmias in above substrate, which we will explain in details later. The ANS is likely to act on the properties of the first two factors through adrenergic stimulation, which makes it possible to increase the sensitivity of the arrhythmogenic substrate and to increase the conductivity of the tissues, thus facilitating the trigger of the arrhythmia.

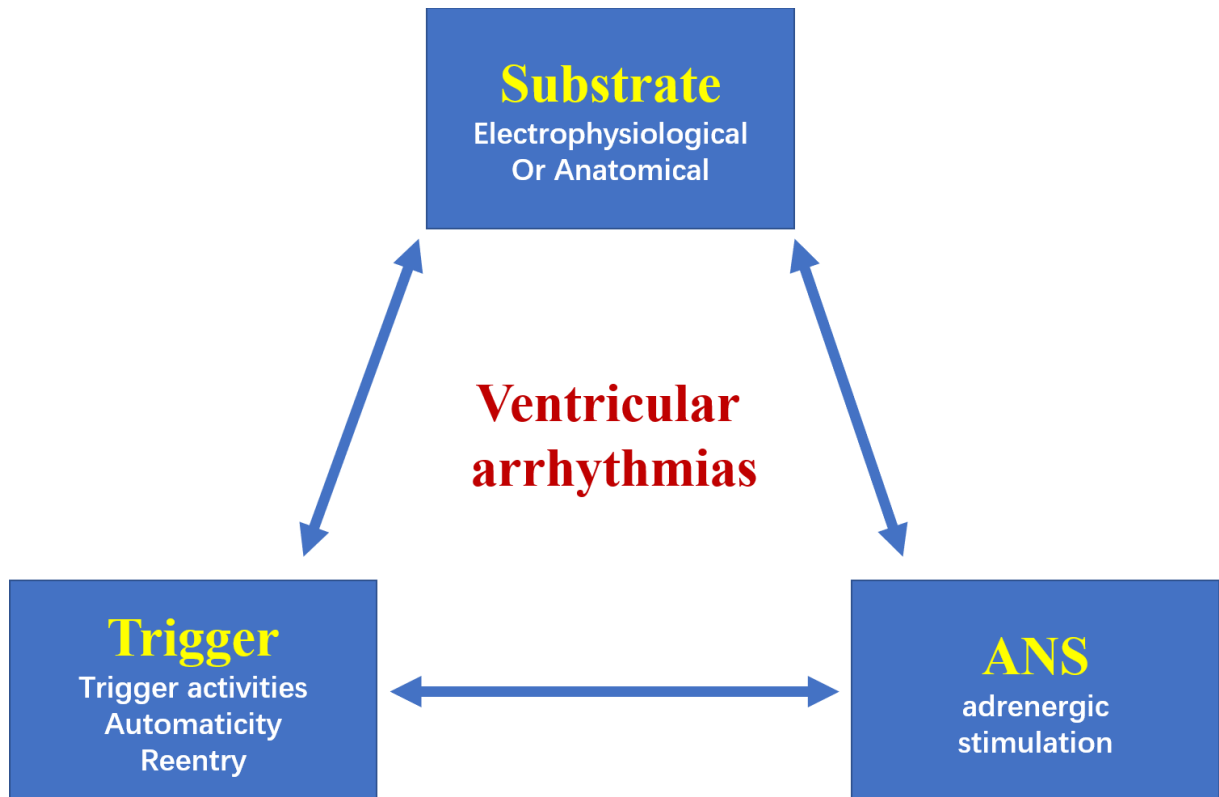


**Figure 10. Coulmel triangle of ventricular arrhythmias.** ANS: autonomic nervous system.

Several schemes have been used to classify the triggers of cardiac arrhythmias. Here we adopt the schemes by dividing them into those occurring at the cellular and tissue levels (Anumonwo and Pandit, 2015)(Tse, 2016). At the cellular level, arrhythmogenesis can occur as a result of focal activities, which includes enhanced automaticity and trigger activity (early or delayed depolarizations, i.e., EADs and DADs) as shown in Fig 10. At the tissue level, reentry is the main cause in the initiation of arrhythmogenesis, which includes anatomical reentry (reentry involving an anatomical obstacle or block) and functional reentry (Reentry not involving an obstacle) as shown in Figure 11.

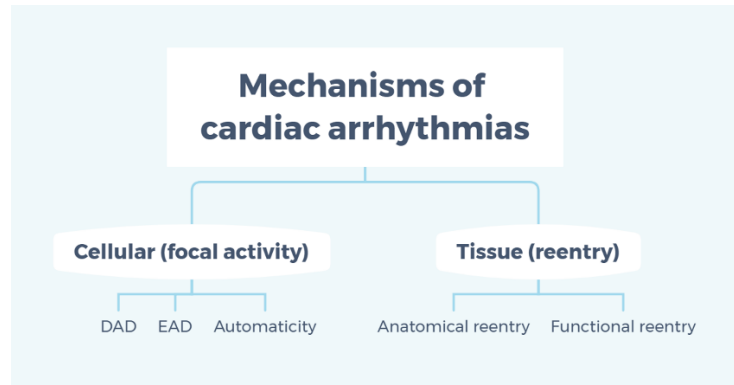


**Figure 11. Triggers of arrhythmias.** The various cellular and tissue triggers of arrhythmias are depicted. (modified from (Anumonwo and Pandit, 2015))

### A. Delayed Afterdepolarizations (DADs)

In order to explain Delayed Afterdepolarizations (DADs), it is necessary to understand Diastolic sarcoplasmic reticulum (SR)  $\text{Ca}^{2+}$  leak. In physiology, the ideal condition for SR release during diastole is completely shut off, but in fact, there is still a small amount of  $\text{Ca}^{2+}$  leak as calcium sparks which was firstly identified by confocal microscopy in 1993 (Cheng, Lederer and Cannell, 1993). The  $\text{Ca}^{2+}$  spark frequency is independent of local  $\text{Ca}^{2+}$  influx (Sato, Blatter and Bers, 1997), but directly affected by open probability ( $P_o$ ) of individual cardiac RyRs events and free or total SR  $\text{Ca}^{2+}$  concentration. At resting intracellular  $\text{Ca}^{2+}$  concentration, the  $P_o$  of a given normal RyR may be  $10^{-5}$ - $10^{-4}$ , but when the SR  $\text{Ca}^{2+}$  content increase or RyRs is altered, it may grow. The spontaneous increased local  $\text{Ca}^{2+}$  may trigger neighboring  $\text{Ca}^{2+}$  release units by  $\text{Ca}^{2+}$ -induced  $\text{Ca}^{2+}$  release mechanism, thereby forming cell-wide  $\text{Ca}^{2+}$  waves. A small amount of diastolic SR  $\text{Ca}^{2+}$  leak as occasional  $\text{Ca}^{2+}$  sparks in physiology may be favorable for preventing the SR content from getting over load, but increased  $\text{Ca}^{2+}$  leak may result in pathological consequences. Firstly,  $\text{Ca}^{2+}$  constantly released from SR by sparks or waves, or even unnoticeable, as it is extruded out of cells, may gradually lead to SR content decrease, which may reduce heart systolic function (as in heart failure). Moreover, the leaked  $\text{Ca}^{2+}$  extruded by  $I_{\text{NCX}}$  generates a depolarizing current that may underlie DAD. Lastly, the clearance of leaked  $\text{Ca}^{2+}$  from cytosol is energetically costly, because it activates  $\text{Ca}^{2+}$  pumps as the SERCA and PMCA (The plasma membrane  $\text{Ca}^{2+}$  ATPase). This energy expenditure may increase the burden for heart especially when heart is already energetically compromised such as in HF (Bers, 2014). Although detecting  $\text{Ca}^{2+}$  spontaneous release as  $\text{Ca}^{2+}$  sparks or waves by confocal microscopy (Wang *et al.*, 2017)(Gómez, 2012) reflected the SR  $\text{Ca}^{2+}$  leak, there is also  $\text{Ca}^{2+}$  leak through RyR that is undetected and may have

functional consequences. Currently the popular method to detect the SR  $\text{Ca}^{2+}$  leak is by measurement of SR content change with and without RyR2 channel blockage by tetracaine (Shannon, Ginsburg and Bers, 2002)(Pereira *et al.*, 2017).

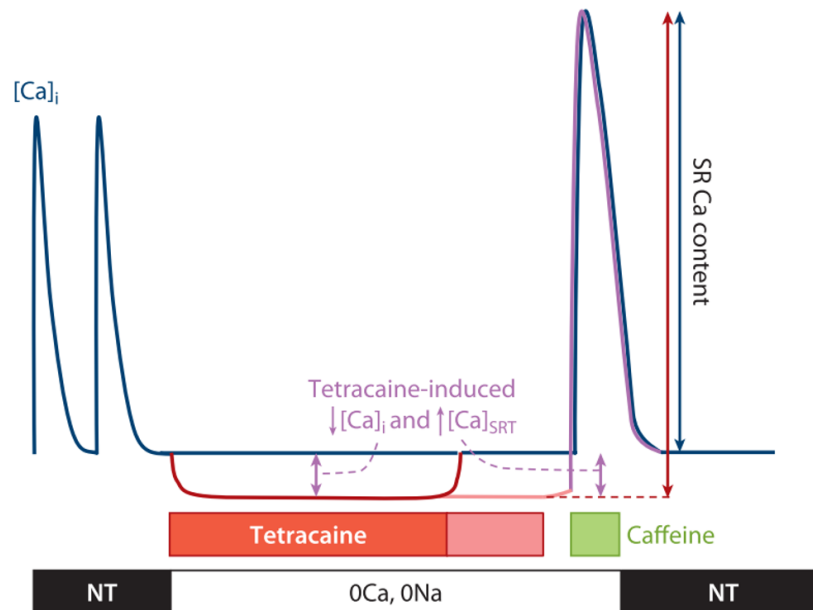


**Figure 12. SR  $\text{Ca}^{2+}$  leak measurements.** Acute block of ryanodine receptor–mediated SR Ca leak by 1 mM tetracaine causes  $[\text{Ca}]_i$  to decline and SR Ca content to rise. Bars indicate series of solution switches, with 10 mM caffeine causing SR Ca release. NT denotes normal Tyrode’s solution. (Adapted from (Bers, 2014))

DADs are spontaneous membrane depolarization that occur during diastole (Qu and Weiss, 2015)(Landstrom, Dobrev and Wehrens, 2017). They are widely considered as being triggered by spontaneous SR  $\text{Ca}^{2+}$  release (Bers, 2008). The increased cytoplasmic  $\text{Ca}^{2+}$  concentration activated NCX to extrude  $\text{Ca}^{2+}$ . Because the NCX exchanges 3  $\text{Na}^+$  for each  $\text{Ca}^{2+}$ , there is a net inward current for each  $\text{Ca}^{2+}$  extruded, thus inducing membrane depolarization. (Bers, Pogwizd and Schlotthauer, 2002)(S M Pogwizd *et al.*, 2001). Since the DADs are generated during diastole, the amplitude of DADs is the result between two opposed currents:  $I_{\text{NCX}}$  and the background current inward-rectifier  $\text{K}^+$ -current  $I_{\text{K1}}$  (Steven M Pogwizd *et al.*, 2001)(Sung *et al.*, 2006), which means a same  $I_{\text{NCX}}$  may result in different amplitude of DAD in different  $I_{\text{K1}}$  condition. An under threshold or limited DAD cannot cause a heart arrhythmia because neighboring cells would provide a current sink which dissipated the  $I_{\text{NCX}}$ , but when a DAD reached the threshold for triggering AP, and occurred in a cluster of neighboring cells, it will become an initiator of arrhythmias as shown in Figure 13. It has been estimated that a total SR

Ca<sup>2+</sup> release of 50 to 60 μmol/L cytosol, or 50% to 70% of the SR Ca<sup>2+</sup> load, is required to produce DADs with an amplitude sufficient to trigger an action potential (Priori and Chen, 2011).

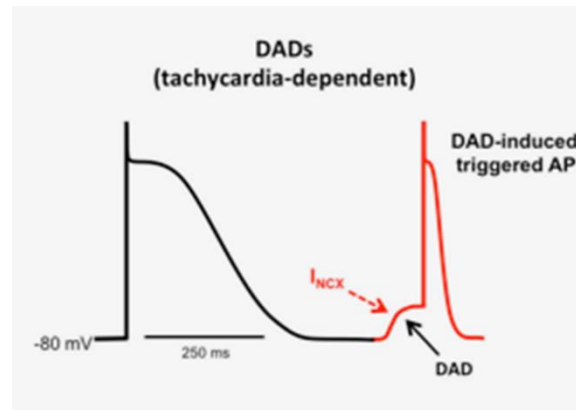


**Figure 13. Delayed Afterdepolarizations (DADs) induced triggered action potential (AP).** (Adapted from (Landstrom et al. 2017))

### B. Early Afterdepolarizations (EADs)

Early Afterdepolarizations (EADs), which was originally called low membrane potential oscillations in Purkinje cells, were identified more than a half century ago (Hauswirth, Noble and Tsien, 1969), but the term EAD was coined later by Cranfield in 1977 (Cranfield, 1977). Unlike DADs, they occur during the AP plateau or phase 3 repolarization as shown in Figure 14. (Weiss *et al.*, 2010)(Qu *et al.*, 2013)(Qu and Weiss, 2015), that is why they were termed similarly as DADs but with “early”. Given that they happen during repolarization, a reduction in outward current or an increase in inward current or both were demanded to reduce the repolarization reserve (Damiano and Rosen, 1984)(January and Riddle, 1989)(January and Moscucci, 1992), which will prolong the AP duration. The L-type Ca<sup>2+</sup> current (I<sub>Ca,L</sub>) and I<sub>NCX</sub> are widely accepted triggers for EADs to date. The two currents usually work together to facilitate the EADs formation, with either one playing the primary role or secondary role (Weiss *et al.*, 2010). For example, when I<sub>Ca,L</sub> exhibits increased window current, the additional Ca<sup>2+</sup> influx will depolarize the cell and also further trigger Ca<sup>2+</sup> release from SR, thus synergistically increasing I<sub>NCX</sub>, and then the two increased inward currents promote EADs formation (Weiss *et al.*, 2010). In other way, if spontaneous Ca<sup>2+</sup> release from SR occurs before repolarization is complete as mentioned above in “SR calcium leak”, the increased intracellular Ca<sup>2+</sup> triggers I<sub>NCX</sub> thereby delaying repolarization, which generated more time for I<sub>Ca,L</sub> to recover from inactivation, secondarily facilitating EADs formation. Both mechanisms have been

demonstrated (Luo and Rudy, 1994)(Choi, Burton and Salama, 2002). However, it is important to note that repolarization reserve reduction is sufficient to prolong APD, but not sufficient to produce EADs. Qu Z.L. et al introduced an integrative view of underlying mechanisms of EADs based on nonlinear dynamics theory. They emphasized that EADs are not simply depolarizations, but are oscillations in membrane voltage (Qu *et al.*, 2013). In addition to the two currents mentioned above, sodium channel ( $I_{Na}$ ) (Song *et al.*, 2006)(Morita *et al.*, 2011) and delayed rectified potassium channels ( $I_{Ks}$  and  $I_{Kr}$ ) (Zeng *et al.*, 1995) may also be underlying factors for EADs generation. Besides triggered activity, the consequence of EADs are dispersion of refractoriness in further triggering reentry.

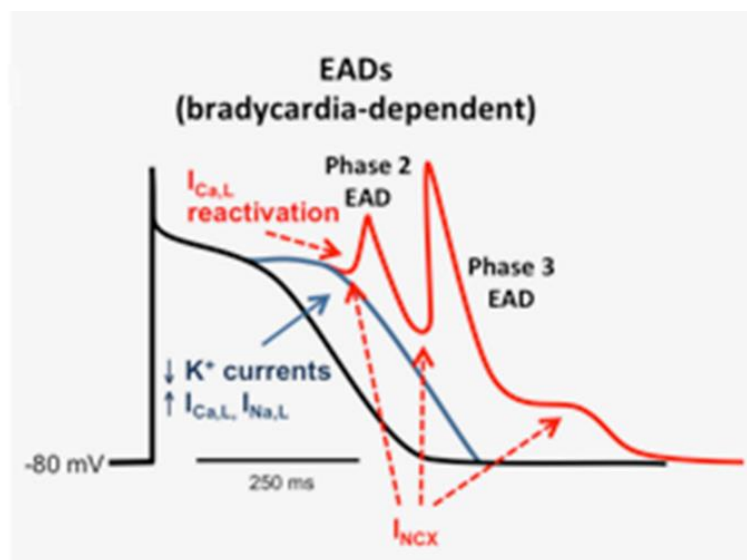


**Figure 14. Triggers of bradycardia-dependent early Afterdepolarizations (EADs).**  $I_{Ca,L}$  indicates L-type  $Ca^{2+}$  current;  $I_{K,Ca}$ ,  $Ca^{2+}$  dependent  $K^+$  current;  $I_{Na,L}$ , late  $Na^+$  current; and  $I_{NCX}$ ,  $Na^+/Ca^{2+}$  exchanger current. (Adapted from (Landstrom et al. 2017))

### C. Abnormal automaticity

There are three kind of cells with automaticity in heart including sinoatrial node myocytes, AV node myocytes and purkinje fibers. The other cardiac myocytes including atrial myocytes and ventricular myocytes are non-automatic. Sinoatrial node myocytes possess the highest spontaneous rates, and are the primary pacemaker determining the whole heart rhythm as mentioned above. However, in abnormal conditions, the non-automatic myocytes could trigger spontaneous impulses or the automaticity of AV node myocytes and purkinje fibers could be increased to suppress the sinoatrial node rhythm, which could lead to arrhythmias. Multiple factors, such as DADs and EADs as mentioned above can induce abnormal automaticity. Apart

from that, many other factors are also underlying factor of abnormal automaticity. Medication, such as aconitine, can cause automaticity by defecting voltage-gated  $\text{Na}^+$  channel inactivation and inducing SR  $\text{Ca}^{2+}$  overload (Sun *et al.*, 2014)(Wang and Wang, 2003)(SCHERF, 1947). Besides, after suppressing 81%  $\text{I}_{\text{K1}}$  in a mathematical model of cardiac ventricular myocytes (Luo-Rudy (LRd)), J. Silva et al observed spontaneous action potentials in guinea pig ventricular myocytes (Silva and Rudy, 2003). Increased cell-cell coupling between cardiac myocytes and cardiac fibroblast also has been found to contribute to ectopic activity (Miragoli and Rohr, 2007)(Kofron *et al.*, 2019), which explained the increased ventricular ectopy in fibrotic hearts. Furthermore, abnormal automaticity could also be triggered in heart failure, which is similar as EADs in the formation mechanism, mediated by  $\text{I}_{\text{Ca,L}}$  (Nuss *et al.*, 1999).

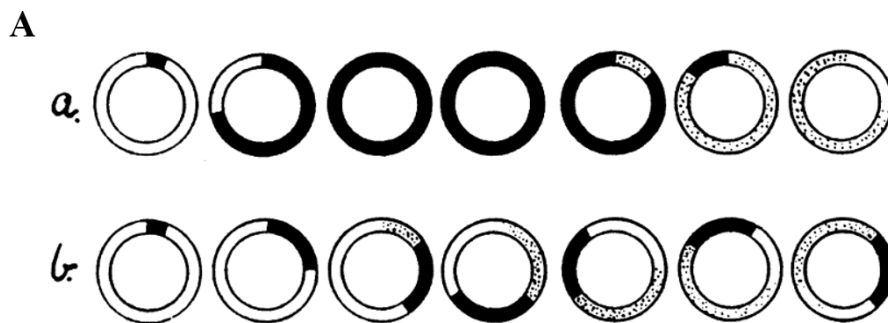
#### **D. Electrical alternans**

Action potential duration (APD) Alternans (AP present long-short-long-short pattern) has been considered to be a diagnostic precursor for more severe arrhythmias (Qu and Weiss, 2015) (Estes *et al.*, 1997) (Rosenbaum DS 1994)(Verrier *et al.*, 2011). Depending on the position of alternans part on the ECG, they could be divided to QRS-complexes alternans and T-Wave alternans (TWA). Since T-wave corresponds to the repolarization of ventricles, TWA is a promising predictor of ventricular arrhythmias. There are several factors contributing to the formation of alternans. Pacing-induced APD alternans was largely considered as depending on the slope of the APD restitution (which disturb the equilibrium state when exceeds 1), but recent investigations demonstrated that no difference in restitution properties between alternans regions and non-alternans regions, which weakens the relationship between the slope of the APD restitution and pacing-induced APD alternans (Orini *et al.*, 2019)(Narayan *et al.*, 2007). They also found that APD restitution slope  $>1$  is prevalent in the human heart. On the other hand, a research in rabbit heart suggested that APD dispersion and conduction velocity restitution are two more important factors (Banville and Gray, 2002). APD alternans can also be secondary to  $\text{Ca}^{2+}$  transient alternans. In principle,  $\text{Ca}^{2+}$  release alternans could be induced by dispersed refractoriness of L-type  $\text{Ca}^{2+}$  channel or RyR channel and alternans of SR content. However, E. Picht et al suggested that formation of the  $\text{Ca}^{2+}$  transient alternans doesn't rely on the SR content alternans in rabbit ventricular myocytes although they happened simultaneously, and another factor, RyR refractoriness, is more important in triggering the pacing-induced APD alternans (Picht *et al.*, 2006). A more recent research performed in langendorff-perfused rabbit hearts showed the similar view which suggested that SR  $\text{Ca}^{2+}$  release alternans is initiated by

RyR refractoriness, but it can be amplified by diastolic SR content alternans, leading to APD alternans (Wang *et al.*, 2014).

### E. Reentry

According to the mechanism of formation, reentry was divided into two categories, anatomical reentry (reentry involving an anatomical obstacle) and functional reentry (Reentry not involving an obstacle). Anatomical reentry is simpler and its mechanism has been explained by G.R. Mines a century ago of which the diagram shown in Figure 15A is still being used today (Mines, 1914)(C. Antzelevitch, 2001)(Silva and Frép, 1997). By the diagram, Mines demonstrated that reentry happened in abnormal tissue with delayed conduction allowing cells to recover from refractory period permitting reentry to occur. Later, investigators found that reentry could also occur without involving an anatomical obstacle in the model of leading circle, spiral waves and rotors (Allessie, Bonke and Schopman, 1973)(Allessie, Bonke and Schopman, 1977)(Salomonsz, Baxter and Jalife, 1992)(Salomonsz, Baxter and Jalife, 1992). Base on refractoriness dispersion theory, A.P Landstorm et all suggested that EADs, DADs and  $Ca^{2+}$  alternans can generate the condition to form reentry as shown in Figure 15B (Landstrom et al 2017).



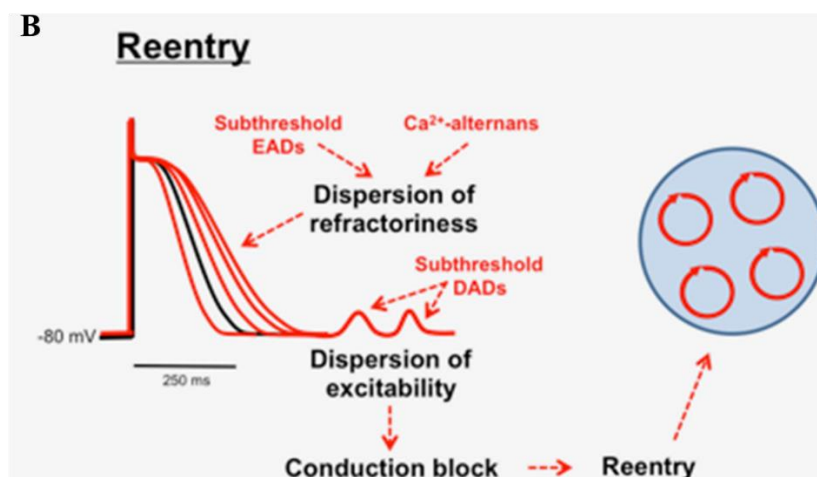


**Figure 15. mechanism of reentry generation.** A. Diagrammatic representation by Mines to demonstrate circulating rhythm in closed circuits in myocardial tissue. a, Normal tissue with rapid conduction with no reentry. b, Abnormal tissue with delayed conduction permitting reentry to occur. Dotted areas = relative refractory phase in the cycle. (Adapted from (Silva and Frpc, 1997)). B. Reentry generated by dispersion of refractoriness and excitability. (Adapted from (Landstrom et al. 2017))

## IV.2.2 Acquired ventricular arrhythmias

Besides the life-threatening ventricular arrhythmias of genetic origin, the acquired arrhythmias are also worth to mention especially for common population, given the rare incidence rate of genetic arrhythmias. In this section, we will talk about the three most common acquired arrhythmias: Medication-induced arrhythmias, Exercise-induced Arrhythmias and Arrhythmias consequences of other diseases.

### A. Medication-induced arrhythmias

Drug-induced arrhythmia or pro-arrhythmia, is the induction or exacerbation of cardiac arrhythmia associated with administration of a drug. The first drug-induced syncope (Quinidine Syncope) has already been described in 1920s, but the mechanism remained unclear until Selzer et al identified a drug-related, pause-dependent form of polymorphic ventricular tachycardia in 1960s (Selzer and Wray, 1964). The most risky drugs for triggering arrhythmias are antiarrhythmic drugs especially the class III (including sotalol, dofetilide, ibutilide, and azimilide) (Arrhythmia, 2010)(Behr and Roden, 2013)(Ramalho and Freitas, 2018). Although noncardiac agents, including but not limited to, antibiotics, antipsychotics antidepressants, and antihistamines, may carry a much smaller risk of marked cardiac toxicity, they may cause undesirable side effects in heart given their much broader clinical use and far less monitoring of cardiac effects (Arrhythmia, 2010). Moreover, the drug-drug interaction is another cannot-

be-ignored factor for drug-induced arrhythmias (Curtis *et al.*, 2003)(Liu *et al.*, 2007). The main mechanism for those drugs to trigger arrhythmias is through inducing QTc prolongation, which may be fulfilled by two ways: firstly and mostly is the inhibition of  $I_{kr}$  (encoded by gene KCNH2/ (HERG) which are analogous to the genetic LQT2 form; secondly is blockade of both  $I_{Kr}$  and  $I_{Ks}$  (Kazmierczak, Peregud-Pogorzelska and Rzeuski, 2007) and inhibition of HERG trafficking to the cell membrane (Cordes *et al.*, 2005). Additionally, drug effects on blockade of sodium channels are an important cause of drug-induced proarrhythmia, which cause prolongation of the QRS interval instead of QTc interval. For example, class IC antiarrhythmic drugs flecainide and encainide, presenting 3.6-fold increase in the risk of fatal arrhythmias and nonfatal cardiac arrests compared with placebo, are both potent sodium channel blockers with little effect on repolarization (Echt, 1991).

## **B. Exercise-induced Arrhythmias**

While regular physical exercise has many health benefits, strenuous physical exercise may have a negative impact on cardiac function (Herm *et al.*, 2017). Although frequent and complex ventricular tachyarrhythmias are common in trained athletes, they are usually unassociated with underlying cardiovascular abnormalities and seem do not convey adverse clinical significance, thus, they got a new description of “athlete’s heart syndrome” (Biffi *et al.*, 2002). However, report from National Collegiate Athletic Association database presented that the SCD rate range from 1 per 53 703 athlete-per year (Harmon *et al.*, 2015), while the number in general population is 1.0 to 1.9/100 000 in adolescents and young adults (Marijon *et al.*, 2011)(Meyer *et al.*, 2012). Furthermore, Gerche et al demonstrated that exercise-induced ventricular arrhythmias could result in right ventricular dysfunction in endurance athletes (La Gerche *et al.*, 2015). Sinus bradycardia and atrioventricular conduction blocks are also very common in athletes (Guasch and Mont, 2017). In adverse, Yankelson et al suggested that heat stroke is more prevalent than arrhythmic death during endurance races by determining the percentage of life-threatening cardiac events manifested in the athletes of long-distance popular races (Yankelson *et al.*, 2014). However, their opinion view was rejected by another group (Scherr, Johannes, 2015) due to two limitations in their report: firstly, the start-time temperature exceeded the standard threshold in Yankelson’s study which tend to induce heat stroke; secondly, the investigated races were too short (10 km), but the serious cardiac events often occur during the last quarter in marathons race (Scherr, Johannes, 2015). Taken together,

intense exercise does seem to trigger ventricular arrhythmias leading to cardiac dysfunction, but their responsiveness to SCD still need to be evaluated.

### **C. Arrhythmias complicated with other diseases**

Many, if not most of, cardiac diseases could result in arrhythmias. During HF, a reduced ejection fraction is the result of changes in ultrastructure and  $\text{Ca}^{2+}$  signaling in cardiomyocyte leading to loss of coordinated excitation-contraction coupling (ECC) and impaired contractility, which in constitutes a complex pro-arrhythmic substrate (Dobrev, Fender and Wehrens, 2018). In addition, the APD prolongation characteristic of HF predisposes ventricular myocytes to EAD (Nuss *et al.*, 1999), which could induce life-threatening arrhythmias as mentioned above. The Valvular Heart Diseases (VHD) are also associated with arrhythmias (Al-Khatib *et al.*, 2018). Urena et al found that a fifth of transcatheter aortic valve replacement (TAVR) candidates presented diagnosed arrhythmias, highlighting the importance of an early diagnosis of arrhythmic events in patients with aortic stenosis (Urena *et al.*, 2015). There are many noncardiac diseases that associate with arrhythmias, such as diabetes. Hypoglycemia in patients with type 2 diabetes could increase bradycardia and atrial and ventricular ectopic counts as well as QT intervals prolongation and abnormal T-wave morphology (Chow *et al.*, 2014). A research in a rat model suggested that cardiac arrhythmias induced by severe hypoglycemia precede sudden death (Chow *et al.*, 2014). In further research, Reno et al found that severe hypoglycemia-induced fatal cardiac arrhythmias could be augmented by diabetes and attenuated by recurrent hypoglycemia (Reno *et al.*, 2017). Patients with chronic kidney disease (CKD) were also demonstrated to possess increased risk of SCD compared with the general population (Bonato and Canziani, 2017)(Wanner, Herzog and Turakhia, 2018).

## **IV.2.3 Genetic ventricular arrhythmias**

### **A. Arrhythmogenic cardiomyopathy (ACM)**

ACM, also known as arrhythmogenic right ventricular cardiomyopathy (ARVC), is an inherited cardiomyopathy that predominantly affects the right ventricle but can affect the left ventricle, causing areas of myocardial replacement with fibrosis and adipose tissue that frequently causes VA and SCD (Al-Khatib *et al.*, 2018). The prevalence of ACM has been estimated to be between 1:1,000 and 1:5,000, depending on the population (Peters, Trummel and Meyners, 2004)(Corrado *et al.*, 2006) (Thiene, Corrado and Basso, 2007). Clinical symptoms typically manifest in the third to fourth decades of life, with arrhythmic

manifestations generally preceding structural features. Thus, ACM affects adolescents infrequently and children rarely (Bauce *et al.*, 2011)(Te Riele *et al.*, 2015). Cardiac MRI provides high-quality assessment of ventricular function, size, regional wall motion abnormalities, and extent of scar and fibrosis (late gadolinium enhancement) that are seen in 30% to 95% of patients with the clinical diagnosis of ACM (Liu *et al.*, 2014)(Marcus *et al.*, 2010). ACM is often due to a mutation involving a desmosomal protein, and it usually has autosomal dominant inheritance with variable penetrance. The most common genes are focused on desmosome, among which, Plakophilin 2 (PKP2) is the most commonly affected gene in adult cohorts, whereas some studies also suggested that the pediatric age group more frequently has mutations in Desmoplakin (DSP) (Bauce *et al.*, 2011)(Te Riele *et al.*, 2015). Besides, more and more genes on other positions such as adheres junction and cytoskeletal structure are identified to be associated with ACM. Interestingly, mutations/variants on RyR<sub>2</sub> has been reported to be associated with ACM (Te Riele *et al.*, 2015) (Roux-Buisson *et al.*, 2014). Thus, RYR2 is associated with two different diseases in the heart, ACM and CPVT, the former presenting structural abnormalities and the latter not. The exact mechanism of the discrepancy remains unclear (Roberts and Brugada, 2003) and whether RYR2 mutations cause ACM is controversial, because identification of RYR2 mutations in ACM is likely to reflect clinical diagnostic overlap between ACM and CPVT (Lazzarini *et al.*, 2015)(Moncayo-Arlandi and Brugada, 2017).

## **B. Congenital Long QT Syndrome (LQTS)**

Congenital LQTS is a genetic cardiac disease characterized by QT interval prolongation in association with stress-induced syncope and SCD in absence of an underlying syndrome or structural heart disease (Bezzina, Lahrouchi and Priori, 2015)(Schwartz *et al.*, 1993). It is a relatively common arrhythmia syndrome affecting around 1 in 2500 patients (Eisner *et al.*, 2017) (Wehrens *et al.*, 2002). The SCD is usually caused by the typical ventricular arrhythmia: torsade de pointes (Roberts and Brugada, 2003). The first family with LQTS was described by Jervell and Lange-Nielsen in 1957 (Kass and Moss, 2003). To date, 17 genes have been demonstrated to be associated with LQTS, but approximately 75% of LQTS related mutations are focused on 3 genes: KCNQ1 (encoded potassium channel - Kv7.1, LQTS-1), KCNH2 (encoded potassium channel - Kv11.1, LQTS-2), and SCN5A (encoded I<sub>Na</sub> sodium channel - NaV1.5, LQTS-3) (Tester *et al.*, 2005)(Landstrom, Dobrev and Wehrens, 2017), whose encoding channels play very important role during AP repolarization. LQTS 1, which is caused by loss-of-function

mutation in the slowly activating delayed rectifier current ( $I_{Ks}$ ) encoding by *KCNQ1*, is the most prevalent form accounting around 35% of cases. LQTS 2 is caused by loss-of-function mutation in the *KCNH2* (also known as *HERG*) encoding rapidly activating delayed rectifier current ( $I_{Kr}$ ), and accounts for around 30% of LQTS cases.  $I_{Na}$  is a depolarizing current, whose gain-of-function mutations in *SCN5A* result in an increase in the late  $I_{Na}$  underlying LQTS 3 which contributes to around 10% of LQTS cases. Although the majority of the accepted LQTS related genes encode channels that govern the flux of  $K^+$  and  $Na^+$ , more and more mutations in genes encoding  $Ca^{2+}$  flux related proteins were identified to be associated with LQTS. For example, LQTS 8 is linked to mutations on *CACNA1C* gene which encode the pore forming subunit ( $Cav1.2 \alpha_{1C}$ ) of L-type  $Ca^{2+}$  channel, responsible for  $I_{Ca,L}$  and essential for EC coupling. LQTS 14-16 are due to the mutations in *CALM* genes, a gene group encoding calmodulin proteins which can bind to the carboxy terminus of the  $Ca^{2+}$  channel to trigger  $Ca^{2+}$ -dependent inactivation (Zühlke *et al.*, 1999)(Bers, 2002). They can also bind to the RyR2 channel and other mutations in *CALM* are linked to CPVT which will be explained latter. LQTS 17 is a recently defined type due to the mutations on gene *TRDN* (Helene M. Altmann *et al.*, 2015). *TRDN* gene is also linked to CPVT-5. In addition, based on the QT Interval-International GWAS (genome-wide association studies) Consortium (QT-IGC) meta-analysis on large population, 35 common variant loci associated with QT interval have been identified, emphasizing the importance of calcium regulation in myocardial repolarization (Arking *et al.*, 2014).

### **C. Brugada Syndrome**

Brugada syndrome (Brs) is a rare inherited cardiac arrhythmogenic disease associated with sudden cardiac death. The Brs phenotype is especially prevalent in males (8:1 ratio of males to females) of Asian origin (Benito *et al.*, 2008)(Charles Antzelevitch, 2001). Currently, it is believed to be responsible for 4-12% of SCD cases and around 20% of SCD in patients with structurally normal hearts (Juang and Huang, 2004)(Sendfeld *et al.*, 2019). It was identified by Brugada brothers who have recorded ECG presenting right bundle branch block and ST segment elevation from 8 clinically similar patients in 1992 (Brugada and Brugada, 1992). Thereafter, the Japanese researchers have coined the term “Brugada syndrome” (Miyazaki *et al.*, 1996), but the controversy regarding the existence of this real new syndrome was initiated after that, until the first mutations in the sodium channel gene *SCN5A* were identified in 1998 (Chen *et al.*, 1998). So far, more than 20 genes have been associated with this disease (Juang

and Horie, 2016), but evidence-based gene validation for Brs indicated that 20 of 21 genes lack sufficient evidence to support causality for Brs, remaining only 1 gene (SCN5A) as demonstrating definitive evidence as a cause for Brs (Hosseini *et al.*, 2018). As mentioned above, mutations in SCN5A gene also cause LQTS, but the functional defect in the Na<sup>+</sup> channel that causes LQTS is the lack of complete inactivation, allowing a continuous leak of Na<sup>+</sup> to the interior of the cell, whereas in Brs there is a faster inactivation of the Na<sup>+</sup> channel, leaving the potassium current I<sub>to</sub> unopposed in phase 1 of the action potential (Charles Antzelevitch, 2001)(Roberts and Brugada, 2003)(Shah, Akar and Tomaselli, 2005). However, the molecular mechanism of the most important characteristic of Brs —ST-segment elevation on the right precordial leads of the ECG—remains unclear to date (Brugada *et al.*, 2014) (Moncayo-Arlandi and Brugada, 2017).

#### **D. Catecholaminergic Polymorphic Ventricular Tachycardia (CPVT)**

CPVT is a genetic disease that manifests by syncope or sudden death in children and young adults under stress conditions without obvious cardiac structural abnormality. Being a rare disease, CPVT is a relative common disease among all genetic cardiac diseases affecting around 1 person among 5000 to 10000 people (Paludan-Müller *et al.*, 2017). In addition, due to its high penetrance and life-threatening nature, CPVT leads to 30% SCD before the age of 40 when untreated. Thus, CPVT became a very important cardiac genetic disease model among academia. So far, there are 5 identified genes contributing to different forms of CPVT, whose encoding proteins are involved in RyR2 complexes (Table 1), playing direct or indirect effect on the Ca<sup>2+</sup> transfer between SR lumen and cytosol. We will discuss the characteristic of each form of CPVT in the following.

In 1978 Coumel *et al.* reported several children without cardiac disease but with reproducible exercise-induced ventricular arrhythmias (Coumel and Fidelle, 1978). Thereafter, the same group did an investigation of 7-years follow-up of 21 patients to fully describe this clinical syndrome (Leenhardt *et al.*, 1995). The genetic study of CPVT was started by Swan *et al.* who demonstrated a linkage of this disease to chromosome 1q42–q43 (Leenhardt *et al.*, 1995). Then, Priori *et al.* (Priori *et al.*, 2001) and Laitinen *et al.* (Päivi J. Laitinen *et al.*, 2001) respectively reported 2 different mutations in the cardiac ryanodine receptor gene (RyR<sub>2</sub>), validating RyR<sub>2</sub> as the first gene related to CPVT. Until now, more than 150 variants associated with CPVT have been identified in RyR<sub>2</sub> gene, presenting autosomal dominant inheritance and accounting around 60% of mutations found in CPVT cases (Landstrom, Dobrev and Wehrens,

2017)(Bezzina, Lahrouchi and Priori, 2015). The second identified gene associated with CPVT is CASQ2 (Lahat, Pras and Eldar, 2001) which encodes calsequestrin-2, a protein that binds free calcium inside of SR. Calsequestrin has been demonstrated to modulate the function of RyR2 by acting as a luminal calcium sensor (Györke *et al.*, 2004). Mutations in CASQ2 cause a less common but more severe autosomal recessive form named as CPVT2 (Lahat, Pras and Eldar, 2001). Subsequently, several genes associated with CPVT have been identified, including Trans-2, 3-enoyl-CoA reductase-like (TECRL), Calmodulin1 (CALM1) and Triadin (TRDN), (Nyegaard *et al.*, 2012)(Roux-buisson *et al.*, 2012)(Bhuiyan *et al.*, 2007)(Devalla *et al.* 2016), mutations in which respectively causing CPVT3, CPVT4 and CPVT5 as shown in table 1, which will be explained in detail latter.

The three remarkable features of CPVT are: no structural abnormality; often presents polymorphic ventricular tachycardia in response to exercise or on exposure to catecholamines as shown in Figure 16, but appears to be asymptomatic in rest state; often causes SCD in children and young adults without proper treatments. SCD or syncope appears in one third of CPVT patients in first degree family members (Priori and Napolitano, 2005). Despite its life threatening nature, CPVT remains difficultly noticed due to the normal baseline electrocardiograms on top of absence of structural abnormality and incomplete penetrance (Postma *et al.*, 2005). Thus, the diagnosis of CPVT is mainly based on the occurrence of arrhythmia during exercise stress-testing or Holter recording (Refaat, Hotait and Tseng, 2014)(Bezzina, Lahrouchi and Priori, 2015), verifying by genetic testing. Furthermore, Hayashi *et al* suggested that the earlier a CPVT is diagnosed the worse the prognosis may be, which is easily to be explained because, on the one side, children have more opportunities to engage in strenuous physical activities, and on the other hand, patients with more severe forms of CPVT, are barely protected by drugs. Moreover,  $\beta$ -blocker dosage based on weight are frequently underdosed due to the age-dependent hepatic clearance (Hayashi *et al.*, 2009).

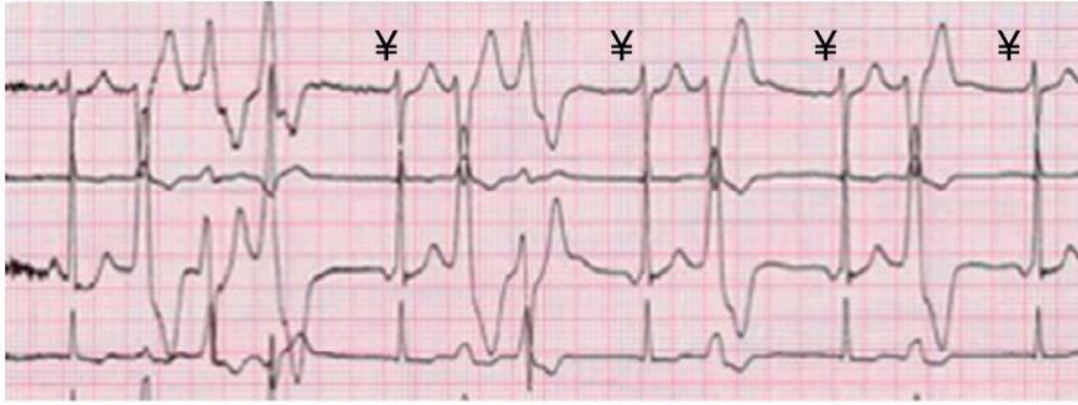


**Figure 16. An example of electrocardiograph from CPVT1 patient.** ventricular premature beats, nonsustained polymorphic ventricular tachycardia, polymorphic ventricular couplet, monomorphic ventricular bigeminy, and atrial ectopic rhythm (¥). (Adapted from (Domingo *et al.*, 2015))

The widely accepted mechanism of arrhythmogenesis in CPVT1 is that the gain-of-function mutations in RyR2, directly or through other related proteins, destabilizing the channel in the closed state to increase the diastolic SR Ca<sup>2+</sup> leak in ventricular myocytes, which induce DADs via the I<sub>NCX</sub>, leading to arrhythmias (Baltogiannis *et al.*, 2019). While most of CPVT1 mutations are gain-of-function, loss-of-function mutations have also been demonstrated, such as RyR2<sup>L433P</sup> in HEK293 cell line (Thomas, George and Lai, 2004) and RyR2<sup>A4860G</sup> in HEK293 cell line (Jiang *et al.*, 2007) and transgenic mice model (Zhao *et al.*, 2015b), complicating the arrhythmogenic mechanism in CPVT. In addition, a series of researches suggested that Purkinje cells (PCs), not VMs, are the major source of triggered arrhythmogenic activity, including biventricular tachycardia and polymorphic ventricular tachycardia (Willis *et al.*, 2016)(Mezu *et al.*, 2012). Thus, we still have long way to go on searching the clear arrhythmogenic mechanism of CPVT.

**Table 1. Summary of CPVT-associated genes (Taken from (Landstrom, Dobrev and Wehrens, 2017))**

Type	MIM*	Gene	Protein	Genetic Locus	Frequency	Inheritance
CPVT 1	604772	<i>RYR2</i>	Ryanodine receptor 2	1q42.1-q43	50%–60%	AD
CPVT 2	611938	<i>CASQ2</i>	Calsequestrin 2	1p13.1	Rare	AR
CPVT 3	614021	<i>TECRL</i>	Trans-2,3-enoyl-CoA reductase-like	7p22-p14	Rare	AR
CPVT 4	614916	<i>CALM1</i>	Calmodulin 1	14q31-q32	Rare	AD
CPVT 5	603283	<i>TRDN</i>	Triadin	6q22.31	Rare	AR

AD indicates autosomal dominant; AR, autosomal recessive; and CPVT, catecholaminergic polymorphic ventricular tachycardia.  
\*Phenotype MIM number.

## ✓ CPVT1

CPVT1, contributing to around 60% of CPVT identified cases, is caused by the mutations on the SR calcium release channel RyR2 in cardiomyocytes. The first CPVT1 mutation in human has been identified in RyR2 gene in 2001 as discussed above (RyR2<sup>R4497C</sup>) (Priori et al 2001). So far, over 150 mutations associated with CPVT1 have been identified, most of which are gain-of-function of RyR2 channels (Bezzerrides *et al.*, 2019).

RyR2 is a Ca<sup>2+</sup> channel located on the membrane of sarcoplasmic reticulum as mentioned above. It plays a vital role during ECC by releasing large amount of Ca<sup>2+</sup> from SR through calcium induced calcium release (CICR), to trigger filaments contraction (Bers, 2002). The gain-of-function mutations of RyR2 channels were widely accepted to destabilize the channel thereby increasing Ca<sup>2+</sup> leak especially under  $\beta$ -adrenergic effect during stress condition, which can be detected as an increase in the frequency or amount of elementary Ca<sup>2+</sup> release events such as calcium sparks (Fernández-Velasco *et al.*, 2009a)(Gómez, 2012). Then what mediate the  $\beta$ -adrenergic effect on RyR2 channels, and how? Protein kinase A (PKA) has been first brought to the view in 1995 by Valdivia et al with the evidence that phosphorylation of the RyR by protein kinase A increased the responsiveness of the channel to Ca<sup>2+</sup> and accelerated the kinetics of adaptation (Valdivia *et al.*, 1995). After that, Marks's group designed a series of provocative experiments and suggested that PKA-mediated (hyper)phosphorylation of RyR2 at S2809 caused increased RyR Ca<sup>2+</sup> sensitivity and abnormal channel activity (Marx *et al.*, 2000). The mechanism they proposed for these effects was shown to phosphorylate RyR2 at S2809 by PKA, which leads to FK-binding protein (FKBP)12.6 (normally bound to RyR and proposed as a stabilizer of its function) dissociation from RyR, resulting in abnormal RyR activity (Marx *et al.*, 2000)(Wehrens *et al.*, 2003). However, the above findings were challenged by the results from Bers's group. In order to exclude the effect of PKA on phospholamban (PLB), Li et al used PLB knockout (PLB-KO) mice and transgenic mice expressing only double-mutant PLB (PLB-DM) that lacks the regulatory phosphorylation sites (S16A/T17A) (Li *et al.*, 2002). PLB is an inhibitor of cardiac muscle sarcoplasmic reticulum Ca<sup>2+</sup>-ATPase (SERCA2), which transports calcium from cytosol into the sarcoplasmic reticulum. When PLB is phosphorylated, it is unbound from the SERCA, thereby releasing its inhibition. Thus, PLB phosphorylation by PKA or CaMKII results in acceleration of the SERCA pump, and increase in the SR Ca<sup>2+</sup> load, which increases by itself the RyR2 open probability (Bers, 2002). They found that PKA activation increased Ca<sup>2+</sup>spark amplitude, duration, and width only in WT, but not in PLB-KO

or PLB-DM, indicating that PKA does not seem to have any appreciable effect on resting RyR function, and suggesting that the effects on WT are indirect, due to increase in the SR Ca<sup>2+</sup> load (Li *et al.*, 2002). Then a following research from Bers's group even demonstrate that FKBP12.6 does not dissociate from RyR2 with PKA-mediated phosphorylation (Guo *et al.*, 2010). In that report, they used 2 or 3 independent techniques to assess FKBP12.6- (and FKBP12)-RyR binding and all of their results support the conclusion that FKBP12.6 binding to RyR is not influenced by PKA phosphorylation (Guo *et al.*, 2010). After refuted PKA RyR-S2809 hyperphosphorylation hypothesis, Bers's group proposed that resting SR Ca<sup>2+</sup> release or leak was increased by CaMKII-dependent phosphorylation of RyR by endogenous associated CaMKII, also using PLB-KO to exclude the PKA effect on PLB (Guo *et al.*, 2006). Mimicking cAMP effect by its analogue 8-(4-chlorophenylthio)-2'-O-methyladenosine-3',5'-cyclic monophosphate (8-CPT), Pereira et al suggested that exchange protein directly activated by cAMP (Epac) can mediate CaMKII-dependent SR Ca<sup>2+</sup> leak upon RyR phosphorylation (Pereira *et al.*, 2007). According to further experiments using Epac1, Epac2, or double knockout mice, Pereira et al demonstrated that  $\beta$ -AR activation causing CaMKII-dependent SR Ca<sup>2+</sup> leak is mediated by Epac2 isoform (Pereira *et al.*, 2013). A more recent study on CPVT patient specific iPS induced human engineered tissue model directly compared the function of CaMKII and PKA by either performing the inhibitors or genetic ablation of the phosphorylation of these two kinases. They found that in CaMKII inhibited or genetic ablated groups, the isoproterenol induced diastolic Ca<sup>2+</sup> leak was significantly prevented while not in PKA inhibited or genetic ablated groups, indicating that CaMKII rather than PKA plays a main role in mediating  $\beta$ -adrenergic SR Ca<sup>2+</sup> leak in this iPS induced human engineered tissue model (Park *et al.*, 2019). Because my thesis subject concerns CPVT1, it will be presented with more detail in section V.

#### ✓ CPVT2

The second subtype of CPVT (CPVT2) is caused by the mutations in CASQ2 gene, encoding calsequestrin protein, accounting only 3% to 5% of CPVT identified cases. Calsequestrin, a Ca<sup>2+</sup>-buffering protein abundantly existing in SR lumen, is encoded by CASQ1 (skeletal) and CASQ2 (cardiac) (Song *et al.*, 2007), which directly and indirectly regulate SR Ca<sup>2+</sup> storage and release (Campbell *et al.*, 1983). Serving as molecular sink for Ca<sup>2+</sup>, its high-binding capacity (40–50 mol of Ca<sup>2+</sup>/mol) and moderate affinity (Kd of 1 mmol/L) nature help to fulfil the large Ca<sup>2+</sup> storage in SR after contraction as well as fast releasing before contraction (Yano and Zarain-Herzberg, 1994)(Chopra and Knollmann, 2009). CASQ2 mutations are

autosomal-recessive variants, so it is less common but usually cause more severe CPVT symptoms (Lahat, Pras and Eldar, 2001). The first CPVT2 mutation is a missense mutation in a highly conserved region of CASQ2 gene that has been identified in 2001 as mentioned above (Lahat, Pras and Eldar, 2001), and in fact, all the identified CPVT2 mutations are missense, deletion, or nonsense mutations, leading to a severe reduction or complete loss of the CASQ2 protein (Faggioni, Kryshtal and Knollmann, 2012). Then the mechanism of CASQ2 mutations effect on SR Ca<sup>2+</sup> release was investigated. By transfecting a canine CASQ2 protein carrying the CPVT2 mutation D307H into adult rat myocytes, Viatchenko-Karpinski et al found that CASQ2<sup>D307H</sup> significantly reduced the SR capacity as well as Ca<sup>2+</sup> transient properties. Further experiments on pacing and exposed myocytes to isoproterenol, they found that myocytes expressing CASQ2<sup>D307H</sup> displayed drastic disturbances of rhythmic oscillations in [Ca<sup>2+</sup>]<sub>i</sub> and membrane potential, as well as the evidence of DADs, but the abnormalities were disappeared after loading SR by a low affinity Ca<sup>2+</sup>- buffer, citrate, suggesting that CASQ2 mutation can impair SR Ca<sup>2+</sup> capacity and destabilize CICR by reducing the Ca<sup>2+</sup> buffering capacity or altering RyR2 sensitivity to luminal Ca<sup>2+</sup> (Viatchenko-Karpinski *et al.*, 2004). This view has been confirmed by another study in CASQ2<sup>D307H</sup> knock-in mice (Song *et al.*, 2007). This study also demonstrated that calreticulin and RyR2 were increased in mutated myocytes, and further experiment that inhibition of RyR2 with Mg<sup>2+</sup> normalized Ca<sup>2+</sup> transient and reduced CPVT in mutated mice, indicating that RyR2 dysfunction was critical to mutant CASQ2 pathophysiology (Song *et al.*, 2007). Gyorke's group proposed that CASQ2 acted as a Ca<sup>2+</sup> luminal sensor to directly modulate the RyR2 function and sensitivity, based on the finding that increasing luminal [Ca<sup>2+</sup>] changed the open channel probability of native RyRs but not of purified RyRs (Györke *et al.*, 2004)(Györke and Terentyev, 2008). However, this view was questioned when Knollmann et al reported that SR Ca<sup>2+</sup> release and SR Ca<sup>2+</sup> load still display a steep and nonlinear relationship in CASQ2-null mice, indicating that CASQ2 is not necessary for RyR2 sensitivity to luminal Ca<sup>2+</sup> (Knollmann *et al.*, 2006). They further presented that CASQ2-null mice displayed normal SR Ca<sup>2+</sup> release and contractile function under basal conditions and causes increased diastolic SR Ca<sup>2+</sup> leak when exposed to catecholamines, indicating that in absence of CASQ2, activation of RyR2 remains unchanged at low SR [Ca<sup>2+</sup>] content but increased at high SR [Ca<sup>2+</sup>] content (Knollmann *et al.*, 2006)(Priori and Chen, 2011). Furthermore, calsequestrin is involved in the RyR2 macromolecular complex that also include another two proteins in the luminal space, junctin and triadin (Dulhunty *et al.*, 2012)(Knollmann *et al.*, 2006), the level of which were dramatically altered in CASQ2-null mice (Knollmann *et*

*al.*, 2006), together with increased calreticulin in CASQ2<sup>D307H</sup> knock-in mice (Song *et al.*, 2007), indicating that the RyR2 functional changes may be partly mediated by those proteins. Taken together, CASQ2 can directly and/or indirectly modulate SR Ca<sup>2+</sup> release by altering RyR2 channel sensitivity to luminal Ca<sup>2+</sup>, which in turn induced proarrhythmic DADs leading to CPVT.

### ✓ CPVT3

CPVT3 is caused by mutations in TECRL gene. It is a very new identified gene associated with CPVT, which has been firstly reported by Devalla's group in 2016 (Devalla *et al.* 2016). In fact, early in 2007, Bhuiyan *et al.* have already noticed a novel variant associated with a novel highly malignant autosomal recessive form of CPVT in an inbred Arab family, which has been predicted to be located in a 25-Mb interval on chromosome 7p14-p22, except SP4, NPY, FKBP9, FKBP14, PDE1C, and TBX20 genes, (Bhuiyan *et al.*, 2007). However, after genetic analysis of another patient from this inbred Arab family, together with genetic analysis of 2 French Canadian females from different families but with similar clinical symptoms, Devalla *et al.* revealed that these novel CPVT related mutations located on chromosome 4q13 but not chromosome 7, and further determined the gene as TECRL. All the patients mentioned here presented VT or CPVT and QT prolongation clinical symptoms leading the diagnoses and genetic studies to LQTS, but no mutation was detected in genes most frequently implicated in LQTS (KCNQ1, KCNH2, SCN5A, KCNE1, or KCNE2). Two variants in TECRL gene have been identified in Devalla's report, one is a missense mutation at position 196 (p.Arg196Gln) identified from the 2 French Canadian female patients, and the other one is a splice site mutation (c.331+1G>A) identified from patient in the inbred Arab family. Further functional study in hiPSC-CMs generated from the patient carrying homozygous splice site mutation (c.331+1G>A) demonstrated that the mutated myocytes presented reduced Ca<sup>2+</sup> transient properties and SR content as well as prolonged action potential duration. In addition, noradrenaline (NA) treatment significantly increased the proarrhythmic activity based on DADs in mutated myocytes, and treatment with flecainide, a class I antiarrhythmic drug, significantly reduced the proarrhythmic activity in these cells (Devalla *et al.* 2016). More recently, a study from China has identified a compound heterozygosity in the TECRL gene (Arg196Gln and c.918+3T > G splice site mutation) in a 13-year-old boy who experienced intermittent palpitations and three syncope episodes triggered by emotional stress or exercises during the last four years (Xie *et al.*, 2019), confirming that TERCL as a new gene associated

with a new form of CPVT. However, the big unknown now is what is the precise function of TECRL (Perry *et al.*, 2016), which is a key to understand the mechanism of TECRL variants resulting in CPVT. Although we have known that TECRL is a high degree of cross-species conserved gene with identical sequence as TECR (a gene that encodes a multi-pass membrane protein in the ER), encoding an ER protein expressed preferentially in the heart based on previous research (Devalla *et al.* 2016), more studies on this novel gene are still needed.

#### ✓ CPVT4

CPVT4 is caused by inherited mutations in protein calmodulin (CaM), an intracellular  $\text{Ca}^{2+}$  sensor widely expressed in all eukaryotic cells (Friedberg and Rhoads, 2001). Three independent genes (CALM1-3) encoding the identical protein, CaM, plays a key role in the proper deciphering of  $\text{Ca}^{2+}$  signaling (Sorensen, Søndergaard and Overgaard, 2013)(Peterson *et al.*, 1999)(Saimi and Kung, 2002). It also presents high degree of conservation with no amino acid changes introduced since the appearance of vertebrates (O’Neil and DeGrado, 1990)(Friedberg and Rhoads, 2001), further verifying its pivotal function. The first CPVT4 mutation was identified in a Sweden family, with members presenting ventricular arrhythmias, syncopes and sudden death, predominantly under stress condition. Applying a genome-wide linkage analysis, Nyegaard *et al* mapped the disease locus to chromosome 14q31-32 (Nyegaard *et al.*, 2012). Subsequent genetic analysis of around 70 known genes within this locus demonstrated a heterozygous CaM-N53I mutation that associated with incidence of disease within the family. According to the presence of phenotypic details of the family members, this mutation was inherited in an autosomal dominant mode and was completely penetrant. A second, *de novo*, missense mutation CaM-N97S, identified in an unrelated individual of Iraqi origin who presented cardiac arrest due to VF at age 4 and was stabilized by treatment with  $\beta$ -adrenergic-receptor blocker, was identified by a systematically screen of 63 individuals (Nyegaard *et al.*, 2012).

CaM is a 148 amino acid  $\alpha$ -helical protein containing four classical  $\text{Ca}^{2+}$ - binding EF hands that bind one calcium ion each. The 4 canonical EF hands locate at the CaM N terminus (N-lobe) and C terminus (C-lobe) separately, and EF hands at the C-lobe have a higher affinity for  $\text{Ca}^{2+}$  than those in the N-lobe (Andersson *et al.*, 1983)(Zhang *et al.*, 2012). Although with relative simple structure, the high degree of flexibility allows CaM physiologically binding with more than 300 target proteins (Vogel, 1994)(Chin and Means, 2000)(Yap *et al.*, 2000). Shaped as a dumbbell, it can sense not only the local  $[\text{Ca}^{2+}]$  but also the  $[\text{Ca}^{2+}]_{\text{cyto}}$  (Dick *et al.*, 2008).

The C-lobe of CaM senses local, large  $\text{Ca}^{2+}$  oscillations due to  $\text{Ca}^{2+}$  influx from the host channel, and the N-lobe senses global, albeit diminutive  $\text{Ca}^{2+}$  changes arising from distant sources (Tadross, Dick and Yue, 2008). CaM has two-sides effect on  $I_{\text{CaL}}$  currents, presenting both inactivation and facilitation of L-type calcium channels, depending on residues within the IQ motif (Van Petegem, Chatelain and Minor, 2005)(Zühlke *et al.*, 1999). Replacement of the native isoleucine by alanine disrupted  $\text{Ca}^{2+}$ -dependent inactivation and unmasked a strong facilitation; conversion of the same residue to glutamate eliminated both forms of autoregulation (Zühlke *et al.*, 1999). The RyR2 sensitivity is also tuned by the binding of CaM (Balshaw *et al.*, 2001)(Yamaguchi *et al.*, 2003), and four CaM-binding domains (CaMBD1a, -1b, -2, and -3) in RyR2 have been proposed. Brohus et al suggested that CaM inhibits RyR2 through anchoring to RyR2 CaMBD2 by C-lobe and saturated with  $\text{Ca}^{2+}$  during  $\text{Ca}^{2+}$  oscillations, while the CaM N-lobe functions as a dynamic  $\text{Ca}^{2+}$  sensor that can bridge noncontiguous regions of RyR2 or clamp down onto CaMBD2 (Brohus *et al.*, 2019). The interfaces between CaM and RyR2 and Cryo-EM structures of the RyR2–CaM complexes have been revealed by high-resolution electron microscopy recently (Gong *et al.*, 2019).

The mutations mentioned above have been demonstrated to alter the  $\text{Ca}^{2+}$  affinity and result in an aberrant interaction with CaMBDs in vitro experiments (Nyegaard *et al.*, 2012). Subsequent studies revealed that the CaM-N97S mutation in the C-lobe demonstrated a significant reduction of  $\text{Ca}^{2+}$  affinity and impaired binding to RyR2 at low  $\text{Ca}^{2+}$  concentration, whereas the CaM-N97S mutation located to the opposing N-lobe demonstrated a small yet significantly increase in the  $\text{Ca}^{2+}$  saturation of the C-lobe, suggesting 2 distinct mechanisms of RyR2 dysfunction regulation by CaM disruption. Furthermore, the mutations in CALM2 (Makita *et al.*, 2014)(Jiménez-Jáimez *et al.*, 2016) and CALM3 (Gomez-Hurtado *et al.*, 2016) have also been revealed to involve in CPVT-like arrhythmias, yet the overlapping features of LQTS and CPVT increase the difficulty to define those mutations.

In CaM mutation linked CPVT, the underlying mechanism was considered as the alteration of the  $\text{Ca}^{2+}$  affinity to EF hands by mutations thereby resulting in an aberrant interaction with RyR2 CaMBDs (Nyegaard *et al.*, 2012). On the other side, the RyR2 CPVT-linked mutations may cause defective interdomain interaction for CaM binding to the RyR2 thereby triggering abnormal SR  $\text{Ca}^{2+}$  release. This hypothesis has been confirmed by a study from Xu et al. They found that cAMP significantly decreased CaM-binding affinity in RyR2<sup>R2474S</sup> knock in mice, and a high concentration of CaM attenuated the aberrant increase of  $\text{Ca}^{2+}$  sparks triggered by

cAMP in saponin-permeabilized cardiomyocytes, indicating the reduction of CaM binding to RyR2 is involved in RyR2<sup>R2474S</sup> related CPVT pathology (Xu *et al.*, 2010).

#### ✓ CPVT5

The initiator of CPVT5 was considered to be the mutation in TRDN gene. TRDN encodes triadin protein, an anchoring protein involved in the SR Ca<sup>2+</sup> release channel macromolecular complex, mediating CASQ2 binding to RyR2 together with junctin protein (Sorensen, Søndergaard and Overgaard, 2013)(Lanner *et al.*, 2010a)(Terentyev *et al.*, 2005). Triadin is a multiprotein family (two isoforms, Trisk 95 and Trisk 51, expressing in skeletal muscle, one isoform, Trisk 32, mainly expressing in cardiac muscle (Marty *et al.*, 2009) arising from the alternative splicing of the single TRDN gene located on Chr6 and containing 41 exons (Thevenon *et al.*, 2003). Ablation of triadin has been demonstrated to cause a decrease of cardiac Ca<sup>2+</sup> release units and impaired excitation-contraction coupling, which in turn induce cardiac arrhythmias (Chopra *et al.*, 2009). The first identification of TRDN mutations are one homozygous deletion c.del53\_56delACAG and two compound heterozygous for a c.176C.G missense mutation (a nonsense variation c.613C.T and a missense mutation p.T59R) separately from two family with probands presenting syncope and cardiac arrest under stress condition yet carry no mutations in RyR2 and CASQ2 genes (Roux-buisson *et al.*, 2012). The 4 bp deletion and the nonsense mutations, resulted in premature stop codons leading either to an absence of protein synthesis, or to the production of a non-functional protein, whereas the missense mutation p.T59R affected a well-conserved position in Trisk 32 and resulted in the introduction of a positively charged amino acid in the transmembrane domain of the protein (Roux-buisson *et al.*, 2012). Subsequent study on mutation p.T59R in COS-7 cells and triadin KO mouse demonstrated that the mutation resulted in instability of the protein, leading to its degradation (Roux-buisson *et al.*, 2012). However, Altmann et al have identified either homozygous or compound heterozygous frameshift mutations in TRDN in 5 patients diagnosed originally with genetically elusive LQTS and experiencing cardiac arrest at very early age ( $\leq 3$  years of age), and they suggested that a novel term triadin knockout syndrome (TKOS) should be used to depict this unique disorder rather than LQT17 or CPVT5 (Helene M Altmann *et al.*, 2015). Recently, the term TKOS has already been used in a study that investigated 21 patients carrying TRDN mutations and exhibiting syncope and cardiac arrest as well as T-wave inversions (Clemens *et al.*, 2019).

## V CPVT1

As stated earlier, CPVT1 is caused by the mutations in RyR2 itself, the core of RyR2 macromolecular complex, and it is the most common form accounting around 60% of all CPVT identified cases. Moreover, mutations on RyR2 often present autosomal-dominant inherited fashion with high penetrance, which highlights its importance among life-threatening arrhythmias. In this session, we will look into the characteristics and molecular foundation of CPVT1 which is the object of my project.

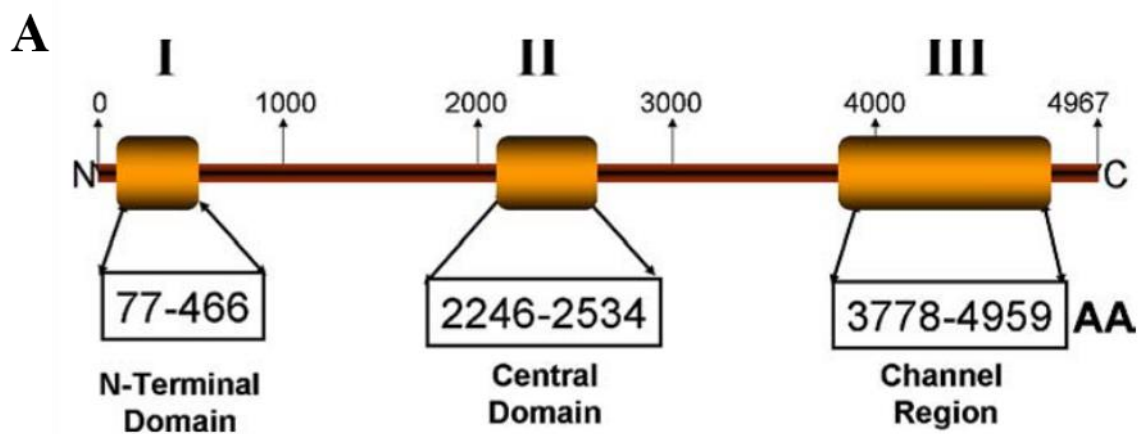
### V.1 CPVT mutations on RyR2

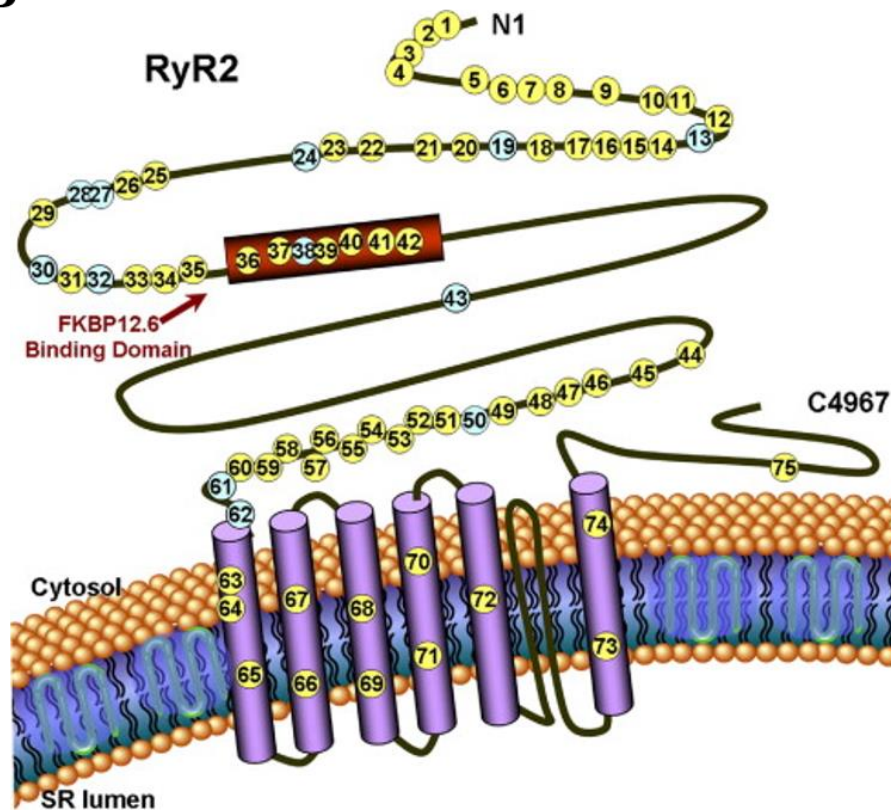
To date more than 150 CPVT-linked mutations have been identified in RyR2 gene as mentioned above. Most of them are located at 3 “hot-spots” including the N-terminal domain (residues 44-466), the central domain (residues 2246-2534) and the C-terminal domain (residues 3778- 4959) as shown in Figure 17A (Bezzina, Lahrouchi and Priori, 2015)(Medeiros-Domingo *et al.*, 2009). Those regions are highly conserved in RyR2 and are superimposable to the localization of RyR1 mutations linked to central core disease and malignant hyperthermia (MacLennan and Zvaritch, 2011)(George *et al.*, 2007), which may be the reason for frequently causing CPVT. The out-of-hotspot polymorphisms also exist, such as G1885E, G1886S and Q2958R (Tiso, 2001)(Milting *et al.*, 2006)(Päivi J Laitinen *et al.*, 2001), but they may be difficult to be detected due to sub-clinical phenotypes.

Most of analyzed CPVT linked mutations in RyR2 have shown gain-of-function, meaning that the mutations increase the SR Ca<sup>2+</sup> release channel activity. For example, the mouse carrying the RyR2<sup>R4496C</sup> mutation (Fernández-Velasco *et al.*, 2009a)(Chen *et al.*, 2012)(Kashimura *et al.*, 2010)(Gómez, 2012), which is the equivalent to the human RyR2<sup>R4497C</sup> mutation located on C-terminal domain, and the mouse carrying the RyR2<sup>R2474S</sup> mutation (Kobayashi *et al.*, 2010) located on central domain, presented an increase in diastolic Ca<sup>2+</sup> release as Ca<sup>2+</sup> sparks or waves which in turn induce DADs as mentioned above. Although rare, a loss-of-function mutation has also been revealed, such as RyR2<sup>A4860G</sup> mutation. According to the research from Jiang *et al.*, single-channel analyses revealed that RyR2<sup>A4860G</sup> mutation diminished the response of RyR2 to activation by luminal Ca<sup>2+</sup>, and HEK293 cells and HL-1 cardiac cells expressing the A4860G mutant displayed attenuated SOICR activity compared with cells transfected with RyR2 WT (Jiang *et al.*, 2007). Functional study of RyR2<sup>A4860G</sup> mutation in heterozygous mice model revealed the novel mechanism that the mutation

decreased the peak of  $\text{Ca}^{2+}$  release during systole, gradually overloading the sarcoplasmic reticulum with  $\text{Ca}^{2+}$ , which in turn caused random bursts of prolonged  $\text{Ca}^{2+}$  release, activating electrogenic  $\text{Na}^+$ - $\text{Ca}^{2+}$  exchanger activity and triggering EADs (Zhao *et al.*, 2015a).

N-terminal domain located the furthest away from transmembrane domain, neither contributing to channel build nor providing binding sites to accessory proteins, but it does harbor many mutations causing severe CPVT symptoms (Figure 17 B), such as mutation R176Q (Kannankeril *et al.*, 2006), G357S (Liu *et al.*, 2017), R420W (Okudaira *et al.*, 2014), R420Q (Domingo *et al.*, 2015)(Wang *et al.*, 2017) are some examples. Cryo-EM structures analysis showed that this region is highly dynamic, tilting upward and outward as the channels transition to activated states (Peng *et al.*, 2016)(Wei *et al.*, 2016)(Samso *et al.*, 2009). One hypothesis is that the N-terminal region acts as a brake on channel opening: inter-subunit interactions which need to be disrupted during channel activation and opening may provide an energetic barrier that impedes channel opening (Kimlicka, Lau, *et al.*, 2013). CPVT linked mutations may facilitate RyR2 channel opening through lowering the energetic barrier by weakening these contacts (Pancaroglu and Van Petegem, 2018).



**B**

**Fig 17. Mutation Clustering in the RyR2.** A. Mutations clustered in the cardiac ryanodine receptor (RyR2) are distributed in 3 “hot-spot” regions, called domains I (N-terminal), II (central), and III (channel region). AA=amino acid number estimated for each domain. B. RyR2 Channel Topology and Localization of Mutations and Polymorphisms. Linear topology of the cardiac ryanodine receptor (RyR2); putative pathogenic mutations (yellow circles) and polymorphisms (blue circles) are shown in the approximate location. The number within the circle corresponds to part of mutations ranging from N-terminal to C-terminal region. (Adopted from Medeiros-Domingo et al (Medeiros-Domingo *et al.*, 2009).)

In this thesis, we mainly studied RyR2<sup>R420Q</sup> mutation, which is located in the N-terminal hot-spot (Figure 18). As mentioned before, the human N-terminal region consists of three domains: A (residues 10–223), B (224–408) and C (409–544)(Borko *et al.*, 2014) as shown by different colors in Figure 18. Arg420 (Fig 18), a residue not conserved between RyRs subtypes, but well conserved among RyRs from different organisms, is crucial for maintaining a stable A/B/C domain arrangement (Borko *et al.*, 2014). As the target of two CPVT1 mutations (RyR2<sup>R420Q</sup>, RyR2<sup>R420W</sup>) also highlighted the importance of Arg420.

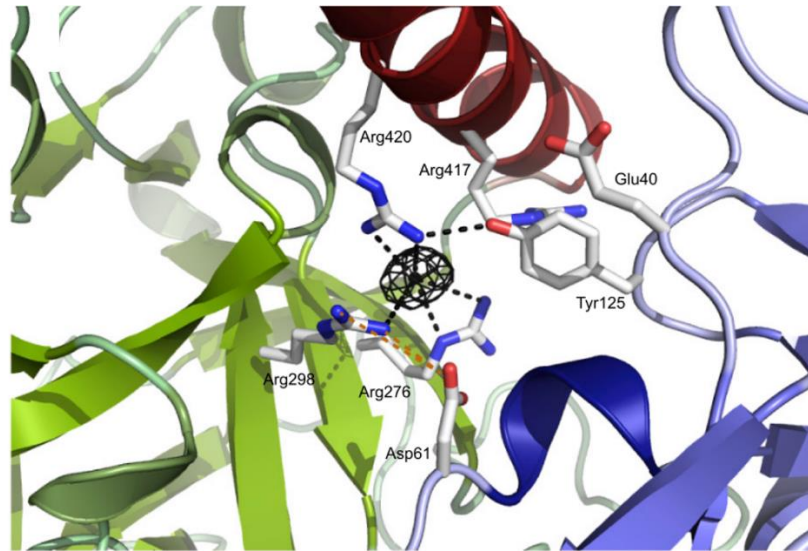


**Figure 18. The corresponding region domain A, B, C and Arg420 residue in N-terminal domain of RyR2.** Blue, domain A; green, domain B; red, domain C. Fo-Fc density, contoured at  $3\sigma$ , is shown for the chloride site. Dashed lines indicate contacts with positively charged arginine atoms and a hydrogen bond between Tyr125 and Arg420. (adapted from (Kimlicka, Tung, et al., 2013)).

## V.2 Experimental models using in CPVT study

In order to determine the mechanisms involved in CPVT by different mutations, different experimental models have been used. Thus, I will briefly describe them before exposing the conclusions taken from the analyzed RyR2 mutations.

### V.2.1 Expression systems

To get insights into the mechanisms involved in RyR2 mutations, heterologous expression systems have been used. Plasmids for RyR2 genes carrying mutations identified in CPVT patients are typically transfected into cell lines, such as human embryonal kidney 293 cell line (HEK293) transformed by exposing cells to sheared fragments of adenovirus type 5 DNA (Graham *et al.*, 1977) and HL-1 cardiac myocyte line generated from the AT-1 mouse atrial cardiomyocyte tumor lineage (Claycomb *et al.*, 1998). Expression systems are used to decipher the biophysical properties of both, wild type and mutant RyR2 channels in single cells and help in understanding the molecular mechanisms underlying CPVT. Given the low demand for culture and high transfected efficiency, HEK293 cell line become the first choice for the initial functional study of RyR2 CPVT linked mutations. For example, the first functional study of RyR2<sup>R420Q</sup> mutation in HEK293 cells demonstrated that the mutation acted as gain-of-function in low  $\text{Ca}^{2+}$  concentration (Domingo *et al.*, 2015). Due to its short growing period, expression

systems have also been used to compare the different mutations or verify the common mechanism among different mutations of CPVT. For instance, Jiang et al studied Q4201R and I4867M from the C-terminal region, S2246L and R2474S from the central region, and R176Q(T2504M) and L433P from the N-terminal region in HEK293 cell line and HL-1 cardiac cell line and concluded that increased Store-overload-induced  $\text{Ca}^{2+}$  release (SOICR) activity and increased the channel sensitivity to luminal  $\text{Ca}^{2+}$  are common defects of RyR2 mutations associated with VT and sudden death (Jiang *et al.*, 2005). However, the limitation of the expression system is its restriction to the examination of known genetic causes, yet the genetic cause for many patients remains unidentified. Besides, it can't give insight into the heterogeneity of phenotypes between family members carrying the same mutation (Sendfeld *et al.*, 2019). More importantly, it is irrefutable that neither of these two cell lines closely resembles human cardiomyocytes. Therefore, other experimental models are still in need for CPVT research.

### **V.2.2 Animal model**

The main advantage of using an animal model rather than an expression system is that the target mutation can be investigated in its physiological environment and during different developmental stages. Mouse, rat and rabbit are three kind of popular animal model for research. Considering of the economic factor, mouse model is the most popular one. The heterozygous knock-in of RyR2 mutation in mice generated a mouse model that replicates many features associated with the CPVT including sex-dependent disease progression and drug response. Numerous of CPVT mutations have been investigated in a mouse models (see table 2), proving it a valuable tool for exploring the underlying cause of ventricular tachycardia in patients (Kannankeril *et al.*, 2006)(Fernández-Velasco *et al.*, 2009a)(Gómez et al. 2012)(Okudaira *et al.*, 2014)(Zhao et al. 2015a)(Wang et al. 2017). However, there are still some limitations when extrapolating the repolarization findings obtained with the mouse model to the human heart. Besides the obvious difference in size and faster beating rate (4-8 times faster), the mouse heart present differences in their ion channel patterns compared to the human heart, such as TTX-sensitive sodium channels transcript levels decreased with increasing heart size (Zimmer et al. 2014) and the huge difference of contribution of NCX for removing  $\text{Ca}^{2+}$  from cytosol (Bers, 2002). Rabbit has been proved to possess more similar ion channel patterns as human being (Bers, 2002), while limited to the technical difficulties and higher cost, no heterozygous knock-in CPVT rabbit model has been reported so far.

### V.2.3 New breakthrough: hiPSC line

Takahashi and Yamanaka discovered in 2006 how intact mature cells in mice could be reprogrammed to become immature stem cells (Takahashi and Yamanaka, 2006). Surprisingly, by introducing only a few genes, they could reprogram mature cells to become pluripotent stem cells, i.e. immature cells that are able to develop into all types of cells in the body. Lately and introducing the same 4 factors (Oct3/4, Sox2, Klf4 and c-Myc) they succeeded in obtaining stem cells from human fibroblasts, which were then able to differentiate into cardiac cells (Takahashi *et al.*, 2007). Like embryonic stem cells, differentiated iPS cells may be used for regenerative therapies, cardiotoxicity screening, basic research and drug screening, but without the ethical issues of embryonic stem cells. Several investigators have described methods to differentiate iPS cells into functional cardiomyocytes (Narazaki *et al.*, 2008)(Mummery *et al.*, 2012). iPSC-CM express cardiac specific markers and structural proteins from well-organized sarcomeres. iPSC-CM cells from both mice and human can generate cells with typical nodal/pacemaker, atrial and ventricular electrical properties (Zhang *et al.*, 2009). Interestingly, they express channels and transporters involved in  $\text{Ca}^{2+}$  handling (Satin *et al.*, 2008). Although they have an immature phenotype compared to adult cardiomyocytes, the fact that they retain channels and transporters from human cardiomyocytes makes them a valuable tool. Because iPSC-CM can be generated from any patient to produce genetically identical pluripotent cells, they are very interesting to analyze genetic diseases such as inherited arrhythmic disorders including CPVT (Hoekstra *et al.*, 2012). To our knowledge, only several RyR2 CPVT mutations have been studied in iPSC-CM (summarized in Table 2). Proposed mechanisms are a gain-of-function defect due to an alteration in the zipping-unzipping mechanism in RyR2<sup>S406L</sup> (Jung *et al.*, 2012a) or store overload induced  $\text{Ca}^{2+}$  release in RyR2<sup>M4109R</sup> (Itzhaki *et al.*, 2012a). However, more mutations and completed analyses are needed. Interestingly, although the CPVT has been suggested to arise in ventricular myocytes as DADs (delayed after depolarizations), patch-clamp analysis of iPSC-CM from RyR2<sup>P2328S</sup> patients have revealed EAD (early after depolarizations) (Kujala *et al.*, 2012). Thus, much it is still unknown, prompting more and in depth analysis of different mutations.

### V.3 Pathologic mechanism of CPVT1

Given the alteration of RyR2 channel is the direct factor causing CPVT, any factor that regulate the RyR2 channel properties could be involved in the underlying mechanism that causing CPVT. To date several mechanisms have been proposed to explain the pathologic

mechanism of CPVT1, such as RyR2 channel sensitivity to cytosol/luminal  $\text{Ca}^{2+}$ , N-terminal domain unzipping, FKBP 12.6 unbinding and so on, but most of them are still under debate, demanding more strong supported studies.

### **V.3.1 Increased RyR2 channel sensitivity to $\text{Ca}^{2+}$**

Unlike RyR1, which is activated by protein-protein interactions between L-type  $\text{Ca}^{2+}$  channels (DHPRs, Cav1.1s) and RyR1 channel, RyR2 is activated by  $\text{Ca}^{2+}$  coming through L-type  $\text{Ca}^{2+}$  channels (DHPRs, Cav1.2s) that was known as CICR as mentioned above (Meissner, 2017). Thus,  $\text{Ca}^{2+}$  is a very important regulator of RyR2 channel. It has been demonstrated that RyR2 can be activated by micromolar cytosolic  $\text{Ca}^{2+}$  and inhibited by millimolar cytosolic  $\text{Ca}^{2+}$  in the absence of other channel regulators (Xu, Mann and Meissner, 1996), suggesting that there are at least two  $\text{Ca}^{2+}$ -binding sites: a high-affinity activation site and a low-affinity inactivation site (Meissner, 2017). Therefore, many researchers have analyzed the  $\text{Ca}^{2+}$  sensitivity of the CPVT1 mutations. For instance, functional study of mutation RyR2<sup>R4496C</sup> demonstrated that diastolic  $\text{Ca}^{2+}$  release as  $\text{Ca}^{2+}$  sparks were more frequent in RyR2<sup>R4496C</sup> myocytes, indicating the mutation increased RyR2 channel activity. The following experiment by exposing the permeabilized cells to different cytosolic  $[\text{Ca}^{2+}]$  confirmed that the mutated channel sensitivity dramatically increased (Fernández-Velasco *et al.*, 2009a). Besides higher sensitivity to cytosolic  $\text{Ca}^{2+}$ , using single channel analysis, Jiang *et al.* held the opinion that increased channel sensitivity to luminal  $\text{Ca}^{2+}$  activation is a common phenomenon in RyR2 mutations linked to CPVT1 (Jiang *et al.*, 2005)(Jiang *et al.*, 2004), proposing the mechanism of store overload induced  $\text{Ca}^{2+}$  release in CPVT.

### **V.3.2 Store-overload-induced $\text{Ca}^{2+}$ release (SOICR)**

Store-overload-induced  $\text{Ca}^{2+}$  release (SOICR) was first mentioned by Chen's group when they tried to describe the depolarization-independent  $\text{Ca}^{2+}$  overload-induced SR  $\text{Ca}^{2+}$  release (Jiang *et al.*, 2004). In their opinion, the CPVT mutations may reduce the threshold for SOICR (Figure 19) by enhancing RyR2 sensitivity to luminal  $\text{Ca}^{2+}$  activation, which in turn increases the propensity for triggered arrhythmia. They highlighted CPVT-linked RyR2 mutations primarily increase the channel sensitivity to luminal  $\text{Ca}^{2+}$  rather than cytosolic  $\text{Ca}^{2+}$  (Jiang *et al.*, 2005), because they considered that activation of RyR2 by cytosolic  $\text{Ca}^{2+}$  underlies the physiological release of  $\text{Ca}^{2+}$  from SR (CICR), whereas activation of RyR2 by luminal  $\text{Ca}^{2+}$  during SR  $\text{Ca}^{2+}$  overload leads to spontaneous  $\text{Ca}^{2+}$  release (SOICR) (Priori and Chen, 2011).

However, their hypotheses are not widely accepted. For example, as mentioned above, Fernández-Velasco et al demonstrated that exposing the permeabilized mutated cells to higher cytosolic  $[Ca^{2+}]$  could increase  $Ca^{2+}$  sparks frequency, indicating that RyR channels are also hypersensitive to  $[Ca^{2+}]_{cytosolic}$  (Fernández-Velasco *et al.*, 2009a). Another example highlighted that  $\beta$ -adrenergic stimulation induced  $Ca^{2+}$  waves by increasing SR  $Ca^{2+}$  content and not by decreasing the threshold for Ca waves in the RyR2<sup>R4496C</sup> CPVT mouse model (Kashimura *et al.*, 2010), indicating that decreased SR threshold by increased RyR channel luminal  $Ca^{2+}$  sensitivity may not be a common phenomenon.

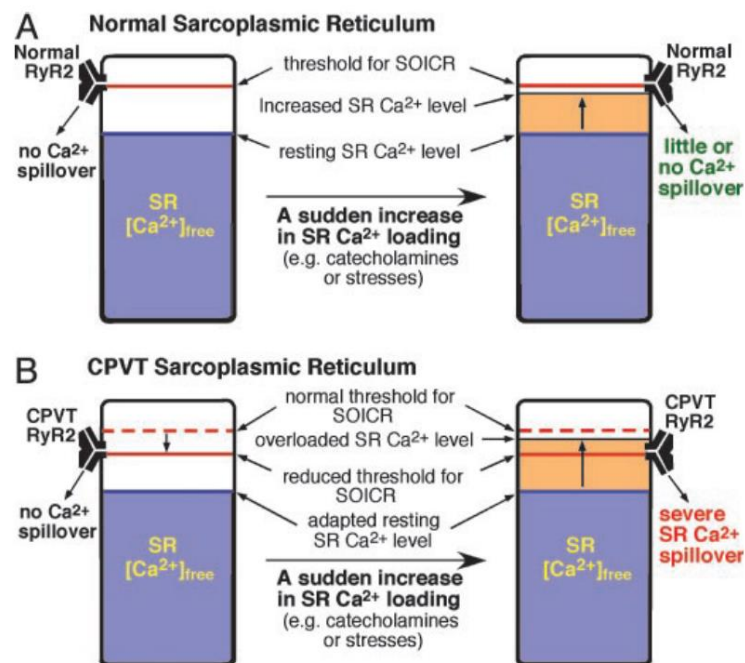


**Figure 19. A proposed mechanism for CPVT associated with RyR2 mutations.** The relationship between the threshold for SOICR and the SR-free  $Ca^{2+}$  level in normal (A) and CPVT SR (B) in the resting and stimulated states is schematically shown. The threshold for SOICR is depicted by a red bar. Note that the threshold for SOICR is reduced in the CPVT SR as a consequence of the RyR2 mutations. The SR free  $Ca^{2+}$  level is represented by the blue area. Note that the resting level of SR-free  $Ca^{2+}$  in the CPVT SR might have adapted to a reduced level due to the existence of SR autoregulation. An abrupt increase of SR-free  $Ca^{2+}$  as a result of stimulations by catecholamines or stresses is depicted by the yellow area. When the SR-free  $Ca^{2+}$  level reaches the SOICR threshold, SOICR occurs, leading to a large SR  $Ca^{2+}$  spillover, which in turn can generate DAD and triggered arrhythmia. (Adapted from (Jiang *et al.*, 2004))

### V.3.3 Altered domain zipping-unzipping

Based on the previous investigations on ECC, Yamamoto et al proposed the hypothesis of zipping and unzipping between N-terminal (amino acids 1 to 600) and central (amino acids 2000 to 2500) domains (Yamamoto, El-Hayek and Ikemoto, 2000)(Ikemoto and Yamamoto,

2002) (Figure 20). Then they created an unzipping model by adding a domain-unzipping peptide, DPc10 (amino acids 2460 to 2495), to decrease the interaction between N-terminal and central domains, by which they found that domain unzipping resulted in  $\text{Ca}^{2+}$  leak through the RyR and facilitating cAMP-dependent hyperphosphorylation of RyR and FKBP12.6 dissociation from RyR (Oda *et al.*, 2005), confirming their previous hypothesis. A more recent research in CPVT knock in mice also supported their view. Uchinoumi *et al.* found that interaction between the N-terminal and central domains of the RyR2 was weakened (domain unzipping) in RyR2<sup>R2474S</sup> knock in mice and adding DPc10 to the wild type cardiomyocytes perfectly mimicked the channel disorder in the RyR2<sup>R2474S</sup> mutated mice, indicating the disruption of zipping state is an underlying mechanism in CPVT (Uchinoumi *et al.*, 2010). Moreover, the high-resolution crystal structures analysis of N-terminal region revealed that most of CPVT-linked RyR2 mutations are located on the surface of domains and within domain interfaces (Tung *et al.*, 2010)(Lobo and Van Petegem, 2009)(Amador *et al.*, 2009)(Kimlicka, Lau, *et al.*, 2013), also supporting the domain zipping-unzipping hypothesis.

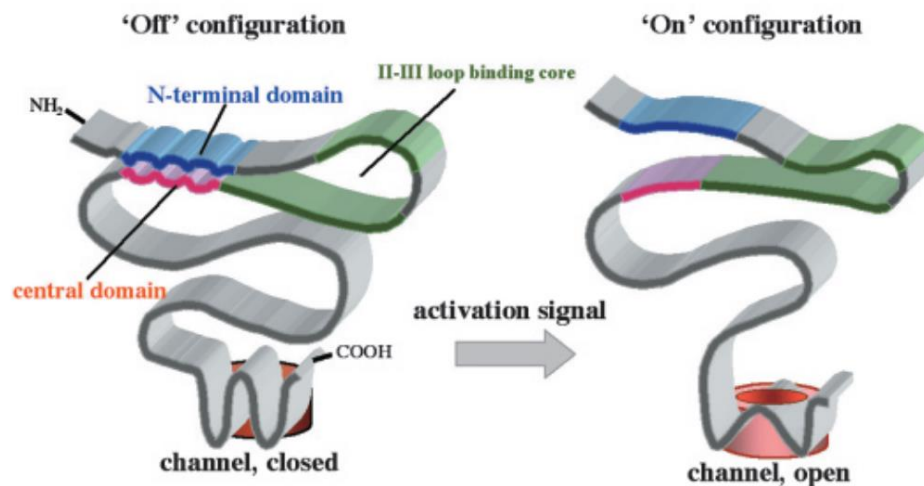


**Figure 20. Hypothetical model illustrating how opening and closing of the  $\text{Ca}^{2+}$  channel is controlled by the inter-domain interactions.** The model assumes that the interaction between the N-terminal domain and the central domain stabilizes the inactive (closed) state (“Off” configuration). The activation signal removes such interaction, producing the active (open) state (“On” configuration). The channel domain recognizes changes in the configuration of the interacting domain pair by mediation of a global conformational change in the polypeptide chain network that connects the domain pair with the channel domain. (Adapted from (Yamamoto, El-Hayek and Ikemoto, 2000))

### V.3.4 Defective FKBP Binding

FK506 binding proteins (FKBPs) are a large family of proteins that belong to the immunophilins, a family of highly conserved proteins that bind immunosuppressive drugs such as FK506 and rapamycin (Lanner *et al.*, 2010b). All the family members are named according to their molecular mass. The founding member of this family is FKBP12, a small molecule weighting 12 kDa and containing 108 amino acid peptide (Tong and Jiang, 2015). FKBP12.6 is the closest homologue of FKBP12 that presents 83% sequence identity to FKBP12 (Timerman *et al.*, 1994). Both FKBP12 and FKBP12.6 (also known as calstabin1 and calstabin2) can physically interact with all three isoforms of RyRs, stabilizing the channel in the closed state (Ahern *et al.* 1994)(Marx *et al.*, 2000)(Ahern *et al.* 1997). Numerous cryo-EM structures analyses have demonstrated that the two FKBP12 isoforms bind in the same position and orientation to the periphery of the cytosolic cap, at the junction between the ‘clamp’ and ‘handle’ domains (Samsó, Shen and Allen, 2006)(Sharma *et al.*, 2006)(Samsó *et al.*, 2009)(Cornea *et al.*, 2010). Recently, Yuchi *et al.* revealed a more precise FKBP binding location that is a SPRY1 loop and highlighted that mutations in the SPRY1 domain can affect FKBP binding through interfering with the folding (Yuchi *et al.*, 2015). Thus, it is reasonable to consider defective FKBP binding as a pathologic mechanism in CPVT. In fact, several CPVT1 mutations, such as RyR2<sup>L433P</sup> located in N-terminal domain, RyR2<sup>S2246L</sup> and RyR2<sup>R2474S</sup> located in central domain, and RyR2<sup>R4496C</sup> located in C-terminal domain, have been shown to reduce the affinity of FKBP12.6 binding to RyR2 (Wehrens *et al.*, 2003)(Lehnart *et al.*, 2008)(Shan *et al.*, 2012). On the other side, overexpression of FKBP12.6 either in cardiac myocytes or in mouse model reduced diastolic Ca<sup>2+</sup> leak that is often related to proarrhythmic DADs (Gómez *et al.*, 2004)(Gellen *et al.*, 2008). A latest report demonstrated that RyRs became more sensitive to Ca<sup>2+</sup> triggers by L-type Ca<sup>2+</sup> channels in the absence or inhibition of FKBP12.6 in cardiomyocytes (Zhao *et al.*, 2017), indicating the stabilization effect of FKBP12.6 on RyR2 channel. However, the opposite evidences also exist. For example, Liu *et al.* found that RyR2–FKBP12.6 interaction in RyR2<sup>R4496C+/-</sup> mice is identical to that of WT both before and after epinephrine and caffeine, and further performing K201, a compound promoting FKBP binding to RyR, failed to prevent DADs in RyR2<sup>R4496C+/-</sup> myocytes and ventricular arrhythmias in RyR2<sup>R4496C+/-</sup> mice, suggesting that R4496C mutation doesn’t interfere with the RyR2/FKBP12.6 complex (Liu *et al.*, 2006). Therefore, it is hard to conclude that decrease in FKBP affinity is common defect in CPVT1 and more investigations are still needed to reveal the real role of FKBP in CPVT mechanism.

**Table 2. The functional studied of CPVT1 mutations and related mechanisms.**

Amino Acid Change	Location	Exon	Experimental Model	Mechanism	References
Exon3 del	NT	2	HL-1, HEK293	reduced the threshold for Ca <sup>2+</sup> release termination and increased fractional release	(Tang et al 2012)
			hiPSC-CM	Shorter APD, lower AP amplitude, upstroke velocity and more depolarized diastolic potential, increased DADs and EADs after adrenaline exposure	(Pölonen et al 2019)
A77V	NT	3	HL-1, HEK293	reduced the threshold for Ca <sup>2+</sup> release termination and increased fractional release	(Tang et al 2012)
R176Q/ T2504M	NT	8	HL-1, HEK293	reduced the threshold for Ca <sup>2+</sup> release termination and increased fractional release	(Tang et al 2012)
			HEK293	reduced the threshold for SOICR	(Jones <i>et al.</i> , 2008)
			HL-1, HEK293	enhanced propensity for SOICR	(Jiang <i>et al.</i> , 2005)
			mice	predisposes the heart to catecholamine-induced oscillatory calcium-release events	(Kannankeril <i>et al.</i> , 2006)
			HEK293	increased duration of elevated cytoplasmic Ca <sup>2+</sup> levels following channel activation	(Thomas et al 2004)
E189D	NT	8	HEK293	increases the propensity for SOICR without altering the affinity for FKBP12.6	(Jung <i>et al.</i> , 2012b)
G230C	NT		HEK293	reduced calstabin2 binding and increased sensitivity cytosolic Ca <sup>2+</sup> but not luminal Ca <sup>2+</sup>	(Meli <i>et al.</i> , 2011)
			HEK293	increased the propensity for SOICR, increased the sensitivity of single RyR2 channels to both cytosolic and luminal Ca <sup>2+</sup> activation	(Liu <i>et al.</i> , 2013)

G357S	NT	13	HEK293	reduced the thresholds for the activation and termination of SOICR, decreased the thermal stability of the N-terminal domain and total RyR2 protein expression	(Liu <i>et al.</i> , 2017)
			HEK293	increased caffeine sensitivity and store overload-induced calcium release activity	(Wangüemert <i>et al.</i> , 2015)
S404R	NT	14	hiPSC-CM	abnormal spontaneous Ca <sup>2+</sup> release events consisting of EADs, DADs, and waves	(Bezzarides <i>et al.</i> , 2019)
S406L	NT	14	hiPSC-CM	elevated diastolic Ca <sup>2+</sup> concentrations, reduced SR Ca <sup>2+</sup> content and increased susceptibility to DADs and arrhythmia	(Jung <i>et al.</i> , 2012b)
R420W	NT	14	mice	impairs depolarization-induced Ca <sup>2+</sup> oscillation	(Okudaira <i>et al.</i> , 2014)
			HL-1, HEK293	reduced the threshold for Ca <sup>2+</sup> release termination and increased fractional release	(Tang <i>et al.</i> 2012)
R420Q	NT	14	HEK293	increased Ca <sup>2+</sup> release at diastolic cytosolic Ca <sup>2+</sup> concentration	(Domingo <i>et al.</i> , 2015)
			mice	Induced bradycardia by disturbing the coupled clock pacemaker	(Wang <i>et al.</i> , 2017)
			hiPSC-CM	iso was either ineffective, caused arrhythmias, or markedly increased diastolic [Ca <sup>2+</sup> ] <sub>i</sub> , and positive inotropic and lusitropic effects were not induced in mutated cardiomyocytes	(Novak <i>et al.</i> , 2015)
L433P	NT	15	HEK293	reduction in sensitivity to channel activation	(Thomas <i>et al.</i> 2004)
			HL-1, HEK293	enhanced propensity for SOICR	(Jiang <i>et al.</i> , 2005)
			HL-1, HEK293	reduced the threshold for Ca <sup>2+</sup> release termination and increased fractional release	(Tang <i>et al.</i> 2012)

			mice	diastolic SR Ca <sup>2+</sup> leak in atrial myocytes	(Shan <i>et al.</i> , 2012)
			yeast	Disrupts RyR2 N-terminus self-association	(Seidel <i>et al.</i> , 2015)
A1107M	CL	28	HL-1, HEK293	increased the threshold for Ca <sup>2+</sup> release termination and reduced fractional release	(Tang et al 2012)
G2145R	CL	41	HEK293	Mild gain-of-function defect in native unphosphorylated mutated channel	(Marjamaa <i>et al.</i> , 2011)
			HEK293	Dissociation of FKBP12.6 from the channel	(Wehrens <i>et al.</i> , 2003)
S2246L	CL	44	HL-1	Increased Ca <sup>2+</sup> release and RyR2: FKBP12.6 dissociation	(George, Higgs and Lai, 2003)
			HL-1, HEK293	enhanced propensity for SOICR	(Jiang <i>et al.</i> , 2005)
			HEK293	reduced the threshold for SOICR	(Jones <i>et al.</i> , 2008)
			mice	induces defective interaction between the N-terminal and central domains	(Suetomi <i>et al.</i> , 2011)
R2267H	CL	45	HEK293	increased Ca <sup>2+</sup> release at diastolic cytosolic Ca <sup>2+</sup> concentration	(Tester, 2007)
E2311D	FKBP	46	hiPSC-CM	CPVT cells presented DADs both in basal and after β-adrenergic stimulation, developed multiple calcium transients	(Di Pasquale <i>et al.</i> , 2013)
P2328S	FKBP	46	HEK293	decreased binding of calstabin2 (FKBP12.6), gain-of-function defect	(Lehnart <i>et al.</i> , 2004)
			mice	alterations in cellular Ca <sup>2+</sup> homeostasis, gene dosage effect arrhythmogenic properties	(Goddard <i>et al.</i> , 2008)

			mice	Homozygous RyR2 <sup>P2328S</sup> was associated with alternans, particularly at short baseline cycle lengths	(Sabir <i>et al.</i> , 2010)
			HEK293	reduced calstabin2 binding and increased sensitivity cytosolic Ca <sup>2+</sup> but not luminal Ca <sup>2+</sup>	(Meli <i>et al.</i> , 2011)
			mice	Acute atrial arrhythmogenicity and altered Ca <sup>2+</sup> homeostasis	(Zhang <i>et al.</i> , 2011)
			hiPSC-CM	aberrant Ca <sup>2+</sup> cycling, DADs and EADs	(Kujala <i>et al.</i> , 2012)
			mice	Abnormal intracellular Ca <sup>2+</sup> homeostasis produces both arrhythmic triggers and a slow-conducting arrhythmic substrate in atria	(J. H. King <i>et al.</i> , 2013)
			RyR2 amino acid sequence	An evidence of conserved ATP binding sequence motifs but no evidence of FKBP12.6 association in central domain	(Blayney <i>et al.</i> , 2013)
			mice	raised [Ca <sup>2+</sup> ] <sub>i</sub> resulted from increased SR leak produces both acute and chronic inhibition of Na <sup>+</sup> channel function, which in turn reduce conduction velocity and thereby induce reentry	(James H. King <i>et al.</i> , 2013)
			mice	altered ventricular myocardial conduction velocity potentially resulting in arrhythmogenic substrate	(Y. Zhang <i>et al.</i> , 2013)
			hiPSC-CM	increased non-alternating variability of Ca <sup>2+</sup> release and slower depolarization by β - Agonists	(Paavola <i>et al.</i> , 2016)
			mice	reduced conduction velocity to downregulated Nav1.5 reducing I <sub>Na</sub>	(Ning <i>et al.</i> , 2016)
			mice	Both activated and inactivated activities of RyR2 channel increased in P2328S heart, but not associated with sub-conductance activity	(Salvage <i>et al.</i> , 2019)

				(S2806 or S2814 phosphorylation or the level of bounded FKBP12)	
N2386I	FKBP	47	HEK293	increased duration of elevated cytoplasmic Ca <sup>2+</sup> levels following channel activation	(Thomas <i>et al.</i> 2004)
			mice	diastolic SR Ca <sup>2+</sup> leak in atrial myocytes	(Shan <i>et al.</i> , 2012)
			RyR2 amino acid sequence	An evidence of conserved ATP binding sequence motifs but no evidence of FKBP12.6 association in central domain	(Blayney <i>et al.</i> , 2013)
R2474S	FKBP	49	HL-1, HEK293	enhanced propensity for SOICR	(Jiang <i>et al.</i> , 2005)
			HEK293	Dissociation of FKBP12.6 from the channel	(Wehrens <i>et al.</i> , 2003)
			mice	decreased binding of the calstabin2 (FKBP12.6) subunit	(Lehnart <i>et al.</i> , 2008)
			mice	causes defective interdomain interaction, significant reduction in the ability of CaM binding to the RyR2, spontaneous Ca <sup>2+</sup> leak	(Xu <i>et al.</i> , 2010)
			mice	diastolic SR Ca <sup>2+</sup> leak in atrial myocytes and depleted calstabin2 from RyR2	(Shan <i>et al.</i> , 2012)
			mice	SR Ca <sup>2+</sup> leak increases the susceptibility to Ca <sup>2+</sup> alternans and Ca <sup>2+</sup> waves increasing the incidence of atrial arrhythmias.	(Xie <i>et al.</i> , 2013)
			mice	increased spontaneous Ca <sup>2+</sup> leak, delayed afterdepolarization, triggered activity and Ca <sup>2+</sup> spark frequency can be corrected to a normal function by increasing the affinity of CaM binding to the RyR	(Fukuda <i>et al.</i> , 2014)
			mice	exercise training reduced ventricular tachycardia episodes in CPVT mice through	(Manotheepan <i>et al.</i> , 2016)

				lower CaMKII-dependent phosphorylation of RyR2	
			mice	increased cytosolic RyR2 Ca <sup>2+</sup> sensitivity and both heart rate and sympathetic stimulation have pro-arrhythmic effects	(Danielsen <i>et al.</i> , 2018)
V2475F	FKBP	49	mice	increased cytosolic Ca <sup>2+</sup> activation, abnormal PKA phosphorylation, and increased activation by luminal Ca <sup>2+</sup>	(Loaiza <i>et al.</i> , 2013)
F2483I	FKBP	49	hiPSC-CM	Increased arrhythmias and DADs by catecholaminergic stimulation and higher local Ca <sup>2+</sup> release events at basal state, CICR continued after repolarization and were abolished by increased cytosolic cAMP levels	(Fatima <i>et al.</i> , 2011)
			hiPSC-CM	longer and wandering Ca <sup>2+</sup> sparks, aberrant unitary Ca <sup>2+</sup> -signaling, smaller Ca <sup>2+</sup> -stores, higher CICR gains, and sensitized adrenergic regulation	(X. H. Zhang <i>et al.</i> , 2013)
			hiPSC-CM	longer and wandering Ca <sup>2+</sup> sparks, elevated diastolic Ca <sup>2+</sup> leaks, and smaller SR Ca <sup>2+</sup> stores	(Wei <i>et al.</i> , 2018)
N3308S	Cytosol	69	HEK293	open probabilities of mutated channels are similar to the wild type channels	(Marjamaa <i>et al.</i> , 2011)
R3570W	Cytosol	75	HEK293	gain-of-function defect in native unphosphorylated mutated channel	(Marjamaa <i>et al.</i> , 2011)
D3638A	Cytosol		hiPSC-CM	In stress condition, lower maximal Ca <sup>2+</sup> transient amplitude, more irregular Ca <sup>2+</sup> release events in CPVT hiPSC-CMs	(Acimovic <i>et al.</i> , 2018)
L3741P	Cytosol	83	hiPSC-CM	Reduced amplitude of Ca <sup>2+</sup> transients and SR content, increased Ca <sup>2+</sup> fractional release of SR	(Preininger <i>et al.</i> , 2016)
G3946S	Cytosol	88	hiPSC-CM	abnormal spontaneous Ca <sup>2+</sup> release events consisting of EADs, DADs, and waves	(Bezzarides <i>et al.</i> , 2019)

N4104K	TMD	90	HL-1	Increased Ca <sup>2+</sup> release and RyR2: FKBP12.6 dissociation	(George, Higgs and Lai, 2003)
			HEK293	enhanced RyR2 luminal Ca <sup>2+</sup> activation, reduced threshold for SOICR	(Jiang <i>et al.</i> , 2004)
M4109R	TMD	90	hiPSC-CM	internal Ca <sup>2+</sup> stores play an important role in the pathogenesis of DADs, [Ca <sup>2+</sup> ] transient irregularities in mutated cells that worsened with adrenergic stimulation and Ca <sup>2+</sup> overload and improved with beta-blockers, reduced threshold for SOICR	(Itzhaki <i>et al.</i> , 2012b)
L4115F	TMD	90	hiPSC-CM	Shorter APD90, increased DADs and EADs after adrenaline exposure	(Pölonen <i>et al.</i> 2019)
Q4201R	TMD	90	HEK293	reduced the threshold for SOICR	(Jones <i>et al.</i> , 2008)
			HL-1, HEK293	enhanced propensity for SOICR	(Jiang <i>et al.</i> , 2005)
			HEK293	decreased binding of calstabin2 (FKBP12.6), gain-of-function defect	(Lehnart <i>et al.</i> , 2004)
R4497C/ R4496C	TMD	93	HEK293	Increased RyR2 channel activity in particular at low Ca <sup>2+</sup> concentrations, the charge and polarity at residue 4496 plays an essential role in RyR2 channel gating	(Jiang <i>et al.</i> , 2002)
			HL-1	Increased Ca <sup>2+</sup> release and RyR2: FKBP12.6 dissociation	(George, Higgs and Lai, 2003)
			HEK293	Dissociation of FKBP12.6 from the channel	(Wehrens <i>et al.</i> , 2003)
			HEK293	enhancing RyR2 luminal Ca <sup>2+</sup> activation, reduce the threshold for SOICR	(Jiang <i>et al.</i> , 2004)
			mice	the first experimental demonstration that the R4496C RyR2 mutation predisposes the	(Cerrone <i>et al.</i> , 2005)

				murine heart to VT and VF in response caffeine and/or adrenergic stimulation	
			mice	induce abnormal calcium transients in the absence of adrenergic stimulation, RyR2–FKBP12.6 interaction is not involved	(Liu <i>et al.</i> , 2006)
			mice	the His–Purkinje system is an important source of focal arrhythmias in CPVT. monomorphic VT was clearly unifocal, whereas bidirectional VT was bifocal. Polymorphic VT was initially multifocal but eventually became reentrant and degenerated into ventricular fibrillation	(Cerrone <i>et al.</i> , 2007)
			mice	higher spontaneous Ca <sup>2+</sup> release during diastole, because of a dramatic increase in Ca <sup>2+</sup> sensitivity	(Fernández-Velasco <i>et al.</i> , 2009b)
			mice	RyR leak lowers both SR Ca content and the threshold for waves. β -Adrenergic stimulation produces Ca <sup>2+</sup> waves by increasing SR Ca <sup>2+</sup> content and not by lowering threshold	(Kashimura <i>et al.</i> , 2010)
			mice	Purkinje cells display a greater propensity to develop abnormalities in intracellular Ca <sup>2+</sup> handling than ventricular myocytes	(Kang <i>et al.</i> , 2010)
			mice	focally activated arrhythmias originate in the specialized electrical conducting cells of the His-Purkinje system	(Herron <i>et al.</i> , 2010)
			mice	Na <sup>+</sup> -dependent SR Ca <sup>2+</sup> overload—in the absence of β -adrenergic stimulation—is sufficient to increase the propensity for triggered arrhythmias	(Sedej <i>et al.</i> , 2010)
			mice	Overexpression of CaMKII δ c in RyR2 <sup>R4496</sup> <sub>C+/-</sub> knock-In mice leads to altered intracellular Ca <sup>2+</sup> handling and increased	(Dybkova <i>et al.</i> , 2011)

				mortality, indicating that CaMKII contributes to further destabilization of a mutated RyR2	
			mice	CaMKII inhibition prevented catecholamine-induced sustained VT in vivo and blunted triggered activity and transient inward currents induced by iso in vitro, mechanistically by an attenuation of SR Ca <sup>2+</sup> leak and blunting catecholamine-mediated SERCA activation	(Liu <i>et al.</i> , 2011)
			mice	an unanticipated decrease in SAN automaticity by a Ca <sup>2+</sup> -dependent decrease of I <sub>Ca,L</sub> and SR Ca <sup>2+</sup> depletion during diastole	(Neco <i>et al</i> 2012)
			mice	mutated RyR2s are functionally normal at rest but display a high degree of Ca <sup>2+</sup> release variability (CRV) on intense adrenergic stimulation. CRV is a Ca <sup>2+</sup> release abnormality, resulting from electric defects rather than the failure of the Ca <sup>2+</sup> release response to action potentials in mutated ventricular myocytes	(Chen <i>et al.</i> , 2012)
			mice	increased RyR2 activity, Ca <sup>2+</sup> spark and wave frequencies	(Savio-Galimberti and Knollmann, 2015)
			mice	the constitutive [Na <sup>+</sup> ] <sub>i</sub> excess of Purkinje cells promotes triggered activity and arrhythmogenesis at lower levels of stress than ventricular myocytes	(Willis <i>et al.</i> , 2016)
			mice	Reduced positive inotropic responses due to larger SR Ca <sup>2+</sup> leakage resulting from faster recovery from inactivation of the RyR2 <sup>R4496C</sup> channels	(Ferrantini <i>et al.</i> , 2016)
			mice	selectively silenced mutant RYR2 <sup>R4496C</sup> mRNA reduces iso-induced DADs and triggered activity, adrenergically mediated	(Bongianino <i>et al.</i> , 2017)

				VT, ultrastructural abnormalities and mitochondrial abnormalities	
S4565R	TMD	94	HEK293	displayed a significant gain-of-function phenotype during diastole	(Tester, 2007)
I4587V	TMD	94	hiPSC-CM	At 1Hz stimulation, iso induced an abnormal diastolic Ca <sup>2+</sup> increase and DADs in AP more frequently in CPVT, but not in spontaneous beating	(Sasaki <i>et al.</i> , 2016)
V4653F	TMD	97	HEK293	increased the sensitivity of RyR2 to activation by luminal Ca <sup>2+</sup>	(Jones <i>et al.</i> , 2008)
			HEK293	decreased binding of calstabin2 (FKBP12.6), gain-of-function defect	(Lehnart <i>et al.</i> , 2004)
V4653F	TMD	96	HEK293	decreased binding of calstabin2 (FKBP12.6), gain-of-function defect	(Lehnart <i>et al.</i> , 2004)
A4860G	TMD	101	HEK293, HL-1	diminished the response of RyR2 to activation by luminal Ca <sup>2+</sup> , but had little effect on the sensitivity of the channel to activation by cytosolic Ca <sup>2+</sup>	(Jiang <i>et al.</i> , 2007)
			HEK293	increased the threshold for SOICR	(Jones <i>et al.</i> , 2008)
			mice	decreased the peak of Ca <sup>2+</sup> release during systole, gradually overloading the sarcoplasmic reticulum with Ca <sup>2+</sup> , activating electrogenic Na <sup>+</sup> -Ca <sup>2+</sup> exchanger activity and triggering early afterdepolarizations	(Zhao <i>et al.</i> , 2015a)
I4867M	CT	102	HL-1, HEK293	enhanced propensity for SOICR	(Jiang <i>et al.</i> , 2005)
V4880A	CT	102	HEK293	Increased the sensitivity to cytosolic and luminal Ca <sup>2+</sup> activation and increased the propensity and reduced the threshold for arrhythmogenic spontaneous Ca <sup>2+</sup> release	(Sun <i>et al.</i> , 2016)

N4895D	CT	103	HEK293	enhancing RyR2 luminal Ca <sup>2+</sup> activation, reduce the threshold for SOICR	(Jiang <i>et al.</i> , 2004)
--------	----	-----	--------	---	---------------------------------

## VI Treatment of CPVT

### VI.1 Traditional treatments

Given the cardiac events are directly induced by catecholamines, the most initial and typical treatment of CPVT is to block the adrenergic receptor by  $\beta$ -blockers. According to experience,  $\beta$ -blockers have been considered the best therapeutic option in CPVT (Leenhardt *et al.*, 1995). By doing a follow-up study of 101 CPVT patients, Hayashi et al compared cardiac event rates between patients with and without  $\beta$ -blockers and confirmed that patients with  $\beta$ -blockers presented significantly lower cardiac fatal or near-fatal event rates (Hayashi *et al.*, 2009). They also suggested that  $\beta$ -blockers should be prescribed in every CPVT patient regardless of any prior syncopal events or patients with an implantable cardioverter-defibrillator (ICD) because ICDs do not always terminate CPVT. Meanwhile, they also noticed that  $\beta$ -blockers hardly gave protection to children because  $\beta$ -blockers dosage based on weight might be insufficient in children due to age-dependent hepatic clearance of  $\beta$ -blockers (Hayashi *et al.*, 2009). Numerous other reports also highlighted that  $\beta$ -blockers are not completely effective in preventing life-threatening arrhythmias (Priori *et al.*, 2002)(Bauce *et al.*, 2002)(Sumitomo *et al.*, 2003)(Haugaa *et al.*, 2010). Thus, ICD, another efficacious traditional treatment for CPVT, is often recommended to the patients who continue to have ventricular arrhythmias despite  $\beta$ -blockers therapy. However, ICDs are still not fully protective and can be proarrhythmic in CPVT patients because both appropriate and inappropriate ICD shocks can trigger catecholamine release, subsequently resulting in multiple shocks (arrhythmic storm), and death (Mohamed *et al.*, 2006)(Pizzale *et al.*, 2008), not to mention the complicated operations and high costs of ICDs. Therefore, searching for more effective and more convenient treatment can never stop.

### VI.2 Novel exploring treatments

As mentioned above, CPVT is a life-threatening disease and traditional treatment only provide partial protection, so many investigators endeavor to explore new treatments or concomitant therapies to improve outcome in CPVT patients. For example, Park's group found that RyR2-serine 2814 phosphorylation by CaMKII is necessary to unmask the latent

arrhythmic potential of the RYR2<sup>R4651I</sup> CPVT mutation (Park *et al.*, 2019). They subsequently created a gene therapy platform by inhibiting CaMKII in mouse model and demonstrated that AAV9-mediated delivery of a CaMKII peptide inhibitor to the heart was effective in suppressing arrhythmias in a CPVT mouse model (RyR2<sup>R176Q</sup>) (Bezzarides *et al.*, 2019). Another group designed a gene therapeutic approach to silence mutant mRNA by siRNAs and found that it rescues ultrastructural and arrhythmic phenotype in mice carriers of the RyR<sup>R4496C</sup> Mutation (Bongianino *et al.*, 2017). However, due to the technical complexity and risky, it has long way to go for these gene therapies in clinical application. In contrast, some concomitant therapies in combination with  $\beta$ -blockers have been confirmed to increase efficacy, such as flecainide, a Na<sup>+</sup> channel blocker which has been demonstrated to inhibit arrhythmogenic Ca<sup>2+</sup> waves and reduce Ca<sup>2+</sup> spark mass (Van Der Werf *et al.*, 2011) and verapamil, a Ca<sup>2+</sup> channel blocker which has been demonstrated to prevent exercise-induced arrhythmias in treatment with  $\beta$ -blockers on CPVT (Rosso *et al.*, 2007), which both have already been used in clinics. Moreover, dantrolene, a therapeutic agent for malignant hyperthermia (MH, an autosomal dominant pharmacogenetic disorder of skeletal muscle related to RyR1 mutation) (Roesl *et al.*, 2014), has also been found to inhibit CPVT arrhythmias in a RyR2<sup>R2474S/+</sup> knock-in mouse model presumably by inhibiting Ca<sup>2+</sup> leak through the RyR2 (Kobayashi *et al.*, 2010) as well as in patient-specific hiPSC-CM model (Penttinen *et al.*, 2015)(Jung *et al.*, 2012a). Thus, testing the antiarrhythmic function of present blockers or medicines may be an effective way for exploring new treatment of CPVT, while hiPSC-CM may provide a valuable tool for patient-specific drugs screening (Acimovic *et al.*, 2018)(Maizels *et al.*, 2017)(Preininger *et al.*, 2016).

We have gotten an information that a CPVT patient carrying RyR2<sup>C2277R</sup> who has undergone several effort syncope, doesn't present CPVT syndrome during evaluation after having taken several medicines (including venlafaxine, pregabalin, terazosin, Oxycodone, naloxone, and tetrazepam) to cure other diseases. So, we are curious about the possible effects of those medicines on calcium handling in cardiomyocytes. As mentioned above, the ion channel blockers such as flecainide and verapamil present antiarrhythmic function, thus we started by venlafaxine and pregabalin since they were demonstrated to block sodium channel and calcium channel respectively, which will be explained in detail later.

### **VI.2.1 Venlafaxine**

Venlafaxine, chemically named 1-[2-(dimethylamino)-1-(4-methoxyphenyl) ethyl] cyclohexanol, is used to treat major depressive disorder, anxiety, and panic disorder, which has been

synthesized and clinically evaluated by Wyeth Laboratories (Muth *et al.*, 1986)(Yardley *et al.*, 1990) and was first marketed in United States in 1993 (Holland and Brown, 2017). Its chemical molecular formula is  $C_{17}H_{27}NO_2$  and chemical 2D structure and 3D conformer as shown in Figure 21. Venlafaxine works as a serotonin-norepinephrine reuptake inhibitor (SNRI) to cure depression through blocking the serotonin and norepinephrine transporters (SERT, also known as Slc6a4, and NET, also known as Slc6a2, respectively) (Laurent *et al.*, 2016), but it blocks the two transporters in sequential manner, which means that it initially inhibit serotonin reuptake followed by the inhibition of norepinephrine reuptake at higher dose (Sansone and Sansone, 2014). Venlafaxine has been reported to block  $I_{Na}$  following its binding to the resting state of the channel (Khalifa, Daleau and Turgeon, 1999). Indeed, case reports about the cardiotoxicity of venlafaxine include bradycardia caused by interaction of venlafaxine and cyclosporine (Azizi, Elyasi and Roodposhti, 2019), risk of congenital heart disease in newborns with prenatal exposure (Desai *et al.*, 2019) and heart failure (Singh *et al.*, 2019). However, comparing the effect of duloxetine, another SNRI, and venlafaxine on blockage of Nav1.5, a research study demonstrated that venlafaxine almost failed to induce use-dependent block on Nav1.5 in cardiomyocytes while low concentrations of duloxetine (1, 10 mM) induced prominent use-dependent block, and they further emphasized that an inhibition of  $Na^+$ -channels does not predict a clinically relevant cardiotoxicity (Stoetzer *et al.*, 2016).

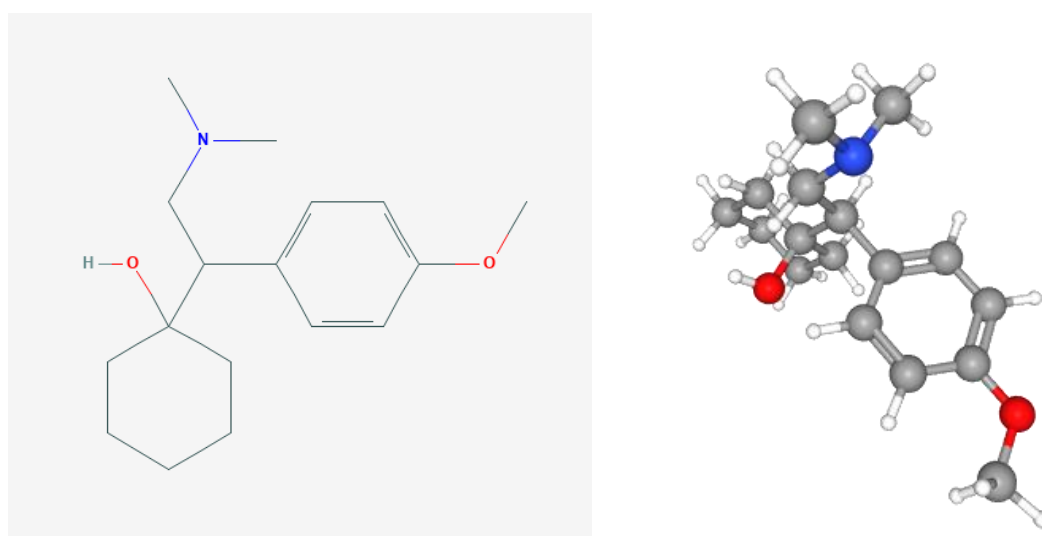


**Figure 21. 2D chemical structure and 3D conformer structure of venlafaxine.** (adapted from PubChem URL: <https://pubchem.ncbi.nlm.nih.gov>)

## VI.2.1 Pregabalin

Pregabalin ((S-(+)-3-isobutylgaba)) was synthesized as an anticonvulsant (Taylor, Angelotti and Fauman, 2007) and was approved for medical use in the United States in 2004. Then it is widely used in the treatment of postherpetic neuralgia, diabetic neuropathic pain, partial seizures, anxiety disorders and fibromyalgia (Ho *et al.*, 2013)(Fink *et al.*, 2002). Its chemical molecular formula is  $C_{17}H_{27}NO_2$  and chemical 2D structure and 3D conformer as shown in Figure 22. Pregabalin has been reported to achieve its anxiolytic effect by binding to the  $\alpha 2\delta$  subunit of the P/Q-type of neuronal voltage-gated calcium channel (Mico and Prieto, 2012)(Bian *et al.*, 2006) that wasn't widely accepted as potential antiepileptic drugs target (Taylor, Angelotti and Fauman, 2007). The  $\alpha 2\delta$  subunit has been demonstrated to be essential in E-C coupling by siRNA knockdown computer model (Tuluc *et al.*, 2007). Indeed, some reports indicate that pregabalin caused heart failure, an adverse outcome that has not been found with the less potent calcium channel antagonist gabapentin (Murphy *et al.*, 2007)(Page *et al.*, 2008)(De Smedt *et al.*, 2008). However, after studying 9855 older patients with a seizure disorder who initiated pregabalin and an equal number treated with gabapentin, Ho et al demonstrated that pregabalin was not associated with an increased risk of heart failure relative to gabapentin, and in contrast, they observed a trend toward a lower risk of heart failure with pregabalin compared to gabapentin in those patients, which may reflect pregabalin's greater vasodilatory effect on arterial myocytes that could reduce afterload and enhance cardiac function (Ho *et al.*, 2017). Moreover, by reviewing the present reported cases, pregabalin has been demonstrated to be a well-tolerated and consistently effective treatment for generalized anxiety disorder, with a unique mechanism of action that makes it a useful addition to the therapeutic armamentarium (Baldwin *et al.*, 2015).

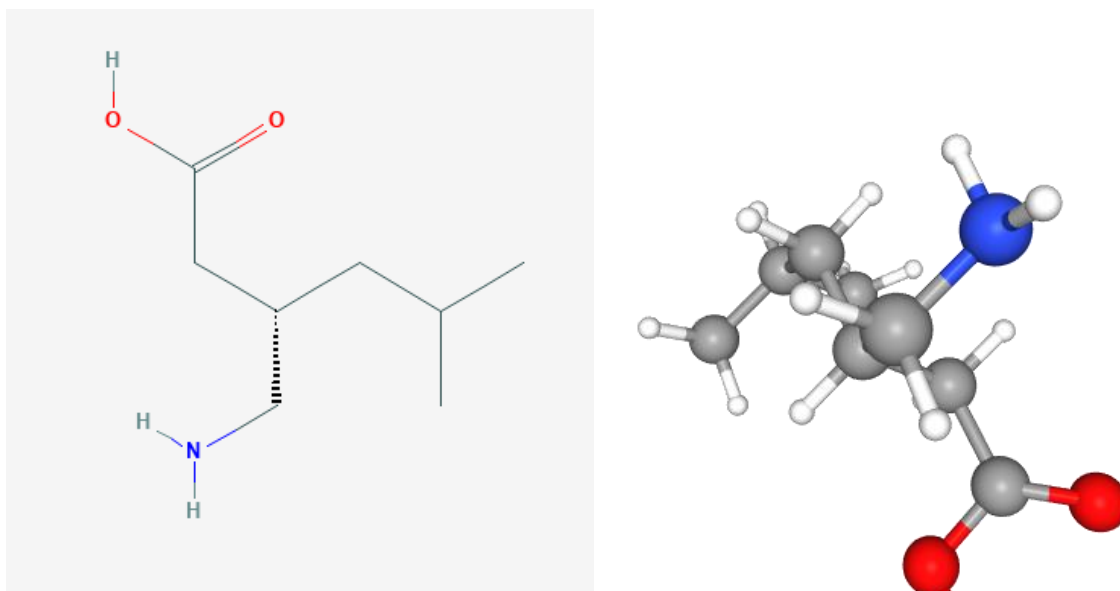


**Figure 22. 2D chemical structure and 3D conformer structure of Pregablin.** (adapted from PubChem URL: <https://pubchem.ncbi.nlm.nih.gov>)

## VII objectives

CPVT1 is a life-threatening genetic disease caused by mutations on RyR2. RyR2 mediate rapid  $\text{Ca}^{2+}$  efflux from SR thereby triggering numerous  $\text{Ca}^{2+}$ -activated physiological processes. RyR2 mutations can induce  $\text{Ca}^{2+}$  handling dysregulation and damage the physiological processes, thereby triggering life-threatening arrhythmias. So far, RyR2 mutations in three hotspots (N-terminal domains, central domain and C-terminal domains) as well as mutations out of those hotspots have been found to be involved in CPVT1. However, the mechanisms of RyR2 mutations causing CPVT may vary from domain to domain, even from mutation to mutation, which are under huge controversy until now. Thus, in this thesis, based on the previous researches from our team and our collaborators, my **first objective** was to functionally study a novel N-terminal mutation RyR2<sup>R420Q</sup>, which has been identified in a Spanish family by our collaborators, in patient specific iPSC-CM, hoping to gain the knowledges of underlying mechanisms of CPVT1 in human cardiomyocytes.

Given the life-threatening characteristic of CPVT, without proper treatment, it can cause SCD in early age. However, the present treatment of CPVT are limited and can't provide complete protection. Moreover, numerous researches found the effects of many medications vary among different mutations even among different patients. Thus, it is urgent to explore more effective treatments and to establish personal treatment. We have gotten an information that a CPVT patient carrying RyR2<sup>C2277R</sup> who has undergone several effort syncope, doesn't

present CPVT syndrome during evaluation after taken several medicines to cure other diseases. It's reasonable to doubt that one or some of those medicines may provide protection of CPVT. Thus, my **second objective** was to detect the effects of those medicines on Ca<sup>2+</sup> handling and SR Ca<sup>2+</sup> leak in our established RyR2<sup>R420Q</sup> knock-in mouse model, and in CPVT (RyR2<sup>R420Q</sup>) patient specific iPSC-CM, hoping to make contribution to CPVT treatment.

# **Methods and materials**



In this project, we aimed to analyze the dysfunction of RyRs variants and mutants to see if and how they can underlie arrhythmic behavior. We also tried to do some pharmacology to test if it can be solved.

To do that we used different materials:

- ✓ Human cardiomyocytes derived from induced pluripotent cells from 2 individuals of the same family in which has been identified a CPVT mutation RyR2<sup>R420Q</sup>.
- ✓ Mice KI for the mutation RyR2<sup>R420Q</sup>
- ✓ HEK293 cells expressing the variant RyR2<sup>D3291V</sup> found in a French family with sudden death.

We also used different techniques:

- ✓ Because the RyR2 is an internal channel responsible of Ca<sup>2+</sup> release, we measured intracellular calcium handling by **confocal microscopy**
- ✓ To see how the potential intracellular Ca<sup>2+</sup> mishandling can induce proarrhythmic behavior, we measured the action potential by **microelectrodes technique**
- ✓ In order to analyze the level and localization of the proteins, we used **biochemical techniques** such as immunolabelling and Western Blots.

## **I. CPVT (RyR2<sup>R420Q</sup>) patient specific iPSC cell culture and differentiation into cardiomyocytes**

A novel CPVT mutation located on RyR2 N terminal portion (RyR2<sup>R420Q</sup>) has been identified in a Spanish family (Domingo *et al.*, 2015). According to the studies of RyR2 function in HEK293 cell line, this mutation presented gain of function in low cytosolic intracellular Ca<sup>2+</sup> concentration and loss of function at high Ca<sup>2+</sup>. Moreover, KI mice heterozygous for this mutation presented bradycardia and sino-atrial node (SAN) dysfunction (Wang *et al.*, 2017). In order to further study the dysfunction of this mutation in human cells, we generated induced pluripotent stem cell (hiPSC) from peripheral blood mononuclear cells (PBMC) of two brothers (one with mutation, the other without mutation as control) by introducing the 4 factors (Oct3/4, Sox2, Klf4 and c-Myc) (Takahashi *et al.*, 2007). This step has been done by the stem cell platform at Nantes. The volunteers for blood donation were indicated by red arrows in pedigree of this family as shown in Figure 23. Then the hiPSC were differentiated into cardiomyocytes (hiPSC-CM) in my lab. hiPSCs are pluripotent stem cells as embryonic stem cells (ESCs)

generated by reprogramming four transcription factors (Oct4, Sox2, cMyc, Klf4) of the adult cells, which were first obtained and termed by Shinya Yamanaka's team at Kyoto University, Japan, in 2006 (Takahashi and Yamanaka, 2006). With the improving of the methods, the new generation of iPSCs possess identical function as ESCs, except the ability to form a completed individual, which perfectly avoids the ethical issues. Since iPSCs can be made in a patient-matched manner, it became a very popular and useful tool for patient-specific disease study (especially for genetic disease) and patient-specific curing.

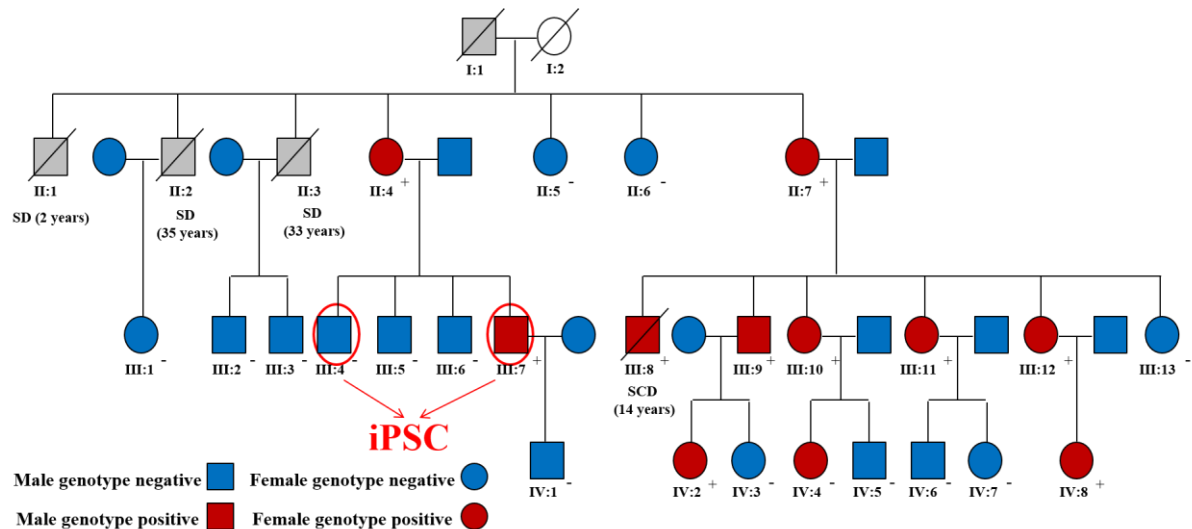


**Figure 23. Pedigree of the Spanish family with CPVT1 caused by RyR2<sup>R420Q</sup>.** The red circle depicts the members that donated blood to generate hiPSCs. (modified from (Domingo *et al.*, 2015))

## I.1 hiPSCs culture

In order to keep its pluripotent function, the hiPSCs culturing is much stricter than for other cells lines. Since the compositions of fetal bovine serum (FBS) is complicated and hard to control, it should be absent in the iPSCs culture. Antibiotics are also forbidden during iPSCs culturing, thus contamination risk increased. StemMACS iPS-BrewXF and mTeSR<sup>TM</sup>1 are two kind of generally used culture medium for iPSCs. We have tested both and found mTeSR<sup>TM</sup>1 is better for our hiPS clones. mTeSR<sup>TM</sup>1 is a highly defined, feeder-free medium suitable for hESC and iPSCs. It contains only the most critical components required to maintain hESC and hiPSCs, providing a simpler condition for pluripotent stem cell culture. The commercial mTeSR<sup>TM</sup>1 containing two parts, mTeSR<sup>TM</sup>1 basal medium and mTeSR<sup>TM</sup>1 5x supplement, once mixed, it should be stored in 4°C less than 2 weeks and in -20°C less than 2 months. Extracellular matrix component is also necessary for maintaining the pluripotent,

undifferentiated state (self-renewal) of hiPSCs in the absence of feeder cells. In this project, we used diluted Matrigel. A new bottle of Matrigel was aliquoted according to the instruction book and stored in  $-20^{\circ}\text{C}$ . Each time an aliquot was diluted in 24 mL Dulbecco's Modified Eagle Medium/Nutrient Mixture F-12 (DMEM/F12 medium, a 1:1 mixture of DMEM and Ham's F-12 combining DMEM's high concentrations of glucose, amino acids, and vitamins with F-12's wide variety of components providing basal medium for supporting the growth of a variety of mammalian cultures.). Then certain volume was added to each well and each dish needed (the volumes are shown in table 3). During the Matrigel preparing, it is important to not overheat it above  $4^{\circ}\text{C}$  which demand an ice bath. Before all the application of hiPSCs, the first thing is to prepare plates with diluted Matrigel, because it takes at least 1 h to form a membrane covering the surface of the plates in room temperature to support the cell culture as well as make the vision for cell observation.

✓ **Table 3: volumes of Matrigel for different type of plates**

<i>Type of plate</i>	<i>Volume of Matrigel</i>
<i>dish 10 cm</i>	6 mL
<i>6-wells plate</i>	1 mL
<i>12-wells plate</i>	500 $\mu\text{L}$
<i>24-wells plate</i>	250 $\mu\text{L}$

### **I.1.1 Thaw the hiPSCs**

The plates covered with Matrigel and culture medium were prepared before taking out the cell from the nitrogen. Rho-Associated Coil Kinase (ROCK) inhibitor Y27632 ( $5\ \mu\text{M}$ ) was added to mTesR<sup>TM</sup>1 culture medium to increases the survival of hiPSC. Once all the materials were ready, a tube of hiPSC was taken from the nitrogen and defrost quickly in a water bath at  $37^{\circ}\text{C}$  without immersing the cork (only a small ice cube should remain after 2-3 minutes). Then the tube was well disinfected with 70% ethanol to avoid contamination and the contents of the tube was transferred to a 15 mL falcon in hood. Following that, mTesR<sup>TM</sup>1 with Y27632 was

added dropwise with homogenizing by rotation to a final volume of about 10 mL. After Centrifuge at 200g for 5 minutes, the supernatant was aspirated and the pellet was resuspended in 3 mL of mTesR™1 with Y27632 and mixed gently with a pipette. Then 2 mL of cells was seeded in 1 well of 6-well plate, and the remaining volume of this cell was seeded in another well of the same plate with adding 1 mL of fresh mTesR™1. There is thus a 2/3 - 1/3 distribution for the 2 wells inoculated providing the choice of different density for next passage. Then homogenize crosswise and incubate at 37 °C, 5% CO<sub>2</sub> overnight. The medium was changed next day and every other day until the passage.

### **I.1.2 Passage of hiPSCs**

There are 3 general methods for passage of hiPSCs. The first, also the original one, is to cut the choosing clusters by needle into small squares and detach the small square of clusters by the needle or pipette. However, this method is less frequently used nowadays because it is more laborious, time-consuming and not useful for large scale expansion. The second one is the passage of single cell by dissociated the cells using Accutase. Accutase is a marine-origin enzyme with proteolytic and collagenolytic activity for the detachment of primary and stem cell lines and tissues. This method results in high expansion rate since seeding by single cells, but the handling time is still relatively long since it need to centrifuge before seeding, and overall, it is more stressful to the cells. The third one, also the one we used, is to pass the cells in small clusters by using Ethylenediaminetetraacetic acid (EDTA) as passage solution. The usefulness of EDTA arises because of its role as a hexadentate ("six-toothed") ligand and chelating agent which make it able to sequester metal ions such as Ca<sup>2+</sup> and Fe<sup>3+</sup>. Ca<sup>2+</sup> is necessary for hiPSCs touching to the bottom and it is removed by EDTA gently detaching hiPSCs without over breaking the clusters. Then the small clusters can be directly diluted (1/6, 1/9, or 1/12 depending on demand and cell line) and seeded in new plates. Thus, this method is less laborious, time-saving, and the more important thing is less stressful to the cells.

The passage could be done when the cells grow into 70% -80% confluence. The pass ratio is usually 1/6 but can be modified according to lineage and/or experimental needs. The materials such as mTesR™1, 6-well plate with Matrigel and passage solution (0.5 mM EDTA) were prepared before starting the procedure. A plate of hiPS cells was taken out of incubator, and after a visual check of the cells, culture medium was completely removed. Then cells were rinsed once by PBS and 1 mL of passage solution was added to each well. The incubation time with EDTA are given as an indication (about 3 min) and can also vary greatly from one cell

line to another. Once the colonies edge starts to detach, the passage solution was removed and replaced by fresh medium. Then the colonies were dissociated by gentle pipetting up and down. The passage should be done carefully to avoid breaking cell clusters too much. The necessary amount of the resulting clusters was distributed to new pro-coated plates in mTesR<sup>TM</sup>1. The plates were homogenized crosswise and incubated at 37 °C, 5% CO<sub>2</sub> overnight. The medium was changed every day until the next passage.

### **I.1.3 Freeze hiPSCs**

HiPSCs can be frozen at the time of a passage, by which we can make a cell bank for each hiPSCs line. PSC Cryomedium was used as the freeze solution in this project. The protocol for harvesting the cell clusters was similar as cell passage. Instead of distributed into the new plates, the resulting clusters were centrifuged at 200g for 5 minutes in room temperature. Then cold Cryomedium PSC (approximately 4 °C) was added to the pellet dropwise while rotating to homogenize at the same time. The harvested cells in cryomedium were aliquoted into cryotubes and placed in a cryo-box. Then the cryo-box was quickly placed in -80 °C freezer and quickly transferred into liquid nitrogen the following day.

## **I.2 hiPS cell differentiation into cardiomyocytes**

The first reported method for differentiating PSCs into cardiomyocytes was using embryoid bodies (EBs) (Kehat *et al.*, 2001). The main principle of this method is to grow the PSCs on feeder cells to form EBs. Then differentiate the EBs by changing the culture medium to differentiation medium. At beginning, the efficiency was only 5% to 10%, but after a series of improvement, it is still a general used method nowadays. Since the three families of protein growth factors, bone morphogenetic proteins (BMPs), the Wingless/INT proteins (WNTs) and the fibroblast growth factors (FGFs), which control early stages of mesoderm formation and cardiogenesis are expressed in the endoderm, co-cultured with visceral endodermal-like cells was also demonstrated to be a practical method for cardiac differentiation of PSCs (Mummery *et al.*, 2003), but the complicated handling and unconfirmed effect of the new introduced cell line hampered its development. The third method is monolayer differentiation which is feeder cell free. Benefit from the simplification of the protocol and well controlled culture materials, it became the most widely used method especially for large scale expansion. More recently, in order to eliminate more uncontrolled factors, Paul W. Burridge and X Lian launched a

chemically defined and small molecule-based differentiation method successfully (Paul W. Burridge, 2014), which ideally avoided using animal-derived products. We tried a protocol adapted from their methods firstly, but unfortunately, the efficiency and success rate were unstable for our cell lines. So, lastly we changed to Gsk3 inhibitor and Wnt inhibitor (GiWi) protocol (X. Lian et al. 2012) (X Lian et al. 2013) in which the chemical molecules were replaced by B27 without insulin or completed B27.

When hiPSCs in maintenance reach to 70% - 80% confluence, they can be used to launch a differentiation protocol. Accutase was used to dissociate iPSC colonies into single cells and rock inhibitor Y27632 (5  $\mu$ M) was used to protect single cells from damage. Briefly, the medium was completely removed from the plates followed by washing the cells once with PBS. Then accutase was added to cells and stay for 5 min at 37 °C. After getting single cells, accutase was removed by centrifugation at 200g for 5 minutes and the pellet was suspended by mTesR™1 medium with Y27632. Then the cell density was counted on Mallasez chamber diluted (1/2) in Trypan Blue. The seeding density is pretty important since proper density will help to form the good monolayer for differentiation. In this method, the cell density must be between 100,000 and 200,000 cells/cm<sup>2</sup>. At last, the plates were homogenized cross-cell distribution and incubated at 37 °C, 5% CO<sub>2</sub>, which counted as Day-2. Then following the protocol as shown in figure 24, the medium was changed every other day and the 6  $\mu$ M Wnt activator CHIR99021 was added on day 0 and the inhibitor of Wnt was added on day 3. Before day 7, insulin was eliminated from B27 since it has been reported to strongly inhibit cardiac differentiation by promoting ectoderm development but restricting the others germ layers. Obvious spontaneous beating part start to form at day5 to day7. After that, cells were maintained with complete B27 until detached and transferred to new dishes around day 18. With maintaining in B27, more and more cells start to contract until the whole well formed a beating wave, so the cells shouldn't be transferred before day 15.

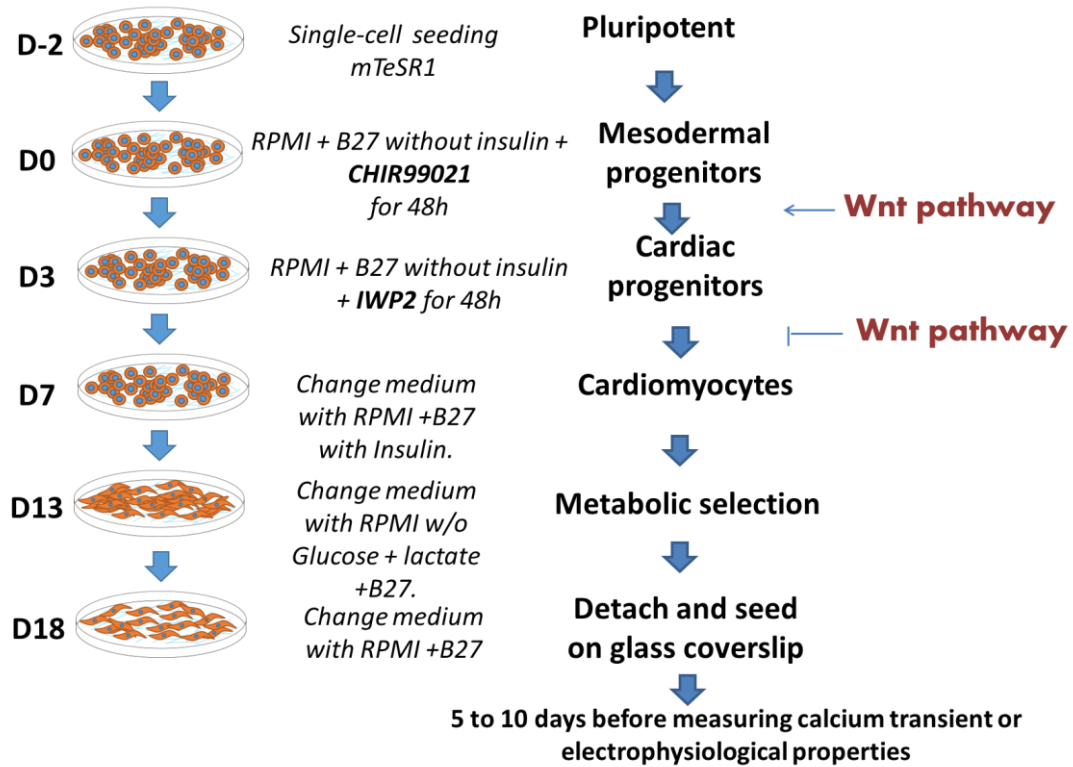


**Figure 24: Protocol of hiPSCs differentiation into cardiomyocytes.** 6  $\mu\text{M}$  CHIR99021, 5  $\mu\text{M}$  IWP2 were used to treat cells.

### I. 3 Recovery and maturation of hiPSC-CMs

The hiPSCs derived cardiomyocytes were detached and seeded into new containers after day 18 as shown in Figure 24 depending on the experiments, seeding in seeded in 35 mm  $\mu$ -dish with glass bottom with small chambers (Ibidi, Clinisciences, France) for calcium handling measurement, immune labeling and action potentials recording by micro-electrode technique, seeding in 12-well plates for protein and RNA extraction, and seeding on small glass coverslips for patch clamp. Briefly, the cardiomyocytes were rinsed once by PBS after culture medium completely removed. TrypLE was used to detach and dissociate the cells to get single cells. TrypLE Express is an animal origin-free, recombinant enzyme used for dissociating a wide range of adherent mammalian cells, which cleaves peptide bonds on the C-terminal sides of lysine and arginine, and is a direct replacement for trypsin. Its exceptional purity increases specificity and reduces damage to cells that can be caused by other enzymes present in some trypsin extracts. Cells were incubated with TrypLE two times with 5 min for each time at 37 °C, first incubation for detaching the cells and second incubation for dissociating the cells into

single cells. Then the equivalent volume of RPMI 1640 with 20% FBS was added to make TrypLE lose efficacy. RPMI 1640 is a widely used basal medium for many cells culture especially for suspension cells culture. It contains the reducing agent glutathione and high concentrations of vitamins as well as biotin, vitamin B12, and PABA, which are not found in DMEM. TrypLE was removed by centrifugation and the pellet was resuspended in RPMI 1640 with B27. Finally, the cells were seeded in certain density according to applications. Then the cells were maturing in RPMI 1640 with B27 until day 32.

## II Dissociation of ventricular cardiomyocytes from RyR2<sup>R420Q</sup> knock-in mice

In this project, we use langendorff method for ventricular cardiomyocytes dissociation. It is a traditional method and demands a lot of experience for operation. In order to decrease the difficulties for novices, many langendorff free methods were exploited. Since we already had great experience and good experts for langendorff method to ensure success rate in our lab, we still chose it for our cell dissociation.

### II.1 solution preparation

✓ **Table 4: basal solution for mice ventricular cardiomyocytes dissociation**

<i>Reagent</i>	<i>Molar mass (g/mol)</i>	<i>Concentration (mM)</i>	<i>g/250 ml</i>	<i>g/500 ml</i>
<i>NaCl</i>	58.4	113	1.65	3.30
<i>KCl</i>	74.5	4.7	0.087	0.175
<i>MgSO<sub>4</sub></i>	246.47	1.2	0.073	0.147
<i>or</i>	120.40		0.036	0.072
<i>KH<sub>2</sub>PO<sub>4</sub></i>	136.09	0.6	0.020	0.040
<i>NaH<sub>2</sub>PO<sub>4</sub></i>	156.02	0.6	0.023	0.046
<i>HEPES</i>	238	10	0.595	1.190
<i>NaHCO<sub>3</sub></i>	84.01	1.6	0.033	0.067
<i>Taurine</i>	125.15	30	0.940	1.880

<i>Glucose</i>	180.00	20	0.900	1.800
<b>Adjust pH to 7.4 with 10N NaOH</b>				

## II.2 Ethics statement

All animal experiments were performed in accordance to the European Community guiding principles, the local ethics committee guide lines, and the French decree in the care and use of animals. Authorizations were manipulated according to the decree obtained from the French Ministry of Agriculture, Fisheries and Food.

## II.3 dissociation process

The mouse was anesthetized by intraperitoneal injection of Pentobarbital (150 mg /kg) and the whole heart including adipose tissue was removed and placed into pre-cooled basal dissociation solution immediately. After removed the redundant tissue and vessels, the heart was cannulated through ascending aorta. Once the cannulated heart set into the langerdorff system, the perfusion was started to rinse the blood by basal solution around 4 min and softened the heart by massaging with two fingers several seconds meanwhile. Then the Liberase™ diluted by basal solution was added to the perfusion system. At beginning, the perfuse drop goes rather slower, but once the aortic valve digested, it accelerates suddenly, which is the sign for ending the perfusion. Then the atria were discarded and the ventricles were placed into warm recovery solution 1 (basal solution containing 0.2 mM Ca<sup>2+</sup> and 5 mg/mL BSA). The ventricles were cut into small pieces and homogenized by pipetting up and down several times to dissociate the cells. Then the suspension was filtered through a nylon mesh to remove the tissue. The cells suspension in recovery solution 1 was incubated at 37°C for 10 min to deposit the cells. Then the supernatant was removed and recovery solution 2 (basal solution containing 0.5 mM Ca<sup>2+</sup> and 5 mg/mL BSA) was used to resuspend the cells. After another 10 min incubation with recovery solution 2, the cells were suspended in store solution (basal solution containing 1 mM Ca<sup>2+</sup>) until use at room temperature.

## III HEK293 cell line culture and transfection by RyR2<sup>D3291V</sup> plasmid

This part belongs to Malorie Blancard's thesis project directed by Pascale Guichenay, and the HEK293 cells were taken from her lab (UMRS 1166, Paris, France). As they didn't had

experience with the RyR2, I was involved in this project as a collaboration. We choose the fastest method to analyze the dysfunction of a new discovered RyR2 variant D3291V in a French family with history of sudden cardiac deaths. HEK293 cell line was originally derived from human embryonic kidney cells grown in tissue culture. They have been widely used in cell biology research due to their reliable growth and propensity for transfection. Since there is no endogenous RyRs expression in HEK293 cells, the transfected RyRs are the only ones.

### **III.1 HEK293 cell line culture**

Firstly, fetal bovine serum and Penicillin / Streptomycin were dissolved and aliquoted for preparing the culture medium. DMEM (Dulbecco's Modified Eagle's) with 10% fetal bovine serum and 1% Penicillin / Streptomycin was used to culture HEK293 cells. The cells stored in liquid nitrogen was thawed in 37°C water bath and seeded in T25 flask filling by 6 mL culture medium for the first new passage. The culture medium was changed every 2 days. The cells were ready for passage when they grew into about 80% confluence. 0.05% trypsin-EDTA was used to detach the cells. Briefly, the cells were rinsed once by DPBS after culture medium completely removed. 4 mL of trypsin-EDTA (0.05%) was added and incubated with cells at 37°C for 2 min. Then the cells suspension was divided into T75 flask for scale expansion and ibidi dishes for transfection.

### **III.2 transfect HEK293 cell by RyRD3291V plasmid**

The HEK293 cells seeding in 35 mm  $\mu$ -dish with glass bottom (Ibidi, Clinisciences, France) were used to observe calcium oscillations. Since there is no RyR present in this cells line, the WT RyR and RyR with D3291V mutation have been transfected into cells by lipofectamine before experiments. Transfection solution was composed of 1.5 uL lipofectamine 3000 and 50 uL opti-MEM medium for each dish. The diluted WT and mutated plasmid were mixed with 50 uL opti-MEM with 0.670 uL P3000. Then the plasmid mixture was mixed into transfection solution to get 100 uL total volume for transfection of each dish. The incubation time was increased to 48 h to get higher transfected efficiency because of the large molecular of RyR2.

## **IV Confocal microscopy technique**

The key technique for the confocal microscopy to distinguish from standard fluorescence microscopy is the pinhole. The pinhole is an aperture diaphragm inserting in the conjugate focal plane where “conjugate” come from (Figure 25). In standard microscopy, unless the specimen

is very thin then areas of the specimen above and below the focal plane still contribute to the image as "out of focus blur". With the pinhole, fluorescence emission from planes outside of the primary focus point can be obstructed, which make the resulting image much clearer, even for the thick specimens (Figure 25.). In this project, we use confocal microscopy to observe the  $\text{Ca}^{2+}$  dynamics by fluorescence dye fluo4-AM in mouse ventricular cardiomyocytes and Calbryte™ 520 AM in hiPSC-CMs.

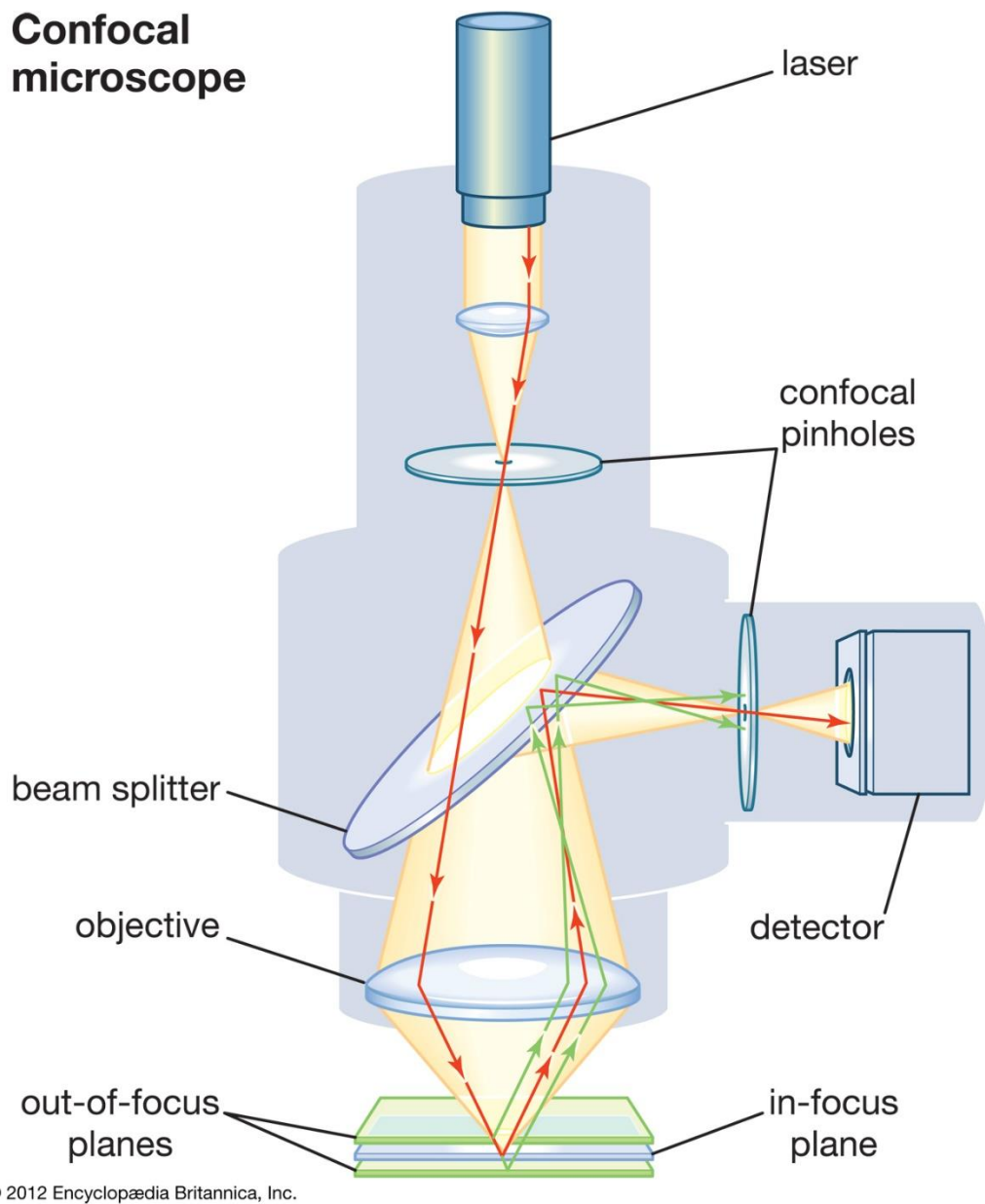


**Figure 25. Schematic diagram of confocal microscopy.** (adapted from <https://www.britannica.com/technology/microscope/Confocal-microscopes>)

## **IV.1 The application of confocal microscopy on hiPSC-CMs**

### **IV.1.1 preparation**

In order to increase the lifetime and keep the good activity of cells, after testing, we decided to use RPMI 1640, the basal medium for hiPSC-CMs maintaining, as basal solution during experiments. Calbryte™ 520 AM (AAT bioquest) has been used as dye for hiPSC-CMs due to its lower toxicity and higher efficiency, excited at 492 nm with a white light laser and emission collected at >514 nm. The cells on 32 to 38 days after differentiation were used to detect the calcium handling. Firstly, cells were dyed by 10  $\mu$ M of Calbryte™ 520 AM for 1 h in incubator at 37°C followed by 15 min at room temperature. Then the cells were ready for recording after removing the medium containing Calbryte™ 520 AM and adding warm fresh RPMI 1640. Meanwhile, all the solutions used for this experiment such as 10 mM caffeine, used for detecting SR content, and 100 nM/1  $\mu$ M iso, used as  $\beta$ -adrenergic receptor activator were prepared. For the pharmacology experiments, 5/2.5  $\mu$ g/mL venlafaxine and pregabalin were also prepared.

### **IV.1.2 record**

**Two-dimension recording mode** with the following parameters: format 512 pixels x 250 pixels, speed 1000 Hz bidirectional, minimize interval, 250 frames was used to record cell's spontaneous contraction. Every recording position was marked by machine so that to observe the same cells in different condition. Then **Line-scan recording mode** with the following parameters: speed 700 Hz, zoom x 2.5, 2000 lines, was used to record the calcium transient of electrically paced cells at 1 Hz. Then 10 mM caffeine was used to measure the SR content. The caffeine effect was recorded by line-scan mode with following parameters: speed 400 Hz, zoom x 2.5, 15000 lines.

### **IV.1.3 Perfusions**

In this project, the effect of iso and two drugs (venlafaxine and pregabalin) has been detected. In each perfusion, the recordings procedures were similar as mentioned above. Cells were perfused with iso for 1 min and drugs for 2 min before recording.

## IV.2 The application of confocal microscopy on mice ventricular cardiomyocytes

### IV.2.1 Solutions

✓ **Table 5: 10 x Tyrode (stock)**

<i>reagent</i>	<i>Molar mass</i> <i>(g/mol)</i>	<i>Concentration</i> <i>(mM)</i>	<i>g/500mL</i>
	PW		
<i>NaCl</i>	58.44	140	<b>40.91</b>
<i>KCl</i>	74.55	4	<b>1.49</b>
<i>HEPES</i>	238.3	10	<b>11.92</b>
<i>MgCl<sub>2</sub></i>	203.3	1.1	<b>1.12</b>
<i>CaCl<sub>2</sub></i>	147.02	1.8	<b>1.32</b>
<b>Adjust PH to 7.4 with NaOH</b>			

✓ **Table 6: 1 x Tyrode**

<i>reagent</i>	<i>Molar mass</i> <i>(g/mol)</i>	<i>Concentration</i> <i>(mM)</i>	<i>g/100mL</i>
	PW		
<i>Tyrode x10</i>	-	-	<b>10 mL</b>
<i>Glucose</i>	180.156	10	<b>0.18 g</b>
<b>Adjust PH to 7.4 with NaOH</b>			

### IV.2.2 Process of experiment

The dissociated ventricular cardiomyocytes were dyed by 7.5  $\mu\text{M}$  of Fluo4-AM dissolved in DMSO-Pluronic for 30 min at room temperature following by 5 min of deposition. Meanwhile, all the solutions used for this experiment such as 10 mM caffeine, used for detecting SR content, and 100 nM/1  $\mu\text{M}$  iso, used as  $\beta$ -adrenergic receptor activator were prepared. For the

pharmacology experiments, 5  $\mu\text{g}/\text{mL}$  venlafaxine and pregabalin were also prepared. Then the Fluo4-AM was removed and fresh 1 x Tyrode solution was added to suspend the cells.

For the recording, the first step is to discern a “good” cell which appears to be well-insulated and well-rectangular with smooth edges as well as responses to electrical stimulation. Then the focused cell was rotated to horizontal position so that the line can go through the longitudinal axis of the cell to measure the cell contraction as shown in figure 26 in line-scan mode. Images were recorded with a resonant scanning confocal microscope Leica SP5, equipped with a white light laser fitted to 500 nm and excitation was collected at  $> 510$  nm. The calcium transient was recorded by line-scan mode with following parameters: speed 400 Hz bidirectional, 1024 lines with electrical stimulation at 2 Hz.

### Principle of Line scan

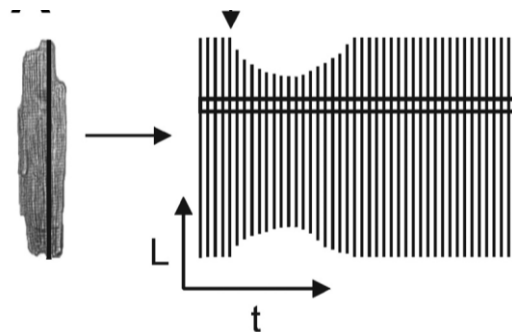


**Figure 26. Schematic diagram of Line scan recording by confocal microscopy.** L=length, t=time. (Adapted from (William H et al. 2002))

After 2 Hz electrical field stimulation, cell was left to be quiescent for 1 min. Then the calcium waves and calcium sparks were recorded in line-scan mode with following parameters: speed 700 Hz, zoom x 4, 1024 lines. 10 images were recorded automatically and 3 times repeat was done for each cell. After sparks measurement, 10 mM caffeine was perfused to measure the SR content of ventricular cardiomyocytes by line-scan mode with the following parameters: 15000 lines, speed 400 Hz. The recording was started when the cell was quiescent and then the cells were stimulated at 2 Hz followed by caffeine perfusion for several seconds. In this way, we could measure the post rest potentiation as well as the fractional release.

### IV.2.3 Perfusions

In this project, the effect of iso and several drugs has been measured. For each perfusion, the recording is the same as mentioned above. The cells were perfused with 100 nM ISO for 1min, and with drugs for 2 min before recording. The procedure of perfusion as shown in figure 27.

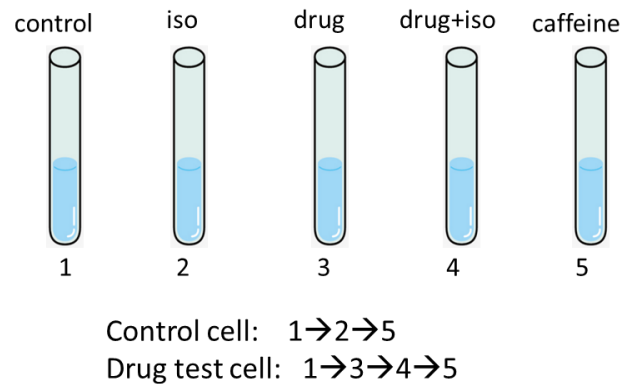


**Figure 27: perfusion procedure for mice ventricular cardiomyocytes.**

## IV.3 The application of confocal microscopy on HEK293 cells

### IV.3.1 Preparation

48 h after transfection, the cells were dyed with fluo4-AM for 25 min at room temperature. In the meantime, 1 x Tyrode solution with different  $\text{Ca}^{2+}$  concentration (0, 0.1, 0.2, 0.3, 0.5, 1, 2 mM) were prepared. Then the fluo4-AM was removed and cells were rinsed once with 1 x Tyrode solution without  $\text{Ca}^{2+}$ . Then the dish was mounted into heating box at 37°C for recording.

### IV.3.2 recording

The calcium oscillations of HEK293 cells transfected by WT and mutated RyR2 plasmids were recorded by 2D time mode with the following parameters: format 512 x 512, speed 400 Hz, zoom x 1.5, 180 frames. 4 to 6 positions from each dish were recorded and each position was marked by the machine to be able to observe the same cells in raising  $\text{Ca}^{2+}$  concentration from 0.1 to 2 mM.

## V Micro-electrode technique

### V.1 The main principles of micro-electrode technique

Microelectrodes were introduced in 1946 by the American scientists R. Gerard and G. Ling to obtain the electric potential of a neural fiber (mouse) and, later, of a single cell (Graham and Gerard, 1946). Micro-electrode technique used in this project is a traditional intracellular electrophysiological recording method. Even though with less advantages than whole cell recording of patch-clamp for ion current recording, it possesses unique advantage for spontaneous action potentials recording since the intracellular solution is kept and not replaced by artificial one as in whole cell patch-clamp. Thus, it is still widely used for recording the field potentials in brain slices or action potentials in cardiac tissue. The micropipette electrode was injected directly into the cell to form a close circuit as shown in Figure 28. With this circuit, the action potentials outside cells are amplified by an AC-coupled amplifier to levels that are suitable for recording on a computer, as shown in figure 28. Unlike patch-clamp, the hand vibration during positioning and exact placement of electrodes are not so sensible, so the micromanipulators can be of the coarse mechanical type, but a rather complex warm system with temperature controlling and perfusion system were needed to improve the environments for the cells. The intracellular solution must be high concentrated solutions, usually 2-4 M  $K^+$  salt, which minimizes the rectifying current flow, lowers voltage noise and provides a wider recording bandwidth. The high concentrated intracellular solution demands much smaller diameter of the pipette tip (0.01-0.1  $\mu M$ ) than patch pipette (1-2  $\mu M$ ), in order to prevent the solution from entering the cells.

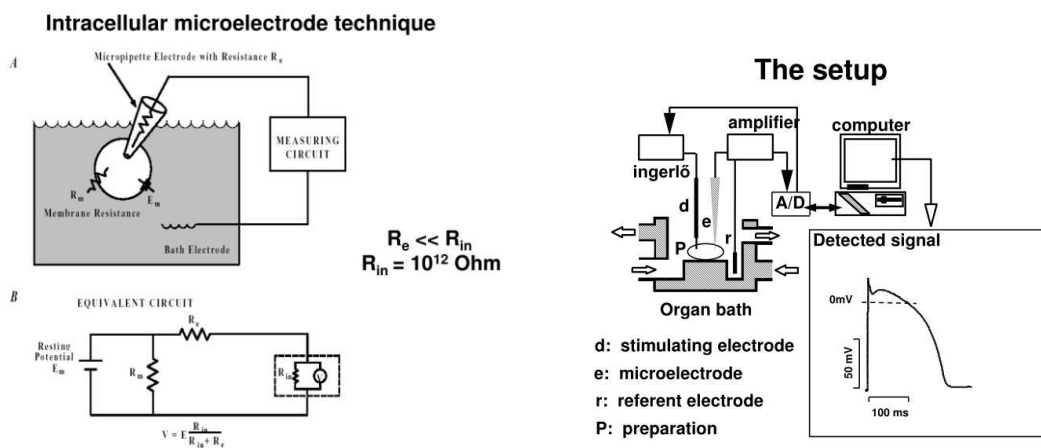


**Figure 28. structural and schematic diagram of intracellular microelectrode technique.**  
<https://www.slideserve.com/darva/cellular-cardiac-electrophysiological-techniques>.

## V.2 The application of micro-electrode on hiPSC-CM

### V.2.1 Solutions:

The basal external solution for micro-electrode on hiPSC-CMs was Sol. Tyrode, but a little modification has been made from the one used for confocal recording, as shown in the following table. The internal solution was 3 M KCl solution.

✓ **Table 7: 1 x Tyrode solution for micro-electrode**

<i>Reagent</i>	<i>Molar mass (g/mol)</i>	<i>Concentration (mM)</i>	<i>g/500mL</i>
<i>NaCl</i>	58.44	137	4.0003
<i>KCl</i>	74.55	5.4	0.2015
<i>CaCl<sub>2</sub>.2H<sub>2</sub>O</i>	147.00	1.8	0.1325
<i>MgCl<sub>2</sub>.6H<sub>2</sub>O</i>	203.30	1	0.1015
<i>HEPES</i>	238.30	10	1.1915
<b>Adjust PH to 7.4 with NaOH</b>			

### V.2.2 Pipettes:

The pipettes were made of fire polished borosilicate capillary glass tube with filament by DMZ-Universal puller (Ser.No.39543/1309, Zeitz-Instruments, Germany). The program used generated pipettes with resistances above 20 MΩ.

### V.2.3 Recording

The double heating system for both dish and solution at 37°C was switched on around 10 min before experiments to leave it pre-warm. Then the hiPSC-CMs seeded in ibidi dishes on 32 to 40 days after differentiation were taken out of incubator and perfused with the warm basal solution for a while to make it adapt to the detected environment. Once the cells got to the stable condition, the experiment can be started. The well beating cell with rod shape membrane were chosen to do the AP recording. Before pipette injected into the cell, the resistance of pipette

was tested to check the tip diameter, and the values above 20 M $\Omega$  were considered to be used. Firstly, the pipette was adjusted to the vision field by micromanipulators set on the electrode holder. Then it was moved close to the cell step by step by the separated micromanipulators. The record was started before the pipette went into the cell to get the baseline value before recording. Then the pipette was manipulated into the cell very slowly, and once the voltage starts to change, it should be stopped. Patience should be taken to see if the action potentials have been gotten. After recording in basal solution for 1-2 min, ISO solution was perfused for 1-2 min to record the action potentials under stress condition. Then the recordings were continued back on basal solution (wash-out condition) until the beating rate recovered to basal condition.

## **VI Immunolabeling of hiPSC-CMs (performed by Pascale GERBAUD and Pierre JAONNE)**

Immunolabeling was performed to verify the differentiated hiPSC-CMs. As mentioned in I.3, on 18 days after differentiation, the differentiated hiPSC-CMs were dissociated and seeded into ibidi dishes. On day 35, the cells in ibidi dishes were used to performed immunolabeling. Briefly, hiPSC-CMs were washed with PBS for 3 times with 5 min each time in room temperature, and then the cells were fixed and permeabilized in cold methanol for 8 minutes at -20°C. After removal of methanol, cells were washed three times in PBS, and were blocked in PBS plus 3% BSA (fatty acid free, Sigma-Aldrich) for 1h at room temperature. Then the cells were incubated with primary antibodies (anti-alpha-actinin monoclonal antibody (sarcomeric) clone EA-53 antibody (1/500, Sigma-Aldrich), or anti-RyR monoclonal antibody (C3-33 MA3-916, 1/500, Thermo scientific, Courtaboeuf, France), or anti-beta catenin monoclonal antibody (1/500, 610154, BD) or anti-connexin43 polyclonal antibody (1/500, C6219, Sigma Aldrich) overnight at 4°C. After removal of first antibodies and rinsed with PBS, cells were incubated with secondary goat anti-mouse or anti-rabbit antibodies coupled to AlexaFluor 488 or 555 for 1h at room temperature avoiding light (1/1000, A11029, Thermo scientific, Courtaboeuf, France). Coverslips were then mounted on the cells incubated in prolong gold antifade reagent containing DAPI to counterstained nuclei over night at room temperature avoiding light (Thermo scientific, Courtaboeuf, France). Images were acquired with an inverted Leica TCS SP8 microscope (Leica, Germany).

## **VII Protein measurement (performed by Pascale GERBAUD)**

The levels of proteins expressing in hiPSC-CMs were measured by western-blot. This technique allows to detect specific proteins in a sample of tissue homogenate. First of all, total cell protein samples were extracted from harvested hiPSC-CMs by lysis buffer (Life Technologies, Villebon-sur-Yvette, France; 50 mM Tris (pH 7.4), 250 mM NaCl, 50 mM NaF, 5 mM EDTA, 1% Nonidet P-40, 0.02% NaN<sub>3</sub>, 1 mM sodium orthovanadate), supplemented with a protease inhibitor cocktail (Merck Millipore, Guyancourt, France) and a phosphatase inhibitor cocktail (Merck Millipore, Guyancourt, France). In order to ensure the protein amount used for detection are equal in all samples, the protein concentrations were measured by BCA method. BCA assay is a high-precision method, which detects the color change of the sample solution from green to purple and present a strong linear absorbance at 562 nm with the increase in protein concentration. Then the protein concentration of the sample is determined by comparing this absorbance with a standard curve of absorbance made from varying bovine serum albumin (BSA). Once the concentrations measured, the protein samples can be aliquoted and stored in -80°C.

After the preparation of samples, the levels of specific proteins were measured by western-blot. Firstly, the protein lysates were loaded with loading buffer which contains anionic denaturing detergent SDS to denature proteins and make them negatively charged so that facilitates the protein separation by molecular weight and the following binding with antibody. Then protein samples were separated on 4%–20% discontinuous gradient polyacrylamide gels, followed by transferred to PVDF membranes. PVDF membranes were incubated with blocking buffer of TBS with Tween-20 (0.1%) and nonfat dry milk (5%) for 45 minutes at room temperature. Membranes were then incubated with primary antibodies diluted in 5% milk TBS overnight at 4°C, followed by the secondary antibodies. Actin (0.8 µg/ml, Sigma-Aldrich, A2066), RyR2 (1µg/ml, Thermo Fisher Scientific, MA3-916), and Cav1.2 primary antibodies were used. Antigen complexes were visualized with ChemiDoc and quantified with Image J (NIH).

## **VIII Materials and reagents**

Putrescine (P5780-5G, Sigma)

Sodium Selenite (S5261-10G, Sigma)

Insulin solution human (I9278-5ML, Sigma) (approximately 10 mg / mL)

Sodium DL Lactate (L4263-100ML, Sigma)

L-ascorbic acid (A8960-5G, Sigma)

Y27632 (10mg, S1049, Selleckchem)

CHIR-99021 (5mg, S1263, Selleckchem)

IWP2 (10 mg, S7085, Selleckchem)

RPMI 1640 (500 mL, 21875-034, Thermo Fisher Scientific)

RPMI 1640 No Glucose (500 mL, 11879-020, Thermo Fisher Scientific)

Matrigel hESC-Qualified (5 mL, 354277, Corning)

DMEM / F12 (500 mL, 31330-038, Thermo Fisher Scientific)

mTeSRTM plus basal medium (400 mL, 05826, stemcell technologies)

mTeSRTM 1 5 x supplement (100 mL, 85852, stemcell technologies)

Trypan Blue (500 mL, 15250-061, Thermo Fisher Scientific)

B27 supplement (10 mL, 17504-044, Thermo Fisher Scientific)

PBS (500 mL, P04-36500, Pan Biotech)

Accutase (100 mL, A11105-01, Thermo Fisher Scientific)

TrypLE Express (500 mL, 12604-021, Thermo Fisher Scientific)

H2O (500 mL, 10977-035, Thermo Fisher Scientific)

0.5 M EDTA, pH = 8 (100 mL, 15575-020, Thermo Fisher Scientific)

Cryomedium PSC (100 mL, 26444-01, Thermo Fisher Scientific)

Penicillin / Streptomycin (100 mL, 15140-122, Thermo Fisher Scientific)

lipofectamine 3000 (life technologies, Saint-Aubinb, France)

Fluo4-AM (F1242 - MW = 1129.86 - 50µg, LifeTech)

Calbryte™ 520 AM (20650 - 10 x 50µg, AAT bioquest)

protease inhibitor cocktail (Merck Millipore, Guyancourt, France)

phosphatase inhibitor cocktail (Merck Millipore, Guyancourt, France)

lysis buffer (Life Technologies, Villebon-sur-Yvette, France)

## **IX statistics**

Results are presented as mean±SEM. Student's t-test, one-way ANOVA and two-way repeated ANOVA statically methods were used according to the experimental setting. P values of less than 0.05 were considered statistically significant and marked by “\*”, less than 0.01 were marked by “\*\*”, and less than 0.001 were marked by “\*\*\*”.

# Results



The results of my thesis are included into two manuscripts. The first manuscript was mainly a transition from the laboratory previous research to my research. As mentioned above, our collaborators have identified the novel N-terminal domain CPVT mutation R420Q in a Spanish family, and the following functional study in HEK293 cells showed that the mutation presented gain-of-function in low  $[Ca^{2+}]_i$  but loss-of-function in high  $[Ca^{2+}]_i$  (Domingo *et al.*, 2015). Thereafter, my lab created a KI mouse model carrying this mutation to further study it in cardiomyocytes. With this KI mouse model, Wang et al have clarified the effect of RyR2<sup>R420Q</sup> in SAN, which was to enhance the Ca<sup>2+</sup> clock and disturb the coupling between Ca<sup>2+</sup> and voltage clocks thereby triggering bradycardia and SAN dysfunction (Wang *et al.*, 2017).

## **I manuscript 1: RyR2<sup>R420Q</sup> mutation in the calcium release channel induces ultrastructural nanoscale alterations involved in arrhythmia and cardiac sudden death**

Since CPVT is ventricular arrhythmia, our highlight work would be in ventricular cardiomyocytes. Thus, we performed a series of experiments in ventricular cardiomyocytes from KI mice to look into the arrhythmogenic mechanism of RyR2<sup>R420Q</sup>. How the mutation located in N-terminal domain of RyR2 disturb the channel gating? Is it similar with that caused by the mutations located in central terminal domain and C-terminal domain or the other mutations in N-terminal domain? The findings in manuscript 1 answered these questions. My work was mainly on hiPSC-CMs, from which many parameters of  $[Ca^{2+}]_i$  handling were consistent with that from KI mouse model, which confirming the patient specific hiPSC-CMs as a good model to study RyR2<sup>R420Q</sup> mutation. On the other side, the consistent results from hiPSC-CMs also improved the reliability of the findings in KI mouse model, which is why we made a relation between the results from both models in manuscript 1. Moreover, I have repeated the measurements of  $[Ca^{2+}]_i$  handling in ventricular myocytes of KI mice when I detected the antiarrhythmic effect of venlafaxine and pregabalin and got the same results as that showed in manuscript 1, further confirming our previous results.

**Title:**

**RyR2<sup>R420Q</sup> mutation induces ultrastructural alterations in the calcium release channel involved in arrhythmia and cardiac sudden death**

Authors:

Liheng Yin<sup>1\*</sup>, Alexandra Zahradnikova Jr<sup>1\*</sup>, Riccardo Rizzetto<sup>1\*</sup>, Simona Boncompani<sup>2#</sup>, Camille Rabesahala de Meritens<sup>3#</sup>, Yadan Zhang<sup>3</sup>, Pierre Joanne<sup>1</sup>, Elena Marqués-Sulé<sup>1,4</sup>, Yuriana Aguilar-Sánchez<sup>5</sup>, Miguel Fernández-Tenorio<sup>6</sup>, Olivier Villejoubert<sup>1</sup>, Linwei Li<sup>1</sup>, Yue Yi Wang<sup>1</sup>, Philippe Mateo<sup>1</sup>, Valérie Nicolas<sup>7</sup>, Pascale Gerbaud<sup>1</sup>, Anthony Lai<sup>8</sup>, Julio L Álvarez<sup>1,9</sup>, Ernst Niggli<sup>6</sup>, Héctor H Valdivia<sup>10</sup>, Carmen R. Valdivia<sup>10</sup>, Josefina Ramos-Franco<sup>5§</sup>, Esther Zorio<sup>11,12§</sup>, Spyros Zissimopoulos<sup>3§</sup>, Feliciano Protasi<sup>2§</sup>, Jean-Pierre Benitah<sup>1§</sup>, Ana M Gómez<sup>1</sup>.

\* Co-first authors

# Co-second authors

§ Contributed equally

**Short title: Nanoscale alterations underlie arrhythmias in RyR2<sup>R420Q/wt</sup> mice**

<sup>1</sup>Signaling in cardiovascular pathophysiology - UMR-S 1180, Inserm, Univ. Paris-Sud, Université Paris-Saclay, 92296 Châtenay-Malabry, France.

<sup>2</sup>Center for Research on Ageing and Translational Medicine (CeSI-MeT), Department of Neuroscience, Imaging and Clinical Sciences (DNICS), Department of Medicine and Ageing Sciences (DMSI), University Gabriele d'Annunzio, Chieti, Italy.

<sup>3</sup>Swansea University Medical School, Institute of Life Science, Swansea, SA2 8PP, UK

<sup>4</sup>Physiotherapy Department, University of Valencia, Valencia, Spain

<sup>5</sup>Department of Physiology and Biophysics. Rush University Medical Center. 1750 West Harrison St. Chicago, IL 60612. USA

<sup>6</sup>Department of Physiology, University of Bern, Bern, Switzerland

<sup>7</sup>IPSIT, 92296 Châtenay-Malabry, France

<sup>8</sup>College of Medicine, QU Health, Qatar University, Doha, Qatar

<sup>9</sup>Institute of Cardiology, Havana, Cuba

<sup>10</sup>Department of Medicine and Cardiovascular Research Center, University of Wisconsin-Madison School of Medicine and Public Health

<sup>11</sup>Cardiology Department and Unidad de Cardiopatías Familiares, Muerte Súbita y Mecanismos de Enfermedad (CaFaMuSMe), Hospital Universitario y Politécnico La Fe and Instituto de Investigación Sanitaria La Fe, Valencia, Spain

<sup>12</sup>Center for Biomedical Network Research on Cardiovascular diseases (CIBERCV), Madrid, Spain

*Address for correspondence:*

Ana M Gómez

Inserm, UMR-S 1180,

Faculté de Pharmacie, Université Paris Saclay,

92296 Châtenay-Malabry, France

Current address: OV: L'Institut Mutualiste Montsouris, 42 boulevard Jourdan, 75014 Paris, France; AZJr : Biomedical Research Center, Slovak Academy of Sciences, Dubravská cesta

9, 84505 Bratislava, Slovakia ; RR : Axxam S.p.A., Bresso, Lombardy, Italy; PJ : UMR 8256,  
Sorbonne Université, 75252 Paris

Catecholaminergic polymorphic ventricular tachycardia (CPVT) is the most frequent rare disease, manifested by syncope or sudden death in children or young adults under stress conditions. The autosomal dominant variant of CPVT is caused by mutations in the  $\text{Ca}^{2+}$  release channel, ryanodine receptor (RyR2) gene, and account for about 60% of the identified mutations. Recently, we described a new mutation in RyR2 N-terminal domain, RyR2<sup>R420Q</sup>, and here we analyzed the arrhythmogenic mechanisms of this mutation in knock-in mice, correlating it to human cardiomyocytes derived from CPVT patients (hiPSC-CMs). Ventricular tachycardia under stress conditions were observed in both CPVT patient and KI mouse. During cardiomyocyte action potentials recording (by patch-clamp in KI mice cardiomyocytes and by microelectrodes in mutant hiPSC-CM) we observed an increased occurrence of delayed after depolarizations (DADs) during isoproterenol stimulation, associated with increased  $\text{Ca}^{2+}$  waves during confocal  $\text{Ca}^{2+}$  recordings in both mice and human RyR2<sup>R420Q</sup> cardiomyocytes. In addition,  $\text{Ca}^{2+}$ -induced  $\text{Ca}^{2+}$ -release, as well as fractional  $\text{Ca}^{2+}$  release, were higher and  $\text{Ca}^{2+}$  sparks lasted significantly longer in the RyR2<sup>R420Q</sup> expressing cells. At the ultrastructural nanodomain level, we observed smaller RyR2 clusters and widened junctional sarcoplasmic reticulum (jSR) measured by g-STED superresolution and electronic microscopy, respectively. The increase in jSR width can increase the local volume, delaying the local depletion and  $\text{Ca}^{2+}$  spark termination. This alteration might be due to the impairment of the RyR2<sup>R420Q</sup> to bind junctophilin-2. At the single current level, we observed that the mutated channel instead of being preferentially in closed state at low  $[\text{Ca}^{2+}]_i$  it opens, although at a subconductance state. The latter might be correlated with an enhanced interaction between the N-terminus and the core solenoid, an RyR2 inter-domain association that has not been previously implicated in the pathogenesis of arrhythmias and sudden cardiac death. In conclusion, the RyR2<sup>R420Q</sup> CPVT mutation presents alterations in RyR2 structure/gating and its association with junctophilin-2, underlying alterations in the nanostructure of the dyad and participating to proarrhythmic behavior. Our study opens new avenues to better understand mechanisms of cardiac sudden death not only in CPVT patients, but also in other acquired most

common diseases where RyR2 function is altered such as in heart failure, or even other diseases affecting organs as brain and pancreas where RyR2 is expressed.

**INTRODUCTION.** Sudden Cardiac Death (SCD) represents about 15% of all deaths in developed countries<sup>1</sup>. It may occur in a structurally diseased heart, but also in apparently normal hearts where a channelopathy, *i.e.*, a genetic disease affecting ion channel activity, is at the origin of the lethal tachyarrhythmia. Catecholaminergic polymorphic ventricular tachycardia (CPVT)<sup>2</sup> is an inherited disease characterized by exercise- or stress-induced ventricular polymorphic tachycardia episodes in the absence of apparent structural heart disease. The disease is highly malignant, often manifesting for the first time in childhood or adolescence as syncopal events and/or SCD. CPVT patients have a mortality rate of ~30-50% by the age of 35 years when untreated. Mutations in the type 2 ryanodine receptor (RyR2) gene account for about 60% of the identified mutations and they are inherited following an autosomal dominant trait. Other CPVT-related genes encode for proteins which may bind to and modulate RyR2 channel<sup>3</sup>. Thus CPVT is clearly an arrhythmogenic disorder affecting directly or indirectly RyR2 function, pointing to intracellular Ca<sup>2+</sup> mishandling the origin of CPVT.

The RyR2 is a homotetramer with hydrophobic segments of the four identical subunits that form a central pore<sup>4</sup>. Usually pathogenic RyR2 CPVT mutations cluster into 3 discrete protein regions or “hot spots” at the N-terminus (32%), central (30%) and C-terminus domain (38%)<sup>5, 6</sup>. While a loss-of-function RyR2 mutation has been described<sup>7, 8</sup>, the vast majority of the mutations studied so far induce gain-of-function changes in RyR2. Different molecular mechanisms underlying defective RyR2 channel regulation have been proposed, including increased sensitivity to cytosolic<sup>9, 10</sup> and luminal<sup>11</sup> Ca<sup>2+</sup>, abnormal regulation by FKBP12.6<sup>12</sup> or calmodulin<sup>13</sup> and defective intra- and inter-subunit interactions<sup>14, 15</sup>.

Recently, we described a new mutation in the RyR2 N-terminal domain (NTD), RyR2<sup>R420Q</sup>, in a Spanish family diagnosed for CPVT<sup>16</sup>. Remarkably, this mutation has also been found in other CPVT families<sup>17-20</sup>, and other pathogenic mutations at the same amino acid have also been identified<sup>19-21</sup> indicating that it might be actually located at a hot spot. Even if several attempts to clarify the functional mechanism for mutations in this region have been performed<sup>22-24</sup>, the pathogenic mechanisms at the molecular and cellular level are still elusive.

Herein, we analyzed the arrhythmogenic mechanism of the N-terminal mutation RyR2<sup>R420Q</sup> using a RyR2<sup>R420Q</sup> KI mouse model as well as human cardiomyocytes derived from induced pluripotent stem cells from CPVT patients. Using multiple state-of-the-art approaches, we showed that the RyR2<sup>R420Q</sup> mutation induces: a) alterations of channel intrinsic properties, with increased interaction between the NTD and the core solenoid, which may underlie enhanced open probability at low Ca<sup>2+</sup>, although at sub-conductance states; and b) impairs the channel association with junctophilin-2, which affects the ultrastructural organization of the dyads, and the distribution and size of the RyR2 clusters.

## RESULTS

### ***Alteration of Ca<sup>2+</sup> homeostasis related to RyR2<sup>R420Q</sup> induced ventricular arrhythmias***

A KI mouse model carrying the RyR2<sup>R420Q</sup> mutation found in CPVT patients<sup>16</sup> presented a CPVT phenotype under stress challenges<sup>25</sup>. Compared to WT littermates, the KI mice showed normal ventricular cardiac function, as assessed by M-Mode echocardiography (Table S1). Under basal conditions, electrocardiogram analysis in freely moving KI and their WT littermates by telemetry did not revealed significant changes, except the heart rate (HR), which was slower in KI females, as previously shown<sup>25</sup> (Supplementary Table 2). However, under emotional stress induced by short episodes (15s) of warm air blowing with a hairdryer, the occurrence of evoked ventricular tachycardia (VT) was doubled in KI compared to WT (Fig. 1A). Likewise, Isoproterenol (ISO) injection elicited ventricular ectopy (VE; Fig. 1B, left), more frequently in KI mice (Fig. 1B, right). Thus, the KI mice recapitulate the human phenotype of RyR2 mutation carriers. Namely, normal cardiac structure and function, and stress-triggered ventricular arrhythmias. Consistent with this *in-vivo* phenotype, during action potentials (AP) recorded in isolated ventricular cardiomyocytes by patch-clamp technique, in the presence of 1- $\mu$ M ISO almost all KI myocytes displayed delayed afterdepolarizations (DADs) and/or triggered activity (TA), whereas less than half WT myocytes showed those pro-arrhythmic events (Fig. 1C). When the Ca<sup>2+</sup> chelator BAPTA (5 mM) was introduced into the patch pipette, ISO-induced DADs and TA were completely prevented in all myocytes, pointing out a central role of intracellular Ca<sup>2+</sup> in triggering this proarrhythmic cellular behavior. Of translational importance, similar electrical abnormalities were observed upon ISO perfusion (1  $\mu$ M) during AP recorded by a microelectrode technique in cell monolayers of human cardiomyocytes derived from iPS cells (hiPSC-CMs) from a carrier patient (III:7) whose stress ECG is presented in Fig.1D (Fig. 1E). In comparison to hiPSC-CMs from his genotype and phenotype negative brother (Ctl) (III:4), while DADs were recorded in both cell groups, the hiPSC-CMs from RyR2<sup>R420Q</sup> patient (Mu) presented higher incidence of them at baseline and especially after ISO treatment (Fig. 1F).

To gain mechanistic insights, we next analyzed in situ the RyR2<sup>R420Q</sup> function by spontaneous Ca<sup>2+</sup> spark recordings in intact quiescent cardiomyocytes. Figure 2A shows examples of line scan confocal images displaying Ca<sup>2+</sup> sparks in WT and KI cells from littermate mouse in basal conditions and during 100 nM ISO perfusion. The spontaneous Ca<sup>2+</sup> sparks frequency was slightly (~1.5 fold) but significantly higher in KI than in WT cells. This overactivity of RyR2<sup>R420Q</sup> function is accompanied by Ca<sup>2+</sup> sparks that lasted significantly longer in cardiomyocytes from KI mice (full duration at half maximum amplitude, FDHM), albeit peak amplitude or width (full width at half maximum amplitude, FWHM) were roughly similar compared to WT (Suppl. Fig.S1). These alterations in Ca<sup>2+</sup> spark characteristics during diastolic periods in KI cells resulted in an enhanced Ca<sup>2+</sup> released per Ca<sup>2+</sup> spark (Ca<sup>2+</sup> spark mass, Fig. 2C) and in enhanced Ca<sup>2+</sup> sparks mediated Ca<sup>2+</sup> leak as evaluated in each cell through averaged Ca<sup>2+</sup> spark mass multiplied by Ca<sup>2+</sup> spark frequency (Fig. 2D). Of note, ISO significantly augmented those Ca<sup>2+</sup> sparks parameters in both cell groups in a similar manner (Fig 2,B,C&D). The enhanced Ca<sup>2+</sup> leak in KI cells, was correlated with decreased capacity of the cardiac myocyte to accumulate Ca<sup>2+</sup> in the sarcoplasmic reticulum (SR) during resting periods, evaluated as the Post Rest Potentiation (at 4 Hz: 1.41±0.067 in 10 WT cells, vs 1.19±0.06 in 11 KI cells, p<0.05).

The exacerbated RyR2<sup>R420Q</sup> activity at rest might underlie the increased occurrence of arrhythmogenic events found in the AP recordings during patch-clamp experiments, which were completely blunted by intracellular Ca<sup>2+</sup> chelation (Fig. 1C). Indeed, KI cardiomyocytes had markedly higher occurrence of Ca<sup>2+</sup> waves following 4-Hz burst pacing, even after 100nM Iso exposure (Fig.2E & F). Similarly, in 1-Hz electrically paced hiPSC-CMs from a RyR2<sup>R420Q</sup> carrier patient, which express RyR2s in a striated pattern (Fig. 1G), ISO elicited aberrant diastolic Ca<sup>2+</sup> release during the diastolic periods (Fig.2H, left), consistent with the DADs presented in Fig. 1E. Pooled data (Fig. 2H, right) showed higher incidence of these aberrant diastolic Ca<sup>2+</sup> releases in mutant carrier hiPSC-CMs compared with control ones.

The above data shows that RyR2<sup>R420Q</sup> increases diastolic SR Ca<sup>2+</sup> leak under resting conditions and increases propensity for Ca<sup>2+</sup>-dependent triggered arrhythmic activities, which are exacerbated by ISO, pointing out a pivotal role of SR Ca<sup>2+</sup> mishandling. Then, we next analyzed global intracellular Ca<sup>2+</sup> ([Ca<sup>2+</sup>]<sub>i</sub>) handling in intact mouse cells by confocal microscopy. Examples of [Ca<sup>2+</sup>]<sub>i</sub> transients evoked at 2 Hz and then exposed to rapid 10-mM caffeine, to evaluate the SR Ca<sup>2+</sup> load, in cardiomyocytes isolated from WT or KI mice before and under isoproterenol application are presented in Fig. 3A. Consistent with the normal heart function detected with echocardiography (Supp Table 1), cardiomyocytes from KI mice showed normal [Ca<sup>2+</sup>]<sub>i</sub> transients amplitude and decay kinetics, both at 2 and 4 Hz (Fig. 3B,C).  $\beta$ -adrenergic stimulation with ISO increased the [Ca<sup>2+</sup>]<sub>i</sub> transient amplitude and accelerated its decay time in both cell types (Fig. 3D). While the ISO effect in accelerating [Ca<sup>2+</sup>]<sub>i</sub> transient decay time was similar between WT and KI, the increase in its peak was significantly smaller in KI mice (Fig. 3D). In regard to the SR Ca<sup>2+</sup> load, cardiomyocytes isolated from KI mice had lower Ca<sup>2+</sup> content in the SR, which was brought to the same level as the WT by  $\beta$ -adrenergic stimulation (Fig. 3E) even if time of decay of the caffeine evoked [Ca<sup>2+</sup>]<sub>i</sub> transient was not different between WT and KI (Fig. 3F), suggesting similar NCX function in the forward mode. The depression in the SR Ca<sup>2+</sup> load with normal [Ca<sup>2+</sup>]<sub>i</sub> transients resulted in the enhanced fractional release in cardiomyocytes from KI mice (Fig. 3G). Namely, for a given amount of Ca<sup>2+</sup> stored in the SR, a larger percentage of Ca<sup>2+</sup> is released during each twitch. Similar findings were made in hiPSC-CM from a RyR2<sup>R420Q</sup> carrier patient compared to hiPSC-CM from his no mutant carrier brother (Fig 3H & I)

Taken together, these data indicate that in a normal twitch, the amount of release Ca<sup>2+</sup> as a function of the SR Ca<sup>2+</sup> stored is higher in RyR2<sup>R420Q</sup> expressing cardiomyocytes. We then wondered whether arrhythmogenic Ca<sup>2+</sup> waves also occur at a lower SR Ca<sup>2+</sup> load. We monitored SR Ca<sup>2+</sup> in permeabilized mice myocytes using SR entrapped Fluo-5N, while bathed in an internal solution that induces Ca<sup>2+</sup> waves. As shown in Fig. 3 J&K, the cardiomyocytes

from RyR2<sup>R420Q</sup> mice presented Ca<sup>2+</sup> waves with a threshold at a significantly lower SR Ca<sup>2+</sup> concentration than in control.

As the presence of the RyR2<sup>R420Q</sup> mutation increases the Ca<sup>2+</sup> release at a given SR Ca<sup>2+</sup> load (fractional release), we decided to analyze whether the RyR2<sup>R420Q</sup> mutation also alters the Ca<sup>2+</sup> release triggered by a given Ca<sup>2+</sup> entry. For this purpose we simultaneously recorded Ca<sup>2+</sup> entry current ( $I_{Ca}$ ) using the whole-cell patch-clamp technique coupled to confocal microscopy to register the evoked  $[Ca^{2+}]_i$  transient. Figure 4A shows examples of such recordings at 0 mV in a WT cell (top) and a KI cell (bottom, red traces). Summary data (Fig. 4 B) show that the RyR2<sup>R420Q</sup> mutation had no effect on the  $I_{Ca}$  density-voltage relationship relative to WT cardiomyocytes (the maximal  $I_{Ca}$  conductance was also similar between both groups (in pS): 205.7±25.1 in 10 WT cells, vs. 219.7±14.8 in 15 KI cells), while the  $[Ca^{2+}]_i$  transient amplitudes in KI cells was significantly increased throughout the entire voltage range. As a result, the Ca<sup>2+</sup>-induced Ca<sup>2+</sup> release (CICR) gain, calculated by normalizing the  $[Ca^{2+}]_i$  transient amplitude by the integral of  $I_{Ca}$ , was increased in KI cells, as exemplified at -20 mV in Fig. 4C, evidencing that there was more SR Ca<sup>2+</sup> release flux through the RyR2<sup>R420Q</sup> over a given Ca<sup>2+</sup> influx in KI than in WT. Of note,  $I_{Ca}$  voltage dependent activation and inactivation properties (Fig 4D) showed no significant differences among groups (activation:  $V_{0.5} = -13.5 \pm 1.7$  mV and  $K = 5.0 \pm 0.4$  in 10 WT cells, and  $V_{0.5} = -14.6 \pm 1.1$  mV and  $K = 5.6 \pm 0.4$  in 15 KI cells; inactivation:  $V_{0.5} = -25.1 \pm 0.8$  mV and  $K = 4.3 \pm 0.1$  in 7 WT cells, and  $V_{0.5} = -26.8 \pm 0.9$  mV and  $k = 5.4 \pm 0.3$  in 11 KI cells). Consequently, the window current delimited by the overlap of activation and inactivation voltage dependencies, which results in a sustained Ca<sup>2+</sup> influx during AP contributing to SR load, but also might underlie arrhythmogenic events <sup>26</sup> is not altered in KI mice.

### ***RyR2 clustering and Ultrastructure of the dyad.***

CICR is initiated at the dyads, where clusters of RyR2 are located at the junctional SR (jSR) in close proximity to the LTCC, located at the transverse tubules. In order to test whether the RyR2<sup>R420Q</sup> affects clustering, we performed superresolution imaging of labelled RyR2. Figure

5A shows deconvoluted images of RyR2 CRUs after threshold analyses on a WT (left) and a KI (right) samples. We found that the clusters mean size was significantly smaller in the KI cardiomyocytes (Fig. 5B). The reduction in the RyR2 cluster size could reflect a decreased number of expressed channels, if the mutation would interfere with expression. We thus measured the total RyR2 expression level by Western Blots. Fig. 5C shows that both WT and KI similarly express RyR2, ruling out this hypothesis. In addition to the smaller cluster size, CRU distribution in KI cells was less aligned, indicating more dispersion along the Z line (Fig. 5D).

Data presented in Fig. 4 shows alteration in  $Ca^{2+}$ -induced  $Ca^{2+}$  release (CICR) gain in RyR2<sup>R420Q</sup> KI cardiomyocytes. We previously found alterations CICR gain in heart failure<sup>27</sup>, proposing changes in the structure of  $Ca^{2+}$  release sites, i.e. often named dyads<sup>28</sup>. Moreover, we aimed to confirm or disregard superresolution results using a technique with more resolution, such as electron microscopy (EM). Hence, here we analyzed dyad structure by EM. RyR2 in cardiomyocytes are clustered in what is called  $Ca^{2+}$  release units (CRUs), specialized intracellular junctions between the SR (labeled in yellow in Fig.5Ea) and T-tubules (labeled in green in Fig.5Ea). CRUs are the functional units for  $Ca^{2+}$  release, basically the sites where  $Ca^{2+}$  sparks arise from. The cytoplasmic domains of RyR2, i.e. the feet, are visible as evenly spaced densities spanning the gap between junctional SR (jSR) and T-tubule in electron microscopy (EM) images at high magnification (pointed by a series of arrows in Fig. 5Eb). In WT cardiomyocytes CRUs are almost exclusively positioned in proximity of Z-lines: the T-tubule present often, but not always, a wide profile (Fig. 5E a & b) with the jSR wrapped around it as in Fig. 5 Ea, or be associated to it forming multiple (two or more) couplons (i.e. individual contact sites between jSR and T-tubule), as in Fig. 5Eb.

We evaluated the number/area of CRUs (a T-tubule with associated jSR, 1 or more) and of couplons, individual jSR profiles associated to T-tubules (in Fig. 5Eb 2 couplons are present) in both WT and KI cardiac cells. This analysis revealed that in KI mice the number of both

CRUs and couplons is significantly reduced (of about 30%; Table 1, columns A and B), indicating that about 1/3 of release sites are missing.

We then analyzed the morphology of CRUs: in WT couplons are usually quite extended, one in Fig. 5 Ea and 2 in Fig. 5 Eb. In KI cardiomyocytes, on the other hand, we may find couplons, which appear fairly normal in length (Fig. 5Ec & e), and other ones in which the jSR is either shorter or apparently fragmented (Fig. 5Ed, f, g & h). The junctional contact between jSR and T-tubules containing RyR2 (Fig. 5Eb small arrows) was measured. The more extended is the area of contact between the two membranes, the larger could be the number of RyR2 contained in that specific couplon. With this in mind, we measured the length of the jSR / T-tubule contacts, or couplons: the average length of individual couplons is shorter in RYR2<sup>R420Q</sup> cardiac cells (Table 1, column C). Based on data in Table 1, column C, we then estimated: a) the average area of contact between jSR and T-tubule in each couplon (Table 3, column D) by assuming that their shape is approximately round and that the EM sections cut a random cord of this circle (see *Materials and Methods* for more detail); and b) the approximate number of RyR2-feet, which would be contained in a couplon of such size (Table 1, column E), assuming that the all area of a couplon is filled with RyR2. These estimates indicate that couplons in RYR2<sup>R420Q</sup> cardiomyocytes are significantly smaller and should contain a significantly lower number of RyR2-feet (Table 1, columns D and E respectively), in agreement with superresolution data.

We also analyzed jSR volume. Whereas in WT the jSR cisternae are narrow and flat (Fig. 5E a & b), in KI *samples* the jSR lumen has a more variable/irregular profile (Fig. 5Ec-f), with slightly wider sections. To confirm the visual observation of dilated and less regular jSR profiles in CRUs of RyR2<sup>R420Q</sup> and to verify possible changes in total SR volume we measured the average width of the jSR and quantified the percentage of fiber volume occupied by the free SR (i.e. longitudinal SR). This analysis indicates that a) the jSR lumen is on the average wider in KI than in WT cardiomyocytes (Fig. 5F). This increase in junctional SR volume is compensated by a significantly reduced free-SR volume (Free SR volume/total volume, in %:

2.1 ± 0.6 (n=109) in WT, vs. 1.3±0.9 (n=214) in KI, mean±SD, p<0.05), so the total SR volume is maintained.

We wondered how a mutation in the RyR2 channel could induce these alterations in the CRU clustering. Junctophilin-2 (JPH2) has recently emerged as an RyR2 accessory protein that directly affects the CRU clustering of RyR2 as well as the Ca<sup>2+</sup> release function<sup>29</sup>. Thus we lay the hypothesis that if the RyR2<sup>R420Q</sup> could interact less with the JPH2, this could contribute to differences in their clustering. We then performed co-immunoprecipitation analyses and found that the Junctophilin-2 binding to the RyR2<sup>R420Q</sup> is strongly depressed (Fig.5G, top), what could partly explain the ultrastructural changes observed in KI cardiomyocytes.

We also analyzed the appearance of the jSR content: the jSR cisternae in WT contain the classic *chain-like* electron dense polymer that runs parallel to the SR membrane (Fig. 5Eb, single arrows), representing Calsequestrin-2 (CASQ2). In KI myocytes, the *chain-like* polymer of condensed CASQ2 is present in some CRUs (Fig. 5 Ec & d), but sometimes missing in others, with the jSR lumen either empty or containing some electron-dense material not well organized/clustered as in normal jSR/T-tubule junctions (Fig. 5Ee-h). This observation suggests inadequate assembly of CASQ2 inside the jSR lumen. Indeed, a similar reduction in size of junctional domains was also observed in other mouse models carrying mutations or ablations of EC coupling proteins<sup>30, 31</sup> such as CASQ<sup>R33Q/R33Q</sup><sup>32</sup>. We therefore evaluated CASQ2 expression level in both groups by WB, to see if there was a reduction in the total amount of CASQ2 in KI, but found no significant difference (Supp. Fig. S2). However, the co-immunoprecipitation of CASQ2 with JP-2 was reduced in the KI hearts (Fig. 5G, bottom), suggesting differences in assembling rather than total expression.

### ***RyR2<sup>R420Q</sup> function***

It is hard to understand how the alteration in ultrastructure might underlie prolonged  $\text{Ca}^{2+}$  spark duration with maintained amplitude in KI cardiomyocytes (Suppl. Fig.S1). It has been proposed however, that  $\text{Ca}^{2+}$  sparks terminate by local depletion in the jSR<sup>33</sup>. Thus it is possible that at the local level, the depletion in KI cells during a  $\text{Ca}^{2+}$  spark takes longer, as its jSR is wider. In order to test this hypothesis, we analyzed the effect of intracellular hypo-osmolarity, which should induce swelling of the SR, on  $\text{Ca}^{2+}$  sparks characteristics in permeabilized rat ventricular cardiomyocytes (Suppl Fig S3). Hypo-osmotic internal solution did not significantly modify  $\text{Ca}^{2+}$  sparks frequency (Suppl Fig. S3A) nor SR  $\text{Ca}^{2+}$  content (Suppl. Fig. S3B). Interestingly, in comparison to normo-osmotic intracellular solution, immersion in hypo-osmotic solution did significantly prolong  $\text{Ca}^{2+}$  spark duration (Suppl. Fig S3C) without significantly affecting  $\text{Ca}^{2+}$  spark width (Suppl. Fig S3D). However, it reduced  $\text{Ca}^{2+}$  sparks amplitude (Suppl. Fig. S3 E) without affecting  $\text{Ca}^{2+}$  sparks mass (Suppl. Fig. S3 F). Thus increased jSR width alone might not completely explain all the  $\text{RyR2}^{\text{R420Q}}$  related alterations, although it can contribute to  $\text{Ca}^{2+}$  spark prolongation. A complementary and/or alternative mechanism that might account for the increased  $\text{Ca}^{2+}$  sparks frequency could be an enhanced  $\text{Ca}^{2+}$  sensitivity of the mutated  $\text{RyR2}$ , as we and others proposed for CPVT C-terminal  $\text{RyR2}$  mutations<sup>8,9</sup>. However, comparison of the  $\text{Ca}^{2+}$  dependent activation of [3H]ryanodine binding to SR microsomes from WT and KI littermates mouse hearts, an index for the  $\text{Ca}^{2+}$  sensitivity of  $\text{RyR2}$  open probability, either normalized to the total amount of  $\text{RyR2}$  present in each sample (Fig 6A) or normalized to maximum binding at pCa5 (Fig.6B), shows no significant differences. Likewise, analysis of  $\text{Ca}^{2+}$  sparks frequency at different  $[\text{Ca}^{2+}]_i$  in permeabilized ventricular cardiomyocytes isolated from WT and KI littermates mice did not show major differences, although significantly higher at 100nM  $[\text{Ca}^{2+}]_i$  (Fig6C), what may underlie the moderately higher  $\text{Ca}^{2+}$  spark occurrence.

### ***RyR2<sup>R420Q</sup> show intrinsic alteration***

Taken together, these results suggest that the  $\text{Ca}^{2+}$  sensitivity of the RyR2<sup>R420Q</sup> is not strikingly different to that of the WT RyR2, and suggests the alteration of other molecular mechanisms resulting from this mutation. To directly assess RyR2<sup>R420Q</sup> function, we used single channel recordings in planar lipid bilayers of SR microsomes from WT and homozygous KI mice to assure that every channel bears the mutation. Figure 6D&F shows examples of unitary current activity from WT and RyR2<sup>R420Q</sup> channels at two different cytosolic  $\text{Ca}^{2+}$  concentrations. Channel transitions to sub-conductance states are a rare occurrence for WT RyR2 when  $\text{Ca}^{2+}$  is used as current carrier (Fig. 6E). In contrast, the common behavior for RyR2<sup>R420Q</sup> was opening to sub-conductance states (Figure 6F&G). The mutation induced sub-conductance states characterized by largely variable dwell times. We detected transitions to sub-conductance states of about one or two thirds of the main conductance, while their frequency was high enough to produce evident components in the amplitude distribution histograms (Fig 6 E&G, n=4). Furthermore, our findings indicate that the probability of occurrence of sub-conductance states was inversely proportional to the cytosolic  $[\text{Ca}^{2+}]$ , meaning that the sub-conductance opening events were more frequently observed at lower cytosolic  $[\text{Ca}^{2+}]$ , while at higher  $[\text{Ca}^{2+}]$  their probability of occurrence was substantially lower (Fig. 6 H&I, Suppl Fig. S4). Of note the phosphorylation status, which could influence sub-conductance states<sup>34</sup>, including RyR2-Ser2814 (phosphorylated by CaMKII) and RyR2-Ser2809 (phosphorylated by both CaMKII and PKA) did not differ in ventricular protein extracts from WT and KI mice (Suppl. Fig.S5).

Alteration of RyR2<sup>R420Q</sup> intrinsic properties might be related to perturbation of molecular interaction within the channel. Indeed, the N terminal domain (NTD) regulates the activity of the homotetrameric RyR2  $\text{Ca}^{2+}$  release channel via two distinct inter-domain interactions: it forms an interface with a neighboring NTD and a separate interface with the core solenoid<sup>4, 35</sup>. Having previously demonstrated that the arrhythmogenic mutations R176Q and L433P disrupt RyR2 N-terminus self-association but do not affect NTD interaction with the core solenoid<sup>15, 35</sup>, we wonder whether this might be the case of RyR2<sup>R420Q</sup> mutation. To ascertain the involvement

of R420Q in RyR2 NTD tetramerization,<sup>15, 35</sup> the cMyc-tagged RyR2 N-terminus (NT, residues 1-906) was expressed in HEK293 cells, subjected to chemical cross-linking with glutaraldehyde and oligomer formation was analyzed by immunoblotting. Surprisingly, the R420Q mutation did not disrupt N-terminus tetramer formation, as indicated by quantification of the anti-cMyc immunoreactive bands corresponding to monomer and tetramer using densitometry analysis (Figure 7A). To assess the effect of R420Q in RyR2 N-terminus interaction with the core solenoid<sup>35</sup> NT<sup>WT</sup>/NT<sup>R420Q</sup> were co-expressed with HA-tagged RyR2-CT (residues 3529-4967), the latter was immunoprecipitated with Ab<sup>HA</sup> and the presence of co-precipitated NT<sup>WT</sup> or NT<sup>R420Q</sup> was analyzed by immunoblotting using Ab<sup>cMyc</sup>. Immunoprecipitation of RyR2-CT with anti-HA, verified by immunoblotting, resulted in successful co-precipitation of both NT<sup>WT</sup> and NT<sup>R420Q</sup>. Notably, quantification using densitometry analysis indicated that the R420Q mutation resulted in statistically significant, two-fold increase in NT interaction with RyR2-CT (Figure 7B).

## DISCUSSION

This integrated study combining human and mouse cardiomyocyte data on the RyR2<sup>R420Q</sup> CPVT mutation is the first description of an ultrastructural defect underlying ventricular arrhythmias in type 1 CPVT. Specifically, we find that RyR2<sup>R420Q</sup> channel binding to Junctophilin-2 is disturbed. This defect can underlie both, the ultrastructural remodeling of the dyad, displaying less frequent and smaller CRUs/couplons and wandering edges of the junctional SR, and the enhanced Ca<sup>2+</sup> release through Ca<sup>2+</sup> sparks in RyR2<sup>R420Q</sup> compared to the WT RyR2. Moreover, we identify the molecular defect underlying RyR2<sup>R420Q</sup> deregulation, namely a tighter interaction between the N-terminus and core solenoid domains, which may underlie openings in subconductances.

We created a mouse model bearing the RyR2<sup>R420Q</sup> we previously identified in CPVT patients<sup>16, 25</sup>. Moreover, we differentiated into cardiomyocytes iPS cells obtained from volunteer family members to correlate data obtained in both human and mouse cardiac cells. We found that RyR2<sup>R420Q</sup> mice present VT under emotional stress, and DADs in both mice and human

cardiomyocytes. These electrical proarrhythmogenic alterations were dependent on spontaneous  $\text{Ca}^{2+}$  release during diastolic periods both in mouse and human cardiomyocytes, which are not surprising in CPVT. However, the molecular mechanism underlying RyR2<sup>R420Q</sup> channel dysfunction we report here is completely novel.

We previously found enhanced  $\text{Ca}^{2+}$  sensitivity of the RyR2<sup>R4496C</sup> CPVT mutation<sup>9,10</sup>, which is located at the C terminal portion of the channel. Hence, we tested this possible mechanism in RyR2<sup>R420Q</sup>, which is located at the N-terminal portion. However our analysis by two different approaches failed to unequivocally point to a difference in  $\text{Ca}^{2+}$  sensitivity of this mutation. The first characteristic that surprised us was the longer  $\text{Ca}^{2+}$  sparks. As we found that the junctional SR cisterna were enlarged, we tested the possibility that  $\text{Ca}^{2+}$  sparks are longer as a result of this fact. Indeed, local SR  $\text{Ca}^{2+}$  depletion at the CRU was proposed as a mechanism for  $\text{Ca}^{2+}$  spark termination<sup>33</sup>. The enhanced junctional SR width in KI could thus induce a delay in local depletion. To try to mimic this condition inducing SR swelling, we bathed permeabilized cardiomyocytes in hypo-osmotic solution and found that in these circumstances, the  $\text{Ca}^{2+}$  sparks indeed lasted significantly longer. Thus, although in permeabilized cells the  $\text{Ca}^{2+}$  spark duration is shorter than in intact cells because  $\text{Ca}^{2+}$  is diffused away faster, the small but significant increase in  $\text{Ca}^{2+}$  spark duration in hypo-osmotic solution suggest that the jSR increase in width in KI cells might participate in  $\text{Ca}^{2+}$  sparks prolongation.

The question then arises, how a mutation in RyR2 can alter the junctional SR shape? We looked at junctophilin-2, which is a protein associated with both SR and plasmalemmal membranes, maintaining the integrity of the dyads<sup>36</sup>. The amount of junctophilin-2, as well as CSQ2, that could be co-immunoprecipitated with RyR2 was severely decreased in RyR2<sup>R420Q</sup>. This is consistent with the reduced size of CRU/couplons and CRU cluster size. In fact, it has been shown that overexpressing junctophilin-2 has the opposite results than the ones we found here, namely, an enlargement of the couplons size<sup>29</sup>. Moreover, data on literature report that junctophilin-2 also affects WT RyR2 function. Indeed, downregulation of junctophilin-2 enhances  $\text{Ca}^{2+}$  sparks frequency, whereas overexpression has the opposite effect<sup>29, 37</sup>. Thus

the decreased binding of RyR2<sup>R420Q</sup> to junctophilin could also explain the enhanced Ca<sup>2+</sup> spark occurrence in RyR2<sup>R420Q</sup> cardiomyocytes. At present, it is unclear how the R420Q mutation impairs the RyR2 interaction with junctophilin-2. It is unlikely that the R420 residue is directly participating in the interaction with junctophilin-2 because it is not surface exposed. The structure of the RyR2 NTD carrying the R420Q mutation has been resolved by X-ray crystallography and showed local conformational alteration<sup>38</sup>. Our data thus suggest that the conformational disturbance of the RyR2<sup>R420Q</sup>, manifested as increased NTD interaction with the core solenoid, results in unbinding of junctophilin-2 producing nano-disturbances in CRUs with uneven and on average wider junctional SR containing less polymerized calsequestrin. Functionally, the Ca<sup>2+</sup> spark probability is enhanced, which together with the longer Ca<sup>2+</sup> spark duration can favor propagation of Ca<sup>2+</sup> release and production of arrhythmogenic Ca<sup>2+</sup> waves.

In our clinical description of this mutation, we started the first in vitro analyses<sup>16</sup>. RyR2<sup>R420Q</sup> expressed in HEK293 cells showed enhanced activity at low [Ca<sup>2+</sup>]<sub>i</sub> and lower activity at high [Ca<sup>2+</sup>]<sub>i</sub>. Suggesting gain of function at low [Ca<sup>2+</sup>]<sub>i</sub> and loss of function at high [Ca<sup>2+</sup>]<sub>i</sub>. The enhanced activity at low [Ca<sup>2+</sup>]<sub>i</sub> can manifest in cardiac myocytes as an increase in the Ca<sup>2+</sup> sparks and waves frequency. HEK cells should not express junctophilin-2 and thus the dysfunction found in heterologous systems cannot be due to alterations in the dyad. In fact, the RyR2<sup>R420Q</sup> also exhibits functional alterations as seen in RyR2<sup>R420Q</sup> unitary current analyses. At low [Ca<sup>2+</sup>]<sub>i</sub>, the RyR2<sup>R420Q</sup> channel is preferentially open in sub-conductance states, with higher open probability than the WT RyR2. The higher open probability, although in subconductance, can participate into the enhanced Ca<sup>2+</sup> spark frequency, as the opening of one RyR2<sup>R420Q</sup>, even at lower conductance, can trigger the opening of other RyRs in the same cluster (mutated or not) and produce a full Ca<sup>2+</sup> spark. However, the intrinsic alteration in RyR2<sup>R420Q</sup> openings, which favors sub-conductance states at low [Ca<sup>2+</sup>]<sub>i</sub> suggests that the ultrastructural alteration in the RyR2<sup>R420Q</sup> channel<sup>38</sup> alters its function. However, it is not so clear how a mutation in the N terminal domain can alter conductance. The R420 site seems to be an important residue for RyR2 function. While most of the CPVT RyR2 mutations have been

found in a single family, the RyR2<sup>R420Q</sup> mutation has been reported, as far as we know, in four apparently unrelated families<sup>16-18, 25</sup>, and the RyR2<sup>R420W</sup> in two<sup>19, 20</sup>. Unlike other RyR2 NTD mutations (e.g. R176Q, L433P)<sup>15, 35</sup>, the R420Q does not perturb N-terminus self-association. Instead, R420Q strengthens the interaction of N-terminus with the core solenoid within the C-terminal pore-forming region. Residue 420, which is buried within the NTD structure, does not form part of the NTD-core solenoid (nor NTD-NTD) interface(s)<sup>4</sup>. Thus, substitution of arginine-420 by glutamine does not directly impact inter-domain interactions but is likely to induce local conformational changes enabling the NTD to make more stable contacts with the core solenoid, probably reducing conductance.

In conclusion, our data show that the CPVT mutation RyR2<sup>R420Q</sup>, which induces a tighter interaction between the NTD and core solenoid domains of the channel, produces both a dysfunction at the single channel level and an impaired association with the junctophilin-2 protein responsible for nanostructural alterations of the dyad, representing a new mechanism for the genesis of CPVT.

## MATERIALS AND METHODS

Experiments were performed in male and female mice heterozygous RyR2<sup>R420Q</sup> knock in (KI) mice and wild-type (WT) littermates (4- 6 months old). Mice were created by PHENOMIN, Institut Clinique de la Souris (ICS), France (<http://www.phenomin.fr/»><sup>25</sup>). Experiments were made in accordance with the ethics principles laid down by the French Ministry of Agriculture and ECC directive 86/609/ECC under protocol agreement n° B9201901. h-iPS were obtained from patients' blood samples (after personal consent and ethical approval) in "Plate-forme iPSC Nantes, (<https://sfrsante.univ-nantes.fr/plates-formes/modeles-cellulaires-et-geniques/plate-forme-ipsc-nantes-cellules-souches-pluripotentes-induites-1101640.kjsp>) and differentiated into cardiac myocytes in the laboratory.

Extended methods section can be found in the online Supplementary Material.

## SUPPLEMENTARY MATERIAL

### *In-vivo experiments*

Mice were anaesthetized by isoflurane and DSI captors were implanted subcutaneously. Electrocardiograms (ECG) were recorded not earlier than one week after surgery by Holter telemetry in conscientious mice. Data were analyzed by ECG auto (EMKA technologies). For additional detail see<sup>25</sup>. Transthoracic echocardiography was made using a Vivid 9 (General Electric Healthcare) in M mode, as detailed earlier<sup>39</sup>

### *Single cell experiments*

Ventricular cardiac myocytes were isolated as previously detailed.<sup>40</sup> Patch-clamp and confocal experiments were performed at room temperature (~21°C) as in<sup>41</sup>.

### *Patch-clamp.*

Action potentials and ion currents were recorded using the patch clamp technique in the whole cell configuration (Axoclamp 1D). Standard intracellular solution to record AP and K<sup>+</sup>

currents contained (in mM): KCl 135, MgCl<sub>2</sub> 4, Na<sub>2</sub>-ATP 5, Na<sub>2</sub>-PC 3, glucose 10, HEPES 10 (pH 7.2). Standard extracellular solution contained (in mM): NaCl 140, KCl 4, MgCl<sub>2</sub> 1.1, CaCl<sub>2</sub> 1.8, HEPES 10 and glucose 10 (pH 7.4). To induce  $\beta$ -adrenergic activation, 100 nM isoproterenol (ISO) was added in some experiments.

Action potentials were evoked at 1 Hz in current-clamp configuration. In some experiments, 5 mM BAPTA was included in the intracellular solution to fully buffer intracellular Ca<sup>2+</sup>.

#### *Ca<sup>2+</sup> -induced Ca<sup>2+</sup> -release*

Simultaneous measurements of I<sub>Ca</sub> and [Ca<sup>2+</sup>]<sub>i</sub> transients were performed by the patch clamp technique (Axopatch 2A, Axon instruments) and confocal imaging (Leica SP5) in the line scan model.

Both extracellular and intracellular K<sup>+</sup> was replaced by equimolar Cs<sup>+</sup>; The Ca<sup>2+</sup> dye fluo-4 (50  $\mu$ M pentaK<sup>+</sup> salt) was added to the intracellular solution.

I<sub>Ca</sub> was recorded by 150 ms step depolarizations ranging from -50 mV to +60 mV in 10 mV increments. To inactivate the fast Na<sup>+</sup> current, each step was preceded by a slow ramp (700ms) from the holding potential (-80 mV) to -40 mV.

Raw fluorescence signals (F) were normalized to basal fluorescence (F<sub>0</sub>), measured at -80 mV. Ca<sup>2+</sup> -induced Ca<sup>2+</sup>- release (CICR) gain was calculated by dividing the peak of the [Ca<sup>2+</sup>]<sub>i</sub> transient to the area underlying the respective I<sub>Ca</sub>.

#### *Intracellular [Ca<sup>2+</sup>]<sub>i</sub> dynamics*

Isolated mice ventricular myocytes were loaded with the membrane permeant Fluo-3 AM as previously described<sup>40</sup>. Confocal Ca<sup>2+</sup> images were obtained exciting the cell at 500 nm with a white light laser and emission were collected at > 510 nm using laser scanning confocal microscope (Leica SP5) equipped with a 63x n.a. 1.2 water immersion objective in the line scan mode. To record [Ca<sup>2+</sup>]<sub>i</sub> transients, myocytes were electrically field stimulated by two Pt electrodes at 2 or 4 Hz. Before recording, Fluo-3 loaded myocytes were stimulated for 1 min to reach steady state. Ca<sup>2+</sup> sparks were recorded in quiescent cells after the [Ca<sup>2+</sup>]<sub>i</sub> transients

recordings.  $\text{Ca}^{2+}$  spark mass was calculated as the product of  $\text{Ca}^{2+}$  spark peak x duration at half peak x width at half peak.  $\text{Ca}^{2+}$  sparks in permeabilized cells were recorded as earlier explained<sup>40</sup> adjusting dextran concentration to reach a calculated osmolarity of 300 mOsm for the normal solution and 250 mOsm for the hypo-osmotic solution. The actual osmolarity values measured with an osmometer were 296 mOsm for the normal solution and 242 mOsm for the hypo-osmotic solution.

hi-PS-CM were loaded with Calbryte™ 520 AM (AAT bioquest), and viewed with the same confocal microscope than mice cells, but excited at 492 nm and emission collected at >514 nm. H-iPSC-CM were field stimulated at 1 Hz. The fluorescence values (F) were normalized to the basal fluorescence ( $F_0$ ) in order to obtain  $F/F_0$ . Spontaneous  $\text{Ca}^{2+}$  sparks and  $\text{Ca}^{2+}$  waves were recorded in quiescent cells, after  $[\text{Ca}^{2+}]_i$  transients recordings.

For SR  $\text{Ca}^{2+}$  load estimation, ventricular myocytes were rapidly perfused with 10 mmol/L caffeine just after field-stimulation. The amplitude of caffeine-evoked  $\text{Ca}^{2+}$  transients was used to assess global SR  $\text{Ca}^{2+}$  load. Fractional SR release was measured by normalizing the steady state of  $\text{Ca}^{2+}$  transient (peak  $F/F_0$ ) by the caffeine-evoked intracellular  $\text{Ca}^{2+}$  transient (peak  $F/F_0$  evoked by 10 mmol/L rapid caffeine application). Post-rest-potential was calculated by normalizing the first intracellular  $\text{Ca}^{2+}$  transient (peak  $F/F_0$ ), following a period of rest from about 2 minutes, to the steady-state  $[\text{Ca}^{2+}]_i$  transient, as previously<sup>40</sup>.

All confocal  $\text{Ca}^{2+}$  images analyses were performed by home-made routines using IDL software (Exelis Visual Information Solutions, Inc.)

*Simultaneous measurement of intra-SR  $\text{Ca}^{2+}$  and cytosolic  $\text{Ca}^{2+}$ .*

Changes in the intra-SR  $[\text{Ca}^{2+}]$  were measured using the low affinity  $\text{Ca}^{2+}$  fluorescent indicator Fluo-5N AM (Invitrogen) (as previously described<sup>42</sup>). Briefly, cells were incubated with a modified Tyrode's solution supplemented with Fluo-5N AM (20  $\mu\text{M}$  of dye in 20% pluronic acid-DMSO solution) at 37°C during 3 hours. Then, cells were washed with Tyrode's solution (250  $\mu\text{M}$   $\text{Ca}^{2+}$ ) and they were kept in this solution at room temperature.

Rhod-2 tripotassium salt was used to record cytosolic  $\text{Ca}^{2+}$  signals. This  $\text{Ca}^{2+}$  indicator was added to the internal solution obtaining a final concentration of 25  $\mu\text{M}$ .

$\text{Ca}^{2+}$  images were acquired with a FluoView 1000 (Olympus) confocal laser-scanning microscope. Fluo-5N was excited at 473 nm with a solid-state laser and fluorescence was detected between 515 and 585 nm. Rhod-2 was excited at 561 nm or 488 nm with a solid-state laser and fluorescence was detected at  $>585$  nm. Images were processed and analyzed using the software ImageJ. A custom macro was developed to align and de-skew the  $\text{Ca}^{2+}$  waves before analyzing these signals. Line-scan images were corrected for dye bleaching. The measurements are expressed as  $\Delta F/F_{\text{Caff}}$ , where  $F_{\text{Caff}}$  is the fluorescence recorded after emptying the SR with 10 mM caffeine (see <sup>42</sup> for details).

To remove any residual Fluo-5N from the cytosol the cells were irreversibly permeabilized using a protocol based on the disruption of the plasma membrane with saponin. Cardiomyocytes pre-incubated with Fluo-5N, were permeabilized in three steps using different solution: 1) washed twice with a  $\text{Ca}^{2+}$ -free Tyrode's solution (supplemented with 100  $\mu\text{M}$  of EGTA) to remove  $\text{Ca}^{2+}$  and avoid  $\text{Ca}^{2+}$  overload during the permeabilization; 2) cells were exposed to the internal solution (in mM: K-Asp 120,  $\text{K}_2\text{ATP}$  3,  $\text{MgCl}_2$  3, EGTA 0.1, phosphocreatine 10, HEPES 10 and creatine phosphokinase 5 U/L, pH was adjusted to 7.2 with KOH) for 30 s; 3) myocytes were incubated in a saponin permeabilization solution (in mM: K-Asp 100, KCl 20,  $\text{MgCl}_2$  3.7, EGTA 1, HEPES 10 and saponin 0.005%; pH was adjusted to 7.2 with KOH) at room temperature during 30 s. Between each step cells were centrifuged at 0.4 g for 1 min. The supernatant was discarded and the pellet was re-suspended into the next solution. Immediately following permeabilization the myocytes were centrifuged at 0.4 g, 1 min and the pellet was re-suspended in internal solution (in mM: K-Asp 120,  $\text{K}_2\text{ATP}$  3,  $\text{MgCl}_2$  3, EGTA 0.1, phosphocreatine 10, HEPES 10, creatine phosphokinase 5 U/L, Dextran 4% and Rhod-2 0.05). The  $[\text{Ca}^{2+}]_{\text{free}}$  in the internal solution was 100 nM. Then, cells were seeded onto coverslip and the experiments were carried out within 15 min after permeabilization.

### ***Protein expression***

RyR2 and calsequestrin-2 (CSQ2) protein expression was measured by western blot from ventricle lysates. Anti-RyR2 (#MA3-916, Affinity Bioreagents), Anti-CSQ2 (#PA1-913, Thermo Scientific) antibodies were used. GAPDH (#2118, Cell signalling) was used as reference.

### ***Super-resolution microscopy***

For STED microscopy, ventricular myocytes were obtained from 4 heterozygous RyR2<sup>R420Q</sup> males mice and 4 of their WT littermates. Cardiomyocytes isolation was performed as described before <sup>43</sup>. At the end of the procedure, cardiomyocytes were allowed to adhere on glass coverslips coated with laminin (1 µg/cm<sup>2</sup>) at room temperature for 2-4 hours. Then, non-adherent cells were removed with PBS and remaining cells were immediately fixed in cold methanol (-20°C) for 5 minutes. Cells were washed with PBS and stored at 4°C until immunocytostaining. Fixed cardiomyocytes were labelled with a primary RyR2 antibody (MA3-916, ThermoFischer Scientific) and a goat anti-mouse secondary antibody coupled to Alexa 488 (A-11001, ThermoFischer Scientific). Then, coverslips were mounted on glass slides with Mowiol®. Samples were imaged on a TCS SP8-gated STED confocal microscope (Leica) on the MIPSIT cell imaging platform of Paris Sud University. Using Huygens (SVI), images were then deconvolved with the CMLE algorithm using an experimental PSF calculated from the acquisition of at least ten fluorescent nanobeads. For the deconvolution, the signal to noise ratio was set to 7 and the threshold intensity was automatically calculated for the different images. Preprocessing was carried out in ImageJ with the help of home-made macros. The intracellular regions were selected for analysis. An automated threshold was calculated (Otsu method) on deconvolved STED images of RyR2 stained cells. The size of each cluster is determined and the clusters were grouped into functional calcium release unit (CRU) based on the edge-to-edge distance between clusters. A functional CRU was defined as a group of cluster having a distance <150 nm of each other (PMID: 26490742, Macquaide et al., Cardiovascular research, 2015).

***Electron microscopy (EM).*** WT and RyR2<sup>R420Q</sup> KI hearts were fixed by retrograde aortic perfusion using 3.5% glutaraldehyde in 0.1 M NaCaCo buffer, pH 7.2. Small bundles of cells

teased from the papillary muscles were then post-fixed in 2% OsO<sub>4</sub> in NaCaCo buffer for 2 hours and block-stained in saturated uranyl acetate. After dehydration, specimens were embedded in an epoxy resin (Epon 812). Ultrathin sections were cut using a Leica Ultracut R microtome (Leica Microsystem) with a Diatome diamond knife (DiatomeLtd. CH-2501 Biel, Switzerland) and double-stained with uranyl acetate and lead citrate. Sections were viewed in a Morgagni Series 268D electron microscope (FEI Company, Brno, Czech Republic), equipped with Megaview III digital camera.

*Quantitative Analysis of EM images.*

a. The frequency of calcium release units (CRUs) and of couplons was calculated in random micrographs taken at 22.000X of magnification. Specifically we collected two pictures for each cardiac cell. We defined as CRU a T-tubule with associated jSR vesicle(s), either single, multiple, or surrounding it. Each panel in Figure 1 shows a single CRU, which may contain multiple couplons, such those in panels B to F.

b. The jSR/T-tubule contact length was measured in random images at 72.000X of magnification. Electron micrographs of all the CRUs encountered during sample examination were taken randomly in different fibers until a sufficient sample size was collected. The length of the jSR/T-tubule contact regions were measured using the Soft Imaging System of the digital camera. Dyads that did not show clear membrane outlines were not photographed.

c. Average area of individual couplons was estimated assuming that EM section cuts across an approximately “circular” junction produces a random cord of such circles. The average measured chord ( $y$ ) is related to the diameter of the average circle ( $D$ ) by the equation:  $y = \pi D/4$ . We have used this equation to calculate the average diameter of each couplon and from that the average area.

d. The number of RYR2-feet in each couplon was estimated assuming that: a) the couplon is filled with RYR2-feet, which form ordered arrays touching each other as in <sup>44-46</sup>; and b) each RYR2-foot occupies an area of approximately 29x29nm <sup>44, 45</sup>.

e. The average width of jSR cisternae was measured in digital images taken at high magnification (72.000x) using the Soft Imaging System of the digital camera. For each group a high number of jSR profile (see Table II for more detail) showing clear membrane outline were collected. Three to six lines (depending on the length of the junctional profile) were randomly drawn across the jSR and measured.

f. The SR volume fraction was calculated by the well-established stereology point counting technique<sup>47, 48</sup> in electron micrographs taken at 22.000 X from cross-sections. In each fiber 2 pictures were taken in internal areas of the fibers, excluding the nuclei and regions. The images were then covered with an orthogonal arrays of dots at a spacing of 0.17  $\mu\text{m}$ , and the ratio of the number of dots falling over the jSR to the total number of dots covering the whole micrograph was used to calculate the percentage of fiber volume occupied by SR.

#### **Human induced pluripotent Stem cells derived cardiomyocytes (hiPSC-CM)**

Human induced pluripotent stem cells (hiPSCs) were thawed mTeSR<sup>TM</sup>1 (Stemcell Technologies) containing 10  $\mu\text{M}$  of Y27632 and plated on Matrigel<sup>®</sup> hESC-Qualified Matrix (Corning). The maintenance medium (mTeSR<sup>TM</sup>1) was changed every day and colonies of hiPSCs were passaged after reaching 80% confluency using 0.5 mM EDTA diluted in PBS without calcium and magnesium. Cell clumps were then diluted in fresh mTeSR<sup>TM</sup>1 and plated on new dishes coated with hESC-Qualified Matrigel<sup>®</sup>. The cardiac differentiation protocol was based on the protocols of Lian et al., and Burrige et al., with minor modifications<sup>49, 50</sup>. Briefly, cardiac differentiation was induced from cells at 80% of confluency that were detached using StemPro<sup>®</sup> Accutase<sup>®</sup> (ThermoFisher Scientific), diluted in mTeSR<sup>TM</sup>1 containing 5  $\mu\text{M}$  of Y27632 and counted. Cells were then plated at the density of 200'000 cells/cm<sup>2</sup> in 12-well plates coated with hESC-Qualified Matrigel<sup>®</sup>. The mTeSR<sup>TM</sup>1 was changed the next day and 2 days after plating (considered as day 0), the medium was exchanged by differentiation medium composed of RPMI containing 2% of B-27<sup>TM</sup> supplement without insulin (ThermoFisher Scientific). Between day 0 and day 2, 6  $\mu\text{M}$  of CHIR99021 was added in the differentiation medium. Between day 3 and day 5, 5  $\mu\text{M}$  of IWP2 was added into the

differentiation medium. From day 7, B-27<sup>TM</sup> supplement was used instead of B-27<sup>TM</sup> without insulin in the differentiation medium and was changed every two days. From day 11 to day 15, RPMI without glucose was used in the differentiation that was supplemented with lactate to increase the purity of the cell preparation. At day 18 of differentiation, cardiomyocytes were gently detached using TrypLE<sup>TM</sup> Express and 70'000 hiPSC-CMs were plated in a 2 well culture insert (ibidi) placed at the center of a 35 mm  $\mu$ -Dish (ibidi) coated with hESC-Qualified Matrigel®. The differentiation medium was changed every two days and cells were analysed between day 30 and 35.

### *Microelectrodes*

Microelectrodes were made of borosilicate capillary glass tubes using a DMZ-Universal puller (Zeitz-Instruments, Germany) with resistances above 20 M $\Omega$  and filled with 3M KCl. A double controlling warm system for both dish and perfused solution was used to maintain the temperature at around 35 °C. The iPSC-CM iPSC-CMsh iPSC-CMs seeded in ibidi dishes on 32 to 40 days after differentiation were used to record the spontaneous action potentials. The cells were taken out of incubator and perfused with the warm (37°C) basal solution (Tyrode solution: NaCl 137 mM, KCl 5.4 mM, CaCl<sub>2</sub>·2H<sub>2</sub>O 1.8 mM, MgCl<sub>2</sub>·6H<sub>2</sub>O 1 Mm, HEPES 10 mM). Beating cells with rod shape membranes were chosen to record AP recording. The APs were recorded under basal conditions for 2 min, and then during perfusion with 1  $\mu$ M ISO. After ISO perfusion, the record continued for washout.

### ***Single channels recordings***

Sarcoplasmic reticulum microsomes from mouse heart ventricles were prepared following Chamberlain et al., procedure (1983) with minor modifications. Briefly, tissue was homogenized in 290 mM sucrose, 3 mM NaN<sub>3</sub>, 10 mM Imidazole buffer, pH= 6.9. A heavy microsomal fraction was then isolated from the homogenate by differential centrifugation. The SR microsomal fractions were collected and diluted into a solution containing 0.29 M sucrose,

10 mM imidazole-HCl, pH 6.7. These samples were then aliquoted, flash frozen and stored at  $-80^{\circ}\text{C}$  until used.

Single-channel studies were carried out as described previously (Ramos-Franco et al., 2010). Bilayers were made from a mixture of phosphatidylethanolamine, phosphatidylserine, and phosphatidylcholine in a 5:4:1 ratio (50 mg/ml in decane). Lipids were obtained from Avanti Polar Lipids (Alabaster, AL) and Matreya LLC (State College, PA). Lipid bilayers were formed across a 100- $\mu\text{m}$  hole in a thin Teflon partition separating two aqueous compartments where the cytosolic compartment (Cis chamber) was virtually grounded and filled with a HEPES–Tris solution (250 mM/118 mM) at pH 7.4 and ATP (1 mM). The luminal compartment (trans chamber) was filled with HEPES–Ca<sup>2+</sup> (250 mM/50 mM), pH 7.4 and was here that voltage was applied. Membrane voltage was controlled using an Axopatch 200B (Molecular Devices, San Jose, CA). Unitary (single-channel) currents represent net ion currents in the lumen-to-cytosol direction. The current signal was digitized at 20 kHz through a Digidata 1322A interface (Molecular Devices, San Jose, California). and subsequently filtered at 2 kHz, unless specified otherwise. Data acquisition and analysis were carried out using pClamp software (Molecular Devices, San Jose, CA). The free Ca<sup>2+</sup> concentration in the cytosolic solution was buffered using BAPTA (1,2-Bis(2-aminophenoxy) ethane-N,N,N',N'-tetraacetic acid tetrapotassium salt) and dibromoBAPTA. Free Ca<sup>2+</sup> concentrations were calculated using 0.1 ionic equivalence and 21°C in the MaxChelator program (WinMaxC Stanford University, CA).

#### *Chemical cross-linking*

HEK293 cells were transiently transfected with plasmid DNA encoding for RyR2 N-terminus (residues 1-906 tagged with cMyc epitope) NT<sup>WT</sup> or NT<sup>R420Q</sup> using TurboFect (Thermo Scientific) according to the provider's instructions. 24 h post-transfection, cells were homogenized on ice in homogenization buffer (5 mM HEPES, 0.3 M sucrose, 10 mM DTT, pH 7.4) by 20 passages through a needle (0.6 x 30 mm) and dispersing the cell suspension through half volume of glass beads (425-600 microns, Sigma). Cell nuclei and glass beads were removed by centrifugation at 1500 x g for 5 min at 4 °C. The supernatant obtained

following a subsequent centrifugation step (20000 x *g* for 10 min at 4 °C) was retained and protein concentration was measured using the bicinchoninic acid (BCA) colorimetric assay (Thermo Scientific). Cell homogenate (20 µg) was incubated with glutaraldehyde (0.0025% or 260 µmol/l) for the following time-points: 0 min, 2 min, 5 min, 10 min, 15 min, 20 min, 30 min and 1 h. The reaction was stopped with the addition of hydrazine (2%) and SDS-PAGE loading buffer (60 mM Tris, 2% SDS, 10% glycerol, 5 mM EDTA, 0.01% bromophenol blue, pH 6.8). Samples were analyzed by SDS-PAGE and immunoblotting with Ab<sup>cMyc</sup> (mouse 9E10, Santa Cruz Biotechnology; used at 1:1000 dilution). Tetramer to monomer ratio was determined by densitometry using a GS-900 Scanner (Bio-Rad) and Image Lab software (Bio-Rad). Tetramer formation was calculated as follows:  $T = OD_T / (OD_T + OD_M) \times 100$ , where OD<sub>T</sub> and OD<sub>M</sub> correspond to optical density obtained for tetramer and monomer bands respectively.

#### *Co-immunoprecipitation*

HEK293 cells were transiently co-transfected with plasmid DNA for HA-RyR2-CT (residues 3529-4967 tagged with HA epitope) together with NT<sup>WT</sup> or NT<sup>R420Q</sup> using TurboFect. 24 h post-transfection cells were homogenized on ice in buffer (20 mM Tris, 150 mM NaCl, pH 7.4) as described above. Cell nuclei and glass beads were removed by centrifugation at 1500 x *g* for 5 min at 4 °C and the supernatant was incubated overnight at 4 °C in the presence of 0.5% CHAPS under rotary agitation. Following overnight solubilization and centrifugation at 20000 x *g* for 10 min at 4 °C to remove the insoluble material, the supernatant was incubated at 4 °C for 6 h with protein A sepharose beads (GE Healthcare) and 2 µg of Ab<sup>HA</sup> (rabbit ab9110, Abcam) under rotary agitation (2 µg of normal, non-immune rabbit IgG (Santa Cruz Biotechnology) was used as negative control). Beads were recovered at 1500 x *g* for 2 min at 4 °C, washed two times (10 min at 4 °C) with the IP buffer (20 mM Tris, 150 mM NaCl, 0.5% CHAPS, pH 7.4) and proteins were eluted with SDS-PAGE loading buffer. A small amount (1/10<sup>th</sup>) of the IP samples was analyzed by SDS-PAGE and immunoblotting with Ab<sup>HA</sup> (mouse 16B12, Biolegend; used at 1:1000 dilution) to assess HA-RyR2-CT expression and immunoprecipitation. The rest (9/10<sup>th</sup>) of the IP samples was analyzed by SDS-PAGE and

immunoblotting with Ab<sup>cMyc</sup> (mouse 9E10, Santa Cruz Biotechnology; used at 1:1000 dilution) to assess the amount of the co-precipitated RyR2 NT construct. The amount of co-precipitated RyR2 NT proteins was determined by densitometry (using GS-900 Scanner and Image Lab software), normalized against the amount of the input protein in the lysate and specific binding was calculated by subtracting the non-immune IgG IP signal from the anti-HA IP signal.

### **Acknowledgements**

This work was funded by Inserm and University Paris Sud, and grants from ANR (ANR-19-CE14-0031-01 to AMG), LabEx LERMIT (ANR-10-LABX-33). AZJr was recipient of a post-doctoral position from University Paris Sud. R.R was recipient of a postdoctoral fellowship from CORDDIM. LHY was recipient of the CSC.

	A	B	C	D	E
	No. CRUs /20 $\mu\text{m}^2$	No. of couplons /20 $\mu\text{m}^2$	Average length of each couplon (in nm)	Estimated average area of each couplon	Estimated No. of RYR- feet /couplon
WT	3.0 $\pm$ 1.1 (109)	3.8 $\pm$ 1.7 (109)	344 $\pm$ 236 (76)	0.151 $\mu\text{m}^2$	179
KI	1.9* $\pm$ 1.8 (214)	2.6* $\pm$ 1.8 (214)	286* $\pm$ 191 (108)	0.104 $\mu\text{m}^2$	123

**Table 1: Quantitative analysis of frequency and size of calcium release units (CRUs).**

The table shows: the number of CRUs (column A), the number of contacts between SR and T-tubules or couplons (column B), the average length of each couplon (column C), and finally estimated the average area of each couplon and the approximate number of RYR2-feet that could be contained in each couplon (columns D and E). *All data were collected from 3 WT hearts and 4 KI hearts. In parenthesis, the number of fibers analyzed (columns A and B), and number of couplons analyzed (column C). Data are shown as mean  $\pm$  SD and analyzed with Student's t test: \* $p$ <0.01.*

**Supplementary table 1**

Echocardiographic parameters of WT and KI mice under slight isoflurane anesthesia; heart weight to body weight at time of sacrifice, and membrane capacitance of isolated cardiomyocytes

Young (4-6 months)	HR (bpm)	EF (%)	FS (%)	LV mass (mg)	HW/BW (mg/g)	Cm (pF)
WT n=7	504.9±8.0	68.4±5.0	34.2±3.8	78.3±7.1	7.57±0.22 (n=23)	149.4±5.0 (n=72)
KI n=8	483.0±9.0	68.9±4.2	34.5±3.2	87.4±5.9	7.45±0.26 (n=15)	142.0±4.6 (n=71)
Old (1 year)	HR (bpm)	EF (%)	FS (%)	LV mass (mg)		
WT n=8	465.8±16.3	59.0±3.2	27.1±2.0	126.5±12.9		
KI n=8	468.1±13.1	64.6±2.3	30.6±1.6	110.8±10.9		

### **Supplementary table 2**

ECG parameters of WT and KI mice in awake freely moving animals.

<b>Day time</b>	<b>HR (b.p.m)</b>	<b>PR (ms)</b>	<b>QTc (ms)</b>
WT Male n=13	535.7±8.1	37.4±0.7	41.4±0.8
KI Male n=14	557.1±12.9	37.9±0.6	43.0±0.5
WT Female n=10	583.8±8.5*	39.2±0.8	42.6±1.2
KI Female n=9	557.5±7.3#	38.6±1.0	41.5±0.8
<b>Night time</b>	<b>HR (b.p.m)</b>	<b>PR (ms)</b>	<b>QTc (ms)</b>
WT Male n=10	575.2±12.1	35.5±0.9	41.2±1.1
KI Male N=11	588.7±15.1	36.7±0.8	43.2±0.7
WT Female n=10	613.9±13.2***	37.7±0.9	42.7±1.2
KI Female N=9	590.5±9.6	37.2±0.9	42.2±0.8

\*p<0.05 vs. male \*\*\*p<0.001 vs male

# p<0.05 vs. WT

## FIGURE LEGENDS

**Figure 1. RyR2<sup>R420Q</sup> induce arrhythmias.** **A.** Left. Example of an ECG recording of KI mice showing ventricular tachycardia (arrows) after emotional stress (hairdryer blowing protocol). Right. Average of VT episodes during 10 minutes recording in mice before and under emotional stress. 13 mice of each group were tested. **B.** Left. Ventricular ectopy (VE) occurrence in KI mouse after ISO injection. Right. Incidence of VE after ISO injection in 14 WT mice and 15 KI mice. **C.** Representative AP recordings from WT and KI myocytes with no Ca<sup>2+</sup> chelator (left) or with 5 mM BAPTA (right) in the intracellular solution. 100 nM ISO was superfused in the bath solution (bottom). The extra AP, consistent with triggered activity (TA) is marked by the arrow. The plot on the right shows the occurrence of DADs or Triggered Activity (TA) incidence measured in WT and KI myocytes, either without Ca<sup>2+</sup> chelator in the intracellular solution (left panels) or in the presence of 5 mM BAPTA (right) expressed as % of cells displaying at least one event during 1 Hz stimulation. n (positive cell/total): No chelation: n= 14 WT; n=14 KI. BAPTA: n=11 WT; n=9 KI. **D.** Ventricular arrhythmias during the exercise testing of a patient carrying the mutation RyR2<sup>R420Q</sup> (speed recording at 25mm/s). **E.** AP recorded in an iPSC-CM from the same patient (in E) showing DADs during ISO perfusion (1  $\mu$ M). **F.** DADs incidence in human iPSC-CM/iPSC-CMs in basal conditions and during ISO perfusion in 19 control cells (Ctl) and 30 RyR2<sup>R420Q</sup> carrier cells (Mu). \*p<0.05; \*\*p<0.01; \*\*\*p<0.001

**Figure 2. Mice and human cardiomyocytes expressing RyR2<sup>R420Q</sup> present more diastolic Ca<sup>2+</sup> release.** **A.** Line scan confocal images showing Ca<sup>2+</sup> sparks in ventricular cardiomyocytes isolated from a WT (top) and a KI (bottom) mouse in basal conditions (left) and during 100 nM ISO perfusion. **B.** Ca<sup>2+</sup> sparks frequency measured as number of events recorded per second in a 100  $\mu$ m line of scan in 30 WT cells, 10 WT in ISO presence, 31 KI and 18 KI+ISO. **C.** Ca<sup>2+</sup> spark mass, calculated as the peak F/F<sub>0</sub> multiplied by width at half maximum, by duration at half maximum. N=566 WT, 293 WT+ISO, 806 KI, 566 KI+ISO. **D.** Calculation of total Ca<sup>2+</sup> release as Ca<sup>2+</sup> sparks, calculated by multiplying the Ca<sup>2+</sup> spark mass by the Ca<sup>2+</sup> spark frequency in each cell. N as in B. **E.** Line scan images mouse ventricular cardiac myocyte from

WT (two top) and KI (two bottom) cells without and with ISO. F. percentage of arrhythmic cells in such protocol in 12 WT cells and 19 KI cells. **G.** example of RyR2 immunolabeling of a human iPSC-CM. **H.** Left. Line scan images of a h-iPSC-CM from the CPVT patient electrically stimulated at 1 Hz in absence (top) and presence (bottom) of 1  $\mu$ M ISO. Spontaneous diastolic  $\text{Ca}^{2+}$  release as  $\text{Ca}^{2+}$  waves are marked by the red arrows. Right. Percentage of arrhythmic cells in the presence of ISO in 59 control hi-PS-CM (Ctl-ISO, white hatched bar) and 44 mutant carriers (Mu-ISO, red hatched bar)

\* $p < 0.05$ ; \*\* $p < 0.01$ .

**Supplemental Figure S1.  $\text{Ca}^{2+}$  sparks characteristics in ventricular cardiomyocytes isolated from WT and KI mice.** **A.**  $\text{Ca}^{2+}$  spark amplitude (measured as the maximal value of fluorescence (F) normalized by the basal fluorescence (F<sub>0</sub>)). **B.**  $\text{Ca}^{2+}$  spark width measured at half maximum; **C.**  $\text{Ca}^{2+}$  spark duration at half maximum. N=566 WT, 293 WT+ISO, 806 KI, 566 KI+ISO from the cells presented in Fig. 2B. \* $p < 0.05$ ; \*\* $p < 0.01$ ; \*\*\* $p < 0.001$

**Figure 3. Mouse and human cardiomyocytes expressing RyR2<sup>R420Q</sup> show enhanced fractional release.** **A** Line scan images of a cardiomyocyte isolated from a WT (left) and a KI (right) mouse before (top) and during (bottom) 100nM isoproterenol perfusion. **B.**  $[\text{Ca}^{2+}]_i$  transient amplitude represented as the maximum value of F/F<sub>0</sub> where F is the fluorescence signal and F<sub>0</sub> the diastolic fluorescence during field stimulation at 2 Hz in 39 cells WT cells (white bar) and 38 KI (red bar); and at 4 Hz in 16 WT cells (gray bar), and 12 KI cells (dark red). **C.** decay time constant of the  $[\text{Ca}^{2+}]_i$  transients from the same cell groups than in B obtained by fitting the descending portion of the fluorescence trace to a single exponential function. **D.** Isoproterenol effect on  $[\text{Ca}^{2+}]_i$  transient amplitude (left bars) and on decay time (right bars) obtained by normalizing in each cell the values in ISO presence by the values before ISO application. \*\*\*  $p < 0.001$  within its own control (paired t-test) \* $p < 0.05$  between WT (n=15) and KI (n=17). **E.** SR  $\text{Ca}^{2+}$  load estimated by rapid caffeine application (10 mM) provided as peak fluorescence evoked by caffeine (F) during electrical stimulation at 2 Hz, normalized to the resting fluorescence (F<sub>0</sub>) in cardiomyocytes from both groups in absence

and presence of ISO (white bar: 11 WT cells, hatched bar, 10 WT cells after ISO, red bar: 11 KI cells, red hatched bar, 8 KI cells in the presence of ISO). **F.** decay time constant obtained as in C but during caffeine application in the same cells than in E. **G.** Fractional release, calculated as the peak  $F/F_0$  evoked by electrical stimulations at 4 Hz, normalized by the caffeine-evoked peak  $F/F_0$  in 10 WT cardiomyocytes (white bar) and in 11 KI myocytes (red bar). **H.** Left. Line scan of human cardiomyocytes derived from iPS from a control (Ctl, top) and mutant carrier (Mu, bottom) during field stimulation at 1 Hz. Right, Line scan images from h-iPS during caffeine application (time of caffeine presence is noted by the green thick line). **I.** Averaged values of fractional release (obtained as for mice cells in G) for 38 control cells (white bar) and 46 RyR2<sup>R420Q</sup> carriers (red bar). **J.** The intra-SR  $Ca^{2+}$  threshold for spontaneous  $Ca^{2+}$  wave generation is lower in R420Q mice. Representative line-scans (upper panel) and traces (lower panel) of cytosolic and luminal (SR)  $Ca^{2+}$  signal in permeabilized cardiomyocytes from WT and KI mice. High concentration of caffeine (10mM) was used to determine the minimal fluorescence signal when the SR is empty. **K.** Quantitative analysis of SR  $Ca^{2+}$  wave threshold in permeabilized cardiomyocytes with a  $[Ca^{2+}]_{cyt}$  of 100 nM.  $N > 8$   $n > 4$  for each group of animals. \*  $p < 0.05$ .

**Figure 4.  $I_{Ca}$  in KI mice is normal, but triggers more  $Ca^{2+}$  release.** **A** Representative examples of  $I_{CaL}$  traces and their evoked intracellular  $Ca^{2+}$  transients simultaneously recorded in WT and KI myocytes. **B** Average ( $\pm$ SE)  $Ca^{2+}$  transient amplitude (Top panel) and  $I_{CaL}$  density (lower panel) voltage dependence in WT and KI myocytes.  $N=9$  WT cells,  $n=15$  KI cells. Peak fluorescence signal at each depolarizing step (F) was normalized by basal fluorescence measured at -80 mV ( $F_0$ ). **C** Average ( $\pm$ SE)  $Ca^{2+}$  induced  $Ca^{2+}$  release gain, measured in each cell as pic of  $F/F_0$  normalized to the  $I_{Ca}$  integral during depolarization at -20 mV. **D** Average ( $\pm$ SE)  $I_{CaL}$  activation/inactivation curves. Activation in 10 WT and 15 KI cells. Inactivation in 7 WT and 11 KI cells. Color code: WT myocytes= white; KI myocytes= red. \*  $p < 0.05$ .

**Figure 5 RyR2<sup>R420Q</sup> induces nanodomains structural alterations.** **A.** Deconvoluted superresolution image of RyR2 in a cardiomyocyte from a WT mouse (left) and KI mouse (right).

**B.** Cluster size in WT and KI cells (9516 clusters in 49 cells from 3 WT, 14165 clusters in 147 cells from 5 KI). **C.** Representative examples of western blot bands corresponding to RyR2 and GAPDH in WT and KI mice, as indicated. Right panel shows the quantification of the RyR2 bands, normalized to GAPDH in the two experimental groups (18 WT hearts, white bar; and 20 KI mice hearts, black bar). **D.** Normalized Frequency count of the distance of each cluster to the line connecting most, measured in WT cells (white wider bars), and KI cells (black narrower bars). Proportion test  $p < 0.05$ . **E.** CRUs, specialized intracellular junctions between the jSR (labeled in yellow in a) and T-tubules (labeled in green in a). The cytoplasmic domains of RyR2, i.e. the feet, are visible as evenly spaced densities (pointed by a series of arrows in panel b) spanning the gap between jSR and T-tubule. The jSR is wrapped around the T-tubule to form a CRU (panel a), or associated to form a CRU with multiple (two or more) couplons (panel b). In WT, couplons are usually quite extended (panels a and b), while in cardiomyocytes we may find couplons, which appear fairly normal in length (panels c & e), and other ones in which the jSR is either shorter or apparently fragmented (panels d, f, g & h). The jSR contains a classic chain-like electron dense polymer (single arrows in panels b and d), representing CASQ2: in KI myocytes, the chain-like polymer of condensed CASQ2 may be sometimes missing in some portions of the jSR. **F.** junctional SR width (jSR) measured in 76 images from 4 WT mice hearts (white bar) and 108 images from 4 KI hearts (black bar).  $*p < 0.01$   $***p < 0.001$ . **G.** Co-ip examples of RyR2 with Junctophilin 2 (JPH2). At left, the co-IP, at right, the total RyR2. Experiments were repeated in 2 WT hearts and 4 KI hearts.

**Supplemental Figure S2. Calsequestrin expression.** Representative examples of western blot bands corresponding to CSQ2 and GAPDH in WT and KI mice, as indicated. Lower panel shows the quantification of CSQ2, normalized to GAPDH in 8 hearts each.

Supplemental Fig. 3. **Ca<sup>2+</sup> sparks characteristics in normal and hypo-osmotic internal solution.** **A.** Ca<sup>2+</sup> sparks frequency calculated as number of events per second per 100 $\mu$ m line of scan in 12 cells in internal solution of normal osmolarity (calculated for 300 mOsm,

measured 296 mOsm, dark green) or in 8 cells in an hypo-osmotic internal solution (calculated for 250 mOsm, measured 242 mosm, light green). **B.** SR Ca<sup>2+</sup> load estimated by rapid caffeine (20mM) solution and calculated as in Fig. 3B in 7 cells of each group. **C.** Ca<sup>2+</sup> spark amplitude measured in 3479 Ca<sup>2+</sup> sparks in normal solution and in 2563 sparks in hypo-osmotic solution. **D.** Duration at half maximum measured in the same Ca<sup>2+</sup> sparks. **E.** Width at half maximum measured in the same Ca<sup>2+</sup> sparks. **F.** Ca<sup>2+</sup> sparks mass calculated from data in C-E. \*\*\*p<0.001.

**Figure 6. RyR2<sup>R420Q</sup> unitary current recordings show alterations.** **A** 3H-Ryanodine binding to SR microsomes from 4 WT (open squares) and from 4 KI hearts (gray circles) normalized to the protein content. **B.** 3H-Ryanodine binding to SR microsomes normalized to the binding of each sample at pCa5. Symbols as in A. **C.** Ca<sup>2+</sup> sparks frequency (measured as in Fig. 2B) recorded in permeabilized cells plotted as a function of the [Ca<sup>2+</sup>]<sub>i</sub>. Symbols as in A. \*p<0.05. **D.** WT RyR2 single-channel conducting Ca<sup>2+</sup>. Traces obtained at 0 mV of membrane potential, in the cytosolic presence of 500 nM free Ca<sup>2+</sup> (top) and 1 μM free Ca<sup>2+</sup> (bottom). **E** Amplitude histograms obtained from 3-min single-channel recordings and fitted with multi-Gaussian functions (ordinate shown as square root of the bin counts). **F** Single-channel recordings of RyR2<sup>R420Q</sup> conducting Ca<sup>2+</sup>, where s1, s2 and s3 indicate the conductance to the different substates obtained at +20 mV. The amplitude levels (s1, s2 and s3) are indicated by dashed lines. In all traces c denotes the closed state. Filtering, 800 Hz. **G.** As in E but for RyR2<sup>R420Q</sup>. **H.** Single-channel recordings of RyR2<sup>R420Q</sup> conducting Ca<sup>2+</sup> (left) and amplitude histograms (right) at higher cytosolic [Ca<sup>2+</sup>]<sub>i</sub>. **I.** Open probability of the full conductance (black squares) and added sub-conductance (blue circles) states plotted as a function of the cytosolic free [Ca<sup>2+</sup>]<sub>i</sub>. Full conductance open probability fitted with a sigmoidal function.

**Supplemental Fig. S4. A** Representative single-channel recordings illustrating current fluctuations of a RyR2<sup>R420Q</sup> channel, recorded at +30 mV of membrane potential, in symmetrical 250 mM Cs-methanesulfonate, 20 mM HEPES, 1 mM BAPTA, and at the

indicated cytosolic free  $[Ca^{2+}]$ , & pH 7.4. Channel openings shown as positive deflections with dashed lines indicating the sub-conductance states, and the solid lines the current levels for the closed and open states. Filtering, 800 Hz. Amplitude histograms were constructed and fitted with multi-Gaussian functions in each condition (ordinate is shown as square root of the bin counts). Vertical scale bar is 10 pA

**Supplementary Fig. S5. Phosphorylation of the RyR2.** **A.** Representative examples of western blot bands corresponding to phosphorylated RyR2 compared to the total RyR2. **B.** quantitative analysis of RyR2 phosphorylation at the S2808 normalized to total RyR2 in 18 WT hearts (white bar) and 19 KI hearts (gray bar). **C.** The same as in B but for the S2814 equivalent position.

**Figure 7. A.** Chemical cross-linking assays of HEK293 cell homogenates expressing cMyc-tagged NT<sup>WT</sup> (RyR2 residues 1-906) or NT<sup>R420Q</sup>. Cell homogenates were incubated with glutaraldehyde for the indicated time points under reducing (10 mM DTT) conditions and analyzed by immunoblotting using Ab<sup>cMyc</sup>; monomer (M) and tetramer (T) are indicated with the arrows. Densitometry analysis (n = 10) performed on the bands corresponding to tetramer and monomer moieties was used to calculate tetramer formation. Data are normalized for WT and given as mean value  $\pm$  SEM; statistical analysis was carried out using Student's t-test. **B.** Co-immunoprecipitation assays from HEK293 cells co-expressing NT<sup>WT</sup> or NT<sup>R420Q</sup> together with HA-tagged RyR2-CT (residues 3529-4967). HA-RyR2-CT was immunoprecipitated with Ab<sup>HA</sup> from CHAPS-solubilized cell lysates and the presence of co-precipitated NT<sup>WT</sup>/NT<sup>R420Q</sup> was analyzed by immunoblotting using Ab<sup>cMyc</sup> (top). To detect immuno-isolated HA-RyR2-CT, 1/10<sup>th</sup> of IP samples was analyzed by immunoblotting using Ab<sup>HA</sup> (bottom). Non-immune rabbit IgG served as negative control. An aliquot of HEK293 cell lysate corresponding to 1% of the amount processed in the co-IP assay was included in the gels to assess protein expression. Data summary (n  $\geq$  8) for NT specific binding (non-immune IgG IP signal subtracted from anti-HA IP signal) following densitometry analysis and

normalization to each construct's respective lysate (taken as 100%). Data are given as mean value  $\pm$  SEM.; statistical analysis was carried out using Student's t-test.

1. Mehra R. Global public health problem of sudden cardiac death. *Journal of electrocardiology*. 2007;40:S118-22.
2. Leenhardt A, Lucet V, Denjoy I, Grau F, Ngoc DD and Coumel P. Catecholaminergic polymorphic ventricular tachycardia in children. A 7-year follow-up of 21 patients. *Circulation*. 1995;91:1512-9.
3. Imberti JF, Underwood K, Mazzanti A and Priori SG. Clinical Challenges in Catecholaminergic Polymorphic Ventricular Tachycardia. *Heart, lung & circulation*. 2016;25:777-83.
4. Peng W, Shen H, Wu J, Guo W, Pan X, Wang R, Chen SR and Yan N. Structural basis for the gating mechanism of the type 2 ryanodine receptor RyR2. *Science*. 2016;354.
5. George CH JH, Thomas NL, Fry DL, Lai FA. Ryanodine receptors and ventricular arrhythmias: Emerging trends in mutations, mechanisms and therapies. *J Mol and Cell Cardiol*. 2007;42:34-50.
6. Yano M, Yamamoto T, Ikeda Y and Matsuzaki M. Mechanisms of Disease: ryanodine receptor defects in heart failure and fatal arrhythmia. *Nat Clin Pract Cardiovasc Med*. 2006;3:43-52.
7. Jiang D CW, Wang R, Zhang L, Chen SR. . Loss of luminal Ca<sup>2+</sup> activation in the cardiac ryanodine receptor is associated with ventricular fibrillation and sudden death. *Proc Natl Acad Sci U S A* 2007;104:18309-14.
8. Zhao YT, Valdivia CR, Gurrola GB, Powers PP, Willis BC, Moss RL, Jalife J and Valdivia HH. Arrhythmogenesis in a catecholaminergic polymorphic ventricular tachycardia mutation that depresses ryanodine receptor function. *Proc Natl Acad Sci U S A*. 2015;112:E1669-77.
9. Fernandez-Velasco M, Rueda A, Rizzi N, Benitah J-P, Colombi B, Napolitano C, Priori SG, Richard S and Maria Gomez A. Increased Ca<sup>2+</sup> Sensitivity of the Ryanodine Receptor Mutant RyR2(R4496C) Underlies Catecholaminergic Polymorphic Ventricular Tachycardia. *Circulation Research*. 2009;104:201-U116.
10. Neco P, Torrente AG, Mesirca P, Zorio E, Liu N, Priori SG, Napolitano C, Richard S, Benitah J-P, Mangoni ME and Gomez AM. Paradoxical Effect of Increased Diastolic Ca<sup>2+</sup> Release and Decreased Sinoatrial Node Activity in a Mouse Model of Catecholaminergic Polymorphic Ventricular Tachycardia. *Circulation*. 2012;126:392-+.
11. Jiang D XB, Zhang L, Chen SR. Enhanced basal activity of a cardiac Ca<sup>2+</sup> release channel (ryanodine receptor) mutant associated with ventricular tachycardia and sudden death. *Circ Res* 2005;97:1173-1181.
12. Lehnart SE, Wehrens XH, Laitinen PJ, Reiken SR, Deng SX, Cheng Z, Landry DW, Kontula K, Swan H and Marks AR. Sudden death in familial polymorphic ventricular tachycardia associated with calcium release channel (ryanodine receptor) leak. *Circulation*. 2004;109:3208-14.
13. Hwang HS, Nitu FR, Yang Y, Walweel K, Pereira L, Johnson CN, Faggioni M, Chazin WJ, Laver D, George AL, Jr., Cornea RL, Bers DM and Knollmann BC. Divergent regulation of ryanodine receptor 2 calcium release channels by arrhythmogenic human calmodulin missense mutants. *Circ Res*. 2014;114:1114-24.
14. Uchinoumi H, Yano M, Suetomi T, Ono M, Xu X, Tateishi H, Oda T, Okuda S, Doi M, Kobayashi S, Yamamoto T, Ikeda Y, Ohkusa T, Ikemoto N and Matsuzaki M. Catecholaminergic polymorphic ventricular tachycardia is caused by mutation-linked defective conformational regulation of the ryanodine receptor. *Circ Res*. 2010;106:1413-24.
15. Seidel M, Thomas NL, Williams AJ, Lai FA and Zissimopoulos S. Dantrolene rescues aberrant N-terminus intersubunit interactions in mutant pro-arrhythmic cardiac ryanodine receptors. *Cardiovasc Res*. 2015;105:118-28.
16. Domingo D, Neco P, Fernandez-Pons E, Zissimopoulos S, Molina P, Olague J, Suarez-Mier MP, Lai FA, Gomez AM and Zorio E. Non-ventricular, Clinical, and Functional Features of the RyR2(R420Q) Mutation Causing Catecholaminergic Polymorphic Ventricular Tachycardia. *Rev Esp Cardiol (Engl Ed)*. 2015;68:398-407.

17. Medeiros-Domingo A BZ, Tester DJ, et al. . The RYR2-encoded ryanodine receptor/calcium release channel in patients diagnosed previously

with either catecholaminergic polymorphic ventricular tachycardia or genotype negative, exercise-induced long QT syndrome: a comprehensive open reading frame mutational analysis. . *J Am Coll Cardiol*. 2009;54:2065–2074.

18. Arad M, Glikson M, El-Ani D and Monserrat-Inglesias L. A family with recurrent sudden death and no clinical clue. *Annals of noninvasive electrocardiology : the official journal of the International Society for Holter and Noninvasive Electrocardiology, Inc*. 2012;17:387-93.

19. Nishio H, Iwata M and Suzuki K. Postmortem molecular screening for cardiac ryanodine receptor type 2 mutations in sudden unexplained death: R420W mutated case with characteristics of status thymico-lymphatics. *Circ J*. 2006;70:1402-6.

20. Baucé B, Rampazzo A, Basso C, Bagattin A, Daliento L, Tiso N, Turrini P, Thiene G, Danieli GA and Nava A. Screening for ryanodine receptor type 2 mutations in families with effort-induced polymorphic ventricular arrhythmias and sudden death: early diagnosis of asymptomatic carriers. *J Am Coll Cardiol*. 2002;40:341-9.

21. Tester DJ, Spoon DB, Valdivia HH, Makielski JC and Ackerman MJ. Targeted mutational analysis of the RyR2-encoded cardiac ryanodine receptor in sudden unexplained death: a molecular autopsy of 49 medical examiner/coroner's cases. *Mayo Clinic proceedings*. 2004;79:1380-4.

22. Okudaira N, Kuwahara M, Hirata Y, Oku Y and Nishio H. A knock-in mouse model of N-terminal R420W mutation of cardiac ryanodine receptor exhibits arrhythmogenesis with abnormal calcium dynamics in cardiomyocytes. *Biochem Biophys Res Commun*. 2014;452:665-8.

23. Borko L, Bauerova-Hlinkova V, Hostinova E, Gasperik J, Beck K, Lai FA, Zahradnikova A and Sevcik J. Structural insights into the human RyR2 N-terminal region involved in cardiac arrhythmias. *Acta crystallographica Section D, Biological crystallography*. 2014;70:2897-912.

24. Novak A, Barad L, Lorber A, Gherghiceanu M, Reiter I, Eisen B, Eldor L, Itskovitz-Eldor J, Eldar M, Arad M and Binah O. Functional abnormalities in iPSC-derived cardiomyocytes generated from CPVT1 and CPVT2 patients carrying ryanodine or calsequestrin mutations. *Journal of cellular and molecular medicine*. 2015;19:2006-18.

25. Wang YY, Mesirca P, Marques-Sule E, Zahradnikova A, Jr., Villejoubert O, D'Ocon P, Ruiz C, Domingo D, Zorio E, Mangoni ME, Benitah JP and Gomez AM. RyR2R420Q catecholaminergic polymorphic ventricular tachycardia mutation induces bradycardia by disturbing the coupled clock pacemaker mechanism. *JCI Insight*. 2017;2.

26. Hirano Y, Moscucci A and January CT. Direct measurement of L-type Ca<sup>2+</sup> window current in heart cells. *Circ Res*. 1992;70:445-55.

27. Gómez AM, Valdivia HH, Cheng H, Lederer MR, Santana LF, Cannell MB, McCune SA, Altschuld RA and Lederer WJ. Defective excitation-contraction coupling in experimental cardiac hypertrophy and heart failure. *Science*. 1997;276:800-6.

28. Gomez AM, Guatimosim S, Dilly KW, Vassort G and Lederer WJ. Heart failure after myocardial infarction: altered excitation-contraction coupling. *Circulation*. 2001;104:688-93.

29. Munro ML, Jayasinghe ID, Wang Q, Quick A, Wang W, Baddeley D, Wehrens XH and Soeller C. Junctophilin-2 in the nanoscale organisation and functional signalling of ryanodine receptor clusters in cardiomyocytes. *Journal of cell science*. 2016;129:4388-4398.

30. Knollmann BC, Chopra N, Hlaing T, Akin B, Yang T, Etensohn K, Knollmann BE, Horton KD, Weissman NJ, Holinstat I, Zhang W, Roden DM, Jones LR, Franzini-Armstrong C and Pfeifer K. Casq2 deletion causes sarcoplasmic reticulum volume increase, premature Ca<sup>2+</sup> release, and catecholaminergic polymorphic ventricular tachycardia. *J Clin Invest*. 2006;116:2510-20.

31. Chopra N and Knollmann BC. Triadin regulates cardiac muscle couplon structure and microdomain Ca(2+) signalling: a path towards ventricular arrhythmias. *Cardiovasc Res*. 2013;98:187-91.

32. Qin J, Valle G, Nani A, Nori A, Rizzi N, Priori SG, Volpe P and Fill M. Luminal Ca<sup>2+</sup> regulation of single cardiac ryanodine receptors: insights provided by calsequestrin and its mutants. *J Gen Physiol.* 2008;131:325-34.
33. Cannell MB, Kong CH, Imtiaz MS and Laver DR. Control of sarcoplasmic reticulum Ca<sup>2+</sup> release by stochastic RyR gating within a 3D model of the cardiac dyad and importance of induction decay for CICR termination. *Biophys J.* 2013;104:2149-59.
34. Marx SO, Reiken S, Hisamatsu Y, Jayaraman T, Burkhoff D, Rosemblyt N and Marks AR. PKA phosphorylation dissociates FKBP12.6 from the calcium release channel (ryanodine receptor): defective regulation in failing hearts. *Cell.* 2000;101:365-76.
35. Seidel M, de Meritens CR, Johnson L, Parthimos D, Bannister M, Thomas NL, Ozekhome-Mike E, Lai FA and Zissimopoulos S. Identification of an amino-terminus determinant critical for ryanodine receptor/Ca<sup>2+</sup> release channel function. *Cardiovasc Res.* 2020.
36. Takeshima H, Komazaki S, Nishi M, Iino M and Kangawa K. Junctophilins: a novel family of junctional membrane complex proteins. *Molecular cell.* 2000;6:11-22.
37. Reynolds JO, Quick AP, Wang Q, Beavers DL, Philippen LE, Showell J, Barreto-Torres G, Thuerauf DJ, Doroudgar S, Glembotski CC and Wehrens XH. Junctophilin-2 gene therapy rescues heart failure by normalizing RyR2-mediated Ca<sup>2+</sup> release. *International journal of cardiology.* 2016;225:371-380.
38. Kimlicka L, Tung CC, Carlsson AC, Lobo PA, Yuchi Z and Van Petegem F. The cardiac ryanodine receptor N-terminal region contains an anion binding site that is targeted by disease mutations. *Structure.* 2013;21:1440-9.
39. Llach A, Mazevet M, Mateo P, Villejouvert O, Ridoux A, Rucker-Martin C, Ribeiro M, Fischmeister R, Crozatier B, Benitah JP, Morel E and Gómez AM. Progression of excitation-contraction coupling defects in doxorubicin cardiotoxicity. *J Mol Cell Cardiol.* 2019;126:129-139.
40. Ruiz-Hurtado G, Li L, Fernandez-Velasco M, Rueda A, Lefebvre F, Wang Y, Mateo P, Cassan C, Gellen B, Benitah JP and Gomez AM. Reconciling depressed Ca<sup>2+</sup> sparks occurrence with enhanced RyR2 activity in failing mice cardiomyocytes. *Journal of General Physiology.* 2015;146:295-306.
41. Fernandez-Velasco M, Ruiz-Hurtado G, Rueda A, Neco P, Mercado-Morales M, Delgado C, Napolitano C, Priori SG, Richard S, MariaGomez A and Benitah JP. RyRCa(2+) Leak Limits Cardiac Ca<sup>2+</sup> Window Current Overcoming the Tonic Effect of Calmodulin Mice. *Plos One.* 2011;6:10.
42. Fernandez-Tenorio M and Niggli E. Real-time intra-store confocal Ca(2+) imaging in isolated mouse cardiomyocytes. *Cell Calcium.* 2016;60:331-340.
43. Leroy J, Richter W, Mika D, Castro LR, Abi-Gerges A, Xie M, Scheitrum C, Lefebvre F, Schittl J, Mateo P, Westenbroek R, Catterall WA, Charpentier F, Conti M, Fischmeister R and Vandecasteele G. Phosphodiesterase 4B in the cardiac L-type Ca(2)(+) channel complex regulates Ca(2)(+) current and protects against ventricular arrhythmias in mice. *J Clin Invest.* 2011;121:2651-61.
44. Franzini-Armstrong C and Nunzi G. Junctional feet and particles in the triads of a fast-twitch muscle fibre. *J Muscle Res Cell Motil.* 1983;4:233-52.
45. Block BA, Imagawa T, Campbell KP and Franzini-Armstrong C. Structural evidence for direct interaction between the molecular components of the transverse tubule/sarcoplasmic reticulum junction in skeletal muscle. *J Cell Biol.* 1988;107:2587-600.
46. Protasi F, Sun XH and Franzini-Armstrong C. Formation and maturation of the calcium release apparatus in developing and adult avian myocardium. *Dev Biol.* 1996;173:265-78.
47. Mobley BA and Eisenberg BR. Sizes of components in frog skeletal muscle measured by methods of stereology. *J Gen Physiol.* 1975;66:31-45.
48. Loud AV. A Method for the Quantitative Estimation of Cytoplasmic Structures. *J Cell Biol.* 1962;15:481-7.
49. Lian X, Zhang J, Azarin SM, Zhu K, Hazeltine LB, Bao X, Hsiao C, Kamp TJ and Palecek SP. Directed cardiomyocyte differentiation from human pluripotent stem cells by modulating Wnt/beta-catenin signaling under fully defined conditions. *Nat Protoc.* 2013;8:162-75.

50. Burrige PW, Holmstrom A and Wu JC. Chemically Defined Culture and Cardiomyocyte Differentiation of Human Pluripotent Stem Cells. *Curr Protoc Hum Genet*. 2015;87:21 3 1-21 3 15.

Figure 1

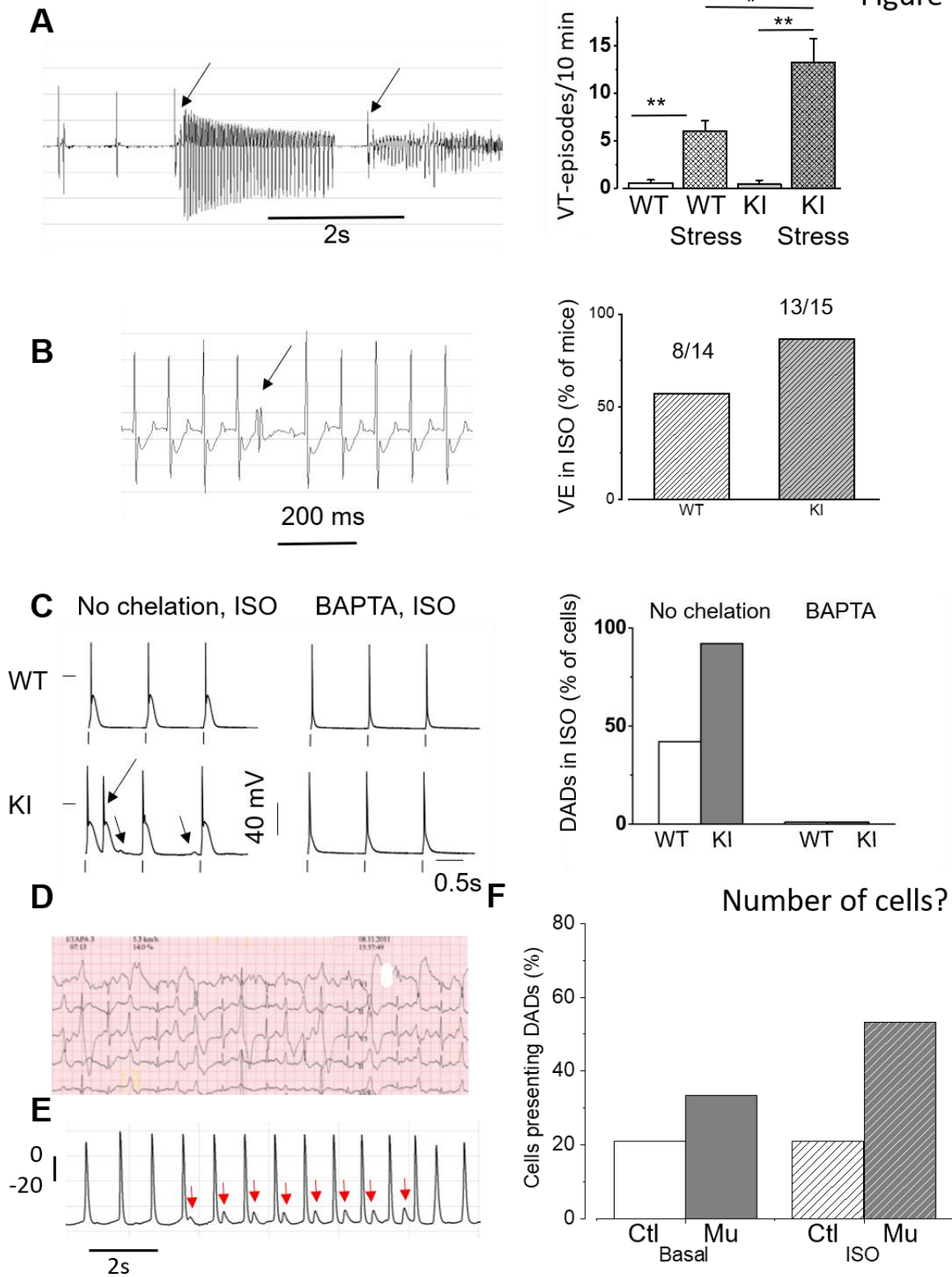


Figure 2

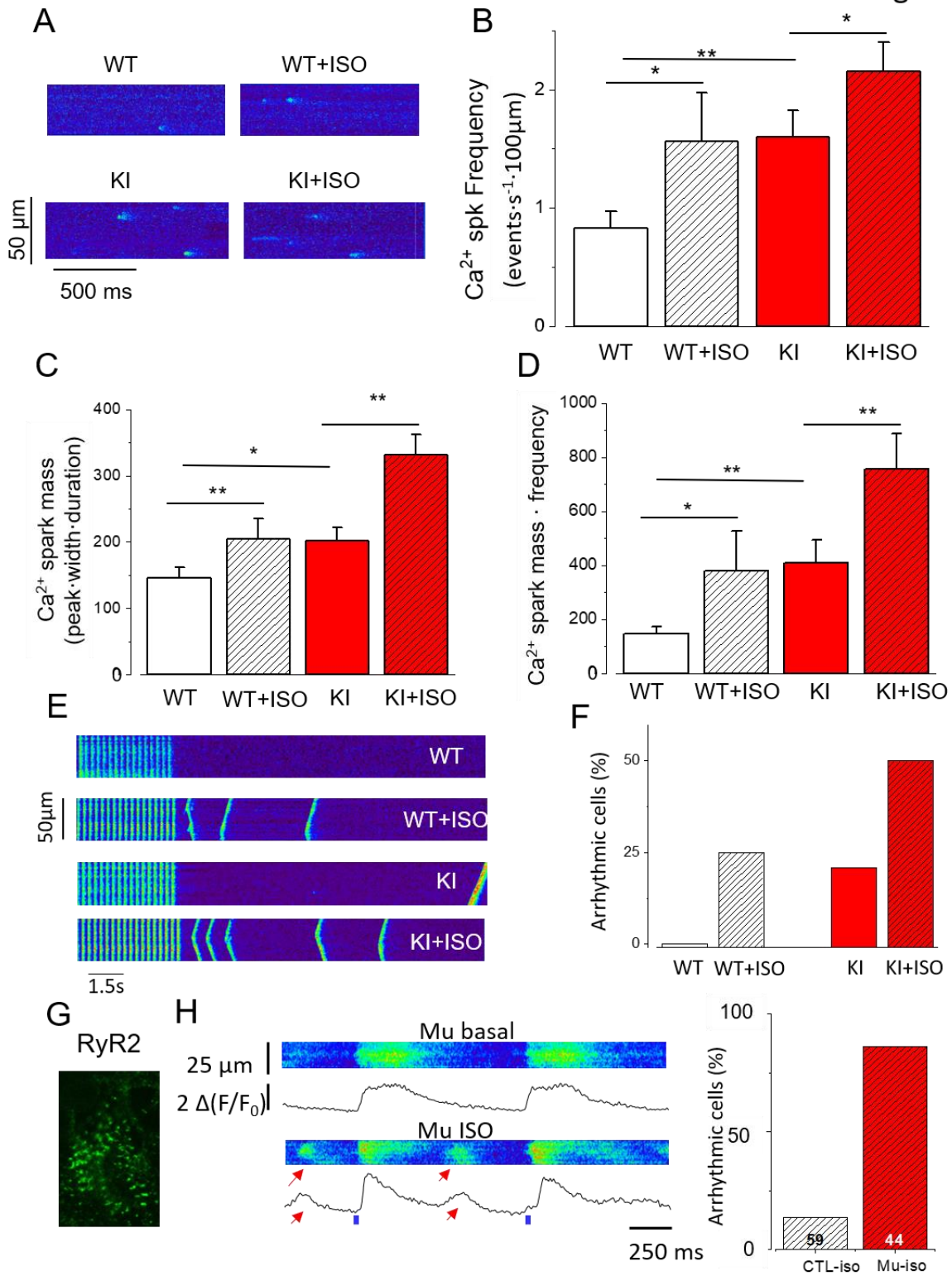


Figure 3

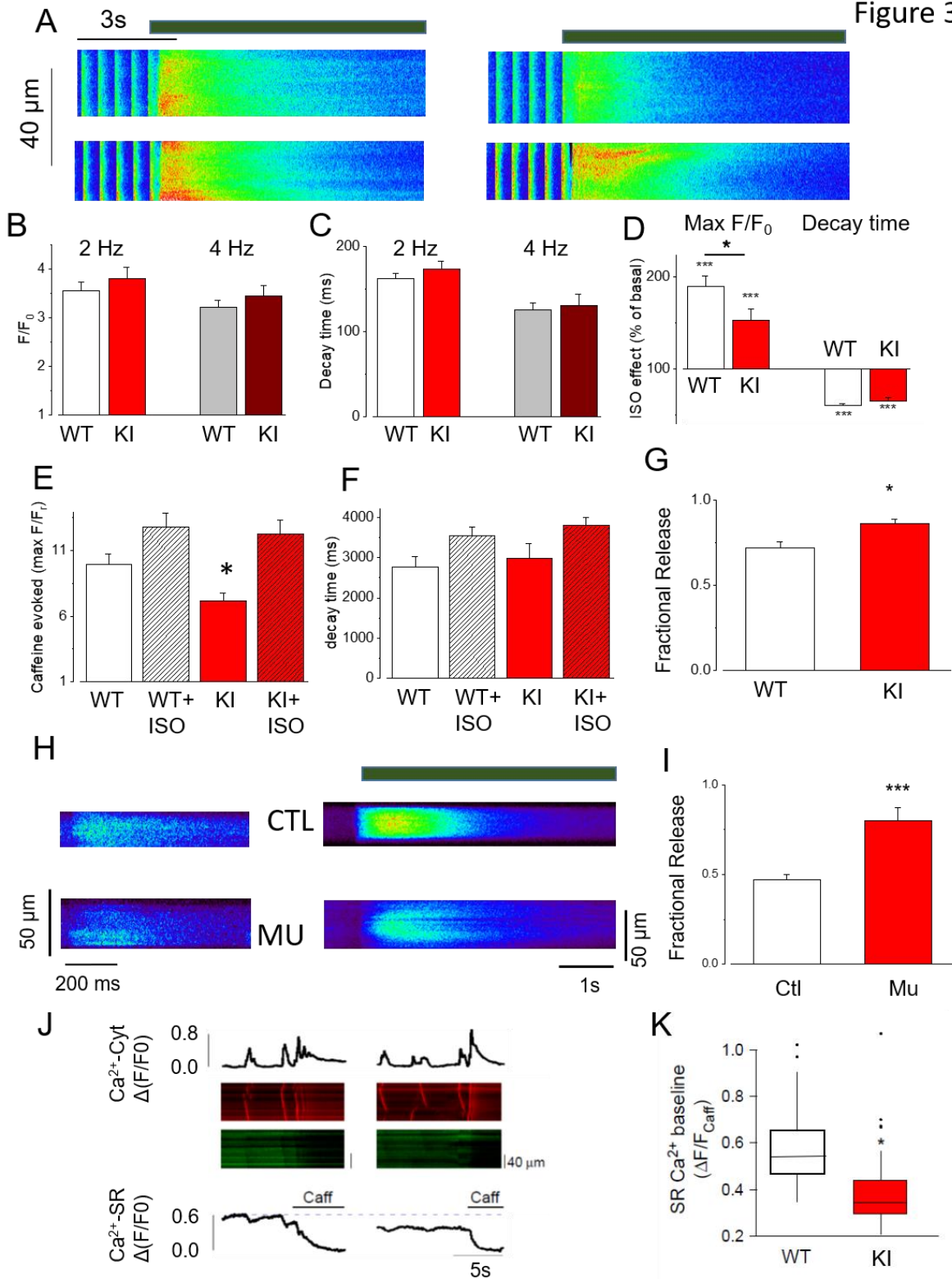
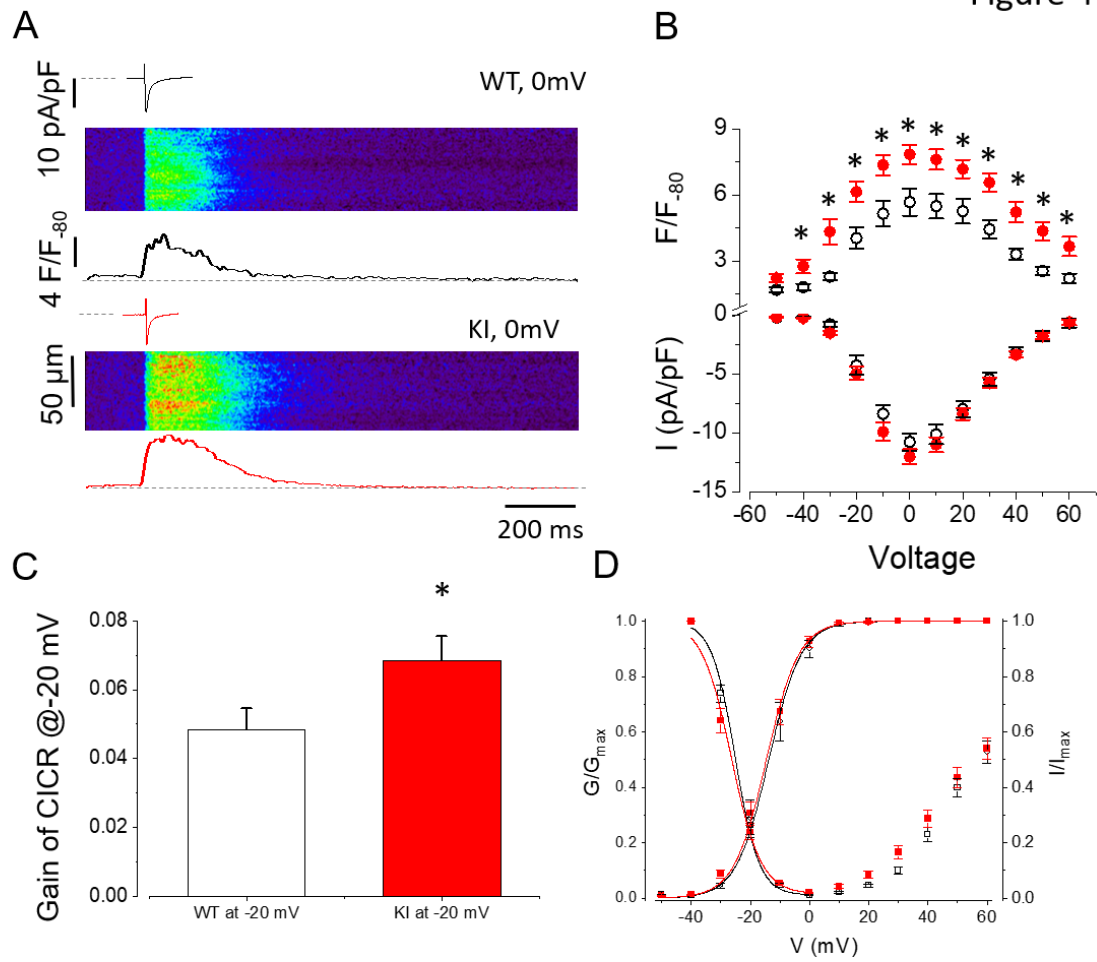


Figure 4



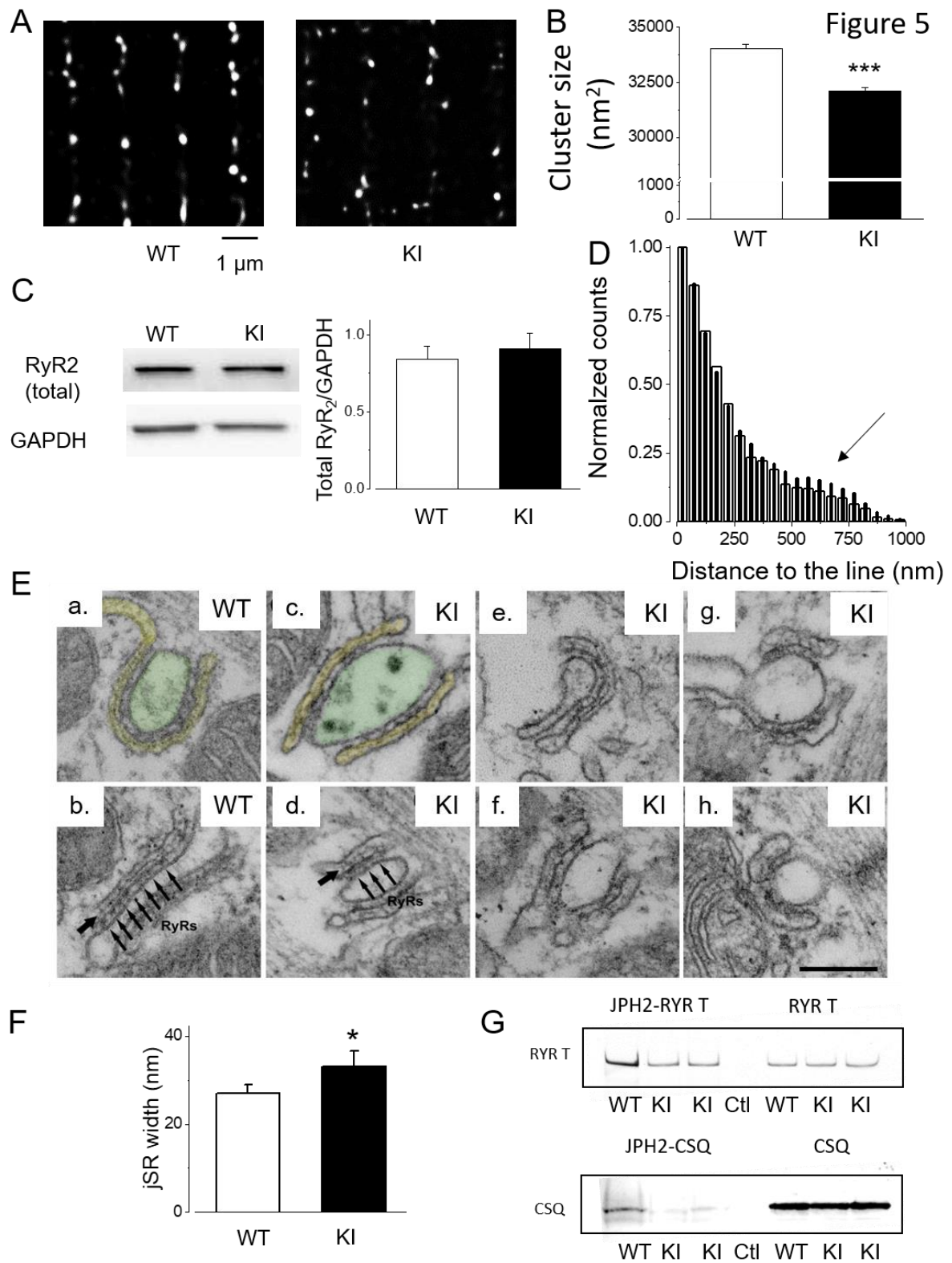


Figure 6

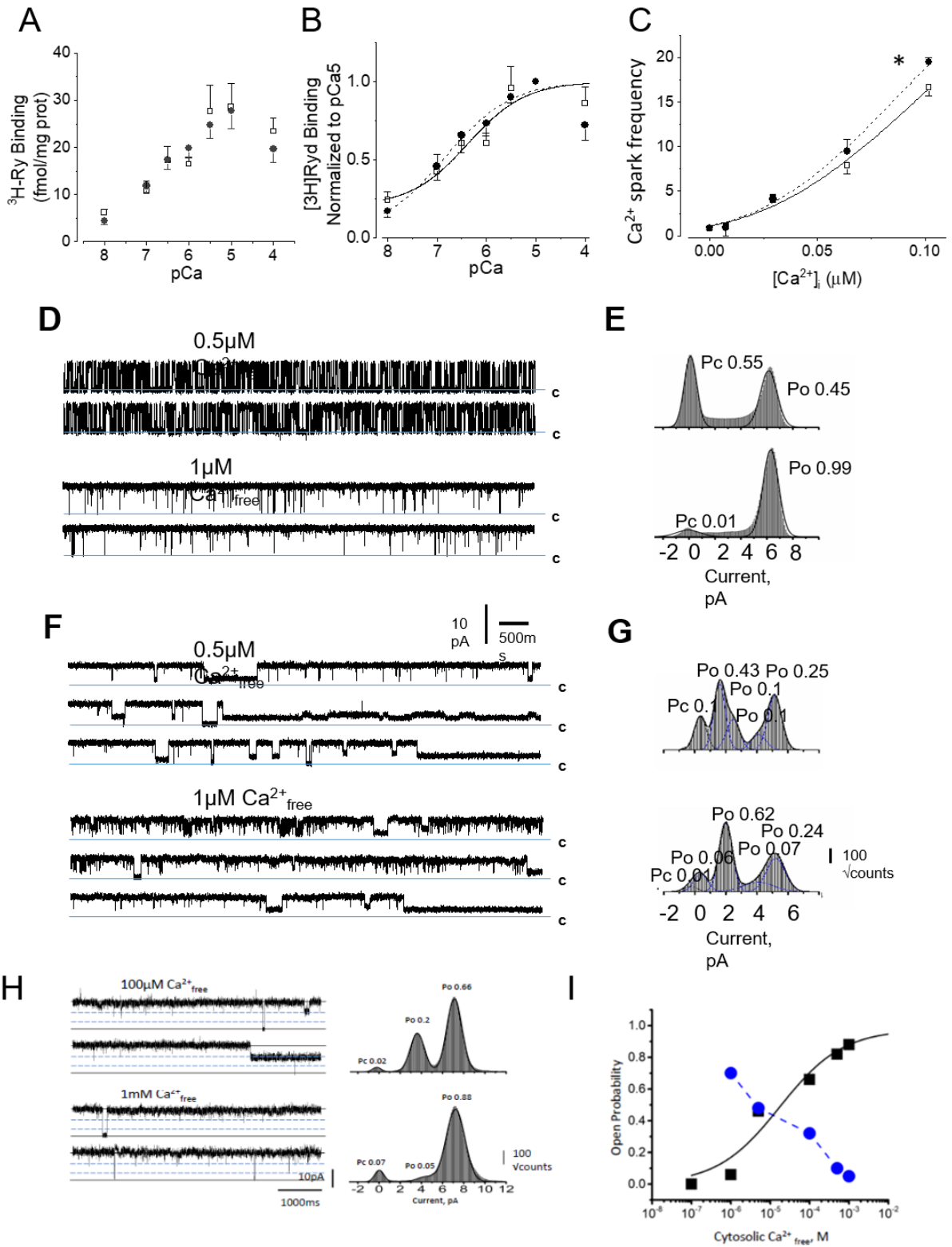
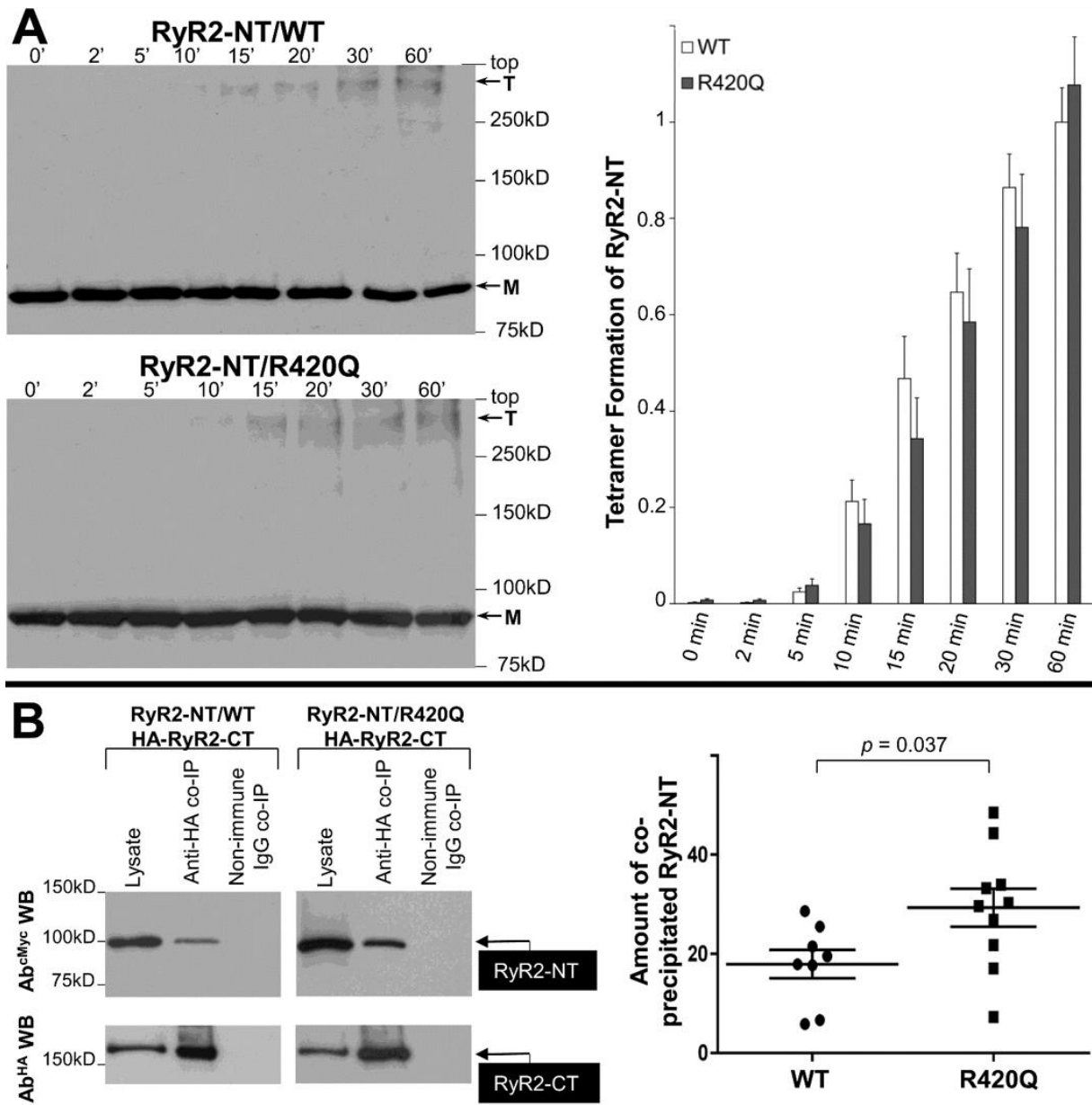
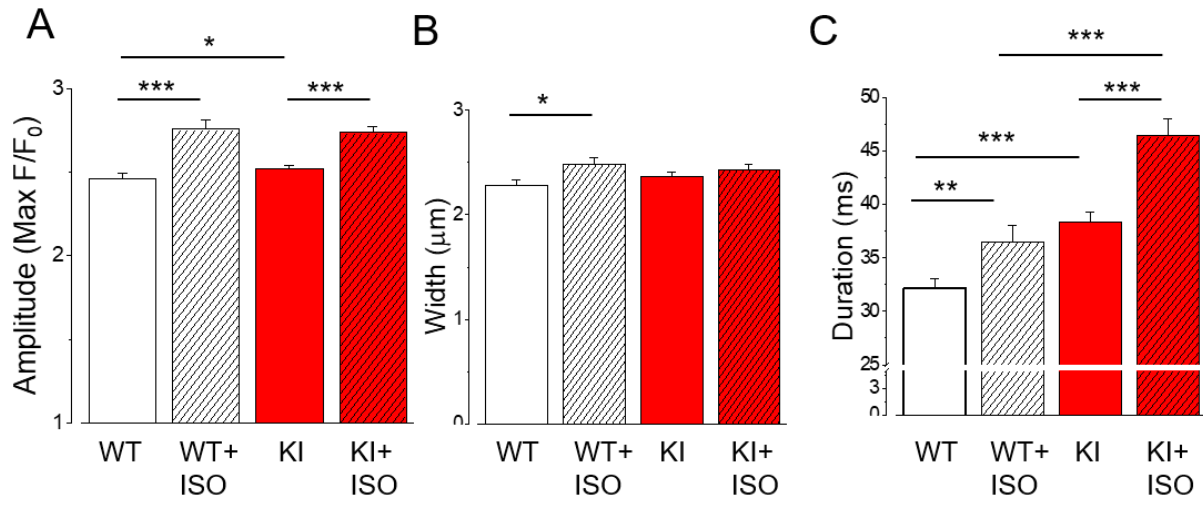


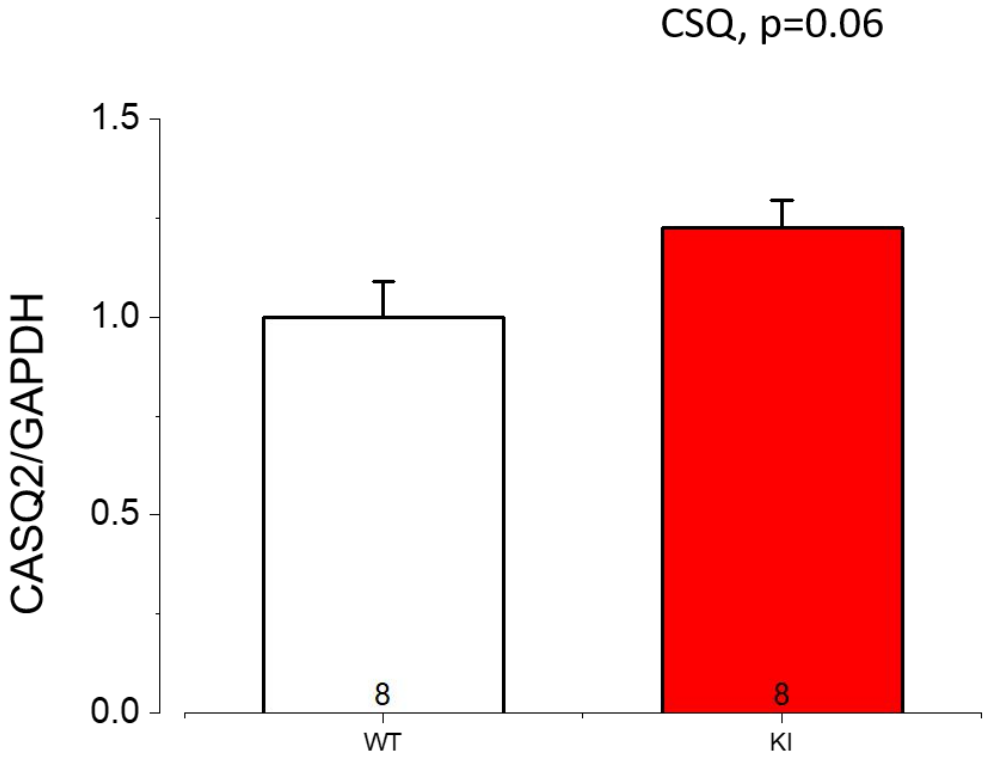
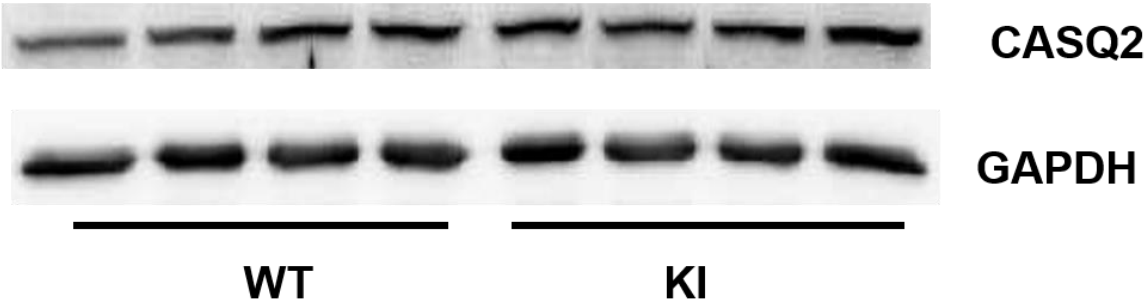
Figure 7



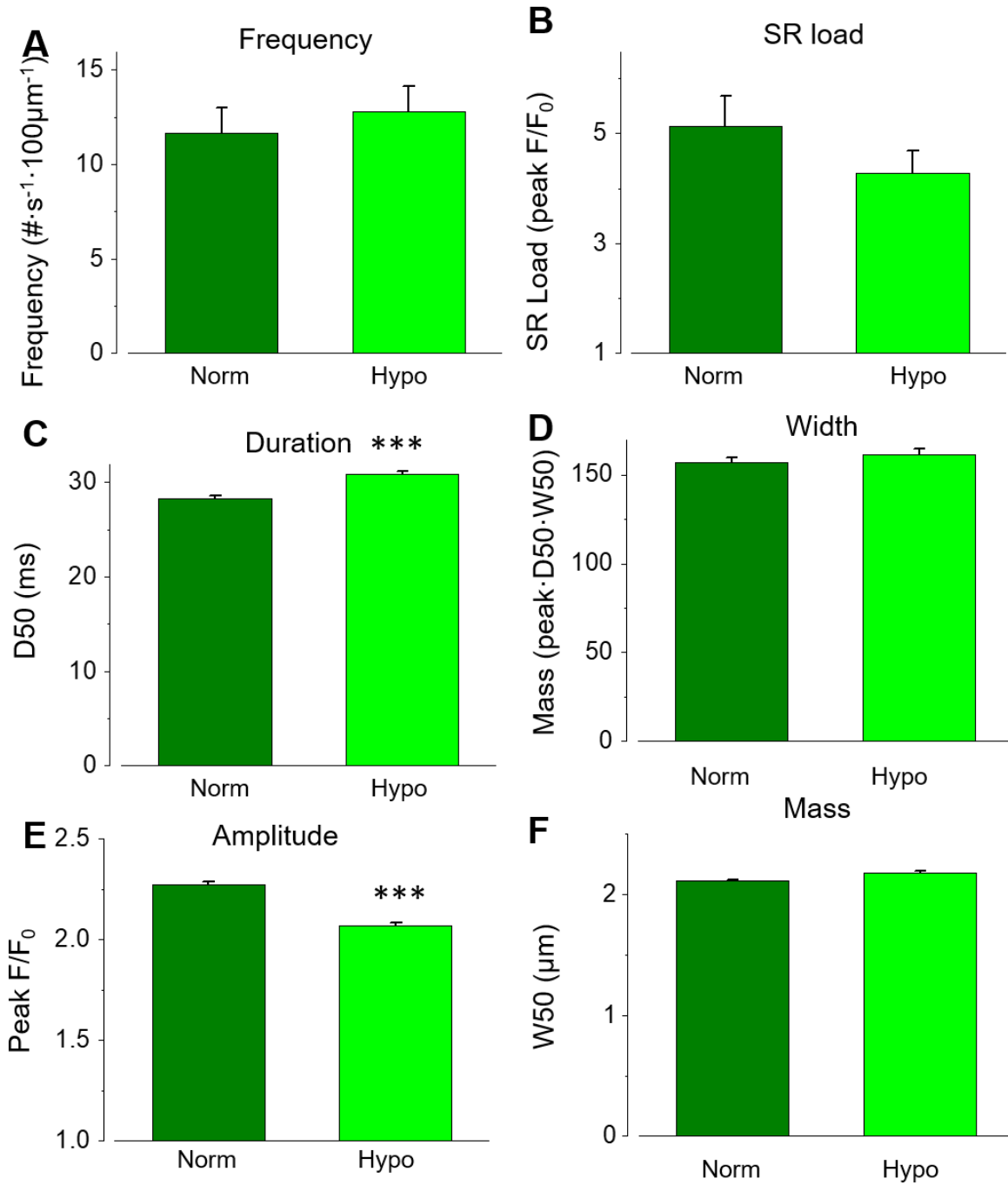
Supplement Fig. 1



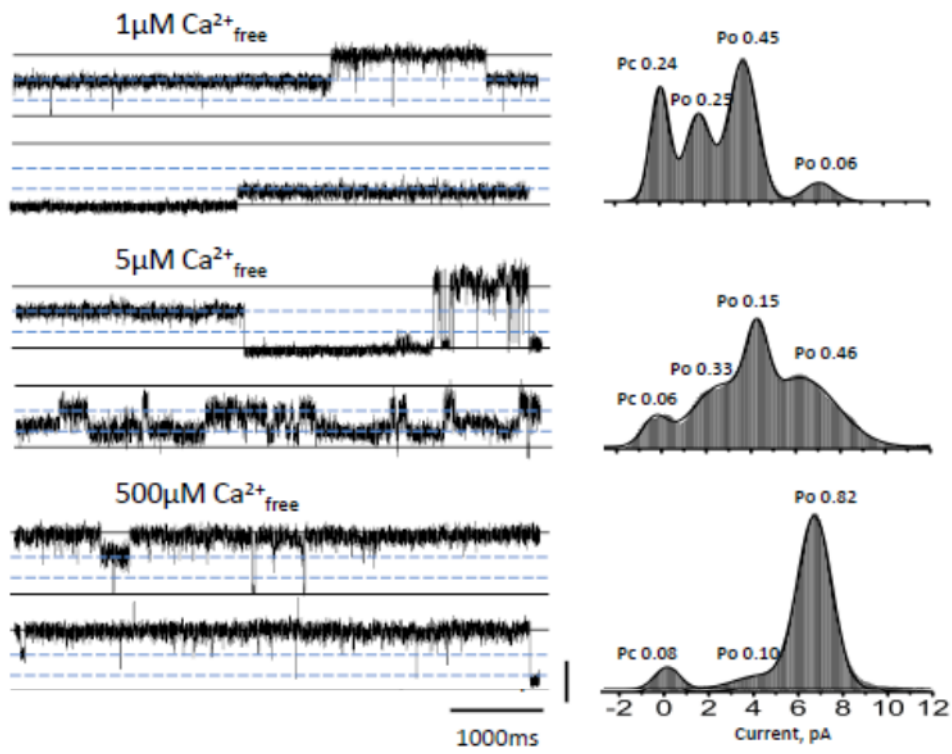
Supplement Fig. 2



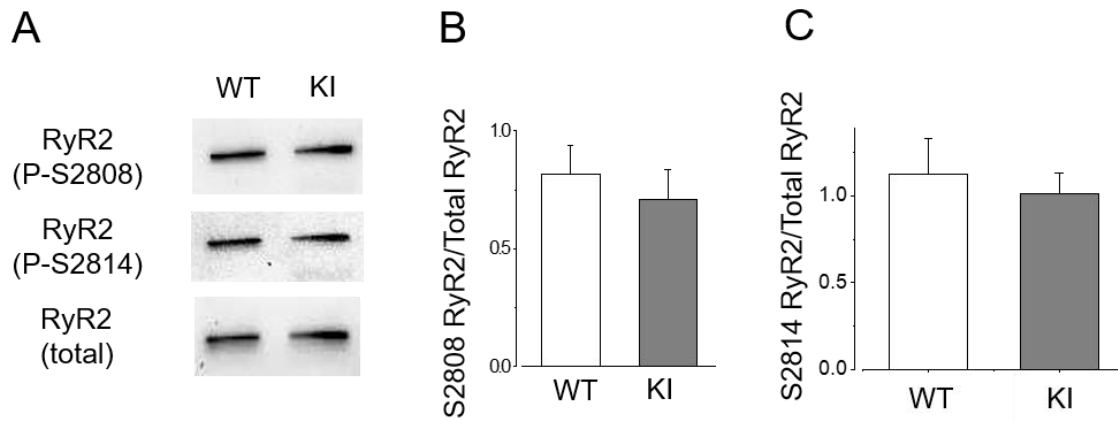
Supplement Fig. 3



## Supplement Fig. 4



## Supplement Fig. 5



## **II manuscript 2: A functional study of a N-terminal CPVT mutation RyR2<sup>R420Q</sup> in patient specific hiPSC-CMs model**

The following manuscript 2 contains the results got from hiPSC-CMs model, as well as the results of pharmacology in KI mouse model. As mentioned above, after studying the N-terminal CPVT mutation RyR2<sup>R420Q</sup> in KI mouse model, my lab also tried to establish a patient specific hiPSC-CMs model from the blood of that Spanish family members. The hiPSC clones have been generated from 4 family members, two from a pair of brothers to study the mutation in male and the other two from a pair of sisters to study that in female. It took about one year to get the hiPSC-CM model working, as it was the first time made in the lab. In the time that the hiPSC were made in Nantes, I did other experiments in HEK293 cells expressing an RyR2<sup>D3291V</sup> variant found in a family with sudden death to analyze Ca<sup>2+</sup> handling. The data I got are included in a collaborative paper that can be found in the annexes. We started the research in hiPSC-CM from the two brothers, so the results shown in manuscript 2 were got from males. For female, I have gotten some results of [Ca<sup>2+</sup>]<sub>i</sub> handling as well as action potential in CPVT hiPSC-CMs, which are not shown in the thesis.

## A functional study of a N-terminal CPVT mutation RyR<sub>2</sub><sup>R420Q</sup> in patient specific hiPSC-CMs model

L.H. Yin<sup>1</sup>, P. Joanne<sup>1,2</sup>, R. Perrier<sup>1</sup>, P. Gerbaud<sup>1</sup>, P. Lechène<sup>1</sup>, J.L. Álvarez<sup>1,3</sup>, J.P. Benitah<sup>1</sup>, A.M. Gomez<sup>1</sup>

<sup>1</sup> UMR-S 1180, Inserm Signaling and cardiovascular pathophysiology, Université Paris-Saclay, 92160 Châtenay-Malabry, France.

<sup>2</sup> Sorbonne Université, UMR 8256, 75252 PARIS CEDEX.

<sup>3</sup> Laboratory of Electrophysiology, Institute of Cardiology and Cardiovascular Surgery, Havana, Cuba.

**Abstract:** Catecholaminergic polymorphic ventricular tachycardia (CPVT) is a lethal genetic arrhythmia that manifests by syncope or sudden death in children and young adults under stress conditions without obvious cardiac structural abnormality. A novel CPVT mutation located in the RyR<sub>2</sub> N terminal portion has been identified in a Spanish family (RyR<sub>2</sub><sup>R420Q</sup>). According to the studies of RyR<sub>2</sub> function in HEK293 cell line, this mutation presented gain of function at low cytosolic intracellular Ca<sup>2+</sup> concentration ( $[Ca^{2+}]_i$ ) and loss of function at high  $[Ca^{2+}]_i$ . Moreover, KI mice heterozygous for this mutation presented bradycardia and sino-atrial node (SAN) dysfunction. Here we generated induced pluripotent stem cell (hiPSC) from two brothers (one with mutation, the other without mutation as control) of this family and differentiated them into cardiomyocytes (hiPSC-CM). In order to verify that the differentiated cells were well cardiomyocytes, we did immunofluorescence labelling to detect the alpha-actinin expression and found that around 90% cells were alpha-actinin positive in both groups of hiPS-CMs. Then the calcium transient was studied by confocal microscopy and the action potential (AP) by micro-electrode technique. The characteristics of spontaneous AP of mutated cells were mostly similar to that of control cells, but more mutated cells presented proarrhythmic behaviors under adrenergic stimulation. hiPSC-CM are immature cardiomyocytes and contract spontaneously. In order to be able to analyze  $[Ca^{2+}]_i$  transient characteristics, we paced the cells at a constant rate of 1 Hz by field stimulation through two Pt electrodes. Sarcoplasmic reticulum (SR) Ca<sup>2+</sup> load was estimated by rapid caffeine (10 mM) application. hiPSC-CMs from the RyR<sub>2</sub><sup>R420Q</sup> carrier presented smaller SR Ca<sup>2+</sup> load than those from the control person, whereas their fractional release (the  $[Ca^{2+}]_i$  transient normalized by the amount of Ca<sup>2+</sup> stored in the SR) was higher than that in control group, indicating a gain-of-function mutation. Even if SR Ca<sup>2+</sup> load was smaller in RyR<sub>2</sub><sup>R420Q</sup> cells, they often presented proarrhythmogenic behavior such as Ca<sup>2+</sup>

waves. The fact was further enhanced during beta-adrenergic stimulation, pointing to this model as a valuable tool to study the CPVT disease in human cells. The effect of Venlafaxine and Pregabalin, two neural system drugs, on  $[Ca^{2+}]_i$  transients were tested in hiPSC-CMs and adult mouse ventricular myocytes on a basis of a confidential case report. Our results suggest that venlafaxine blocks ISO induced proarrhythmic  $Ca^{2+}$  release events in these two cell models. Pregabalin shows block effect on arrhythmic events in adult mouse ventricular myocytes. These findings provide a good chance for exploring novel antiarrhythmic drugs.

**Key words:** CPVT, hiPSC-CMs,  $Ca^{2+}$  handling, action potential, antiarrhythmics

## Introduction

Catecholaminergic polymorphic ventricular tachycardia (CPVT) is a lethal genetic arrhythmia that manifests by syncope or sudden death in children and young adults under stress conditions without obvious cardiac structural abnormality. So far, 5 genes have been reported to be involved in CPVT, including type 2 Ryanodine Receptor (RyR2), Calsequestrin 2, Trans-2,3-enoyl-CoA reductase-like, Calmodulin 1 and Triadin (Landstrom, Dobrev and Wehrens, 2017). All these genes encoding proteins are involved in RyR2 complexes, playing direct or indirect effect on the  $Ca^{2+}$  transfer between sarcoplasmic reticulum (SR) lumen and cytosol. Thus, CPVT is expected to be caused by  $Ca^{2+}$  handling dysfunction, which further trigger lethal arrhythmias. Due to its high penetrance and life-threatening nature, CPVT leads to 30% SCD before the age of 40 (Paludan-Müller *et al.*, 2017). CPVT1, which is caused by the mutations in RyR2, accounts for 60% of CPVT identified cases. To date, more than 150 mutations in RyR2 have been found to be related to CPVT1 (Bezzarides *et al.*, 2019). Most of them are located at 3 “hot-spots” including the N-terminal domain, the central domain and the C-terminal domain (Bezzina, Lahrouchi and Priori, 2015). Up to now, most of functional researches of CPVT1 were carried out in heterologous expression systems, with small part of them characterized in knock in or knock out mouse models. According to those reports, most of mutations presented gain-of-function, while the loss-of-function mutations have also been reported, such as RyR2<sup>A4860G</sup> (Jiang *et al.*, 2007)(Zhao *et al.*, 2015a) and RyR2<sup>L433P</sup> (Thomas, George and Lai, 2004). Moreover, the molecular and cellular pathogenic mechanism of

mutations causing CPVT1 may vary among different locations, such as an increase of RyR2 sensitivity to  $\text{Ca}^{2+}$  for mutations located in C-terminal domain (Fernández-Velasco *et al.*, 2009a), or dissociation of FKBP12.6 proteins for mutations located in central domain (Lehnart *et al.*, 2008)(Meli *et al.*, 2011). With the establishment of human induced pluripotent stem cell derived cardiomyocytes (hiPSC-CMs) (Zhang, Wilson and Soerens, 2009), more and more mutations have been studied in the patient specific hiPSC-CM, providing further valuable information to gain the knowledge of CPVT mechanism. In this study, we generated hiPSCs from a CPVT1 (RyR2<sup>R420Q</sup>) patient as well as his negative genotyping brother, and compared the  $\text{Ca}^{2+}$  handling and action potentials of these two groups of cells. We found that the mutated cells presented more diastolic  $\text{Ca}^{2+}$  release as well as more afterdepolarizations, which recapitulate the disease phenotype of CPVT, validating hiPSC-CMs as a valuable model for CPVT functional study. Furthermore, based in a case report (personal communication) we evaluated the possible antiarrhythmic effect of two neural system drugs, venlafaxine and pregabalin, which have been reported to inhibit sodium channel (Khalifa, Daleau and Turgeon, 1999) and calcium channel (Mico and Prieto, 2012)(Bian *et al.*, 2006) respectively. Our preliminary data showed that venlafaxine blocked proarrhythmic events ( $\text{Ca}^{2+}$  waves) both in hiPSC-CMs and mouse ventricular myocytes. Pregabalin was only performed in mouse ventricular myocytes and also showed inhibited effect on  $\text{Ca}^{2+}$  waves. Our results, if confirmed and extended to *in-vivo* analyses, may be promising antiarrhythmic drugs.

## Methods

### CPVT (RyR2<sup>R420Q</sup>) patient and control (RyR2<sup>WT</sup>) specific iPS cell generation and culture

Patient-specific iPS cell lines were generated from the blood cells of two members of a Spanish family, after patient consent and approval of the ethical committee of Hospital Universitario La Fe, Valencia, Spain. One of the volunteers is the mutation carrier and the other one is the patient's brother presenting negative genotype as control, identified as III-4 and III-7 in family pedigree (Domingo *et al.* 2015). The hiPS cells were produced at Nantes, France (Plate-formed iPSC Nantes - Cellules sources pluripotent inducts). Then, iPS cells thawed from the liquid nitrogen were cultured in mTeSR<sup>TM</sup> (stemcell technologies) medium in plates that covered by diluted Matrigel (Corning) as extracellular matrix component. The culture medium was changed every other day before each passage. To do the passage, the cells were detached by ethylenediaminetetraacetic acid (EDTA) and transferred into small clusters. Differentiation was induced in cells that were passed at least 4 times.

## **Cardiomyocyte differentiation from iPS cells**

The differentiation protocol was referenced to Gsk3 inhibitor and Wnt inhibitor (GiWi) protocol (Lian *et al.*, 2012) (X Lian *et al.* 2013). Accutase (Thermo Fisher Scientific) was used to dissociate iPSC colonies into single cells and rock inhibitor Y27632 (5  $\mu$ M)(Selleckchem) was used to protect single cells from damage. Briefly, the medium was completely removed from the plates followed by washing the cells once with PBS. Then accutase was added for 5 min at 37 °C. After getting single cells, accutase was removed following centrifugation at 200g for 5 minutes, and the pellet was suspended in mTesR<sup>TM</sup> medium with 5  $\mu$ M Y27632. Then the cell density was counted on Mallasez chamber diluted ( $\frac{1}{2}$ ) in Trypan Blue. By this method, the cell density was between 100,000 and 200,000 cells/cm<sup>2</sup>. Lastly, the plates were incubated at 37 °C, 5% CO<sub>2</sub>, which counted as Day-2. Then the medium was changed every other day and the Gsk3 inhibitor CHIR99021 (6  $\mu$ M) was added on day 0 to activate Wnt protein expression, and then CHIR99021 was removed after 48 h followed by the Wnt inhibitor IWP2 (2.5  $\mu$ M) added on day 3. Then IWP2 was removed after 48 h. Before day 7, B27-insulin (without insulin) (Thermo Fisher Scientific) was used to maintain the cells since insulin has been reported to strongly inhibit cardiac differentiation by promoting ectoderm development but restricting the others germ layers. Obvious spontaneous beating regions start to form at day 5 to day 7. After that, cells were maintained with B27 (Thermo Fisher Scientific) until detached and transferred into new dishes around day 18.

## **Immunolabeling of hiPSC-CMs**

Immunolabeling was performed to verify the differentiated hiPSC-CMs. Briefly, iPSC-CMs were washed with PBS for 3 times with 5 min each time in room temperature, and then the cells were fixed and permeabilized in cold (-20°C) methanol for 8 minutes. After methanol removal, cells were washed three times in PBS, and were blocked in PBS plus 3% BSA (fatty acid free, Sigma-Aldrich) for 1h at room temperature. Then the cells were incubated with primary antibodies (anti-alpha-actinin monoclonal antibody (sarcomeric) clone EA-53 antibody (1/500, Sigma-Aldrich), overnight at 4°C. After removal of primary antibodies and rinsed with PBS, cells were incubated with secondary goat anti-mouse antibodies coupled to AlexaFluor 488 or 555 for 1h at room temperature avoiding light (1/1000, A11029, Thermo scientific, Courtaboeuf, France). Coverslips were then mounted on the cells incubated in prolong gold antifade reagent containing DAPI to counterstained nucleus over night at room temperature avoiding light

(Thermo scientific, Courtaboeuf, France). Images were acquired with an inverted Leica TCS SP8 microscope (Leica, Germany).

### **Measurement of expression of proteins from hiPSC-CMs**

Total cell protein samples were extracted from harvested iPSC-CMs by lysis buffer (Life Technologies, Villebon-sur-Yvette, France; 50 mM Tris (pH 7.4), 250 mM NaCl, 50 mM NaF, 5 mM EDTA, 1% Nonidet P-40, 0.02% NaN<sub>3</sub>, 1 mM sodium orthovanadate), supplemented with a protease inhibitor cocktail (Merck Millipore, Guyancourt, France) and a phosphatase inhibitor cocktail (Merck Millipore, Guyancourt, France). Then protein samples were separated on 4%–20% discontinuous gradient polyacrylamide gels, followed by transferred to PVDF membranes. PVDF membranes were incubated with blocking buffer of TBS with Tween-20 (0.1%) and nonfat dry milk (5%) for 45 minutes at room temperature. Membranes were then incubated with primary antibodies diluted in 5% milk TBS overnight at 4°C, followed by the secondary antibodies. Actin (0.8 µg/ml, Sigma-Aldrich, A2066), RyR2 (1 µg/ml, Thermo Fisher Scientific, MA3-916), and Cav1.2 primary antibodies were used. Antigen complexes were visualized with ChemiDoc and quantified with Image J (NIH).

### **Record of action potentials by micro-electrode**

Micro-electrodes were made of borosilicate capillary glass tubes using a DMZ-Universal puller (Zeitz-Instruments, Germany) with resistances above 20 MΩ and filled with 3M KCl. A double controlling warm system for both dish and perfused solution was used to maintain the temperature at around 35 °C. The hiPSC-CMs seeded in two small chambers of 35 mm µ-dish with glass bottom (Ibidi, Clinisciences, France) on 32 to 40 days after differentiation were used to record the spontaneous action potentials. The cells were taken out of incubator and perfused with the warm (37°C) basal solution (Tyrode solution: NaCl 137 mM, KCl 5.4 mM, CaCl<sub>2</sub>·2H<sub>2</sub>O 1.8 mM, MgCl<sub>2</sub>·6H<sub>2</sub>O 1 Mm, HEPES 10 mM). Beating cells with rod shape membranes were chosen to record AP recording. The APs were recorded under basal conditions for 2 min, and then during perfusion with 1 µM ISO. After ISO perfusion, the record continued for washout.

### **Measurements of Ca<sup>2+</sup> handling by confocal microscopy**

RPMI 1640 (Thermo Fisher Scientific) was used as solution during confocal recording. Calbryte™ 520 AM (AAT bioquest), a highly sensitive dye for tracking local events (Tada *et al.*, 2014)(Usselman, 2017), has been used as dye for hiPSC-CMs, excited at 492 nm with a

white light laser and emission collected at  $>514$  nm. The hiPSC-CMs seeded in two small chambers of 35 mm  $\mu$ -dish with glass bottom (Ibidi, Clinisciences, France) on 32 to 38 days after differentiation were used to record the calcium signals. Firstly, cells were loaded with 10  $\mu$ M of Calbryte™ 520 AM in 20% pluronic acid-DMSO solution for 1 h in cell incubator at 37°C followed by 15 min wash out at room temperature avoiding light. Two-dimension images of spontaneous activity were recorded at speed 2000 Hz by confocal microscope Leica SP5 equipped with a resonant scanner. Then Line-scan images were recorded at speed 700 Hz to record the calcium transients of electrically paced cells through 2 Pt electrodes at 1 Hz. After the recording in basal condition, cells were perfused by 100 nM ISO to check the sympathetic effect. 10 mM caffeine was rapidly perfused to measure the SR content. In other experiments 1  $\mu$ M ISO was used to check for proarrhythmic behavior induction.

## Statistics

Results are presented as mean $\pm$ SEM. Student's t-test, one-way/two-way ANOVA and two-way repeated ANOVA statically methods were used according to the experimental setting. P values  $< 0.05$  were considered statistically significant and marked by \* $< 0.05$ , \*\* $p < 0.001$ , and \*\*\* $p < 0.0001$ .

## Results

### Characteristics of hiPSC-CM

RyR2<sup>R420Q</sup> is a CPVT1 mutation located in the N-terminal, which has been identified in a Spanish family by our collaborators (Domingo *et al.*, 2015). The hiPSC-CMs were generated from the blood of two volunteers from this Spanish family. The two volunteers are brothers with the same parents, one without mutation, named control (III:4), the other one (III:7) (Domingo *et al.*, 2015) carrying mutation and presenting CPVT as shown in his ECG in Figure 1A. The hiPSCs as presented in Fig 1B showed spontaneous contractions (supplemental video) and positive immunolabeling of myocyte specific protein  $\alpha$ -actinin (Figure 1C) and cardiomyocyte specific protein RyR2 (manuscript 1), validating cardiomyocyte differentiation. Moreover, the percentage of  $\alpha$ -actinin<sup>+</sup> cells was similar in two groups of cells (Figure 1C), indicating the differentiation efficiency was comparable for CPVT and control iPSC. DAPI was used to dye nucleus as shown in blue fluorescence (Figure 1C). The protein expression of total

RyR2 (Figure 1D) and Cav1.2 (Figure 1E) were measured by western-blot, and results showed no difference of these proteins in CPVT and control hiPSC-CMs, indicating the normal structure of CPVT hiPSC-CMs.

### **Characteristics of spontaneous action potentials in hiPSC-CM**

The spontaneous APs were recorded by microelectrode technique in RyR2<sup>WT</sup> and RyR2<sup>R420Q</sup> expressing hiPSC-CMs as exemplified in Fig 2A. The cycle lengths of spontaneous APs under basal conditions were similar between the two groups, and was shortened by 1  $\mu$ M ISO in both cell groups (Figure 2A, B), suggesting normal automatic activity and  $\beta$ -adrenergic responsiveness of the RyR2<sup>R420Q</sup> expressing hiPSC-CMs. The maximal diastolic potential (MDP) was comparable in both groups of cells. However, after ISO, both groups of hiPSC-CMs presented more depolarized MDP (Figure 2C). The AP duration was similar in both cell groups (Figure 2D, supplemental Figure 1 D) and shortened by ISO in both groups. Maximal upstroke velocity was unaltered by the mutant, but it was decreased by ISO in CPVT hiPSC-CMs (supplemental Figure 1 B). During 1  $\mu$ M ISO perfusion, we denoted that the CPVT hiPSC-CMs presented proarrhythmic behavior, characterized by high incidence of DADs (Figure 2E). In CPVT hiPSC-CMs, 7 out of 30 cells (23.33%) presented proarrhythmic behavior in basal conditions, and 14 out of 30 cells (46.66%) during ISO perfusion, while in control hiPSC-CM, the percentage of cells presenting proarrhythmic behavior were 10.53% and 15.79% in basal and during ISO perfusion respectively (Figure 2F). Thus, more CPVT hiPSC-CMs presented proarrhythmic behaviors than control hiPSC-CM in ISO ( $p=0.0269$ ).

### **[Ca<sup>2+</sup>]<sub>i</sub> transients**

In order to study the characteristics of [Ca<sup>2+</sup>]<sub>i</sub> transients, the two groups of cells were paced at 1 Hz to fix the same beating rate in every cell. The two cell groups presented no significant difference in amplitude of [Ca<sup>2+</sup>]<sub>i</sub> transients (Figure 3A, B). After 1 min 1  $\mu$ M-ISO perfusion, many CPVT hiPSC-CMs presented proarrhythmogenic Ca<sup>2+</sup> waves during diastolic periods (Figure 3C). As counted in Figure 3D, 10 positions out of 31 positions with cells presenting waves, which is significantly higher than that in control group. This finding is consistent with the cells presenting proarrhythmogenic behaviors in APs recordings in Figure 2F. Since the occurrence of Ca<sup>2+</sup> waves impeded analysis of ISO effects due to increased basal fluorescence (supplemental Figure 2), in order to check ISO effects in both cell groups, we used ISO at lower concentration (100 nM), in which both groups of hiPSC-CMs didn't present increased basal

fluorescence and  $\text{Ca}^{2+}$  waves. 100 nM-ISO increased  $[\text{Ca}^{2+}]_i$  transient amplitude (supplemental Figure 3A) and accelerated its duration (supplemental Figure 3B) similarly in both groups, consistent with normal  $\beta$ -adrenergic responsiveness of the  $\text{RyR2}^{\text{R420Q}}$  expressing hiPSC-CMs.

### **Sarcoplasmic reticulum $\text{Ca}^{2+}$ load**

We previously characterized in  $\text{RyR2}^{\text{R420Q}}$  KI mice (ref first study) a reduction of Sarcoplasmic Reticulum (SR)  $\text{Ca}^{2+}$  load due to increased diastolic  $\text{Ca}^{2+}$  leak, without alteration of  $[\text{Ca}^{2+}]_i$  transient amplitude. Thus, we evaluated the SR content in control and CPVT hiPSC-CMs both in basal and after perfusion with 1  $\mu\text{M}$  ISO by rapid application of 10 mM caffeine. As Figure 4 shows, the SR content in CPVT hiPSC-CMs was significantly lower than that in control hiPSC-CMs both in basal and during 1  $\mu\text{M}$  ISO challenge (Figure 4B). The depression in the SR  $\text{Ca}^{2+}$  load with normal  $[\text{Ca}^{2+}]_i$  transients resulted in the enhanced fractional release in CPVT hiPSC-CMs (Figure 4C), confirming a gain-of-function mutation.

### **Antiarrhythmic effect of venlafaxine in hiPSC-CMs**

One CPVT1 carrier patient (CPVT resistant patient) of the Spanish family was asymptomatic after taken several drugs (including venlafaxine, pregabalin, terazosin, tetrazepam and naloxone) to treat other diseases. Since venlafaxine has been reported to inhibit sodium channel (Khalifa, Daleau and Turgeon, 1999) and another  $\text{Na}^+$  channel inhibitor flecainide has been experimentally and clinically documented to be efficient as antiarrhythmic drug for CPVT, we wondered whether venlafaxine might be a therapeutic alternative in CPVT. Thus firstly, we perfused hiPSC-CMs with 2.5  $\mu\text{g}/\text{mL}$  venlafaxine in presence of 1  $\mu\text{M}$  ISO, and recorded  $[\text{Ca}^{2+}]_i$  transients to check the effect of venlafaxine on the ISO induced arrhythmic events. Figure 5A shows venlafaxine decreased  $\text{Ca}^{2+}$  sparks in a recording position of CPVT hiPSC-CMs. The ISO induced arrhythmic events in CPVT hiPSC-CMs were significantly decreased by venlafaxine (Figure 5B). Then we also treated hiPSC-CMs with 2.5  $\mu\text{g}/\text{mL}$  venlafaxine in chronic mode (pre-treated by venlafaxine for 24 h). As shown in Figure 5C, in chronic venlafaxine treatment groups, the proarrhythmic  $\text{Ca}^{2+}$  events were fewer than that in basal groups (Figure 5C), and ISO didn't significantly increase arrhythmic events in CPVT hiPSC-CMs, suggesting a protective effect of venlafaxine.

### **Antiarrhythmic effect of venlafaxine and pregabalin in mouse ventricular myocytes**

In order to confirm antiarrhythmic effect of venlafaxine, we analyzed alteration of the diastolic  $\text{Ca}^{2+}$  release events such as  $\text{Ca}^{2+}$  waves (Figure 6A) in adult ventricular myocytes isolated from WT and RyR2<sup>R420Q</sup> KI littermate mice. During confocal recording of 2-Hz field stimulated cells, KI cardiomyocytes had markedly higher occurrence of  $\text{Ca}^{2+}$  waves after 100nM ISO exposure than WT cardiomyocytes (Figure 6A) which is consistent to previous data in manuscript 1. In presence of 5  $\mu\text{g}/\text{mL}$  venlafaxine, which did not affect  $\text{Ca}^{2+}$  wave occurrences at basal conditions, the ISO increased  $\text{Ca}^{2+}$  waves incidences were reduced in both groups (Figure 6B). Furthermore, another anti-pain drug taken by the CPVT resistant patient, pregabalin (5  $\mu\text{g}/\text{mL}$ ), also prevented proarrhythmic ISO increased  $\text{Ca}^{2+}$  waves frequencies (Figure 6C). Thus, venlafaxine and pregabalin seemed to present antiarrhythmic effect in CPVT mutation knock-in mouse ventricular myocytes. To gain mechanistic insights of these effects, we further analyzed venlafaxine and pregabalin treatments on  $\text{Ca}^{2+}$  transients and SR  $\text{Ca}^{2+}$  content. As shown in Supplemental Figure 4, venlafaxine and pregabalin didn't significantly modify the  $\text{Ca}^{2+}$  transient and SR  $\text{Ca}^{2+}$  content in WT and KI cardiomyocytes under basal condition or after 100-nM ISO treatment.

## Discussion

Research effort has been directed to explore the mechanism of CPVT for about twenty years, since the discovery of the first mutation of this cardiac genetic disease. In the early stage, heterologous expression systems were widely used for functional studies of CPVT mechanism. For example, after study some CPVT mutations in HEK 293 cell line and HL-1 cell line, Jiang et al proposed the concept of store-overload-induced  $\text{Ca}^{2+}$  release (SOICR), suggesting that the depolarization-independent SR  $\text{Ca}^{2+}$  release is due to the decreased threshold in SR  $\text{Ca}^{2+}$  load to induce spontaneous release by CPVT mutants (Jiang *et al.*, 2004)(Jiang *et al.*, 2005). However, since HEK 293 cell is not cardiomyocyte and HL-1 cell was got from atrial tumor (Elcarpio, Ahinski and Zzo, 1998), they can't fulfil the further functional studies of CPVT. Thus, CPVT mutations KI mouse models were established. The KI mouse models recapitulated disease phenotype of CPVT patients in many ways, like bradycardia and sino-atrial node (SAN) dysfunction (Wang *et al.*, 2017)(Gómez, 2012), abnormal  $\text{Ca}^{2+}$  release viewed as  $\text{Ca}^{2+}$  waves which is consistent with the occurrence of delayed afterdepolarizations (Fernández-Velasco *et al.*, 2009b), as well as loss-of-function characteristics (Zhao *et al.*, 2015b). However, as we all know, mouse heart possesses big differences from human heart no matter in whole organ function, such as heart rate, or in protein expression, such as the SERCA pump or ionic channels

shaping the AP, which can limit its application. For sure, to better understand disease mechanism at molecular and cellular level, the best way is to study it in cardiomyocytes isolated from patients, but it is impossible to obtain sufficient quantities of cardiomyocytes from patient biopsies and the survival time of adult cardiomyocytes is too short (Fatima *et al.*, 2011). Hopefully, the appearance of hiPSCs solved this problem, with which, the functional cardiomyocytes can be established from CPVT patients (Zhang *et al.*, 2009).

Patient-specific hiPSC-CMs has been properly described as “disease-in-a-dish”, which solved the cell-sourcing problem to directly study human cardiomyocytes from CPVT patients (Itzhaki *et al.*, 2012). Indeed, based on previous researches, hiPSC-CMs have demonstrated to be able to recapitulate disease phenotype of CPVT patients in many ways, such as ISO induced abnormal  $\text{Ca}^{2+}$  release during diastole and DADs in action potentials (Itzhaki *et al.*, 2012)(Zhang *et al.*, 2013). In this study we have generated hiPSC lines from a CPVT1 patient carrying a novel mutation in the N-terminal domain of RyR2 as well as from the patient’s brother who presents negative genotype as control. By comparing the  $\text{Ca}^{2+}$  handling and action potentials of hiPSC-CMs generated from these two persons, we found that the hiPSC-CMs from CPVT patient didn’t present significantly higher incidence of diastolic  $\text{Ca}^{2+}$  release such as  $\text{Ca}^{2+}$  waves in  $\text{Ca}^{2+}$  transients and proarrhythmic behaviors such as DADs than that from the control person in basal condition. However, after  $\beta$ -adrenergic stimulation, the two parameters increased remarkably in CPVT hiPSC-CMs but not in control hiPSC-CMs, which largely recapitulated disease phenotype of CPVT as well as was consistent with the data we previously got on the same mutation (RyR2<sup>R420Q</sup>) in KI mice (manuscript 1), validating hiPSC-CM as a good cellular model for CPVT study.

Experimental findings from heterologous expression systems, lipid bilayers, and knock-in or knockout mouse models suggest that the basic mechanism underlying development of arrhythmias in CPVT involves a diastolic  $\text{Ca}^{2+}$  leak from the mutant RyR2 (Priori and Chen, 2011), which leads to a depolarized current generated by sodium calcium exchanger (NCX) that can trigger spontaneous APs thereby being at the origin of lethal arrhythmias. Our data suggest an increase in diastolic  $\text{Ca}^{2+}$  leak in CPVT hiPSC-CMs supported by the increase in diastolic  $\text{Ca}^{2+}$  release events such as  $\text{Ca}^{2+}$  waves. The further study of  $\text{Ca}^{2+}$  handling revealed a decrease in SR  $\text{Ca}^{2+}$  load in CPVT hiPSC-CMs, which most likely resulted from the increased diastolic  $\text{Ca}^{2+}$  leak. However, the  $\text{Ca}^{2+}$  transient amplitude remains unaltered in CPVT hiPSC-CMs which is consistent with the data from RyR2<sup>R420Q</sup> KI mouse (manuscript 1). The  $[\text{Ca}^{2+}]_i$

transient amplitude with regard to the SR  $\text{Ca}^{2+}$  load (fractional release) is higher in CPVT hiPSC-CMs than in control hiPSC-CMs, suggesting gain of function of the RyR2<sup>R420Q</sup>. Previous authors have analyzed hiPSC-CM and found three groups of cells from CPVT patients: one that did not respond to ISO, another that normally responded (increase in the  $[\text{Ca}^{2+}]_i$  transient amplitude), and a third one which responded by inducing arrhythmia (Novak *et al.*, 2015). In fact, the  $[\text{Ca}^{2+}]_i$  transient amplitude is calculated by normalizing the maximum peak fluorescence value (F) by the diastolic fluorescence ( $F_0$ ). If diastolic  $[\text{Ca}^{2+}]_i$  were higher in CPVT hiPSC-CMs, this could result in lower F/ $F_0$  values. Because confocal fluorescence dye with Fluo4-AM is not ratiometric, we cannot compare absolute values between different groups of cells. Measurements using a ratiometric dye, Fura-2 are under way. In our study, although some cells failed to respond in both control and CPVT groups, there were not clear group separations and globally most cells responded normally. Looking closer, the basal fluorescence did not vary in control hiPSC-CMs during stimulation with 1  $\mu\text{M}$  ISO, but increased in CPVT hiPSC-CMs. This could suggest enhanced diastolic  $\text{Ca}^{2+}$  release by RyR2<sup>R420Q</sup> under stress conditions and may be the explanation of weaker increase in F/ $F_0$  in mutated cells, which does not necessarily reflect less  $\beta$ -adrenergic sensitivity.

The striking results of spontaneous action potentials we found was the difference in maximum resting potential under  $\beta$ -adrenergic stimulation in CPVT hiPSC-CMs. ISO induced a depolarization of MDP in both groups. This could be due to the fact that these cells express HCN4 channels, which produce  $I_f$  (funny current), whose activation is shifted by cAMP produced by  $\beta$ -adrenergic stimulation. So  $I_f$  is activated at more positive potentials, starting slow depolarization and limiting the maximum diastolic potential. There is no difference in this fact between two groups, thus suggesting that the presence of RyR2<sup>R420Q</sup> does not secondarily induce any change on MDP.

Besides as a valuable model for functional studies of CPVT, hiPSC-CM also represent a unique platform for drug screening and development of optimized patient-tailored therapies. Flecainide, an approved antiarrhythmic drug known to block sodium channels, has been tested in hiPSC-CMs and its antiarrhythmic performance observed in CPVT hiPSC-CMs demonstrated that hiPSC-CM model replicated well the individual drug responses (Itzhaki *et al.*, 2012). The antiarrhythmic effect of another drug, Dantrolene, a drug effective on malignant hyperthermia, has also been revealed in hiPSC-CM models (Jung *et al.*, 2012)(Penttinen *et al.*, 2015). In this study, we have tested the antiarrhythmic effect of venlafaxine, one drug has been

taken by a CPVT resistant patient, in this CPVT (RyR2<sup>R420Q</sup>) hiPSC-CM model, and also in CPVT (RyR2<sup>R420Q</sup>) KI mouse ventricular myocytes as comparison. We found that venlafaxine blocked ISO induced arrhythmic events both in hiPSC-CM and KI mouse ventricular myocytes. Venlafaxine is a medicine used to treat major depressive disorder, anxiety, and panic disorder, which has been reported to block neuronal I<sub>Na</sub> following its binding to the resting state of the channel (Khalifa, Daleau and Turgeon, 1999). Flecainide has been reported to show remarkable efficacy to suppress spontaneous sarcoplasmic reticulum Ca<sup>2+</sup> release either by directly inhibiting RyR2 (through decreasing its opening probability) (Shah and Hodgson, 2009)(Watanabe *et al.*, 2011) or by increasing the threshold for triggered activity (through its Na<sup>+</sup> channel blocking activity) (Liu *et al.*, 2011). Here we still don't know the mechanism of the antiarrhythmic effect of venlafaxine, but the data from mouse ventricular myocytes suggested that venlafaxine didn't alter [Ca<sup>2+</sup>]<sub>i</sub> transient and SR Ca<sup>2+</sup> load. Thus we speculate that venlafaxine may either block RyR2 in similar way as flecainide, or doesn't affect RyR2 but decrease Ca<sup>2+</sup> release by reducing the availability of I<sub>Na</sub> in plasma membrane. Moreover, we have also tested another drug, pregabalin in KI mouse model since it has also been taken by that CPVT resistant patient. Pregabalin is a medicine widely used in the treatment of postherpetic neuralgia, diabetic neuropathic pain, partial seizures, anxiety disorders and fibromyalgia, which has been reported to inhibit voltage-gated calcium channel by targeting to  $\alpha 2\delta$  isoform of the channel (Mico and Prieto, 2012)(Bian *et al.*, 2006). We found that pregabalin blocked ISO induce Ca<sup>2+</sup> waves, which indicated that pregabalin may protect from arrhythmias. Similar with venlafaxine, pregabalin didn't show alteration of [Ca<sup>2+</sup>]<sub>i</sub> transient and SR Ca<sup>2+</sup> load in mouse ventricular myocytes. We should also test pregabalin in hiPSC-CM. The mechanism of antiarrhythmic effect of both drugs remains unclear and demand for further experiments.

In conclusion, Our data showed gain-of-function characteristic of mutation RyR2<sup>R420Q</sup>, confirming our previous findings in heterologous system (Domingo *et al.*, 2015)(Wang *et al.*, 2017), and validating hiPSC-CM as a valuable model for studying this cardiac genetic disease, and pharmacology tests. Moreover, venlafaxine and pregabalin were demonstrated to show antiarrhythmic effect in a cellular context, *in vivo* analyses are needed to see whether they can be promising antiarrhythmic therapy.

## Figure legends

**Figure 1. The origin of iPSC and Immunolabeling images of cardiomyocytes specific proteins.** A) ECG image recorded from the volunteer carrying mutation RyR2<sup>R420Q</sup> (III: 7), showing polymorphic ventricular tachycardia under stress. B) Morphologies of hiPSC clones. C) The immunolabeling images showing myocytes specific proteins  $\alpha$ -actinin, and the percentage of  $\alpha$ -actinin<sup>+</sup> cells was comparable in two groups. Protein expression of total RyR2 (D) and Cav1.2 (E) are similar in two groups. \*p<0.05, \*\*p<0.01, \*\*\*p<0.001.

**Figure 2. Mutated cells are more prone to present pro-arrhythmic behavior.** A) Represented APs in different cell groups. B) The cycle length of spontaneous AP in 19 control iPSC-CM/iPSC-CM/shiPSC-CMs and 30 CPVT iPSC-CM/iPSC-CM/shiPSC-CMs were recorded at baseline conditions (CTL.BL and CPVT.BL, black and red, respectively) and subsequently recorded in the presence of 1  $\mu$ M ISO (CTL.ISO and MU.ISO, green and blue, respectively) C) Maximal diastolic potential (MDP). D) AP duration (APD) at 90% repolarization. The data between two treatments of same genotype were repeated recorded from 18 control cells and 25 mutated cells respectively. E) representative action potential from a mutated cell showing Delayed After Depolarizations (DADs). The red arrows depict DADs. F) Percentage of cells presenting pro-arrhythmic behavior. The numbers in columns represent the total number of cells in each group, the numbers on top of the column represent the number of cells presenting proarrhythmic behavior. \*p<0.05, \*\*p<0.01, \*\*\*p<0.001.

**Figure 3. CPVT hiPSC-CM show proarrhythmic Ca<sup>2+</sup> release.** A) Examples of line-scan images showing [Ca<sup>2+</sup>]<sub>i</sub> transients in hiPSC-CMs paced at 1Hz (the images here show a recording position of each group with several cells included for each). B) Amplitude of [Ca<sup>2+</sup>]<sub>i</sub> transients (F/F<sub>0</sub>) (N: 138 control hiPSC-CMs, 158 CPVT hiPSC-CMs). C) Line-scan images in control and CPVT hiPSC-CMs before and during ISO perfusion. CPVT hiPSC-CMs show Ca<sup>2+</sup> waves indicated by red arrows, and blue arrows depict electrical stimulations. D) Percentage of hiPSC-CMs presenting Ca<sup>2+</sup> waves in both groups under basal and 1  $\mu$ M ISO condition. The N values here indicate the recorded position, each of which including several (1-4) cells. \*p<0.05, \*\*p<0.01, \*\*\*p<0.001.

**Figure 4. CPVT hiPSC-CMs show lower SR calcium load than control.** A) Representative line-scan images from confocal microscopy showing electrically evoked [Ca<sup>2+</sup>]<sub>i</sub> transients and the caffeine-evoked (10 mM) Ca<sup>2+</sup> transient of control and CPVT hiPSC-CMs both under basal and 1  $\mu$ M ISO condition. The red line on top of the image depicts caffeine perfusion, blue arrows depict electrical stimulations. B) The SR content in CPVT hiPSC-CMs were significantly lower than that in control group both in basal and 1  $\mu$ M ISO. N=52 in control in basal (black), N=68 in CPVT in basal (red), N=50 in control in ISO (green), N=64 in CPVT in ISO (blue). C) The fractional release in CPVT hiPSC-CMs were significantly higher than that in control group both in basal and 1  $\mu$ M ISO. N=37 in control in basal, N=39 in CPVT in basal, N=33 in control in ISO, N=41 in CPVT in ISO. \*p<0.05, \*\*p<0.01, \*\*\*p<0.001.

**Figure 5. venlafaxine effect in spontaneous Ca<sup>2+</sup> release in hiPSC-CMs.** A) line-scan images showing [Ca<sup>2+</sup>]<sub>i</sub> transients of one control hiPSC-CM and one CPVT hiPSC-CM in different treatments. The CPVT hiPSC-CM present Ca<sup>2+</sup> sparks. B) Percentage of hiPSC-CMs presenting spontaneous Ca<sup>2+</sup> sparks or waves in control and CPVT hiPSC-CMs in basal conditions (gray bars), during 1  $\mu$ M ISO perfusion (red bars) and during perfusion with 2.5  $\mu$ g/mL venlafaxine in the continued presence of 1  $\mu$ M ISO (dark red bars). Acute venlafaxine treatment decreased ISO-evoked proarrhythmic events in CPVT hiPSC-CMs. C) Percentage of hiPSC-CMs presenting spontaneous Ca<sup>2+</sup> sparks/waves in cells incubated during 24 hours with 2.5  $\mu$ g/mL venlafaxine (light gray bars) and during 1  $\mu$ M ISO perfusion in the continued presence of Venlafaxine (dark red bars). Chronic venlafaxine treatment decreased ISO induced proarrhythmic events in CPVT hiPSC-CMs. The numbers in the columns indicate the N values of each group and numbers on top of columns indicate the numbers of hiPSC-CMs presenting arrhythmic events. \*p<0.05, \*\*p<0.01, \*\*\*p<0.001.

**Figure 6. Antiarrhythmic effect of venlafaxine and pregabalin in mouse ventricular myocytes.** A) line-scan image shows a  $\text{Ca}^{2+}$  wave in a ventricular myocyte from KI mouse. B)  $\text{Ca}^{2+}$  wave frequency (number of  $\text{Ca}^{2+}$  waves per second in a 49s recording period) in cardiomyocytes from WT and KI mice in baseline (BL) and in 100 nM ISO perfusion. ISO increased  $\text{Ca}^{2+}$  waves frequency in ventricular myocytes from WT and KI mice. N: 11 cells in WT in basal (black box), during 100 nM ISO perfusion (orange box); 28 cells in KI in basal (blue box), during 100 nM ISO perfusion (pink box). C) Venlafaxine decreased ISO induced  $\text{Ca}^{2+}$  waves in ventricular myocytes from WT and KI mice. N: 10 cells in WT in basal (black box), during 5  $\mu\text{g}/\text{mL}$  venlafaxine perfusion (red box), and during perfusion with 100 nM ISO in the continued presence of 5  $\mu\text{g}/\text{mL}$  venlafaxine (green box); 17 cells in KI in basal (blue box), during 5  $\mu\text{g}/\text{mL}$  venlafaxine perfusion (light blue box), and during perfusion with 100 nM ISO in the continued presence of 5  $\mu\text{g}/\text{mL}$  venlafaxine (pink purple box). D) Pregabalin decreased ISO induced  $\text{Ca}^{2+}$  waves in ventricular myocytes from WT and KI mice. N: 10 cells in WT vs. 21 cells in KI. The “\*” directly on top of the data indicate the significant difference of this group compared to that in basal, the “\*\*” on the top of line indicate the significant difference between the two groups on both side of the line. \*  $p < 0.05$ , \*\* $p < 0.01$ , and \*\*\* $p < 0.001$ .

**Supplemental Figure 1. Characteristics of APs of hiPSC-CM in basal and 1  $\mu\text{M}$  ISO.** A) Threshold of the AP, measured at the point where the membrane potential starts depolarization, B) Maximal upstroke velocity ( $dv/dt \text{ max}$ ) of the phase 0 of the AP, C) Overshoot of AP, D) Duration of AP at 20% and D) 50% of repolarization. The data between two treatments of same genotype were repeated recorded from 18 control cells and 25 mutated cells respectively. \*  $p < 0.05$ , \*\* $p < 0.01$ , and \*\*\* $p < 0.001$ .

**Supplemental Figure 2. ISO effect on baseline fluorescence of  $[\text{Ca}^{2+}]_i$  transients.** 100 nM ISO didn't alter baseline fluorescence in both groups, while 1000 nM ISO significantly increase baseline fluorescence in CPVT group but not in control group. 42 cells in CTL vs. 53 cells in CPVT in 100 nM ISO, 91 cells in CTL vs. 106 cells in CPVT in 1000 nM ISO. \*  $p < 0.05$ , \*\* $p < 0.01$ , and \*\*\* $p < 0.001$ .

**Supplemental Figure 3. ISO effect on  $[\text{Ca}^{2+}]_i$  transients in hiPSC-CMs at 100 nM concentration.** A) Peak  $F/F_0$  of the electrically evoked  $[\text{Ca}^{2+}]_i$  transient during 100 nM ISO normalized by the peak  $F/F_0$  of the same hiPSC-CM before ISO application. ISO increased amplitude ( $F/F_0$ ). B) Full time duration of the  $[\text{Ca}^{2+}]_i$  transient at half its amplitude (D50) during isoproterenol normalized by the D50 in the same hiPSC-CM before ISO. Accelerated duration at 50% peak of  $[\text{Ca}^{2+}]_i$  transients in both groups of hiPSC-CMs. N: 62 control hiPSC-CMs vs. 71 CPVT hiPSC-CMs.

**Supplemental Figure 4.  $\text{Ca}^{2+}$  transients and SR load of adult mouse ventricular myocytes haven't been modified by venlafaxine and pregabalin.** A)  $[\text{Ca}^{2+}]_i$  transient amplitude (max  $F/F_0$  baseline), B) Decay time calculated by fitting the descending phase of the  $[\text{Ca}^{2+}]_i$  transient to a single exponential, C) Time to peak; D-F) show the same parameters with A-C but with ISO. In basal, N=33 in WT in basal (black box), N=12 in WT.ven (recorded after 2 min 5  $\mu\text{g}/\text{mL}$  venlafaxine perfusion, red box), N=10 in WT.pre (recorded after 2 min 5  $\mu\text{g}/\text{mL}$  pregabalin perfusion, green box), N=45 in KI in basal (blue box), N=14 in KI.ven (recorded after 2 min 5  $\mu\text{g}/\text{mL}$  venlafaxine perfusion, light blue box), N=7 in KI.pre (recorded after 2 min 5  $\mu\text{g}/\text{mL}$  pregabalin perfusion, pink purple box); in ISO, N=11 in WT.iso, N=9 in WT.ven.iso, N=11 in WT.pre.iso, N=28 in KI.iso, N=18 in KI.ven.iso, N=23 in KI.pre.iso. G) venlafaxine and pregabalin didn't change caffeine evoked peak in basal condition as well as in ISO condition (H), (N: in basal: 9 cells in WT, 8 cells in WT.ven, 8 cells in WT.pre, 7 cells in KI, 8 cells in KI.ven, 6 cells in KI.pre; in ISO: 11 cells in WT.iso, 7 cells in WT.ven.iso, 11 cells in WT.pre.iso, 18 cells in KI.iso, 18 cells in KI.ven.iso, 18 cells in KI.pre.iso).

## Acknowledgement

This work was supported by ANR (Agence Nationale de la Recherche) grants to AMG, (ANR-13-BSV1-0023-01 & ANR-19-CE14-0031-01) and to JPB (ANR-15-CE14-0005). LHY was a recipient of the CSC (Chinese Science Council) doctoral fellowship, and JLA an Alambert grant from Université Paris Sud.

## References

Bezzerrides, V. J. *et al.* (2019) ‘Gene Therapy for Catecholaminergic Polymorphic Ventricular Tachycardia by Inhibition of Ca<sup>2+</sup> /Calmodulin-Dependent Kinase II’, *Circulation*, 140(5), pp. 405–419. doi: 10.1161/circulationaha.118.038514.

Bezzina, C. R., Lahrouchi, N. and Priori, S. G. (2015) ‘Genetics of Sudden Cardiac Death’, *Circulation Research*, 116(12), pp. 1919–1936. doi: 10.1161/CIRCRESAHA.116.304030.

Bian, F. *et al.* (2006) ‘Calcium channel alpha2-delta type 1 subunit is the major binding protein for pregabalin in neocortex, hippocampus, amygdala, and spinal cord: An ex vivo autoradiographic study in alpha2-delta type 1 genetically modified mice’, *Brain Research*, 1075(1), pp. 68–80. doi: 10.1016/j.brainres.2005.12.084.

Domingo, D. *et al.* (2015) ‘Non-ventricular, Clinical, and Functional Features of the RyR2(R420Q) Mutation Causing Catecholaminergic Polymorphic Ventricular Tachycardia.’, *Revista espanola de cardiologia (English ed.)*, 68(5), pp. 398–407. doi: 10.1016/j.rec.2014.04.023.

Elcarpio, J. O. B. D., Ahinski, A. N. B. and Zzo, N. I. J. I. (1998) ‘HL-1 cells : A cardiac muscle cell line that contracts and retains phenotypic characteristics of the adult cardiomyocyte’, *Proc. Natl. Acad. Sci. USA*, 95(March), pp. 2979–2984.

Fatima, A. *et al.* (2011) ‘In vitro modeling of ryanodine receptor 2 dysfunction using human induced pluripotent stem cells’, *Cellular Physiology and Biochemistry*, 28(4), pp. 579–592. doi: 10.1159/000335753.

Fernández-Velasco, M. *et al.* (2009a) 'Increased Ca<sup>2+</sup> sensitivity of the ryanodine receptor mutant RyR2R4496C underlies catecholaminergic polymorphic ventricular tachycardia', *Circulation Research*, 104(2), pp. 201–209. doi: 10.1161/CIRCRESAHA.108.177493.

Fernández-Velasco, M. *et al.* (2009b) 'Increased Ca<sup>2+</sup> sensitivity of the ryanodine receptor mutant RyR2R4496C underlies catecholaminergic polymorphic ventricular tachycardia', *Circulation Research*, 104(2), pp. 201–209. doi: 10.1161/CIRCRESAHA.108.177493.

Gómez, A. M. (2012) 'Paradoxical effect of increased diastolic Ca<sup>2+</sup> release and decreased sinoatrial node activity in a mouse model of catecholaminergic polymorphic ventricular tachycardia', *Circulation*, 126(4), pp. 392–401. doi: 10.1161/CIRCULATIONAHA.111.075382.

Itzhaki, I. *et al.* (2012) 'Modeling of catecholaminergic polymorphic ventricular tachycardia with patient-specific human-induced pluripotent stem cells', *Journal of the American College of Cardiology*. Elsevier Inc., 60(11), pp. 990–1000. doi: 10.1016/j.jacc.2012.02.066.

Jiang, D. *et al.* (2004) 'RyR2 mutations linked to ventricular tachycardia and sudden death reduce the threshold for store-overload-induced Ca<sup>2+</sup> release (SOICR).', *Proceedings of the National Academy of Sciences of the United States of America*, 101(35), pp. 13062–7. doi: 10.1073/pnas.0402388101.

Jiang, D. *et al.* (2005) 'Enhanced store overload-induced Ca<sup>2+</sup> release and channel sensitivity to luminal Ca<sup>2+</sup> activation are common defects of RyR2 mutations linked to ventricular tachycardia and sudden death', *Circulation Research*, 97(11), pp. 1173–1181. doi: 10.1161/01.RES.0000192146.85173.4b.

Jiang, D. *et al.* (2007) '(RyR2-A4860G) Loss of luminal Ca<sup>2+</sup> activation in the cardiac ryanodine receptor is associated with ventricular fibrillation and sudden death.', *Proceedings of the National Academy of Sciences of the United States of America*, 104(46), pp. 18309–14. doi: 10.1073/pnas.0706573104.

Jung, C. B. *et al.* (2012) 'Dantrolene rescues arrhythmogenic RYR2 defect in a patient-specific stem cell model of catecholaminergic polymorphic ventricular tachycardia', *EMBO Molecular Medicine*, 4(3), pp. 180–191. doi: 10.1002/emmm.201100194.

- Khalifa, M., Daleau, P. and Turgeon, J. (1999) 'Mechanism of sodium channel block by venlafaxine in guinea pig ventricular myocytes', *Journal of Pharmacology and Experimental Therapeutics*, 291(1), pp. 280–284.
- Landstrom, A. P., Dobrev, D. and Wehrens, X. H. T. (2017) 'Calcium Signaling and Cardiac Arrhythmias', *Circulation Research*, 120(12), pp. 1969–1993. doi: 10.1161/CIRCRESAHA.117.310083.
- Lehnart, S. E. *et al.* (2008) 'Leaky Ca<sup>2+</sup> release channel / ryanodine receptor 2 causes seizures and sudden cardiac death in mice', *The Journal of Clinical Investigation*, 118(6), pp. 2230–2245. doi: 10.1172/JCI35346DS1.
- Lian, X. *et al.* (2012) 'Robust cardiomyocyte differentiation from human pluripotent stem cells via temporal modulation of canonical Wnt signaling', *Proceedings of the National Academy of Sciences*, 109(27), pp. E1848–E1857. doi: 10.1073/pnas.1200250109.
- Lian, X. *et al.* (2013) 'Directed cardiomyocyte differentiation from human pluripotent stem cells by modulating Wnt/beta-catenin signaling under fully defined conditions', *Nature Protocols*, 8(1), pp. 162–175. doi: 10.1038/nprot.2012.150.Directed.
- Liu, N. *et al.* (2011) 'Short communication: Flecainide exerts an antiarrhythmic effect in a mouse model of catecholaminergic polymorphic ventricular tachycardia by increasing the threshold for triggered activity', *Circulation Research*, 109(3), pp. 291–295. doi: 10.1161/CIRCRESAHA.111.247338.
- Lowri Thomas, N., George, C. H. and Anthony Lai, F. (2004) 'Functional heterogeneity of ryanodine receptor mutations associated with sudden cardiac death', *Cardiovascular Research*, 64(1), pp. 52–60. doi: 10.1016/j.cardiores.2004.06.009.
- Meli, A. C. *et al.* (2011) 'A novel ryanodine receptor mutation linked to sudden death increases sensitivity to cytosolic calcium', *Circulation Research*, 109(3), pp. 281–290. doi: 10.1161/CIRCRESAHA.111.244970.
- Mico, J.-A. and Prieto, R. (2012) 'Elucidating the mechanism of action of pregabalin: alpha(2)delta as a therapeutic target in anxiety.', *CNS drugs. New Zealand*, 26(8), pp. 637–648. doi: 10.2165/11634510-000000000-00000.

- Novak, A. *et al.* (2015) 'RyR420Q-Functional abnormalities in iPSC-derived cardiomyocytes generated from CPVT1 and CPVT2 patients carrying ryanodine or calsequestrin mutations', *Journal of Cellular and Molecular Medicine*, 19(8), pp. 2006–2018. doi: 10.1111/jcmm.12581.
- Paludan-Müller, C. *et al.* (2017) 'Integration of 60,000 exomes and ACMG guidelines question the role of Catecholaminergic Polymorphic Ventricular Tachycardia-associated variants', *Clinical Genetics*, 91(1), pp. 63–72. doi: 10.1111/cge.12847.
- Penttinen, K. *et al.* (2015) 'Antiarrhythmic effects of dantrolene in patients with catecholaminergic polymorphic ventricular tachycardia and replication of the responses using iPSC models', *PLoS ONE*, 10(5). doi: 10.1371/journal.pone.0125366.
- Priori, S. G. and Chen, S. R. W. (2011) 'Inherited dysfunction of sarcoplasmic reticulum Ca<sup>2+</sup> handling and arrhythmogenesis', *Circulation Research*, pp. 871–883. doi: 10.1161/CIRCRESAHA.110.226845.
- Shah, U. and Hodgson, R. (2009) 'Flecainide prevents catecholaminergic polymorphic ventricular tachycardia in mice and humans', *Nature Medicine*, 13(4), pp. 466–480. doi: 10.1038/nm.1942.Flecainide.
- Tada, M. *et al.* (2014) 'A highly sensitive fluorescent indicator dye for calcium imaging of neural activity in vitro and in vivo', *European Journal of Neuroscience*, 39(11), pp. 1720–1728. doi: 10.1111/ejn.12476.
- Usselman, C. W. N. S. S. J. R. B. (2017) 'A comparison of fluorescent Ca<sup>2+</sup> indicators for imaging local Ca<sup>2+</sup> signals in cultured cells', *Physiology & behavior*, 176(3), pp. 139–148. doi: 10.1016/j.physbeh.2017.03.040.
- Wang, Y. Y. *et al.* (2017) 'RyR2R420Q catecholaminergic polymorphic ventricular tachycardia mutation induces bradycardia by disturbing the coupled clock pacemaker mechanism.', *JCI insight*, 2(8). doi: 10.1172/jci.insight.91872.
- Watanabe, H. *et al.* (2011) 'Flecainide inhibits arrhythmogenic Ca<sup>2+</sup> waves by open state block of ryanodine receptor Ca<sup>2+</sup> release channels and reduction of Ca<sup>2+</sup> spark mass', *Journal of molecular and cellular cardiology*, 76(2), pp. 1358–1375. doi: 10.1111/j.1365-2958.2010.07165.x.Characterization.

Zhang, J. *et al.* (2009) 'Functional cardiomyocytes derived from human induced pluripotent stem cells', *Circulation Research*, 104(4), pp. 30–41. doi: 10.1161/CIRCRESAHA.108.192237.

Zhang, J., Wilson, G. and Soerens, A. (2009) 'Functional Cardiomyocytes Derived from Human Induced Pluripotent Stem Cells', *Circulation ...*, 104(4), pp. e30–e41. doi: 10.1161/CIRCRESAHA.108.192237.Functional.

Zhang, X. H. *et al.* (2013) 'Ca<sup>2+</sup> signaling in human induced pluripotent stem cell-derived cardiomyocytes (iPSC-CM) from normal and catecholaminergic polymorphic ventricular tachycardia (CPVT)-afflicted subjects', *Cell Calcium*, 54(2), pp. 57–70. doi: 10.1016/j.ceca.2013.04.004.

Zhao, Y.-T. *et al.* (2015a) '(RyR2-A4860G) Arrhythmogenesis in a catecholaminergic polymorphic ventricular tachycardia mutation that depresses ryanodine receptor function.', *Proceedings of the National Academy of Sciences of the United States of America*, 112(13), pp. E1669-77. doi: 10.1073/pnas.1419795112.

Zhao, Y.-T. *et al.* (2015b) 'Arrhythmogenesis in a catecholaminergic polymorphic ventricular tachycardia mutation that depresses ryanodine receptor function.', *Proceedings of the National Academy of Sciences of the United States of America*, 112(13), pp. E1669-77. doi: 10.1073/pnas.1419795112.

Figure 1

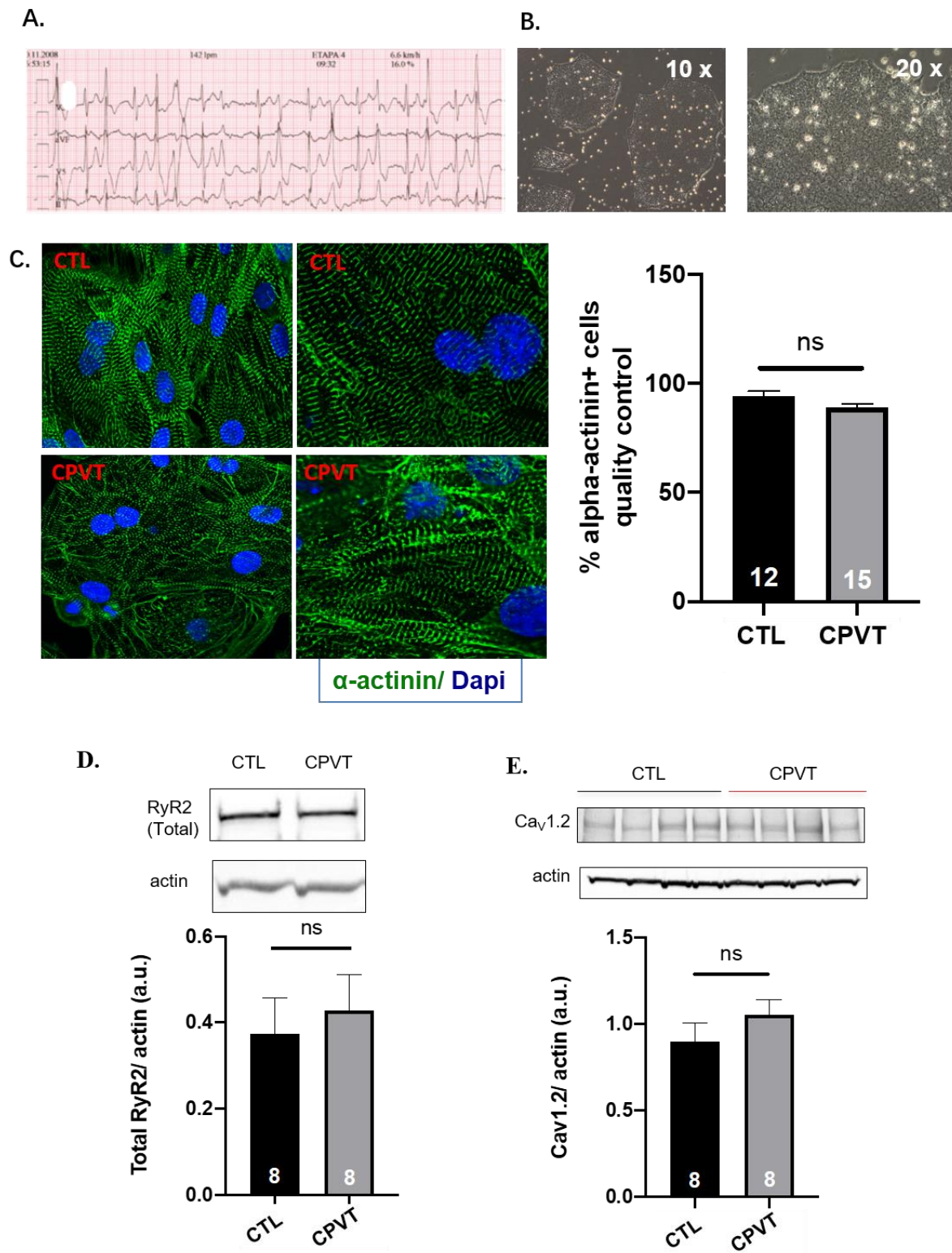


**Figure 2**

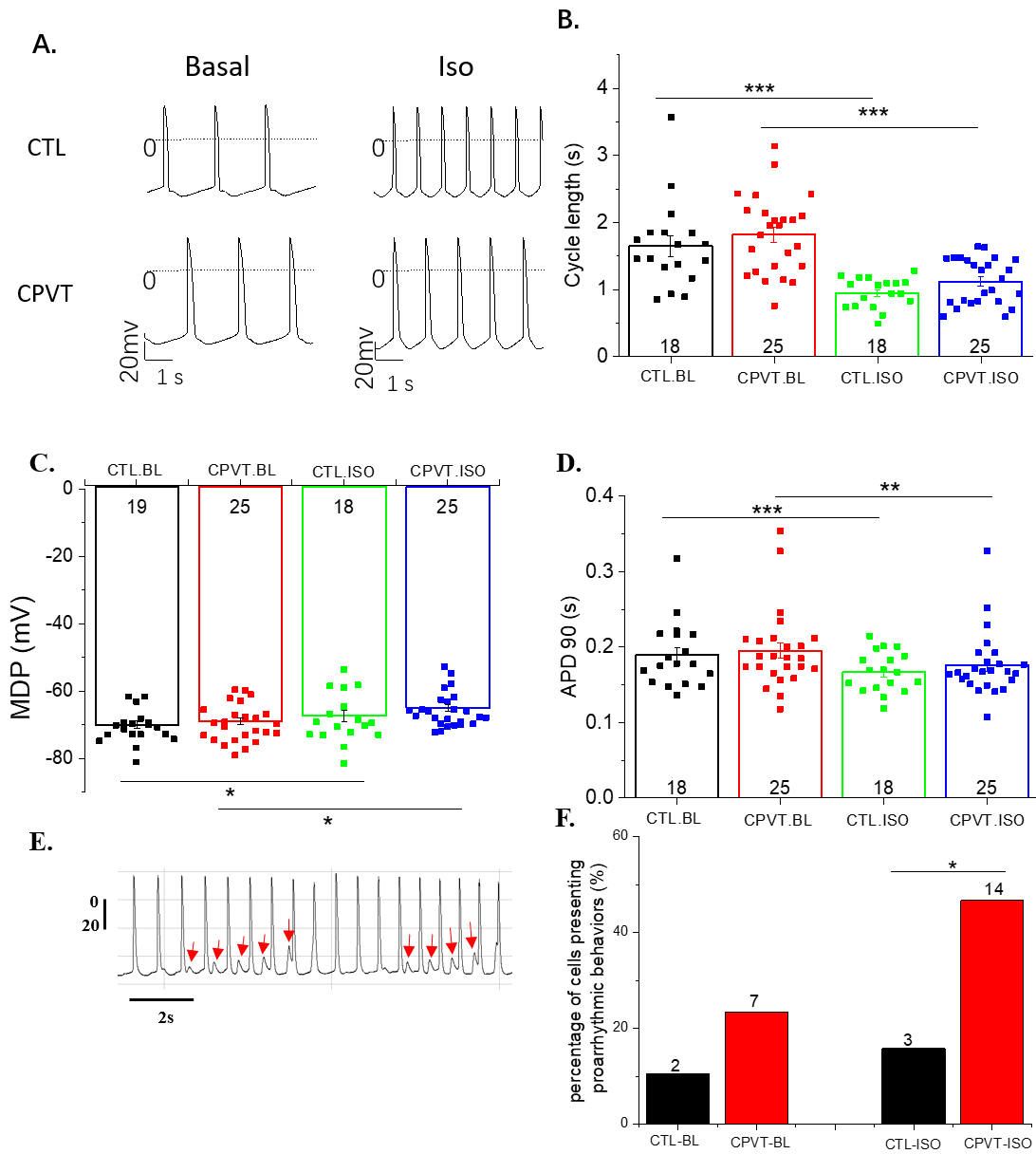


**Figure 3**

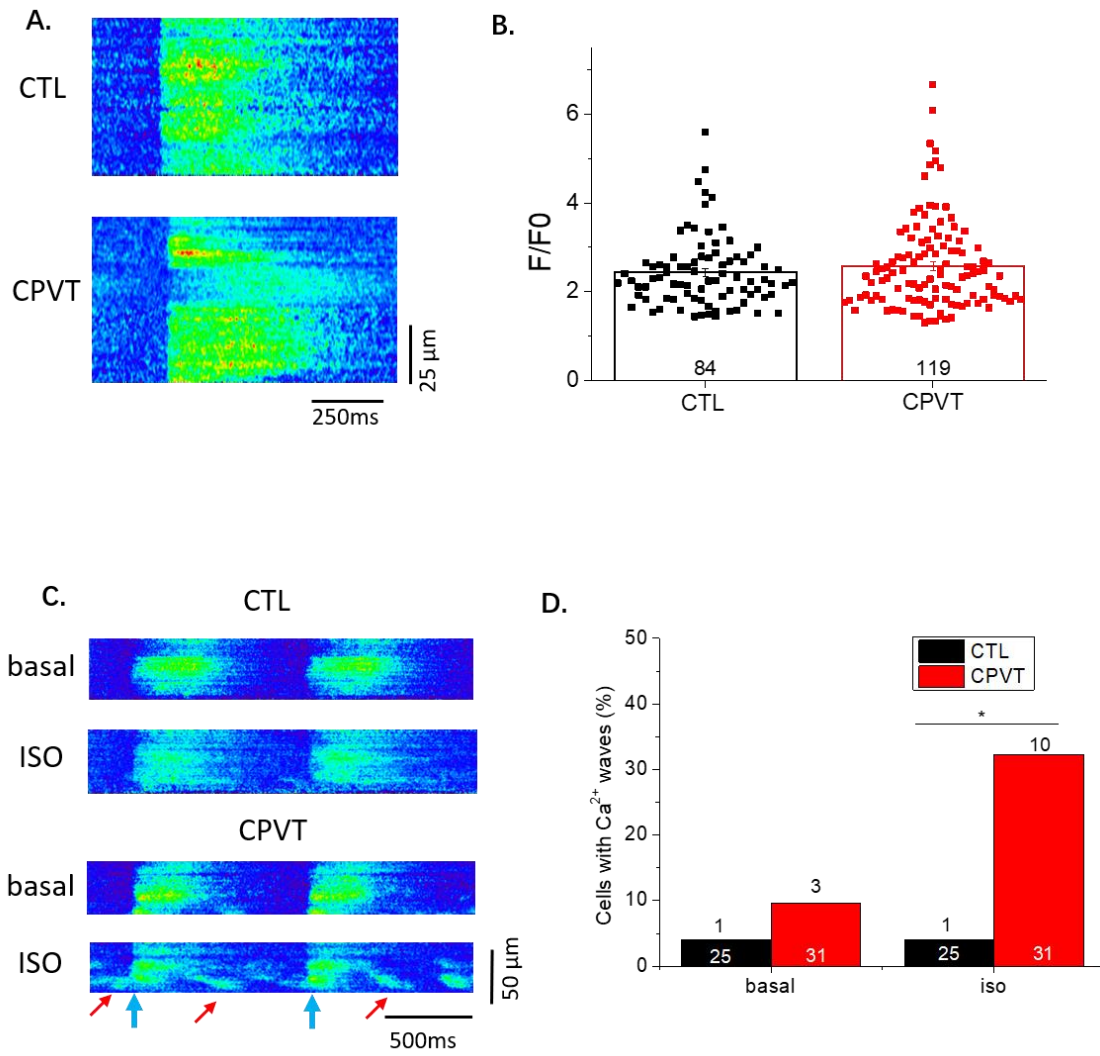


**Figure 4**

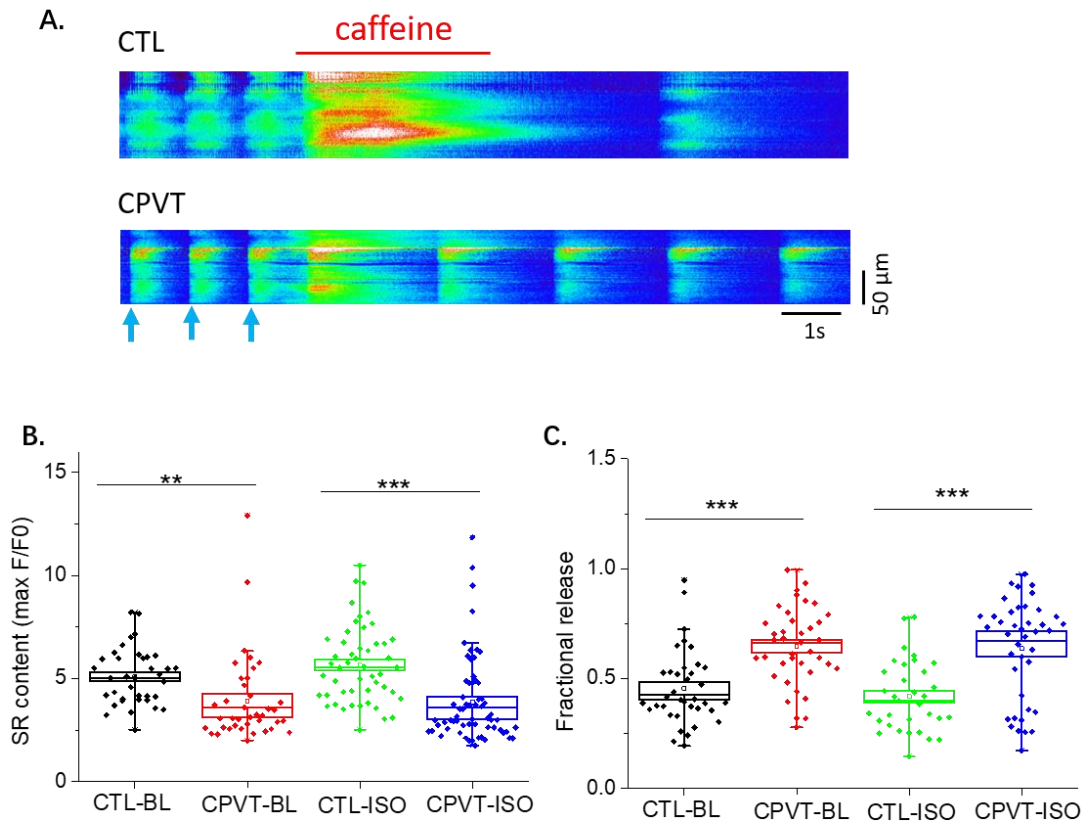


**Figure 5**

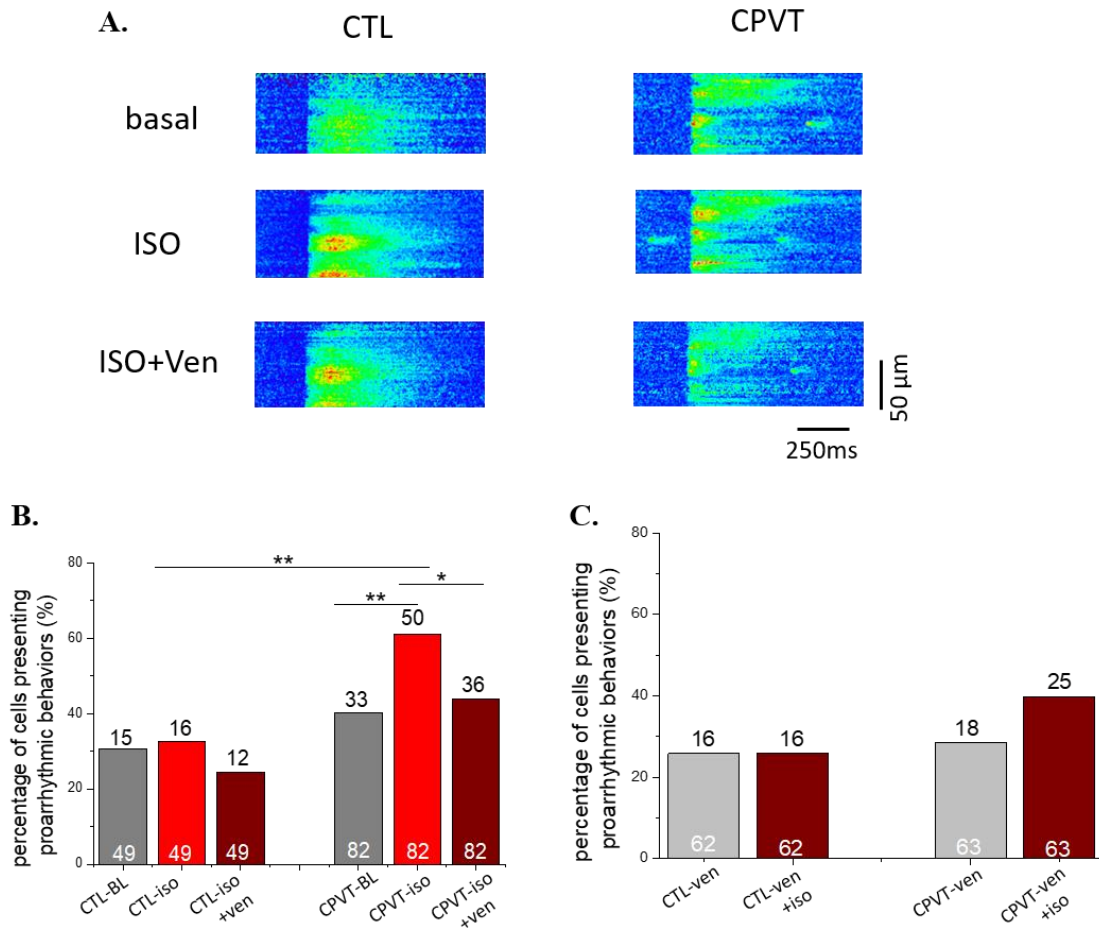
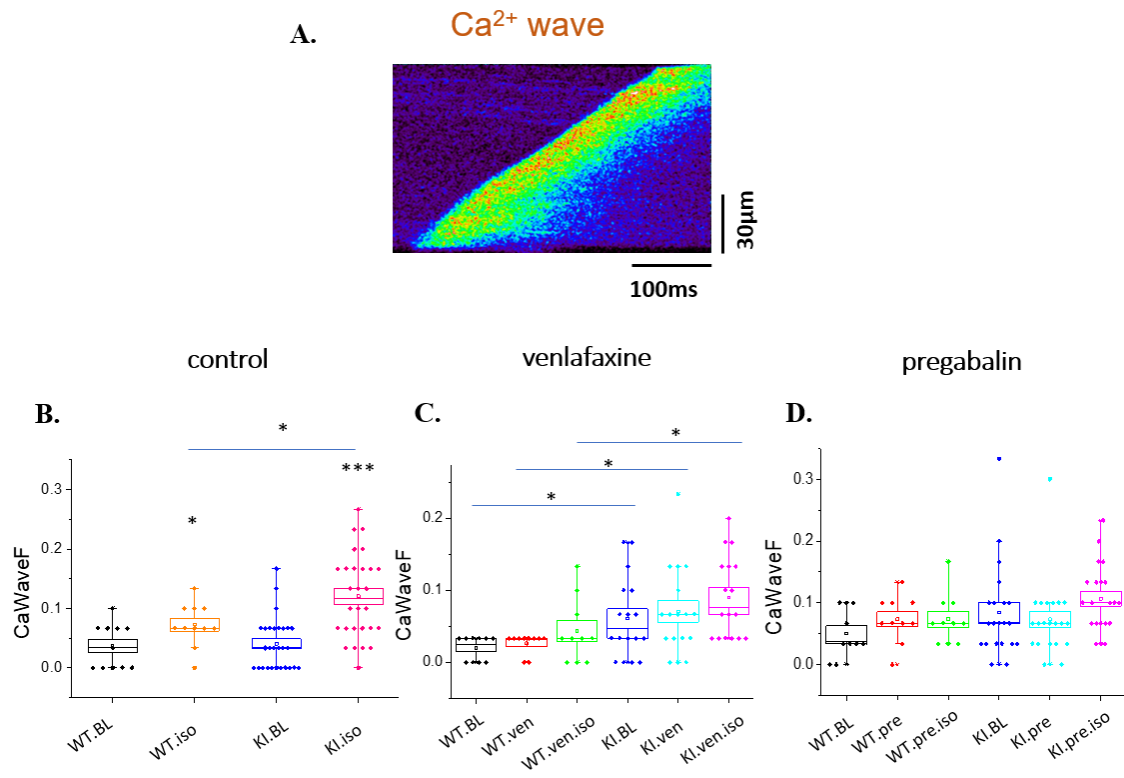
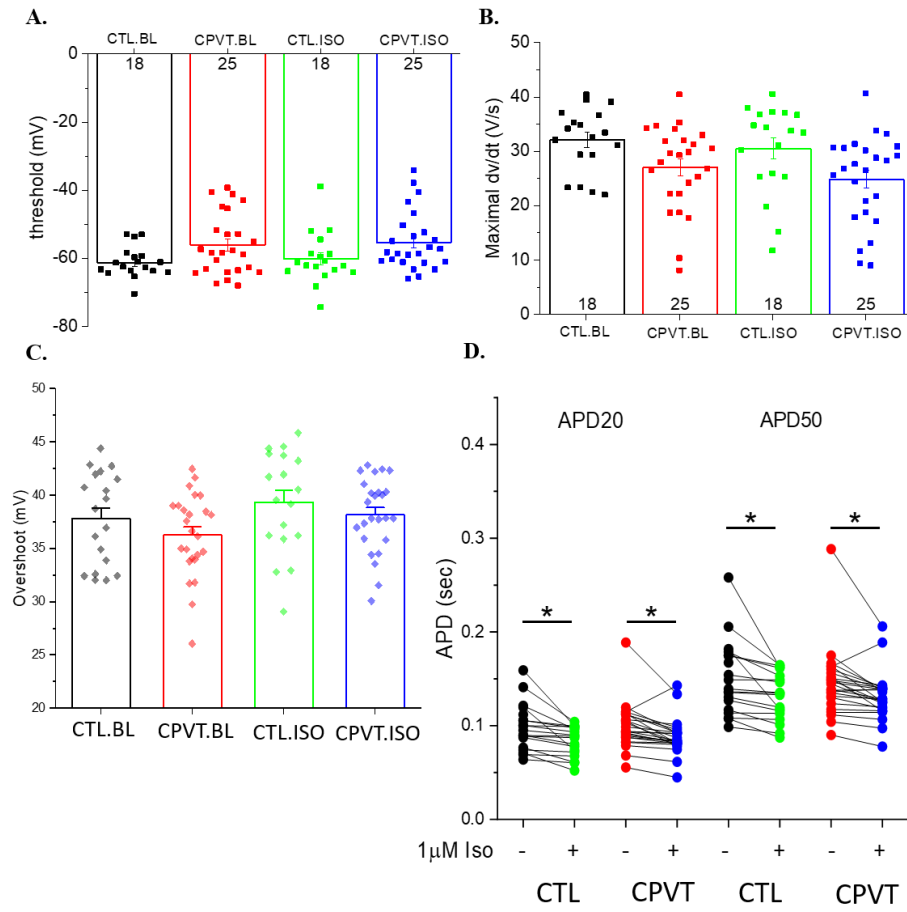


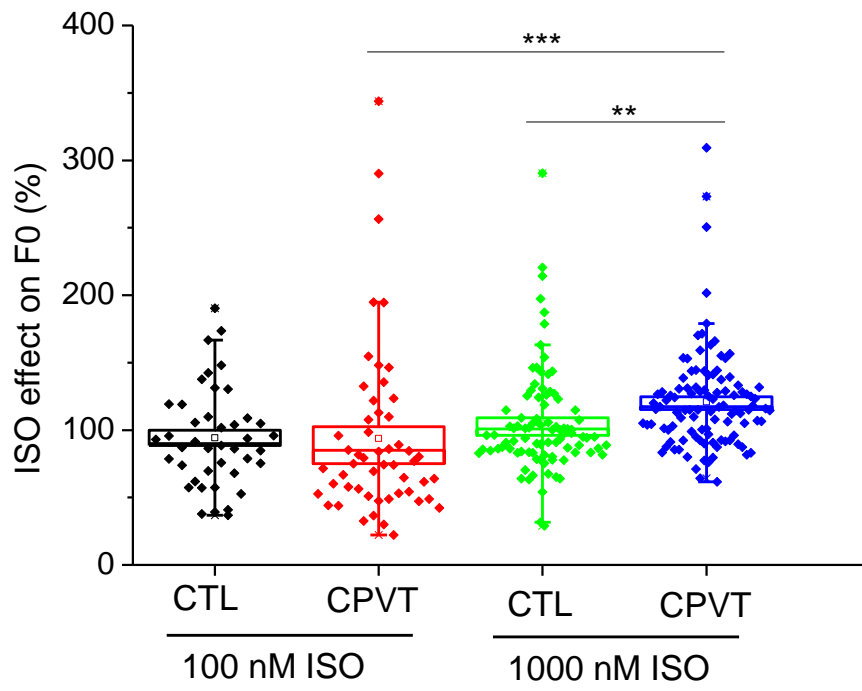
**Figure 6**



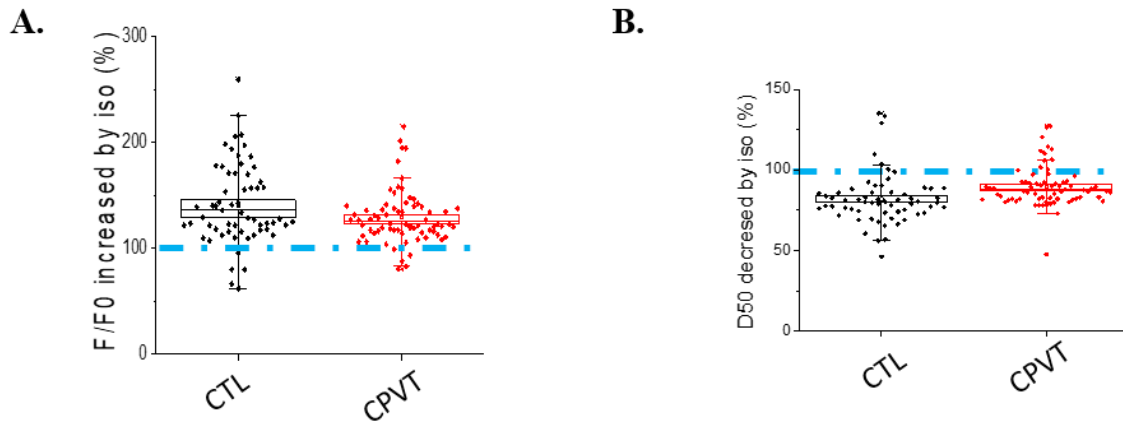
# Supplemental Figure 1



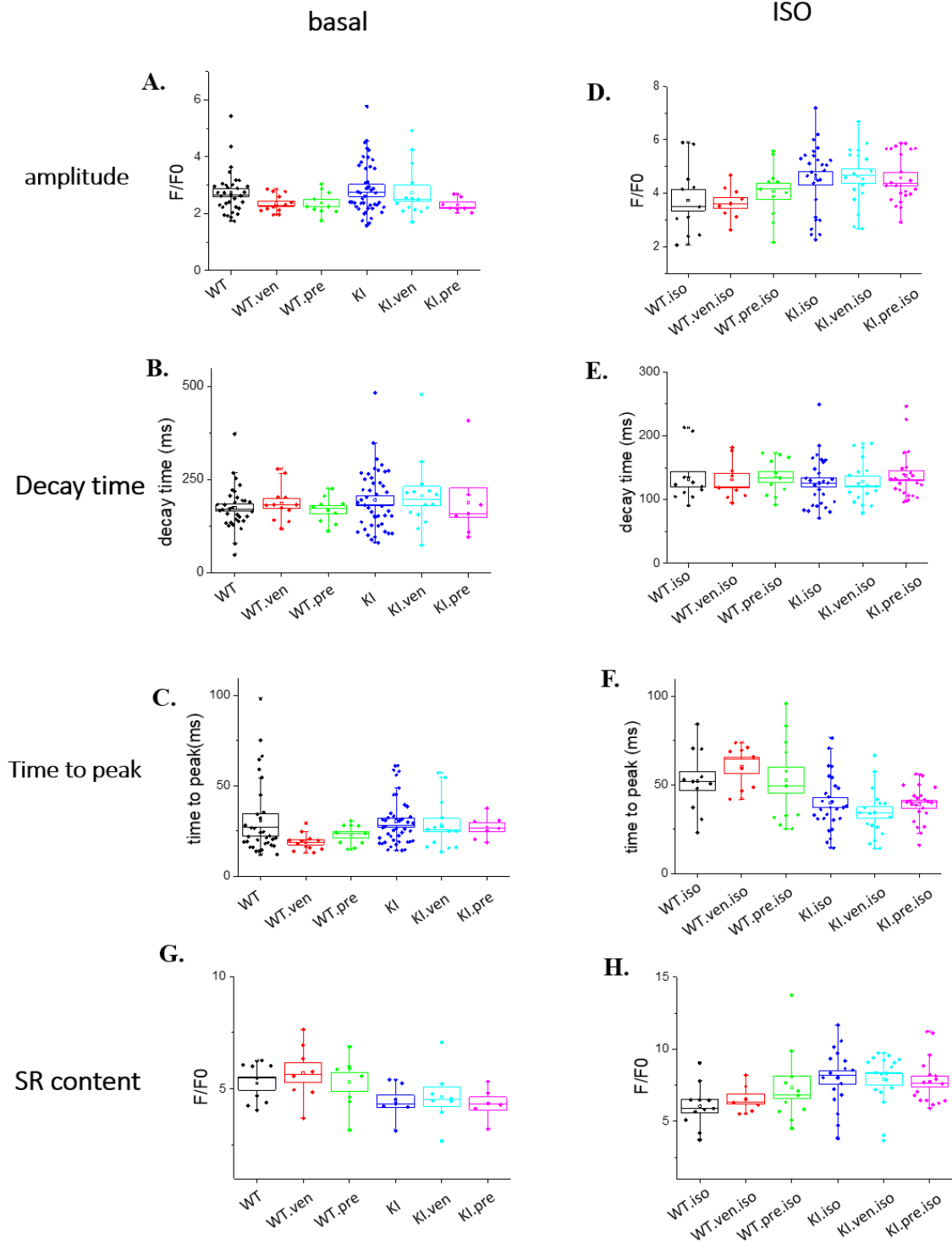
**Supplemental Figure 2**



**Supplemental Figure 3**



**Supplemental Figure 4**



# Discussion



Although CPVT has been unveiled and described more than 40 years ago (Coumel P, Fidelle J 1978), and the first CPVT1 mutation was identified almost 20 years ago (Priori et al. 2001) (Laitinen et al. 2001), the underlying mechanism of CPVT still remains under controversy. One important reason is that the mechanism of mutations causing arrhythmias may vary among different locations as we have summarized in table 2 in Introduction, due to the large molecule and multiple modulatory factors of RyR2. Different mutations even generated totally opposite results, for example, gain-of-function and loss-of-function, but they both cause CPVT. Furthermore, the experimental models used for CPVT studies such as mouse, present large structural and functional differences from human, which also hampered the outcome of researches. After first description by Zhang et al in 2009 (J. Zhang et al. 2009), hiPSC-CMs straightway became the most popular tool for researchers in CPVT field. To date, more than 10 mutations have been functionally studied in hiPSC-CMs, including patient-specific and engineering hiPSC-CMs. In this thesis, we studied the same mutation RyR2<sup>R420Q</sup> both in knock-in mouse model and patient-specific hiPSC-CMs, providing a good insight into the underlying mechanism of RyR2<sup>R420Q</sup> causing CPVT. Moreover, here we for the first time generated the control hiPSCs from the patient's brother who possess the consanguinity, improving the comparability of the data of two groups at difference with other researches who use healthy hiPS cell lines or hiPSCs generated from any people as control.

## **hiPSC culturing and differentiation into cardiomyocytes**

hiPSC is a relative new cell model which has been discovered by Takahashi and Yamanaka in 2006 (Takahashi and Yamanaka 2006), while hiPSC-CM is even later which has firstly been described in 2009 as mentioned above (J. Zhang et al. 2009). Since that, numerous researches were endeavor to optimize the differentiation method to improve the generation of cardiomyocytes as well as promote cell maturation (Parikh et al. 2017)(Garbern et al. 2019)(Ulmer et al. 2018)(Bose and Shenoy P 2016). The hiPSC platform of our lab was set up during my thesis, so at beginning we have done many exploring experiments. We tried different culture medium for hiPSC culturing and finally found that mTesR<sup>TM</sup> stem cell culture medium is the best for our clones. We have also tried different differentiation protocols. At beginning, we used the protocol based on the methods from Lian et al (Lian et al, 2015) and BurrIDGE et al (BurrIDGE et al, 2014). Since the efficiency and success rate were unstable, we changed to Gsk3 inhibitor and Wnt inhibitor (GiWi) protocol which has been created by Lian et al (X. Lian et al. 2012) (X Lian et al. 2013) earlier. Besides, since we were working on the new hiPSC lines, we

needed to optimize the concentrations of all the molecules we used for cell culturing and cell differentiation, as well as test the cell seeding concentration to start the differentiation. After about 8 months, we succeed to get good and stable beating cardiomyocytes for experiments. After immunolabeling of the myocyte specific protein such as  $\alpha$ -actinin and RyR2, we validated the cells we derived from hiPSC were well cardiomyocytes. During this time I was also working in a side project analyzing the variant in RyR2 detected by our collaborators in a family with sudden death. I did the first HEK transfection, confocal calcium imaging at different calcium concentration and response to cAMP elevation (see manuscript in Annexes).

## **Heart rate and spontaneous contraction rate**

In my laboratory previous study in mouse, we have found a significantly slower sinus heart rhythm (SHR) in KI females than WT females, which is consistent with the data from patients (Wang et al. 2017). However, here we found no difference of spontaneous contraction rate between CPVT hiPSC-CMs and control hiPSC-CMs. One of reasons may due to the gender, since the hiPSC-CMs we detected were generated from men which didn't present SHR bradycardia (Wang et al. 2017). Another possible reason maybe that the hiPSC-CMs, although automatic, are not pacemaker cells. Furthermore, ISO was performed to check the sympathetic effect. In mouse model, the RR interval reduced by iso was bigger in KI mice in females but no difference in males (Wang et al. 2017). In hiPSC-CMs, we found CL of spontaneous contraction rate reduction by ISO was similar in both groups. The different in ventricular vs pacemaker cells and the specie (mice vs human) can underlie the difference in the ISO sensitivity to spontaneous rate.

## **Ca<sup>2+</sup> homeostasis**

The dysfunction of Ca<sup>2+</sup> homeostasis is generally considered as the main trigger of CPVT. In this scheme, the irregular SR Ca<sup>2+</sup> leak caused by RyR2 mutations will result in local Ca<sup>2+</sup> accumulating in sub-sarcolemmal space thereby activating membrane Na<sup>+</sup>/Ca<sup>2+</sup> exchanger to remove the extra Ca<sup>2+</sup>, which will generate an inward current that can trigger DADs or EADs (Wei et al. 2018). Measurement of diastolic Ca<sup>2+</sup> leak as Ca<sup>2+</sup> sparks is a good way to evaluate the activity of mutated RyR2 channels, and the RyR2 with gain-of-function mutations often present increased Ca<sup>2+</sup> sparks frequency (Fernández-Velasco et al. 2009a) (Fatima et al. 2011) (Wei et al. 2018). Furthermore, by analyzing the properties of Ca<sup>2+</sup> sparks such as peak, duration

and width, we can figure out how the channel activity change. In previous study, we found that in sinoatrial node, the CPVT cells presented higher frequency and longer duration of  $\text{Ca}^{2+}$  sparks, indicating the mutation  $\text{RyR2}^{\text{R420Q}}$  resulted in higher probability and marked prolonged duration of RyR2 channel opening (Wang et al. 2017). In this thesis, we also analyzed those properties of  $\text{Ca}^{2+}$  sparks in ventricular myocytes, and within expected, we saw the similar phenomenon that higher frequency and longer duration of  $\text{Ca}^{2+}$  sparks resulted in bigger mass of diastolic  $\text{Ca}^{2+}$  leak in ventricular myocytes from KI mice, validating the gain-of-function behavior. In the side project as shown in the manuscript in Annexes, we also analyzed a novel RyR2 variant D3291V, which was found as loss-of-function, since the cells expressing this variant failed to response to forskolin. This variant has been found outside of RyR2 hotspots of CPVT1 mutations.

Moreover, the arrhythmogenic  $[\text{Ca}^{2+}]_i$  events such as  $\text{Ca}^{2+}$  waves have been investigated in pacing ventricular myocytes both in basal and adrenergic stress condition. In basal, almost no WT cells presented  $\text{Ca}^{2+}$  waves, and cells from KI mice significantly presented more  $\text{Ca}^{2+}$  waves than WT group. ISO provoked the appearance of arrhythmogenic  $[\text{Ca}^{2+}]_i$  events in WT cells and further increased them in the KI cells. These results were consistent with the data of VT observed in vivo. Simultaneously, we also calculated the cells presenting  $\text{Ca}^{2+}$  waves in hiPSC-CMs and observed a marked ISO induced augmentation of  $\text{Ca}^{2+}$  waves in CPVT hiPSC-CMs, indicating the higher activity of mutated channels activated by ISO, validating the CPVT phenotype.

In order to know whether those alterations in RyR2 channels change the  $\text{Ca}^{2+}$  handling in cardiomyocytes, we also evaluated intracellular  $\text{Ca}^{2+}$  ( $[\text{Ca}^{2+}]_i$ ) handling in intact mouse cells as well as in hiPSC-CMs by confocal microscopy. We found that cardiomyocytes from KI mice showed normal  $[\text{Ca}^{2+}]_i$  transients characteristics, both at 2 and 4 Hz pacing stimulation. ISO increased the  $[\text{Ca}^{2+}]_i$  transient amplitude and accelerated its decay time in both groups of cells, but the iso effect on amplitude was lower in KI cells than WT cells. Similarly, in hiPSC-CMs, no difference of  $[\text{Ca}^{2+}]_i$  transient amplitude was found between CPVT and control hiPSC-CMs when paced at 1 Hz. It is reasonable since the CPVT patients often appear normally in resting. However, the smaller amplitude in CPVT hiPSC-CMs has also been reported in mutation  $\text{RyR2}^{\text{D3638A}}$  (Acimovic et al. 2018) and  $\text{RyR2}^{\text{L3741P}}$  (Preininger et al. 2016), two mutations located at the C-terminal domain. The difference here may be generated by different location of the mutations.

Since the diastolic SR  $\text{Ca}^{2+}$  leak is often affected by SR  $\text{Ca}^{2+}$  load, we would like to know what happen to  $\text{Ca}^{2+}$  content in the SR. After measuring the SR  $\text{Ca}^{2+}$  content by rapid caffeine application following field stimulation, we found that cardiomyocytes isolated from KI mice had lower SR  $\text{Ca}^{2+}$  content than that from WT mice, but this decrease was overcome by  $\beta$ -adrenergic stimulation, while the decay time of the caffeine evoked  $[\text{Ca}^{2+}]_i$  transient was comparable in WT and KI cardiomyocytes, suggesting similar NCX function in the forward mode. However, in hiPSC-CMs, we found the SR  $\text{Ca}^{2+}$  content was significantly lower in CPVT hiPSC-CMs, while the fractional release was higher in CPVT hiPSC-CMs both in basal and in  $1\mu\text{M}$  ISO, suggesting a gain of function alteration of the RyR2<sup>R420Q</sup>. Similar results have also been reported in other mutations in previous researches. In mutation RyR2<sup>P2328S</sup> (Kujala et al. 2012) and RyR2<sup>L3741P</sup> (Preininger et al. 2016), the SR  $\text{Ca}^{2+}$  content was lower and fractional release was higher in CPVT hiPSC-CMs in basal conditions. In mutation RyR2<sup>F2483I</sup> (X. H. Zhang et al. 2013), smaller SR  $\text{Ca}^{2+}$  content was found in CPVT hiPSC-CMs in basal, while in mutation RyR2<sup>S406L</sup> (Jung et al. 2012b), the significantly smaller SR  $\text{Ca}^{2+}$  content was only found after  $1\mu\text{M}$  ISO but not in basal. However, in mutation RyR2<sup>D3638A</sup> (Acimovic et al. 2018), the fractional release in CPVT hiPSC-CMs presented no significant difference compared to control group. Those smaller SR  $\text{Ca}^{2+}$  content in CPVT hiPSC-CMs may also be due to the diastolic SR  $\text{Ca}^{2+}$  leak. In fact, ISO induced diastolic  $\text{Ca}^{2+}$  increase in CPVT hiPSC-CMs has already been reported in other mutations, such as RyR2<sup>P2328S</sup> (Kujala et al. 2012), RyR2<sup>S406L</sup> (Jung et al. 2012b), RyR2<sup>F2483I</sup> (X. H. Zhang et al. 2013), as well as the same mutation as we studied RyR2<sup>R420Q</sup> (Novak et al. 2015). Indeed, we found  $100\text{ nM}$  iso increased the  $[\text{Ca}^{2+}]_i$  transient amplitude in both CPVT and control hiPSC-CMs, while  $1\mu\text{M}$  ISO failed to increase the amplitude in CPVT hiPSC-CMs due to the significantly increased baseline value, which highlighted the importance of diastolic  $\text{Ca}^{2+}$  level that is partly controlled by SR  $\text{Ca}^{2+}$  leak and SERCA. To address this hypothesis, it is necessary to measure the diastolic  $\text{Ca}^{2+}$  level in next step.

## Electrophysiological properties

The dysfunction of  $\text{Ca}^{2+}$  homeostasis can further affect electrophysiological properties to trigger DADs or EADs thereby triggering arrhythmias. Thus, we recorded the action potentials (APs) of mouse ventricular myocytes by patch clamp and APs of hiPSC-CMs by micro-electrode. We found that no matter in mouse ventricular myocytes or in hiPSC-CMs, more cells carrying mutation presented ISO activated arrhythmogenic events, which was consistent with

the data of  $\text{Ca}^{2+}$  waves in  $\text{Ca}^{2+}$  handling. Especially, almost all the cardiomyocytes from KI mouse presented DADs after adrenergic stimulation, while this ratio came back to zero after adding a  $\text{Ca}^{2+}$  chelator BAPTA to the patch pipette, indicating that intracellular  $\text{Ca}^{2+}$  had a central role in triggering these arrhythmias. For hiPSC-CMs, we only recorded the spontaneous APs in basal condition and under 1  $\mu\text{M}$  ISO perfusion. We found that ISO stimulation significantly increased the ratio of cells presenting arrhythmogenic events. Similar findings have been reported in mutations  $\text{RyR2}^{\text{L4115F}}$  and  $\text{RyR2}^{\text{E3D}}$  (Pölonen, Swan, and Aalto-Setälä 2019). In another research, it has been reported that ISO only significantly increased DADs in 1 Hz paced CPVT ( $\text{RyR2}^{\text{I4587V}}$ )-hiPSC-CMs but not in spontaneously beating cells (Sasaki et al. 2016).

We then further analyzed the other parameters of APs by analyzing the APs without arrhythmic events of two groups. We found that most of parameters were similar in two groups of hiPSC-CMs, indicating that the mutation  $\text{RyR2}^{\text{R420Q}}$  doesn't alter the other ion channels contributing to AP shape. Whereas some reports have demonstrated that another gain-of-function CPVT mutation  $\text{RyR2}^{\text{P2328S}}$  downregulated Nav1.5 in murine (King et al. 2013)(Ning et al. 2016). The durations of AP at 20, 50, and 90% of repolarization were comparable in the two groups both in basal and in 1  $\mu\text{M}$  ISO perfusion. However, the shorter APD has also been reported for mutations  $\text{RyR2}^{\text{L4115F}}$  and  $\text{RyR2}^{\text{E3D}}$  in the previous research (Pölonen, Swan, and Aalto-Setälä 2019). Mutations  $\text{RyR2}^{\text{L4115F}}$  is a C-terminal mutation which is far away from our mutation, while though as an N-terminal mutation,  $\text{RyR2}^{\text{E3D}}$  is located in untranslated regions. Thus, it is reasonable that these two mutations generated different effects on AP properties. After perfused with 1  $\mu\text{M}$  ISO, hiPSC-CMs presented significantly more depolarized maximal diastolic potential (MDP), which may due to the effect of mutation on HCN4 channels that expressing in these immature cells. Activation of HCN4 channels, which produce  $I_f$  (funny current), is shifted by cAMP produced by  $\beta$ -adrenergic stimulation. So  $I_f$  is activated at more positives potentials, starting slow depolarization and limiting the maximum diastolic potential. There is no difference in this fact between two groups, thus suggesting that the presence of  $\text{RyR2}^{\text{R420Q}}$  does not secondarily induces any change on MDP.

## **The antiarrhythmic effect of venlafaxine and pregabalin**

Venlafaxine and pregabalin are central nervous system drugs aiming to cure depression or anxiety respectively, which have never been used as antiarrhythmic drugs. We tested their

antiarrhythmic effects here because one CPVT patient who has already undergone several effort syncope, stopped presenting CPVT symptoms during evaluation after taken several medicines (including venlafaxine, pregabalin, terazosin, Oxycodone, naloxone, and tetrazepam) to cure other diseases. We already knew that the ion channels inhibitors, such as flecainide, a Na<sup>+</sup> channel blocker, and verapamil, a Ca<sup>2+</sup> channel blocker, may possess the characteristics of preventing arrhythmias. While it has been reported that venlafaxine inhibited Na<sup>+</sup> channel (Khalifa, Daleau, and Turgeon 1999) and pregabalin inhibited neuronal voltage-gated calcium channel (Mico and Prieto 2012)(Bian et al. 2006). Thus, we speculated that venlafaxine and pregabalin might play a role in preventing from CPVT in that patient. In order to address our hypotheses, we tested the effect of those two drugs on diastolic Ca<sup>2+</sup> release events such as Ca<sup>2+</sup> waves and sparks both in adult mouse ventricular myocytes and hiPSC-CMs. hiPSC-CMs is a good model for drugs screening, since it is generated from CPVT patient as well as can recapitulate disease phenotype of CPVT patients in many ways (Itzhaki et al. 2012)(X. H. Zhang et al. 2013). Flecainide (Itzhaki et al. 2012), an approved antiarrhythmic drug, and Dantrolene (Jung et al. 2012)(Penttinen et al. 2015), a drug effective on malignant hyperthermia, have already been tested in hiPSC-CMs and their antiarrhythmic performance observed in CPVT hiPSC-CMs demonstrated that hiPSC-CM model replicated well the individual drug responses.

We have treated hiPSC-CMs with venlafaxine by both acute (2 min perfusion) and chronic (24 h) mode and both ways showed that venlafaxine decreased diastolic Ca<sup>2+</sup> release events in CPVT hiPSC-CMs, indicating the antiarrhythmic effect of venlafaxine. It may indicate that venlafaxine can reduce diastolic Ca<sup>2+</sup> leak induced by ISO in hiPSC-CMs, and this is important since increased diastolic Ca<sup>2+</sup> leak seems to be a relative common phenomenon in ISO treated CPVT hiPSC-CMs that have been observed in many previous researches (Jung et al. 2012)(Novak et al. 2015)(Kujala et al. 2012)(Wei et al. 2018). Moreover, acute treated venlafaxine has also been found to decrease Ca<sup>2+</sup> waves in adult ventricular myocytes from CPVT KI mice, further validating the protection role of venlafaxine in CPVT. In order to step to the antiarrhythmic mechanism of venlafaxine, we also detected the effect of venlafaxine on Ca<sup>2+</sup> transient and SR Ca<sup>2+</sup> content in adult mouse ventricular myocytes. We found that venlafaxine didn't alter Ca<sup>2+</sup> transient and SR Ca<sup>2+</sup> content, reminiscent of the effect of flecainide that has been reported to inhibit SR Ca<sup>2+</sup> leak by blocking RyR2 channel in its open state without increasing SR content (Shah and Hodgson 2009) (Watanabe et al. 2011). It has been refuted by another report which suggested that flecainide didn't directly affect RyR2

channel but prevent arrhythmic trigger events by reducing the availability of sodium channels (Liu et al. 2011). Since venlafaxine and flecainide both show inhibition effect on sodium channel, it is reasonable to speculate that venlafaxine may work in the similar way as flecainide. However, to address this hypothesis, more experiments such as single channel technique are needed to detect whether or not venlafaxine block RyR2 channels.

Pregabalin was only tested in mouse ventricular myocytes and the preliminary results also indicated antiarrhythmic effect of pregabalin in ventricular myocytes from RyR<sup>R420Q</sup> KI mice. Moreover, pregabalin didn't alter Ca<sup>2+</sup> transient and SR Ca<sup>2+</sup> content according to our preliminary data which is similar to venlafaxine. Pregabalin has been showed to block voltage gated calcium channels by targeting to  $\alpha 2\delta$  isoform of the channel (Mico and Prieto 2012)(Bian et al. 2006), reminiscent of verapamil, another approved class IV antiarrhythmic drug targeting to calcium channel (Singh, Nademanee, and Feld 1983).

Here we only figured out the antiarrhythmic effect of venlafaxine and pregabalin, but their optimal concentration as well as their cardiotoxicity, which are very important factors for the drugs clinical application, are unclear.

So in summary, the work performed during my thesis established the iPSC-CM in the laboratory and validated the hiPSC-CM model to analyze CPVT phenotype, corroborating a gain of function behavior of RyR<sup>R420Q</sup>, since the ISO induced arrhythmic events were higher both in Ca<sup>2+</sup> transients and APs of CPVT hiPSC-CMs, and moreover, the fractional release of SR Ca<sup>2+</sup> was higher in CPVT hiPSC-CMs. Furthermore, we suggest that venlafaxine and pregabalin, two neural system drugs, could protect from arrhythmias to these CPVT patients since we found that they inhibited the ISO induced arrhythmias in CPVT hiPSC-CMs and/or in CPVT KI mouse ventricular myocytes.

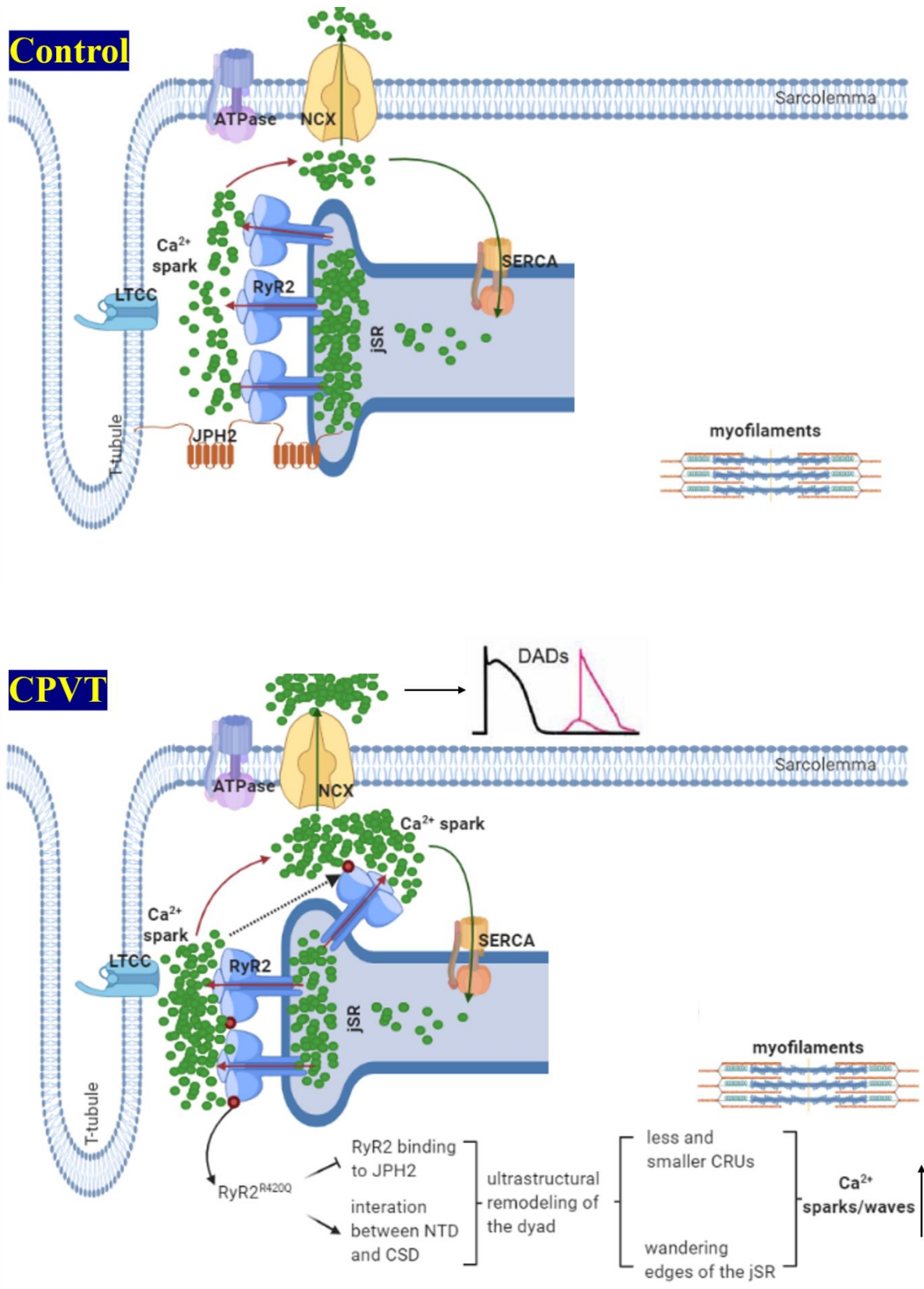


**Figure 29. Schematic diagram showing arrhythmogenic mechanism of CPVT1 mutation RyR<sup>R420Q</sup> demonstrated by this thesis.** In control diagram, Ca<sup>2+</sup> sparks don't trigger Ca<sup>2+</sup> waves. In CPVT diagram, Ca<sup>2+</sup> release as Ca<sup>2+</sup> sparks/waves from sarcoplasmic reticulum (SR) by ryanodine receptor 2 (RyR2) during resting state due to disturbed dyad by RyR<sup>R420Q</sup>

mutation. LTCC: L-type calcium channel, JPH2: Junctophilin-2, jSR: junctional SR, SERCA: sarco/endoplasmic reticulum  $\text{Ca}^{2+}$ -ATPase, NCX: sodium calcium exchanger, DADs: delay afterdepolarizations, NTD: N-terminal domain, CSD: core solenoid domain, CRU: calcium release unit. Red arrows:  $\text{Ca}^{2+}$  released into cytosol, green arrows:  $\text{Ca}^{2+}$  removed from cytosol, dash arrows:  $\text{Ca}^{2+}$  trigger neighboring  $\text{Ca}^{2+}$  release units to release  $\text{Ca}^{2+}$ .

# References



- Acimovic, I. *et al.* (2018) ‘Post-Translational Modifications and Diastolic Calcium Leak Associated to the Novel RyR2-D3638A Mutation Lead to CPVT in Patient-Specific hiPSC-Derived Cardiomyocytes’, *Journal of Clinical Medicine*, 7(11), p. 423. doi: 10.3390/jcm7110423.
- Ahern, G. P., Junankar, P. R. and Dulhunty, A. F. (1994) ‘Single channel activity of the ryanodine receptor calcium release channel is modulated by FK-506’, *FEBS Letters*, 352(3), pp. 369–374. doi: 10.1016/0014-5793(94)01001-3.
- Ahern, G. P., Junankar, P. R. and Dulhunty, A. F. (1997) ‘Subconductance States in Single-Channel Activity of Skeletal Muscle Ryanodine Receptors After Removal of FKBP12’, *Biophysical Journal*. Elsevier, 72(1), pp. 146–162. doi: 10.1016/S0006-3495(97)78654-5.
- Al-Khatib, S. M. *et al.* (2018) *2017 AHA/ACC/HRS Guideline for Management of Patients With Ventricular Arrhythmias and the Prevention of Sudden Cardiac Death: Executive Summary*, *Circulation*. doi: 10.1161/CIR.0000000000000548.
- Allessie, M. A., Bonke, F. I. and Schopman, F. J. (1973) ‘Circus movement in rabbit atrial muscle as a mechanism of tachycardia.’, *Circulation research*. United States, 33(1), pp. 54–62.
- Allessie, M. A., Bonke, F. I. and Schopman, F. J. (1977) ‘Circus movement in rabbit atrial muscle as a mechanism of tachycardia. III. The “leading circle” concept: a new model of circus movement in cardiac tissue without the involvement of an anatomical obstacle.’, *Circulation research*. United States, 41(1), pp. 9–18. doi: 10.1161/01.res.41.1.9.
- Alseikhan, B. A. *et al.* (2002) ‘Engineered calmodulins reveal the unexpected eminence of Ca<sup>2+</sup> channel inactivation in controlling heart excitation’, *Proceedings of the National Academy of Sciences of the United States of America*, 99(26), pp. 17185–17190. doi: 10.1073/pnas.262372999.
- Altmann, Helene M. *et al.* (2015) ‘Homozygous/compound heterozygous triadin mutations associated with autosomal-recessive long-QT syndrome and pediatric sudden cardiac arrest: Elucidation of the triadin knockout syndrome’, *Circulation*, 131(23), pp. 2051–2060. doi: 10.1161/CIRCULATIONAHA.115.015397.
- Altmann, Helene M *et al.* (2015) ‘Homozygous/compound heterozygous triadin mutations associated with autosomal-recessive long-QT syndrome and pediatric sudden cardiac arrest: Elucidation of the triadin knockout syndrome’, *Circulation*, 131(23), pp. 2051–2060. doi: 10.1161/CIRCULATIONAHA.115.015397.
- Amador, F. J. *et al.* (2009) ‘Crystal structure of type I ryanodine receptor amino-terminal  $\beta$ -trefoil domain reveals a disease-associated mutation “hot spot” loop’, *Proceedings of the National Academy of Sciences of the United States of America*, 106(27), pp. 11040–11044. doi: 10.1073/pnas.0905186106.
- Amador, F. J. *et al.* (2013) ‘Type 2 ryanodine receptor domain a contains a unique and dynamic  $\alpha$ -helix that transitions to a  $\beta$ -strand in a mutant linked with a heritable cardiomyopathy’, *Journal of Molecular Biology*. Elsevier Ltd, 425(21), pp. 4034–4046. doi: 10.1016/j.jmb.2013.08.015.
- Amin, A. S., Tan, H. L. and Wilde, A. A. M. (2010) ‘Cardiac ion channels in health and disease’, *Heart Rhythm*. Elsevier Inc., 7(1), pp. 117–126. doi: 10.1016/j.hrthm.2009.08.005.

- Andersson, A. *et al.* (1983) ‘Cadmium-113 nuclear magnetic resonance studies of proteolytic fragments of calmodulin: assignment of strong and weak cation binding sites.’, *Biochemistry*. United States, 22(10), pp. 2309–2313. doi: 10.1021/bi00279a001.
- Anthony Lai, F. *et al.* (1988) ‘Purification and reconstitution of the calcium release channel from skeletal muscle’, *Nature*, 331(6154), pp. 315–319. doi: 10.1038/331315a0.
- Antzelevitch, C. (2001) ‘Basic mechanisms of reentrant arrhythmias’, *Current Opinion in Cardiology*, 16(1), pp. 1–7. doi: 10.1097/00001573-200101000-00001.
- Antzelevitch, Charles (2001) ‘The Brugada syndrome: Ionic basis and arrhythmia mechanisms’, *Journal of Cardiovascular Electrophysiology*, 12(2), pp. 268–272. doi: 10.1046/j.1540-8167.2001.00268.x.
- Anumonwo, J. M. and Pandit, S. V. (2015) ‘Ionic mechanisms of arrhythmogenesis’, *Trends in Cardiovascular Medicine*. Elsevier, 25(6), pp. 487–496. doi: 10.1016/j.tcm.2015.01.005.
- Arking, D. E. *et al.* (2014) ‘Genetic association study of QT interval highlights role for calcium signaling pathways in myocardial repolarization’, *Nature Genetics*, 46(8), pp. 826–836. doi: 10.1038/ng.3014.
- Arrhythmia, D. (2010) ‘Genetic Basis of LQTS’, *Circulation*, pp. 1426–1435. doi: 10.1161/CIRCULATIONAHA.109.894725.
- Austin, K. M. *et al.* (2019) ‘Molecular mechanisms of arrhythmogenic cardiomyopathy’, *Nature Reviews Cardiology*. Springer US. doi: 10.1038/s41569-019-0200-7.
- Avila, G. *et al.* (2020) ‘between Sarcolemma and Sarcoplasmic Reticulum in Muscle Cells’.
- Azizi, M., Elyasi, F. and Roodposhti, F. N. (2019) ‘Bradycardia caused by interaction of venlafaxine and cyclosporine: A case report’, *Caspian Journal of Internal Medicine*, 10(4), pp. 463–467. doi: 10.22088/cjim.10.4.463.
- Bai, X. C. *et al.* (2016) ‘The Central domain of RyR1 is the transducer for long-range allosteric gating of channel opening’, *Cell Research*. Nature Publishing Group, 26(9), pp. 995–1006. doi: 10.1038/cr.2016.89.
- Baldwin, D. S. *et al.* (2015) ‘Efficacy and safety of pregabalin in generalised anxiety disorder: A critical review of the literature’, *Journal of Psychopharmacology*, 29(10), pp. 1047–1060. doi: 10.1177/0269881115598411.
- Balshaw, D. M. *et al.* (2001) ‘Calmodulin Binding and Inhibition of Cardiac Muscle Calcium Release Channel (Ryanodine Receptor)’, *Journal of Biological Chemistry*, 276(23), pp. 20144–20153. doi: 10.1074/jbc.M010771200.
- Baltogiannis, G. G. *et al.* (2019) ‘CPVT: Arrhythmogenesis, Therapeutic Management, and Future Perspectives. A Brief Review of the Literature’, *Frontiers in Cardiovascular Medicine*, 6(July), pp. 8–11. doi: 10.3389/fcvm.2019.00092.
- Banville, I. and Gray, R. A. (2002) ‘Effect of Action Potential Duration and Conduction Velocity Restitution and Their Spatial Dispersion on Alternans and the Stability of Arrhythmias’, *J Cardiovasc Electrophysiol*, 13, pp. 1141–9.

- Bauce, B. *et al.* (2002) ‘Screening for ryanodine receptor type 2 mutations in families with effort-induced polymorphic ventricular arrhythmias and sudden death: early diagnosis of asymptomatic carriers.’, *Journal of the American College of Cardiology*. United States, 40(2), pp. 341–349. doi: 10.1016/s0735-1097(02)01946-0.
- Bauce, B. *et al.* (2011) ‘Clinical phenotype and diagnosis of arrhythmogenic right ventricular cardiomyopathy in pediatric patients carrying desmosomal gene mutations.’, *Heart rhythm*. United States, 8(11), pp. 1686–1695. doi: 10.1016/j.hrthm.2011.06.026.
- Behr, E. R. and Roden, D. (2013) ‘Drug-induced arrhythmia: Pharmacogenomic prescribing?’, *European Heart Journal*, 34(2), pp. 89–95. doi: 10.1093/eurheartj/ehs351.
- Benitah, J. P., Alvarez, J. L. and Gómez, A. M. (2010) ‘L-type Ca<sup>2+</sup> current in ventricular cardiomyocytes’, *Journal of Molecular and Cellular Cardiology*. Elsevier Inc., 48(1), pp. 26–36. doi: 10.1016/j.yjmcc.2009.07.026.
- Benito, B. *et al.* (2008) ‘Brugada Syndrome’, *Progress in Cardiovascular Diseases*, 51(1), pp. 1–22. doi: 10.1016/j.pcad.2008.05.002.
- Berridge, M. J. (2012) ‘Calcium signalling remodelling and disease’, *Biochemical Society Transactions*, 40(2), pp. 297–309. doi: 10.1042/BST20110766.
- Berridge, M. J. (2016) ‘The inositol trisphosphate/calcium signaling pathway in health and disease’, *Physiological Reviews*, 96(4), pp. 1261–1296. doi: 10.1152/physrev.00006.2016.
- Bers, D. M. (2002) ‘Cardiac excitation–contraction coupling’, *nature*, 415(January), pp. 198–205.
- Bers, D. M. (2008) ‘Calcium cycling and signaling in cardiac myocytes.’, *Annual review of physiology*, 70, pp. 23–49. doi: 10.1146/annurev.physiol.70.113006.100455.
- Bers, D. M. (2014) ‘Cardiac Sarcoplasmic Reticulum Calcium Leak: Basis and Roles in Cardiac Dysfunction’, *Annual Review of Physiology*, 76(1), pp. 107–127. doi: 10.1146/annurev-physiol-020911-153308.
- Bers, D. M. (no date) *book-E-C coupling*.
- Bers, D. M., Pogwizd, S. M. and Schlotthauer, K. (2002) ‘Upregulated Na/Ca exchange is involved in both contractile dysfunction and arrhythmogenesis in heart failure.’, *Basic research in cardiology*. Germany, 97 Suppl 1, pp. I36-42.
- Bezzerrides, V. J. *et al.* (2019) ‘Gene Therapy for Catecholaminergic Polymorphic Ventricular Tachycardia by Inhibition of Ca<sup>2+</sup>/Calmodulin-Dependent Kinase II’, *Circulation*, 140(5), pp. 405–419. doi: 10.1161/circulationaha.118.038514.
- Bezzina, C. R., Lahrouchi, N. and Priori, S. G. (2015) ‘Genetics of Sudden Cardiac Death’, *Circulation Research*, 116(12), pp. 1919–1936. doi: 10.1161/CIRCRESAHA.116.304030.
- Bhuiyan, Z. A. *et al.* (2007) ‘A novel early onset lethal form of catecholaminergic polymorphic ventricular tachycardia maps to chromosome 7p14-p22’, *Journal of Cardiovascular Electrophysiology*, 18(10), pp. 1060–1066. doi: 10.1111/j.1540-8167.2007.00913.x.

- Bian, F. *et al.* (2006) 'Calcium channel alpha2-delta type 1 subunit is the major binding protein for pregabalin in neocortex, hippocampus, amygdala, and spinal cord: An ex vivo autoradiographic study in alpha2-delta type 1 genetically modified mice', *Brain Research*, 1075(1), pp. 68–80. doi: 10.1016/j.brainres.2005.12.084.
- Biffi, A. *et al.* (2002) 'Long-term clinical significance of frequent and complex ventricular tachyarrhythmias in trained athletes', *Journal of the American College of Cardiology*. Elsevier Masson SAS, 40(3), pp. 446–452. doi: 10.1016/S0735-1097(02)01977-0.
- Blayney, L. *et al.* (2013) 'ATP interacts with the CPVT mutation-associated central domain of the cardiac ryanodine receptor', *Biochimica et Biophysica Acta - General Subjects*, 1830(10), pp. 4426–4432. doi: 10.1016/j.bbagen.2013.05.038.
- Bonato, F. O. B. and Canziani, M. E. F. (2017) 'Ventricular arrhythmia in chronic kidney disease patients.', *Jornal brasileiro de nefrologia : 'orgao oficial de Sociedades Brasileira e Latino-Americana de Nefrologia*. Brazil, 39(2), pp. 186–195. doi: 10.5935/0101-2800.20170033.
- Bongianino, R. *et al.* (2017) 'Allele-specific silencing of mutant mRNA rescues ultrastructural and arrhythmic phenotype in mice carriers of the R4496C mutation in the ryanodine receptor gene (RYR2)', *Circulation Research*, 121(5), pp. 525–536. doi: 10.1161/CIRCRESAHA.117.310882.
- Borko, ubomír *et al.* (2014) 'Structural insights into the human RyR2 N-terminal region involved in cardiac arrhythmias', *Acta Crystallographica Section D: Biological Crystallography*, 70(11), pp. 2897–2912. doi: 10.1107/S1399004714020343.
- Brandes, R. and Bers, D. M. (1997) 'Intracellular Ca<sup>2+</sup> increases the mitochondrial NADH concentration during elevated work in intact cardiac muscle.', *Circulation research*. United States, 80(1), pp. 82–87. doi: 10.1161/01.res.80.1.82.
- Brohus, M. *et al.* (2019) 'Ca<sup>2+</sup> -dependent calmodulin binding to cardiac ryanodine receptor (RyR2) calmodulin-binding domains', *Biochemical Journal*, 476(2), pp. 193–209. doi: 10.1042/BCJ20180545.
- Bronner, F. (2001) 'Extracellular and intracellular regulation of calcium homeostasis.', *TheScientificWorldJournal*, 1, pp. 919–925. doi: 10.1100/tsw.2001.489.
- Brugada, P. and Brugada, J. (1992) 'Right bundle branch block, persistent ST segment elevation and sudden cardiac death: A distinct clinical and electrocardiographic syndrome. A multicenter report', *Journal of the American College of Cardiology*, 20(6), pp. 1391–1396. doi: 10.1016/0735-1097(92)90253-J.
- Cabra, V., Murayama, T. and Samsó, M. (2016) 'Ultrastructural Analysis of Self-Associated RyR2s', *Biophysical Journal*, 110(12), pp. 2651–2662. doi: 10.1016/j.bpj.2016.05.013.
- Campbell, K. P. *et al.* (1983) 'Purification and characterization of calsequestrin from canine cardiac sarcoplasmic reticulum and identification of the 53,000 dalton glycoprotein.', *The Journal of biological chemistry*. United States, 258(2), pp. 1197–1204.
- Cerrone, M. *et al.* (2005) 'Bidirectional ventricular tachycardia and fibrillation elicited in a knock-in mouse model carrier of a mutation in the cardiac ryanodine receptor.', *Circulation research*, 96(10), pp. 77–82. doi: 10.1161/01.res.0000169067.51055.72.

- Cerrone, M. *et al.* (2007) 'Arrhythmogenic mechanisms in a mouse model of catecholaminergic polymorphic ventricular tachycardia', *Circulation Research*, 101(10), pp. 1039–1048. doi: 10.1161/CIRCRESAHA.107.148064.
- Cerrone, M. and Priori, S. G. (2011) 'Genetics of sudden death: Focus on inherited channelopathies', *European Heart Journal*, 32(17), pp. 2109–2120. doi: 10.1093/eurheartj/ehr082.
- Chen, B. *et al.* (2012) 'In situ confocal imaging in intact heart reveals stress-induced  $Ca^{2+}$  release variability in a murine catecholaminergic polymorphic ventricular tachycardia model of type 2 ryanodine receptor  $R4496C$  mutation', *Circulation: Arrhythmia and Electrophysiology*, 5(4), pp. 841–849. doi: 10.1161/CIRCEP.111.969733.
- Chen, Q. *et al.* (1998) 'Genetic basis and molecular mechanism for idiopathic ventricular fibrillation', *Nature*, 392(6673), pp. 293–296. doi: 10.1038/32675.
- Cheng, H. and Lederer, W. J. (2008) 'Calcium sparks', *Physiological Reviews*, pp. 1491–1545. doi: 10.1152/physrev.00030.2007.
- Cheng, H., Lederer, W. J. and Cannell, M. B. (1993) 'Calcium Sparks : Elementary Events Underlying Excitation-Contraction Coupling in Heart Muscle', 262(October).
- Chin, D. and Means, A. R. (2000) 'Calmodulin: a prototypical calcium sensor.', *Trends in cell biology*. England, 10(8), pp. 322–328.
- Choi, B.-R., Burton, F. and Salama, G. (2002) 'Cytosolic  $Ca^{2+}$  triggers early afterdepolarizations and Torsade de Pointes in rabbit hearts with type 2 long QT syndrome.', *The Journal of physiology*. England, 543(Pt 2), pp. 615–631. doi: 10.1113/jphysiol.2002.024570.
- Chopra, N. *et al.* (2009) 'Ablation of triadin causes loss of cardiac  $Ca^{2+}$  release units, impaired excitation-contraction coupling, and cardiac arrhythmias', *Proceedings of the National Academy of Sciences of the United States of America*, 106(18), pp. 7636–7641. doi: 10.1073/pnas.0902919106.
- Chopra, N. and Knollmann, B. C. (2009) 'Cardiac calsequestrin: The new kid on the block in arrhythmias: Molecular perspectives', *Journal of Cardiovascular Electrophysiology*, pp. 1179–1185. doi: 10.1111/j.1540-8167.2009.01531.x.
- Chow, E. *et al.* (2014) 'Risk of cardiac arrhythmias during hypoglycemia in patients with type 2 diabetes and cardiovascular risk', *Diabetes*, 63(5), pp. 1738–1747. doi: 10.2337/db13-0468.
- Claycomb, W. C. *et al.* (1998) 'HL-1 cells: a cardiac muscle cell line that contracts and retains phenotypic characteristics of the adult cardiomyocyte.', *Proceedings of the National Academy of Sciences of the United States of America*. United States, 95(6), pp. 2979–2984. doi: 10.1073/pnas.95.6.2979.
- Clemens, D. J. *et al.* (2019) 'International Triadin Knockout Syndrome Registry: The Clinical Phenotype and Treatment Outcomes of Patients with Triadin Knockout Syndrome', *Circulation: Genomic and Precision Medicine*, 12(2), pp. 65–75. doi: 10.1161/CIRCGEN.118.002419.

- Cordes, J. S. *et al.* (2005) ‘Pentamidine reduces hERG expression to prolong the QT interval.’, *British journal of pharmacology*. England, 145(1), pp. 15–23. doi: 10.1038/sj.bjp.0706140.
- Cornea, R. L. *et al.* (2010) ‘Mapping the ryanodine receptor FK506-binding protein subunit using fluorescence resonance energy transfer’, *Journal of Biological Chemistry*, 285(25), pp. 19219–19226. doi: 10.1074/jbc.M109.066944.
- Corrado, D. *et al.* (2006) ‘Trends in sudden cardiovascular death in young competitive athletes after implementation of a preparticipation screening program.’, *JAMA*. United States, 296(13), pp. 1593–1601. doi: 10.1001/jama.296.13.1593.
- Coumel P, Fidelle J, L. V (1978) ‘Catecholaminergic-induced severe ventricular arrhythmias with Adams-Stokes syndrome in children: report of four cases.’, *Br. Heart J*, (40), pp. 28 – 37.
- Coumel, P. and Thomas, O. (1997) ‘Cardiac arrhythmias and the autonomic nervous system.’, *Le Journal médical libanais. The Lebanese medical journal*, 45(4), pp. 212–216.
- Coussin, F. *et al.* (2000) ‘Requirement of ryanodine receptor subtypes 1 and 2 for Ca(2+)-induced Ca(2+) release in vascular myocytes.’, *The Journal of biological chemistry*. United States, 275(13), pp. 9596–9603. doi: 10.1074/jbc.275.13.9596.
- Cranefield, P. F. (1977) ‘Action potentials, afterpotentials, and arrhythmias.’, *Circulation research*. United States, 41(4), pp. 415–423. doi: 10.1161/01.res.41.4.415.
- Cronin, E. M. *et al.* (2019) ‘2019 HRS/EHRA/APHRS/LAHR expert consensus statement on catheter ablation of ventricular arrhythmias’, *Journal of Arrhythmia*, pp. 323–484. doi: 10.1002/joa3.12185.
- Curtis, L. H. *et al.* (2003) ‘Prescription of QT-prolonging drugs in a cohort of about 5 million outpatients.’, *The American journal of medicine*. United States, 114(2), pp. 135–141. doi: 10.1016/s0002-9343(02)01455-9.
- Brugada, R. *et al.* (2014) ‘BRUGADA SYNDROME’, (1), pp. 25–28.
- Damiano, B. P. and Rosen, M. R. (1984) ‘Effects of pacing on triggered activity induced by early afterdepolarizations.’, *Circulation*. United States, 69(5), pp. 1013–1025. doi: 10.1161/01.cir.69.5.1013.
- Danielsen, T. K. *et al.* (2018) ‘Arrhythmia initiation in catecholaminergic polymorphic ventricular tachycardia type 1 depends on both heart rate and sympathetic stimulation’, *PLoS ONE*, 13(11), pp. 1–21. doi: 10.1371/journal.pone.0207100.
- Desai, P. H. *et al.* (2019) ‘Risk of Congenital Heart Disease in Newborns with Prenatal Exposure to Anti-depressant Medications’, *Cureus*, 11(5). doi: 10.7759/cureus.4673.
- Devalla, H. D. *et al.* (2015) ‘Atrial-like cardiomyocytes from human pluripotent stem cells are a robust preclinical model for assessing atrial-selective pharmacology’, *EMBO Molecular Medicine*, 7(4), pp. 394–410. doi: 10.15252/emmm.201404757.
- Devalla, H. D., Gélinas, R., Aburawi, E. H., Beqqali, A., Goyette, P., Freund, C., Chaix, Marie-a, *et al.* (2016) ‘TECRL , a new life-threatening inherited arrhythmia gene associated

with overlapping clinical features of both LQTS and CPVT', *EMBO Molecular Medicine*, 8(12), pp. 1390–1408. doi: 10.15252/emmm.201505719.

Devalla, H. D., Gélinas, R., Aburawi, E. H., Beqqali, A., Goyette, P., Freund, C., Chaix, Marie-A, *et al.* (2016) 'TECRL , a new life-threatening inherited arrhythmia gene associated with overlapping clinical features of both LQTS and CPVT ', *EMBO Molecular Medicine*, 8(12), pp. 1390–1408. doi: 10.15252/emmm.201505719.

Dick, I. E. *et al.* (2008) 'LETTERS A modular switch for spatial Ca<sup>2+</sup> selectivity in the calmodulin regulation of Ca<sup>v</sup> channels', 451(February). doi: 10.1038/nature06529.

Dobrev, D., Fender, A. C. and Wehrens, X. H. T. (2018) 'Pro-arrhythmic RyR2 channels in heart failure: do their localisation and mechanism of activation really matter?', *Cardiovascular Research*, 114(11), pp. 1428–1429. doi: 10.1093/cvr/cvy175.

Domingo, D. *et al.* (2015) 'Non-ventricular, Clinical, and Functional Features of the RyR2(R420Q) Mutation Causing Catecholaminergic Polymorphic Ventricular Tachycardia.', *Revista española de cardiología (English ed.)*, 68(5), pp. 398–407. doi: 10.1016/j.rec.2014.04.023.

Dulhunty, A. F. *et al.* (2012) 'Proteins within the intracellular calcium store determine cardiac RyR channel activity and cardiac output', *Clinical and Experimental Pharmacology and Physiology*, 39(5), pp. 477–484. doi: 10.1111/j.1440-1681.2012.05704.x.

Dybkova, N. *et al.* (2011) 'Overexpression of CaMKII $\delta$ c in RyR2R4496C<sup>+/-</sup> knock-in mice leads to altered intracellular Ca<sup>2+</sup> handling and increased mortality', *Journal of the American College of Cardiology*. Elsevier Inc., 57(4), pp. 469–479. doi: 10.1016/j.jacc.2010.08.639.

Echt, D. S. (1991) 'The New England Journal of Medicine Downloaded from nejm.org by EVA SALAS OLLE on September 29, 2015. For personal use only. No other uses without permission. Copyright © 1991 Massachusetts Medical Society. All rights reserved.', *N Engl J Med*, 1(325), pp. 293–302. doi: 10.1186/1476-069X-12-14.

Efremov, R. G. *et al.* (2015) 'Architecture and conformational switch mechanism of the ryanodine receptor', *Nature*. Nature Publishing Group, 517(7532), pp. 39–43. doi: 10.1038/nature13916.

Eisner, D. A. *et al.* (2017) 'Calcium and Excitation-Contraction Coupling in the Heart', *Circulation Research*, pp. 181–195. doi: 10.1161/CIRCRESAHA.117.310230.

Estes, N. A. 3rd *et al.* (1997) 'Electrical alternans during rest and exercise as predictors of vulnerability to ventricular arrhythmias.', *The American journal of cardiology*. United States, 80(10), pp. 1314–1318. doi: 10.1016/s0002-9149(97)00694-2.

Faggioni, M., Kryshnal, D. O. and Knollmann, B. C. (2012) 'Calsequestrin mutations and catecholaminergic polymorphic ventricular tachycardia', in *Pediatric Cardiology*, pp. 959–967. doi: 10.1007/s00246-012-0256-1.

Fatima, A. *et al.* (2011) 'In vitro modeling of ryanodine receptor 2 dysfunction using human induced pluripotent stem cells', *Cellular Physiology and Biochemistry*, 28(4), pp. 579–592. doi: 10.1159/000335753.

- Fernández-Velasco, M. *et al.* (2009a) 'Increased Ca<sup>2+</sup> sensitivity of the ryanodine receptor mutant RyR2R4496C underlies catecholaminergic polymorphic ventricular tachycardia', *Circulation Research*, 104(2), pp. 201–209. doi: 10.1161/CIRCRESAHA.108.177493.
- Fernández-Velasco, M. *et al.* (2009b) 'Increased Ca<sup>2+</sup> sensitivity of the ryanodine receptor mutant RyR2R4496C underlies catecholaminergic polymorphic ventricular tachycardia', *Circulation Research*, 104(2), pp. 201–209. doi: 10.1161/CIRCRESAHA.108.177493.
- Fernández-Velasco, M. *et al.* (2009c) 'Increased Ca<sup>2+</sup> sensitivity of the ryanodine receptor mutant RyR2R4496C underlies catecholaminergic polymorphic ventricular tachycardia', *Circulation Research*, 104(2), pp. 201–209. doi: 10.1161/CIRCRESAHA.108.177493.
- Ferrantini, C. *et al.* (2016) 'R4496C RyR2 mutation impairs atrial and ventricular contractility', *Journal of General Physiology*, 147(1), pp. 39–52. doi: 10.1085/jgp.201511450.
- Fink, K. *et al.* (2002) 'Inhibition of neuronal Ca<sup>2+</sup> influx by gabapentin and pregabalin in the human neocortex', *Neuropharmacology*, 42(2), pp. 229–236. doi: 10.1016/S0028-3908(01)00172-1.
- Friedberg, F. and Rhoads, A. R. (2001) 'Evolutionary aspects of calmodulin', *IUBMB Life*, 51(4), pp. 215–221. doi: 10.1080/152165401753311753.
- Fukuda, M. *et al.* (2014) 'Enhanced binding of calmodulin to RyR2 corrects arrhythmogenic channel disorder in CPVT-associated myocytes', *Biochemical and Biophysical Research Communications*. Elsevier Inc., 448(1), pp. 1–7. doi: 10.1016/j.bbrc.2014.03.152.
- Furuichi, T. *et al.* (1994) 'Multiple types of ryanodine receptor/Ca<sup>2+</sup> release channels are differentially expressed in rabbit brain.', *The Journal of neuroscience : the official journal of the Society for Neuroscience*. United States, 14(8), pp. 4794–4805.
- Garcia, M. I. and Boehning, D. (2017) 'Cardiac inositol 1,4,5-trisphosphate receptors', *Biochimica et Biophysica Acta - Molecular Cell Research*. Elsevier B.V., 1864(6), pp. 907–914. doi: 10.1016/j.bbamcr.2016.11.017.
- Gellen, B. *et al.* (2008) 'Conditional FKBP12.6 overexpression in mouse cardiac myocytes prevents triggered ventricular tachycardia through specific alterations in excitation-contraction coupling', *Circulation*, 117(14), pp. 1778–1786. doi: 10.1161/CIRCULATIONAHA.107.731893.
- George, C. H. *et al.* (2007) 'Ryanodine receptors and ventricular arrhythmias: Emerging trends in mutations, mechanisms and therapies', *Journal of Molecular and Cellular Cardiology*, pp. 34–50. doi: 10.1016/j.yjmcc.2006.08.115.
- George, C. H., Higgs, G. V. and Lai, F. A. (2003) 'Ryanodine receptor mutations associated with stress-induced ventricular tachycardia mediate increased calcium release in stimulated cardiomyocytes', *Circulation Research*, 93(6), pp. 531–540. doi: 10.1161/01.RES.0000091335.07574.86.
- des Georges, A. *et al.* (2016) 'Structural Basis for Gating and Activation of RyR1', *Cell*, 167(1), pp. 145–157.e17. doi: 10.1016/j.cell.2016.08.075.

- La Gerche, A. *et al.* (2015) 'Exercise-induced right ventricular dysfunction is associated with ventricular arrhythmias in endurance athletes', *European Heart Journal*, 36(30), pp. 1998–2010. doi: 10.1093/eurheartj/ehv202.
- Giannini, G. *et al.* (1995) 'The ryanodine receptor/calcium channel genes are widely and differentially expressed in murine brain and peripheral tissues.', *The Journal of cell biology*. United States, 128(5), pp. 893–904. doi: 10.1083/jcb.128.5.893.
- Goddard, C. A. *et al.* (2008) 'Physiological consequences of the P2328S mutation in the ryanodine receptor (RyR2) gene in genetically modified murine hearts', *Acta Physiologica*, 194(2), pp. 123–140. doi: 10.1111/j.1748-1716.2008.01865.x.
- Gomez-Hurtado, N. *et al.* (2016) 'Novel CPVT-Associated Calmodulin Mutation in CALM3 (CALM3-A103V) Activates Arrhythmogenic Ca Waves and Sparks', *Circulation: Arrhythmia and Electrophysiology*, 9(8), pp. 1–10. doi: 10.1161/CIRCEP.116.004161.
- Gómez, A. M. *et al.* (2004) 'FKBP12.6 overexpression decreases Ca<sup>2+</sup> spark amplitude but enhances [Ca<sup>2+</sup>]<sub>i</sub> transient in rat cardiac myocytes', *American Journal of Physiology - Heart and Circulatory Physiology*, 287(5 56-5), pp. 1987–1993. doi: 10.1152/ajpheart.00409.2004.
- Gómez, A. M. (2012) 'Paradoxical effect of increased diastolic Ca<sup>2+</sup> release and decreased sinoatrial node activity in a mouse model of catecholaminergic polymorphic ventricular tachycardia', *Circulation*, 126(4), pp. 392–401. doi: 10.1161/CIRCULATIONAHA.111.075382.
- Gong, D. *et al.* (2019) 'Modulation of cardiac ryanodine receptor 2 by calmodulin', *Nature*. Springer US. doi: 10.1038/s41586-019-1377-y.
- Graham, F. L. *et al.* (1977) 'Characteristics of a human cell line transformed by DNA from human adenovirus type 5.', *The Journal of general virology*. England, 36(1), pp. 59–74. doi: 10.1099/0022-1317-36-1-59.
- Graham, J. and Gerard, R. W. (1946) 'Membrane potentials and excitation of impaled single muscle fibers', *Journal of Cellular and Comparative Physiology*, 28(1), pp. 99–117. doi: 10.1002/jcp.1030280106.
- Guasch, E. and Mont, L. (2017) 'Diagnosis, pathophysiology, and management of exercise-induced arrhythmias', *Nature Reviews Cardiology*. Nature Publishing Group, 14(2), pp. 88–101. doi: 10.1038/nrcardio.2016.173.
- Guo, T. *et al.* (2006) 'Ca<sup>2+</sup>/calmodulin-dependent protein kinase II phosphorylation of ryanodine receptor does affect calcium sparks in mouse ventricular myocytes', *Circulation Research*, 99(4), pp. 398–406. doi: 10.1161/01.RES.0000236756.06252.13.
- Guo, T. *et al.* (2010) 'Kinetics of FKBP12.6 binding to ryanodine receptors in permeabilized cardiac myocytes and effects on Ca sparks', *Circulation Research*, 106(11), pp. 1743–1752. doi: 10.1161/CIRCRESAHA.110.219816.
- Györke, I. *et al.* (2004) 'The Role of Calsequestrin, Triadin, and Junctin Conferring Cardiac Ryanodine Receptor Responsiveness to Luminal Calcium', *Biophysical Journal*, 86(4), pp. 2121–2128. doi: 10.1016/S0006-3495(04)74271-X.

Györke, S. and Terentyev, D. (2008) 'Modulation of ryanodine receptor by luminal calcium and accessory proteins in health and cardiac disease', *Cardiovascular Research*, pp. 245–255. doi: 10.1093/cvr/cvm038.

Harmon, K. G. *et al.* (2015) 'Incidence, cause, and comparative frequency of sudden cardiac death in national collegiate athletic association athletes a decade in review', *Circulation*, 132(1), pp. 10–19. doi: 10.1161/CIRCULATIONAHA.115.015431.

Haugaa, K. H. *et al.* (2010) 'High prevalence of exercise-induced arrhythmias in catecholaminergic polymorphic ventricular tachycardia mutation-positive family members diagnosed by cascade genetic screening', *Europace*, 12(3), pp. 417–423. doi: 10.1093/europace/eup448.

Hauswirth, O., Noble, D. and Tsien, R. W. (1969) 'The mechanism of oscillatory activity at low membrane potentials in cardiac Purkinje fibres.', *The Journal of physiology*. England, 200(1), pp. 255–265. doi: 10.1113/jphysiol.1969.sp008691.

Hayashi, Meiso *et al.* (2009) 'Incidence and risk factors of arrhythmic events in catecholaminergic polymorphic ventricular tachycardia', *Circulation*, 119(18), pp. 2426–2434. doi: 10.1161/CIRCULATIONAHA.108.829267.

Herm, J. *et al.* (2017) 'Frequency of exercise-induced ST-T-segment deviations and cardiac arrhythmias in recreational endurance athletes during a marathon race: Results of the prospective observational Berlin Beat of Running study', *BMJ Open*, 7(8). doi: 10.1136/bmjopen-2016-015798.

Herron, T. J. *et al.* (2010) 'Purkinje cell calcium dysregulation is the cellular mechanism that underlies catecholaminergic polymorphic ventricular tachycardia', *Heart Rhythm*, 7(8), pp. 1122–1128. doi: 10.1016/j.hrthm.2010.06.010.

Ho, J. M.-W. *et al.* (2017) 'Pregabalin and heart failure: A population-based study', *Pharmacoepidemiology and Drug Safety*, (April), pp. 1–6. doi: 10.1002/pds.4239.

Ho, J. M. *et al.* (2013) 'Risk of heart failure and edema associated with the use of pregabalin: a systematic review', *Systematic Reviews*, 2(1), p. 25. doi: 10.1186/2046-4053-2-25.

Hoekstra, M. *et al.* (2012) 'Induced pluripotent stem cell derived cardiomyocytes as models for cardiac arrhythmias', *Frontiers in Physiology*, 3 AUG(August), pp. 1–14. doi: 10.3389/fphys.2012.00346.

Holland, J. and Brown, R. (2017) 'Neonatal venlafaxine discontinuation syndrome: A mini-review', *European Journal of Paediatric Neurology*. Elsevier Ltd, 21(2), pp. 264–268. doi: 10.1016/j.ejpn.2016.11.003.

Hosseini, S. M. *et al.* (2018) 'Reappraisal of reported genes for sudden arrhythmic death: Evidence-based evaluation of gene validity for brugada syndrome', *Circulation*, 138(12), pp. 1195–1205. doi: 10.1161/CIRCULATIONAHA.118.035070.

Ikemoto, N. and Yamamoto, T. (2002) 'Regulation of calcium release by interdomain interaction within ryanodine receptors.', *Frontiers in bioscience : a journal and virtual library*. United States, 7, pp. d671-83.

Itzhaki, I. *et al.* (2012a) 'Modeling of catecholaminergic polymorphic ventricular tachycardia with patient-specific human-induced pluripotent stem cells', *Journal of the American College of Cardiology*. Elsevier Inc., 60(11), pp. 990–1000. doi: 10.1016/j.jacc.2012.02.066.

Itzhaki, I. *et al.* (2012b) 'Modeling of catecholaminergic polymorphic ventricular tachycardia with patient-specific human-induced pluripotent stem cells', *Journal of the American College of Cardiology*. Elsevier Inc., 60(11), pp. 990–1000. doi: 10.1016/j.jacc.2012.02.066.

Janse, M. J. and Rosen, M. R. (2006) 'History of arrhythmias.', *Handbook of experimental pharmacology*. Germany, (171), pp. 1–39.

January, C. T. and Moscucci, A. (1992) 'Cellular mechanisms of early afterdepolarizations.', *Annals of the New York Academy of Sciences*. United States, 644, pp. 23–32. doi: 10.1111/j.1749-6632.1992.tb30999.x.

January, C. T. and Riddle, J. M. (1989) 'Early afterdepolarizations: mechanism of induction and block. A role for L-type Ca<sup>2+</sup> current.', *Circulation research*. United States, 64(5), pp. 977–990. doi: 10.1161/01.res.64.5.977.

Jiang, D. *et al.* (2002) 'Enhanced basal activity of a cardiac Ca<sup>2+</sup> release channel (ryanodine receptor) mutant associated with ventricular tachycardia and sudden death', *Circulation Research*, 91(3), pp. 218–225. doi: 10.1161/01.RES.0000028455.36940.5E.

Jiang, D. *et al.* (2004) 'RyR2 mutations linked to ventricular tachycardia and sudden death reduce the threshold for store-overload-induced Ca<sup>2+</sup> release (SOICR).', *Proceedings of the National Academy of Sciences of the United States of America*, 101(35), pp. 13062–7. doi: 10.1073/pnas.0402388101.

Jiang, D. *et al.* (2005) 'Enhanced store overload-induced Ca<sup>2+</sup> release and channel sensitivity to luminal Ca<sup>2+</sup> activation are common defects of RyR2 mutations linked to ventricular tachycardia and sudden death', *Circulation Research*, 97(11), pp. 1173–1181. doi: 10.1161/01.RES.0000192146.85173.4b.

Jiang, D. *et al.* (2007) '(RyR2-A4860G) Loss of luminal Ca<sup>2+</sup> activation in the cardiac ryanodine receptor is associated with ventricular fibrillation and sudden death.', *Proceedings of the National Academy of Sciences of the United States of America*, 104(46), pp. 18309–14. doi: 10.1073/pnas.0706573104.

Jiménez-Jáimez, J. *et al.* (2016) 'Calmodulin 2 mutation N98S is associated with unexplained cardiac arrest in infants due to low clinical penetrance electrical disorders', *PLoS ONE*, 11(4), pp. 1–10. doi: 10.1371/journal.pone.0153851.

Jones, P. P. *et al.* (2008) 'Endoplasmic reticulum Ca<sup>2+</sup> measurements reveal that the cardiac ryanodine receptor mutations linked to cardiac arrhythmia and sudden death alter the threshold for store-overload-induced Ca<sup>2+</sup> release', *Biochemical Journal*, 412(1), pp. 171–178. doi: 10.1042/BJ20071287.

Juang, J. M. and Huang, S. K. S. (2004) 'Brugada Syndrome - An Under-Recognized Electrical Disease in Patients with Sudden Cardiac Death', *Cardiology*, 101(4), pp. 157–169. doi: 10.1159/000076693.

Juang, J. M. J. and Horie, M. (2016) 'Genetics of Brugada syndrome', *Journal of Arrhythmia*. Nature Publishing Group, 32(5), pp. 418–425. doi: 10.1016/j.joa.2016.07.012.

- Jung, C. B. *et al.* (2012a) ‘Dantrolene rescues arrhythmogenic RYR2 defect in a patient-specific stem cell model of catecholaminergic polymorphic ventricular tachycardia’, *EMBO Molecular Medicine*, 4(3), pp. 180–191. doi: 10.1002/emmm.201100194.
- Jung, C. B. *et al.* (2012b) ‘Dantrolene rescues arrhythmogenic RYR2 defect in a patient-specific stem cell model of catecholaminergic polymorphic ventricular tachycardia’, *EMBO Molecular Medicine*, 4(3), pp. 180–191. doi: 10.1002/emmm.201100194.
- Kang, G. *et al.* (2010) ‘Purkinje cells from RyR2 mutant mice are highly arrhythmogenic but responsive to targeted therapy’, *Circulation Research*, 107(4), pp. 512–519. doi: 10.1161/CIRCRESAHA.110.221481.
- Kannankeril, P. J. *et al.* (2006) ‘Mice with the R176Q cardiac ryanodine receptor mutation exhibit catecholamine-induced ventricular tachycardia and cardiomyopathy’, *Proceedings of the National Academy of Sciences of the United States of America*, 103(32), pp. 12179–12184. doi: 10.1073/pnas.0600268103.
- Karakikes, I. *et al.* (2015) ‘Human Induced Pluripotent Stem Cell-Derived Cardiomyocytes: Insights into Molecular, Cellular, and Functional Phenotypes’, *Circulation Research*, 117(1), pp. 80–88. doi: 10.1161/CIRCRESAHA.117.305365.
- Kashimura, T. *et al.* (2010) ‘In the RyR2R4496C mouse model of CPVT,  $\beta$ -adrenergic stimulation induces Ca waves by increasing SR Ca content and not by decreasing the threshold for Ca Waves’, *Circulation Research*, 107(12), pp. 1483–1489. doi: 10.1161/CIRCRESAHA.110.227744.
- Kass, R. S. and Moss, A. J. (2003) ‘Long QT syndrome: Novel insights into the mechanisms of cardiac arrhythmias’, *Journal of Clinical Investigation*, 112(6), pp. 810–815. doi: 10.1172/JCI19844.
- Kazmierczak, J., Peregud-Pogorzelska, M. and Rzeuski, R. (2007) ‘QT Interval prolongation and torsades de pointes due to a coadministration of ciprofloxacin and azimilide in a patient with implantable cardioverter-defibrillator.’, *Pacing and clinical electrophysiology : PACE*. United States, 30(8), pp. 1043–1046. doi: 10.1111/j.1540-8159.2007.00809.x.
- Keating, M. T. and Sanguinetti, M. C. (2001) ‘Molecular and cellular mechanisms of cardiac arrhythmias’, *Cell*, 104(4), pp. 569–580. doi: 10.1016/S0092-8674(01)00243-4.
- Kehat, I. *et al.* (2001) ‘Human embryonic stem cells can differentiate into myocytes with structural and functional properties of cardiomyocytes.’, *The Journal of clinical investigation*. United States, 108(3), pp. 407–414. doi: 10.1172/JCI12131.
- Khalifa, M., Daleau, P. and Turgeon, J. (1999) ‘Mechanism of sodium channel block by venlafaxine in guinea pig ventricular myocytes’, *Journal of Pharmacology and Experimental Therapeutics*, 291(1), pp. 280–284.
- Kimlicka, L., Lau, K., *et al.* (2013) ‘Disease mutations in the ryanodine receptor N-terminal region couple to a mobile intersubunit interface’, *Nature Communications*. Nature Publishing Group, 4, pp. 1–10. doi: 10.1038/ncomms2501.
- Kimlicka, L., Tung, C.-C., *et al.* (2013) ‘The Cardiac Ryanodine Receptor N-Terminal Region Contains an Anion Binding Site that Is Targeted by Disease Mutations’, *Structure*. Elsevier Ltd, 21(8), pp. 1440–1449. doi: 10.1016/j.str.2013.06.012.

- King, J. H. *et al.* (2013) 'Atrial arrhythmia, triggering events and conduction abnormalities in isolated murine RyR2-P2328S hearts', *Acta Physiologica*, 207(2), pp. 308–323. doi: 10.1111/apha.12006.
- King, James H. *et al.* (2013) 'Loss of Nav1.5 expression and function in murine atria containing the RyR2-P2328S gain-of-function mutation', *Cardiovascular Research*, 99(4), pp. 751–759. doi: 10.1093/cvr/cvt141.
- Knollmann, B. C. *et al.* (2006) 'Casq2 deletion causes sarcoplasmic reticulum volume increase, premature Ca<sup>2+</sup> release, and catecholaminergic polymorphic ventricular tachycardia', *Journal of Clinical Investigation*, 116(9), pp. 2510–2520. doi: 10.1172/JCI29128.
- Kobayashi, S. *et al.* (2010) 'Dantrolene, a therapeutic agent for malignant hyperthermia, inhibits catecholaminergic polymorphic ventricular tachycardia in a RyR2(R2474S/+) knock-in mouse model.', *Circulation journal : official journal of the Japanese Circulation Society*, 74(12), pp. 2579–2584. doi: 10.1253/circj.CJ-10-0680.
- Kofron, C. M. *et al.* (2019) 'Signaling and Stress Response G<sub>q</sub>-activated fibroblasts induce cardiomyocyte action potential prolongation and automaticity in a three-dimensional microtissue environment', pp. 810–827. doi: 10.1152/ajpheart.00181.2017.
- Kujala, K. *et al.* (2012) 'Cell Model of Catecholaminergic Polymorphic Ventricular Tachycardia Reveals Early and Delayed Afterdepolarizations', *PLoS ONE*, 7(9), pp. 1–10. doi: 10.1371/journal.pone.0044660.
- Lahat, H., Pras, E. and Eldar, M. (2001) 'A missense mutation in CASQ2 is associated with autosomal recessive catecholamine-induced polymorphic ventricular tachycardia in Bedouin families from Israel', in *Annals of Medicine*, pp. 87–91. doi: 10.1080/17431380410032517.
- Laitinen, Päivi J. *et al.* (2001) 'Mutations of the cardiac ryanodine receptor (RyR2) gene in familial polymorphic ventricular tachycardia', *Circulation*, 103(4), pp. 485–490. doi: 10.1161/01.CIR.103.4.485.
- Laitinen, Päivi J *et al.* (2001) 'Mutations of the cardiac ryanodine receptor (RyR2) gene in familial polymorphic ventricular tachycardia', *Circulation*, 103(4), pp. 485–490. doi: 10.1161/01.CIR.103.4.485.
- Landstrom, A. P., Dobrev, D. and Wehrens, X. H. T. (2017) 'Calcium Signaling and Cardiac Arrhythmias', *Circulation Research*, 120(12), pp. 1969–1993. doi: 10.1161/CIRCRESAHA.117.310083.
- Lanner, J. T. *et al.* (2010a) 'Calcium Release', *Cold Spring Harbor Perspectives in Biology*, 2, pp. 1–21.
- Lanner, J. T. *et al.* (2010b) 'Ryanodine Receptors: Structure, Expression, Molecular Details, and Function in Calcium Release', *Cold Spring Harbor Perspectives in Biology*, 2, pp. 1–21.
- Laurent, L. *et al.* (2016) 'In utero exposure to venlafaxine, a serotonin–norepinephrine reuptake inhibitor, increases cardiac anomalies and alters placental and heart serotonin signaling in the rat', *Birth Defects Research Part A - Clinical and Molecular Teratology*, 106(12), pp. 1044–1055. doi: 10.1002/bdra.23537.

- Lazzarini, E. *et al.* (2015) 'The ARVD/C genetic variants database: 2014 update.', *Human mutation*. United States, 36(4), pp. 403–410. doi: 10.1002/humu.22765.
- Leenhardt, A. *et al.* (1995) 'Catecholaminergic polymorphic ventricular tachycardia in children. A 7-year follow-up of 21 patients.', *Circulation*. United States, 91(5), pp. 1512–1519. doi: 10.1161/01.cir.91.5.1512.
- Lehnart, S. E. *et al.* (2004) 'Sudden death in familial polymorphic ventricular tachycardia associated with calcium release channel (ryanodine receptor) leak.', *Circulation*, 109(25), pp. 3208–3214. doi: 10.1161/01.CIR.0000132472.98675.EC.
- Lehnart, S. E. *et al.* (2008) 'Leaky Ca<sup>2+</sup> release channel/ryanodine receptor 2 causes seizures and sudden cardiac death in mice', *The Journal of clinical investigation*, 118(6), pp. 2230–2245. doi: 10.1172/JCI35346DS1.
- Li, L. *et al.* (1998) 'Cardiac myocyte calcium transport in phospholamban knockout mouse: relaxation and endogenous CaMKII effects.', *The American journal of physiology*. United States, 274(4), pp. H1335-47. doi: 10.1152/ajpheart.1998.274.4.H1335.
- Li, Y. *et al.* (2002) 'Protein kinase A phosphorylation of the ryanodine receptor does not affect calcium sparks in mouse ventricular myocytes', *Circulation Research*, 90(3), pp. 309–316. doi: 10.1161/hh0302.105660.
- Liu, N., Colombi, B., Memmi, M., Zissimopoulos, S., Rizzi, N., Negri, S., Imbriani, M., Napolitano, C., Lai, F Anthony, *et al.* (2006) 'Arrhythmogenesis in catecholaminergic polymorphic ventricular tachycardia: Insights from a RyR2 R4496C knock-in mouse model', *Circulation Research*, 99(3), pp. 292–298. doi: 10.1161/01.RES.0000235869.50747.e1.
- Liu, N., Colombi, B., Memmi, M., Zissimopoulos, S., Rizzi, N., Negri, S., Imbriani, M., Napolitano, C., Lai, F. Anthony, *et al.* (2006) 'Arrhythmogenesis in catecholaminergic polymorphic ventricular tachycardia: Insights from a RyR2 R4496C knock-in mouse model', *Circulation Research*, 99(3), pp. 292–298. doi: 10.1161/01.RES.0000235869.50747.e1.
- Liu, N. *et al.* (2011) 'Calmodulin kinase II inhibition prevents arrhythmias in RyR2R4496C<sup>+/-</sup> mice with catecholaminergic polymorphic ventricular tachycardia', *Journal of Molecular and Cellular Cardiology*. Elsevier Ltd, 50(1), pp. 214–222. doi: 10.1016/j.yjmcc.2010.10.001.
- Liu, P. *et al.* (2007) 'Pharmacokinetic interaction between voriconazole and methadone at steady state in patients on methadone therapy.', *Antimicrobial agents and chemotherapy*. United States, 51(1), pp. 110–118. doi: 10.1128/AAC.00559-06.
- Liu, T. *et al.* (2014) 'Effect of the 2010 task force criteria on reclassification of cardiovascular magnetic resonance criteria for arrhythmogenic right ventricular cardiomyopathy.', *Journal of cardiovascular magnetic resonance : official journal of the Society for Cardiovascular Magnetic Resonance*. England, 16, p. 47. doi: 10.1186/1532-429X-16-47.
- Liu, Y. *et al.* (2013) 'The CPVT-associated RyR2 mutation G230C enhances store overload-induced Ca<sup>2+</sup> release and destabilizes the N-terminal domains.', *The Biochemical journal*, 454(1), pp. 123–31. doi: 10.1042/BJ20130594.

- Liu, Y. *et al.* (2017) ‘CPVT-associated cardiac ryanodine receptor mutation G357S with reduced penetrance impairs Ca<sup>2+</sup> release termination and diminishes protein expression’, *PLoS ONE*, 12(9). doi: 10.1371/journal.pone.0184177.
- Loaiza, R. *et al.* (2013) ‘Heterogeneity of ryanodine receptor dysfunction in a mouse model of catecholaminergic polymorphic ventricular tachycardia’, *Circulation Research*, 112(2), pp. 298–308. doi: 10.1161/CIRCRESAHA.112.274803.
- Lobo, P. A. *et al.* (2011) ‘The deletion of exon 3 in the cardiac ryanodine receptor is rescued by  $\beta$  strand switching’, *Structure*. Elsevier Ltd, 19(6), pp. 790–798. doi: 10.1016/j.str.2011.03.016.
- Lobo, P. A. and Van Petegem, F. (2009) ‘Crystal Structures of the N-Terminal Domains of Cardiac and Skeletal Muscle Ryanodine Receptors: Insights into Disease Mutations’, *Structure*. Elsevier Ltd, 17(11), pp. 1505–1514. doi: 10.1016/j.str.2009.08.016.
- Lowri Thomas, N., George, C. H. and Anthony Lai, F. (2004) ‘Functional heterogeneity of ryanodine receptor mutations associated with sudden cardiac death’, *Cardiovascular Research*, 64(1), pp. 52–60. doi: 10.1016/j.cardiores.2004.06.009.
- Luo, C. H. and Rudy, Y. (1994) ‘A dynamic model of the cardiac ventricular action potential. II. Afterdepolarizations, triggered activity, and potentiation.’, *Circulation research*. United States, 74(6), pp. 1097–1113. doi: 10.1161/01.res.74.6.1097.
- Ma, J. *et al.* (2011) ‘High purity human-induced pluripotent stem cell-derived cardiomyocytes: electrophysiological properties of action potentials and ionic currents.’, *American journal of physiology. Heart and circulatory physiology*. United States, 301(5), pp. H2006-17. doi: 10.1152/ajpheart.00694.2011.
- Mackenzie, L. *et al.* (2002) ‘The role of inositol 1,4,5,-trisphosphate receptors in Ca<sup>2+</sup> signalling and the generation of arrhythmias in rat atrial myocytes’, *Journal of Physiology*, 541(2), pp. 395–409. doi: 10.1113/jphysiol.2001.013411.
- MacLennan, D. H. and Zvaritch, E. (2011) ‘Mechanistic models for muscle diseases and disorders originating in the sarcoplasmic reticulum’, *Biochimica et Biophysica Acta - Molecular Cell Research*. Elsevier B.V., pp. 948–964. doi: 10.1016/j.bbamcr.2010.11.009.
- Maizels, L. *et al.* (2017) ‘Patient-Specific Drug Screening Using a Human Induced Pluripotent Stem Cell Model of Catecholaminergic Polymorphic Ventricular Tachycardia Type 2’, *Circulation: Arrhythmia and Electrophysiology*, 10(6). doi: 10.1161/CIRCEP.116.004725.
- Makita, N. *et al.* (2014) ‘Novel calmodulin mutations associated with congenital arrhythmia susceptibility’, *Circulation: Cardiovascular Genetics*, 7(4), pp. 466–474. doi: 10.1161/CIRCGENETICS.113.000459.
- Mangoni, M. E. and Nargeot, J. (2008) ‘Genesis and regulation of the heart automaticity’, *Physiological Reviews*, 88(3), pp. 919–982. doi: 10.1152/physrev.00018.2007.
- Manotheepan, R. *et al.* (2016) ‘Exercise training prevents ventricular tachycardia in CPVT1 due to reduced CaMKII-dependent arrhythmogenic Ca<sup>2+</sup> release’, *Cardiovascular Research*, 111(3), pp. 295–306. doi: 10.1093/cvr/cvw095.

- Marcus, F. I. *et al.* (2010) 'Diagnosis of arrhythmogenic right ventricular cardiomyopathy/dysplasia: proposed modification of the task force criteria.', *Circulation*, United States, 121(13), pp. 1533–1541. doi: 10.1161/CIRCULATIONAHA.108.840827.
- Marijon, E. *et al.* (2011) 'Sports-related sudden death in the general population', *Circulation*, 124(6), pp. 672–681. doi: 10.1161/CIRCULATIONAHA.110.008979.
- Marjamaa, A. *et al.* (2011) 'Ryanodine receptor (RyR2) mutations in sudden cardiac death: Studies in extended pedigrees and phenotypic characterization in vitro', *International Journal of Cardiology*. Elsevier Ireland Ltd, 147(2), pp. 246–252. doi: 10.1016/j.ijcard.2009.08.041.
- Marty, I. *et al.* (2009) 'Triadin: What possible function 20 years later?', in *Journal of Physiology*, pp. 3117–3121. doi: 10.1113/jphysiol.2009.171892.
- Marx, S. O. *et al.* (2000) 'PKA phosphorylation dissociates FKBP12.6 from the calcium release channel (ryanodine receptor): Defective regulation in failing hearts', *Cell*, 101(4), pp. 365–376. doi: 10.1016/S0092-8674(00)80847-8.
- Mattei MG, Giannini G, Moscatelli F, S. V. (1994) 'Chromosomal localization of murine ryanodine receptor genes RYR1, RYR2, and RYR3 by in situ hybridization.', p. Genomics1994.
- McPherson, P. S. and Campbell, K. P. (1993) 'Characterization of the major brain form of the ryanodine receptor/Ca<sup>2+</sup> release channel', *Journal of Biological Chemistry*, 268(26), pp. 19785–19790.
- Medeiros-Domingo, A. *et al.* (2009) 'The RYR2-Encoded Ryanodine Receptor/Calcium Release Channel in Patients Diagnosed Previously With Either Catecholaminergic Polymorphic Ventricular Tachycardia or Genotype Negative, Exercise-Induced Long QT Syndrome. A Comprehensive Open Reading Frame Muta', *Journal of the American College of Cardiology*. Elsevier Inc., 54(22), pp. 2065–2074. doi: 10.1016/j.jacc.2009.08.022.
- Meissner, G. (2017) 'The structural basis of ryanodine receptor ion channel function', *Journal of General Physiology*, 149(12), pp. 1065–1089. doi: 10.1085/jgp.201711878.
- Meli, A. C. *et al.* (2011) 'A novel ryanodine receptor mutation linked to sudden death increases sensitivity to cytosolic calcium', *Circulation Research*, 109(3), pp. 281–290. doi: 10.1161/CIRCRESAHA.111.244970.
- Mesirca, P., Torrente, A. G. and Mangoni, M. E. (2015) 'Functional role of voltage gated Ca<sup>2+</sup> channels in heart automaticity', *Frontiers in Physiology*, 6(FEB), p. 19. doi: 10.3389/fphys.2015.00019.
- Meyer, L. *et al.* (2012) 'Incidence, causes, and survival trends from cardiovascular-related sudden cardiac arrest in children and young adults 0 to 35 years of age: A 30-year review', *Circulation*, 126(11), pp. 1363–1372. doi: 10.1161/CIRCULATIONAHA.111.076810.
- Mezu, U. L. *et al.* (2012) 'Accelerated junctional rhythm and nonalternans repolarization lability precede ventricular tachycardia in Casq2<sup>-/-</sup> mice', *Journal of Cardiovascular Electrophysiology*, 23(12), pp. 1355–1363. doi: 10.1111/j.1540-8167.2012.02406.x.

- Mico, J.-A. and Prieto, R. (2012) 'Elucidating the mechanism of action of pregabalin: alpha(2)delta as a therapeutic target in anxiety.', *CNS drugs*. New Zealand, 26(8), pp. 637–648. doi: 10.2165/11634510-000000000-00000.
- Milting, H. *et al.* (2006) 'Composite polymorphisms in the ryanodine receptor 2 gene associated with arrhythmogenic right ventricular cardiomyopathy', *Cardiovascular Research*, 71(3), pp. 496–505. doi: 10.1016/j.cardiores.2006.04.004.
- Mines, G. (1914) 'On circulating excitations in heart muscle and their possible relation to tachycardia and fibrillation', *Trans R Soc Can*, 8 (43-52), p. 1914.
- Miragoli, M. and Rohr, S. (2007) 'Myofibroblasts Induce Ectopic Activity in Cardiac Tissue', pp. 755–758. doi: 10.1161/CIRCRESAHA.107.160549.
- Miyazaki, T. *et al.* (1996) 'Autonomic and antiarrhythmic drug modulation of ST segment elevation in patients with Brugada syndrome', *Journal of the American College of Cardiology*, 27(5), pp. 1061–1070. doi: 10.1016/0735-1097(95)00613-3.
- Mohamed, U. *et al.* (2006) 'Sudden cardiac death despite an implantable cardioverter-defibrillator in a young female with catecholaminergic ventricular tachycardia.', *Heart rhythm*. United States, 3(12), pp. 1486–1489. doi: 10.1016/j.hrthm.2006.08.018.
- Moncayo-Arlandi, J. and Brugada, R. (2017) 'Unmasking the molecular link between arrhythmogenic cardiomyopathy and Brugada syndrome', *Nature Reviews Cardiology*. Nature Publishing Group, 14(12), pp. 744–756. doi: 10.1038/nrcardio.2017.103.
- Morita, N. *et al.* (2011) 'Suppression of re-entrant and multifocal ventricular fibrillation by the late sodium current blocker ranolazine.', *Journal of the American College of Cardiology*. United States, 57(3), pp. 366–375. doi: 10.1016/j.jacc.2010.07.045.
- Mummery, C. L. *et al.* (2012) 'Differentiation of human embryonic stem cells and induced pluripotent stem cells to cardiomyocytes: A methods overview', *Circulation Research*, pp. 344–358. doi: 10.1161/CIRCRESAHA.110.227512.
- Murphy, N. *et al.* (2007) 'Decompensation of Chronic Heart Failure Associated With Pregabalin in Patients With Neuropathic Pain', *Journal of Cardiac Failure*, 13(3), pp. 227–229. doi: 10.1016/j.cardfail.2006.11.006.
- Muth, E. A. *et al.* (1986) 'Antidepressant biochemical profile of the novel bicyclic compound Wy-45,030, an ethyl cyclohexanol derivative', *Biochemical Pharmacology*, 35(24), pp. 4493–4497. doi: 10.1016/0006-2952(86)90769-0.
- Nakai, J. *et al.* (1990) 'Primary structure and functional expression from cDN A of the cardiac ryanodine receptor/calcium release channel', *FEBS Letters*, 271(1–2), pp. 169–177. doi: 10.1016/0014-5793(90)80399-4.
- Narayan, S. M. *et al.* (2007) 'T-Wave Alternans , Restitution of Human Action Potential Duration , and Outcome', 50(25). doi: 10.1016/j.jacc.2007.10.011.
- Narazaki, G. *et al.* (2008) 'Directed and systematic differentiation of cardiovascular cells from mouse induced pluripotent stem cells', *Circulation*, 118(5), pp. 498–506. doi: 10.1161/CIRCULATIONAHA.108.769562.

- Ning, F. *et al.* (2016) ‘The RyR2-P2328S mutation downregulates Nav1.5 producing arrhythmic substrate in murine ventricles’, *Pflugers Archiv European Journal of Physiology*, 468(4), pp. 655–665. doi: 10.1007/s00424-015-1750-0.
- Novak, A. *et al.* (2015) ‘RyR420Q-Functional abnormalities in iPSC-derived cardiomyocytes generated from CPVT1 and CPVT2 patients carrying ryanodine or calsequestrin mutations’, *Journal of Cellular and Molecular Medicine*, 19(8), pp. 2006–2018. doi: 10.1111/jcmm.12581.
- Nuss, H. B. *et al.* (1999) ‘Cellular basis of ventricular arrhythmias and abnormal automaticity in heart failure’, *American Journal of Physiology - Heart and Circulatory Physiology*, 277(1 46-1).
- Nyegaard, M. *et al.* (2012) ‘Mutations in calmodulin cause ventricular tachycardia and sudden cardiac death’, *American Journal of Human Genetics*, 91(4), pp. 703–712. doi: 10.1016/j.ajhg.2012.08.015.
- O’Brien, J., Meissner, G. and Block, B. A. (1993) ‘The fastest contracting muscles of nonmammalian vertebrates express only one isoform of the ryanodine receptor’, *Biophysical Journal*. Elsevier, 65(6), pp. 2418–2427. doi: 10.1016/S0006-3495(93)81303-1.
- O’Neil, K. T. and DeGrado, W. F. (1990) ‘How calmodulin binds its targets: sequence independent recognition of amphiphilic alpha-helices.’, *Trends in biochemical sciences*. England, 15(2), pp. 59–64. doi: 10.1016/0968-0004(90)90177-d.
- Oda, T. *et al.* (2005) ‘Defective regulation of interdomain interactions within the ryanodine receptor plays a key role in the pathogenesis of heart failure’, *Circulation*, 111(25), pp. 3400–3410. doi: 10.1161/CIRCULATIONAHA.104.507921.
- Okudaira, N. *et al.* (2014) ‘Biochemical and Biophysical Research Communications A knock-in mouse model of N-terminal R420W mutation of cardiac ryanodine receptor exhibits arrhythmogenesis with abnormal calcium dynamics in cardiomyocytes’, *Biochemical and Biophysical Research Communications*. Elsevier Inc., 452(3), pp. 665–668. doi: 10.1016/j.bbrc.2014.08.132.
- Orini, M. *et al.* (2019) ‘Mechanistic insights from targeted molecular profiling of repolarization alternans in the intact human heart’, 114, pp. 981–989. doi: 10.1093/europace/euz007.
- Otsu, K. *et al.* (1990) ‘Molecular cloning of cDNA encoding the Ca<sup>2+</sup> release channel (ryanodine receptor) of rabbit cardiac muscle sarcoplasmic reticulum.’, *The Journal of biological chemistry*. United States, 265(23), pp. 13472–13483.
- Ottini, L. *et al.* (1996) ‘ $\alpha$  and  $\beta$  isoforms of ryanodine receptor from chicken skeletal muscle are the homologues of mammalian RyR1 and RyR3’, *Biochemical Journal*, 315(1), pp. 207–216. doi: 10.1042/bj3150207.
- Paavola, J. *et al.* (2016) ‘Slowed depolarization and irregular repolarization in catecholaminergic polymorphic ventricular tachycardia: A study from cellular Ca<sup>2+</sup> transients and action potentials to clinical monophasic action potentials and electrocardiography’, *Europace*, 18(10), pp. 1599–1607. doi: 10.1093/europace/euv380.

- Page, R. L. 2nd *et al.* (2008) ‘Possible heart failure exacerbation associated with pregabalin: case discussion and literature review.’, *Journal of cardiovascular medicine (Hagerstown, Md.)*. United States, 9(9), pp. 922–925. doi: 10.2459/JCM.0b013e3282fb7629.
- Paludan-Müller, C. *et al.* (2017) ‘Integration of 60,000 exomes and ACMG guidelines question the role of Catecholaminergic Polymorphic Ventricular Tachycardia-associated variants’, *Clinical Genetics*, 91(1), pp. 63–72. doi: 10.1111/cge.12847.
- Pancaroglu, R. and Van Petegem, F. (2018) ‘Calcium Channelopathies: Structural Insights into Disorders of the Muscle Excitation–Contraction Complex’, *Annual Review of Genetics*, 52(1), pp. 373–396. doi: 10.1146/annurev-genet-120417-031311.
- Park, S.-J. *et al.* (2019) ‘Insights Into the Pathogenesis of Catecholaminergic Polymorphic Ventricular Tachycardia From Engineered Human Heart Tissue’, *Circulation*, 140(5), pp. 390–404. doi: 10.1161/circulationaha.119.039711.
- Di Pasquale, E. *et al.* (2013) ‘CaMKII inhibition rectifies arrhythmic phenotype in a patient-specific model of catecholaminergic polymorphic ventricular tachycardia’, *Cell Death and Disease*. Nature Publishing Group, 4(10), pp. e843-11. doi: 10.1038/cddis.2013.369.
- Paul W. Burridge<sup>1, 2, 3</sup>, Elena Matsa<sup>1, 2, 3</sup>, Praveen Shukla<sup>1, 2, 3</sup>, Ziliang C. Lin<sup>4</sup>, Jared M. Churko<sup>1, 2, 3</sup>, Antje D. Ebert<sup>1, 2, 3</sup>, Feng Lan<sup>1, 2, 3</sup>, Sebastian Diecke<sup>1, 2, 3</sup>, Bruno Huber<sup>1, 2, 3</sup>, Nicholas M. Mordwinkin<sup>1, 2, 3</sup>, Jordan R. Plews<sup>1, 2, 3</sup>, Oscar, and J. C. W. (2014) ‘Chemically Defined and Small Molecule-Based Generation of Human Cardiomyocytes’, *Nat Methods*, 2(74), pp. 855–860. doi: 10.1126/scisignal.274pe36.Insulin.
- Peng, W. *et al.* (2016) ‘Structural basis for the gating mechanism of the type 2 ryanodine receptor RyR2’, *Science*, 354(6310). doi: 10.1126/science.aah5324.
- Penttinen, K. *et al.* (2015) ‘Antiarrhythmic effects of dantrolene in patients with catecholaminergic polymorphic ventricular tachycardia and replication of the responses using iPSC models’, *PLoS ONE*, 10(5). doi: 10.1371/journal.pone.0125366.
- Pereira, L. *et al.* (2007) ‘The cAMP binding protein Epac modulates Ca<sup>2+</sup> sparks by a Ca<sup>2+</sup>/calmodulin kinase signalling pathway in rat cardiac myocytes’, *Journal of Physiology*, 583(2), pp. 685–694. doi: 10.1113/jphysiol.2007.133066.
- Pereira, L. *et al.* (2013) ‘Epac2 mediates cardiac  $\beta$ 1-adrenergic-dependent sarcoplasmic reticulum Ca<sup>2+</sup> leak and arrhythmia’, *Circulation*, 127(8), pp. 913–922. doi: 10.1161/CIRCULATIONAHA.12.148619.
- Pereira, L. *et al.* (2017) ‘ $\beta$ -Adrenergic induced SR Ca<sup>2+</sup> + leak is mediated by an Epac-NOS pathway’, *Journal of Molecular and Cellular Cardiology*. Elsevier Ltd, 108, pp. 8–16. doi: 10.1016/j.yjmcc.2017.04.005.
- Perry, M. D. *et al.* (2016) ‘TECRL : connecting sequence to’, 8(12), pp. 1–2.
- Van Petegem, F. (2012) ‘Ryanodine receptors: Structure and function’, *Journal of Biological Chemistry*, 287(38), pp. 31624–31632. doi: 10.1074/jbc.R112.349068.
- Van Petegem, F., Chatelain, F. C. and Minor, D. L. J. (2005) ‘Insights into voltage-gated calcium channel regulation from the structure of the CaV1.2 IQ domain-Ca<sup>2+</sup>/calmodulin

- complex.’, *Nature structural & molecular biology*. United States, 12(12), pp. 1108–1115. doi: 10.1038/nsmb1027.
- Peters, S., Trummel, M. and Meyners, W. (2004) ‘Prevalence of right ventricular dysplasia-cardiomyopathy in a non-referral hospital.’, *International journal of cardiology*. Netherlands, 97(3), pp. 499–501. doi: 10.1016/j.ijcard.2003.10.037.
- Peterson, B. Z. *et al.* (1999) ‘Calmodulin is the Ca<sup>2+</sup> sensor for Ca<sup>2+</sup> -dependent inactivation of L-type calcium channels.’, *Neuron*. United States, 22(3), pp. 549–558. doi: 10.1016/s0896-6273(00)80709-6.
- Picht, E. *et al.* (2006) ‘Cardiac Alternans Do Not Rely on Diastolic Sarcoplasmic Reticulum Calcium Content Fluctuations’, pp. 740–748. doi: 10.1161/01.RES.0000244002.88813.91.
- Pizzale, S. *et al.* (2008) ‘Sudden death in a young man with catecholaminergic polymorphic ventricular tachycardia and paroxysmal atrial fibrillation.’, *Journal of cardiovascular electrophysiology*. United States, 19(12), pp. 1319–1321. doi: 10.1111/j.1540-8167.2008.01211.x.
- Pogwizd, S M *et al.* (2001) ‘Arrhythmogenesis and contractile dysfunction in heart failure: Roles of sodium-calcium exchange, inward rectifier potassium current, and residual beta-adrenergic responsiveness.’, *Circulation research*. United States, 88(11), pp. 1159–1167. doi: 10.1161/hh1101.091193.
- Pogwizd, Steven M *et al.* (2001) ‘Arrhythmogenesis and contractile dysfunction in heart failure: Roles of sodium-calcium exchange, inward rectifier potassium current, and residual  $\beta$ -adrenergic responsiveness’, *Circulation Research*, 88(11), pp. 1159–1167. doi: 10.1161/hh1101.091193.
- Pölönen, R. P., Swan, H. and Aalto-Setälä, K. (2019) ‘Mutation-specific differences in arrhythmias and drug responses in CPVT patients: simultaneous patch clamp and video imaging of iPSC derived cardiomyocytes’, *Molecular Biology Reports*. Springer Netherlands. doi: 10.1007/s11033-019-05201-y.
- Postma, A. V. *et al.* (2005) ‘Catecholaminergic polymorphic ventricular tachycardia: RYR2 mutations, bradycardia, and follow up of the patients’, *Journal of Medical Genetics*, 42(11), pp. 863–870. doi: 10.1136/jmg.2004.028993.
- Prajapati, C., Pölönen, R. P. and Aalto-Setälä, K. (2018) ‘Simultaneous recordings of action potentials and calcium transients from human induced pluripotent stem cell derived cardiomyocytes’, *Biology Open*, 7(7). doi: 10.1242/bio.035030.
- Preininger, M. K. *et al.* (2016) ‘A human pluripotent stem cell model of catecholaminergic polymorphic ventricular tachycardia recapitulates patient-specific drug responses’, *Disease Models & Mechanisms*, 9(9), pp. 927–939. doi: 10.1242/dmm.026823.
- Priori, S. G. *et al.* (2001) ‘Underlie Catecholaminergic Polymorphic Ventricular Tachycardia’, pp. 196–200.
- Priori, S. G. *et al.* (2002) ‘Clinical and molecular characterization of patients with catecholaminergic polymorphic ventricular tachycardia’, *Circulation*, 106(1), pp. 69–74. doi: 10.1161/01.CIR.0000020013.73106.D8.

- Priori, S. G. and Chen, S. R. W. (2011) 'Inherited dysfunction of sarcoplasmic reticulum Ca<sup>2+</sup> handling and arrhythmogenesis', *Circulation Research*, pp. 871–883. doi: 10.1161/CIRCRESAHA.110.226845.
- Priori, S. G. and Napolitano, C. (2005) 'Cardiac and skeletal muscle disorders caused by mutations in the intracellular Ca<sup>2+</sup> release channels', *Journal of Clinical Investigation*, pp. 2033–2038. doi: 10.1172/JCI25664.
- Protze, S. I. *et al.* (2016) 'Sinoatrial node cardiomyocytes derived from human pluripotent cells function as a biological pacemaker', *Nature Biotechnology*. Nature Publishing Group, (December), pp. 1–16. doi: 10.1038/nbt.3745.
- Qu, Z. *et al.* (2013) 'Early afterdepolarizations in cardiac myocytes: Beyond reduced repolarization reserve', *Cardiovascular Research*, 99(1), pp. 6–15. doi: 10.1093/cvr/cvt104.
- Qu, Z. and Weiss, J. N. (2015) 'Mechanisms of Ventricular Arrhythmias: From Molecular Fluctuations to Electrical Turbulence', *Annual Review of Physiology*, 77(1), pp. 29–55. doi: 10.1146/annurev-physiol-021014-071622.
- Ramalho, D. and Freitas, J. (2018) 'Drug-induced life-threatening arrhythmias and sudden cardiac death: A clinical perspective of long QT, short QT and Brugada syndromes', *Revista Portuguesa de Cardiologia*. Sociedade Portuguesa de Cardiologia, 37(5), pp. 435–446. doi: 10.1016/j.repc.2017.07.010.
- Refaat, M. M., Hotait, M. and Tseng, Z. H. (2014) 'Utility of the exercise electrocardiogram testing in sudden cardiac death risk stratification', *Annals of Noninvasive Electrocardiology*, pp. 311–318. doi: 10.1111/anec.12191.
- Reno, C. M. *et al.* (2017) 'Severe hypoglycemia-induced fatal cardiac arrhythmias are augmented by diabetes and attenuated by recurrent hypoglycemia', *Diabetes*, 66(12), pp. 3091–3097. doi: 10.2337/db17-0306.
- Reuter, H. *et al.* (2005) 'Na<sup>+</sup>-Ca<sup>2+</sup>exchange in the regulation of cardiac excitation-contraction coupling', *Cardiovascular Research*, 67(2), pp. 198–207. doi: 10.1016/j.cardiores.2005.04.031.
- Te Riele, A. S. J. M. *et al.* (2015) 'Arrhythmogenic Right Ventricular Dysplasia/Cardiomyopathy in the Pediatric Population: Clinical Characterization and Comparison With Adult-Onset Disease.', *JACC. Clinical electrophysiology*. United States, 1(6), pp. 551–560. doi: 10.1016/j.jacep.2015.08.004.
- Roberts, R. and Brugada, R. (2003) 'Genetics and Arrhythmias', *Annual Review of Medicine*, 54(1), pp. 257–267. doi: 10.1146/annurev.med.54.073002.182112.
- Roesl, C. *et al.* (2014) 'Functional characterisation of the R2452W ryanodine receptor variant associated with malignant hyperthermia susceptibility', *Cell Calcium*. Elsevier Ltd, 56(3), pp. 195–201. doi: 10.1016/j.ceca.2014.07.004.
- Rosenbaum DS, Jackson LE, Smith JM, Garan H, Ruskin JN, C. R. 1994. (1994) 'Electrical alternans and vulnerability to ventricular arrhythmias.', *N. Engl. J. Med.*, 330, pp. 235–41.
- Rosso, R. *et al.* (2007) 'Calcium channel blockers and beta-blockers versus beta-blockers alone for preventing exercise-induced arrhythmias in catecholaminergic polymorphic

ventricular tachycardia', *Heart Rhythm*, 4(9), pp. 1149–1154. doi: 10.1016/j.hrthm.2007.05.017.

Roux-buisson, N. *et al.* (2012) 'Absence of triadin, a protein of the calcium release complex, is responsible for cardiac arrhythmia with sudden death in human', *Human Molecular Genetics*, 21(12), pp. 2759–2767. doi: 10.1093/hmg/dds104.

Roux-Buisson, N. *et al.* (2014) 'Prevalence and significance of rare RYR2 variants in arrhythmogenic right ventricular cardiomyopathy/dysplasia: results of a systematic screening.', *Heart rhythm*. United States, 11(11), pp. 1999–2009. doi: 10.1016/j.hrthm.2014.07.020.

Rubart, M. and Zipes, D. P. (2005) 'Mechanisms of sudden cardiac death', 115(9). doi: 10.1172/JCI26381.

Sabir, I. N. *et al.* (2010) 'Alternans in genetically modified Langendorff-perfused murine hearts modeling catecholaminergic polymorphic ventricular tachycardia', *Frontiers in Physiology*, 1 OCT(October), pp. 1–9. doi: 10.3389/fphys.2010.00126.

Saimi, Y. and Kung, C. (2002) 'Calmodulin as an Ion Channel Subunit', *Annual Review of Physiology*, 64(1), pp. 289–311. doi: 10.1146/annurev.physiol.64.100301.111649.

Salomonsz, R., Baxter, W. and Jalife, J. (1992) 'Letters to nature', 355(January), pp. 312–314.

Salvage, S. C. *et al.* (2019) 'Ion channel gating in cardiac ryanodine receptors from the arrhythmic RyR2-P2328S mouse', *Journal of Cell Science*, 132(10). doi: 10.1242/jcs.229039.

Samsó, M. *et al.* (2009) 'Coordinated movement of cytoplasmic and transmembrane domains of RyR1 upon gating.', *PLoS biology*. United States, 7(4), p. e85. doi: 10.1371/journal.pbio.1000085.

Samsó, M., Shen, X. and Allen, P. D. (2006) 'Structural characterization of the RyR1-FKBP12 interaction', *Journal of Molecular Biology*, 356(4), pp. 917–927. doi: 10.1016/j.jmb.2005.12.023.

Sansone, R. A. and Sansone, L. A. (2014) 'Serotonin norepinephrine reuptake inhibitors: A pharmacological comparison', *Innovations in Clinical Neuroscience*, 11(3–4), pp. 37–42.

Sasaki, K. *et al.* (2016) 'Patient-Specific Human Induced Pluripotent Stem Cell Model Assessed with Electrical Pacing Validates S107 as a Potential Therapeutic Agent for Catecholaminergic Polymorphic Ventricular Tachycardia', pp. 1–17. doi: 10.1371/journal.pone.0164795.

Satin, J. *et al.* (2008) 'Calcium Handling in Human Embryonic Stem Cell-Derived Cardiomyocytes', *Stem Cells*, 26(8), pp. 1961–1972. doi: 10.1634/stemcells.2007-0591.

Satoh, H., Blatter, L. A. and Bers, D. M. (1997) 'Effects of  $[Ca^{2+}]_i$ , SR  $Ca^{2+}$  load, and rest on  $Ca^{2+}$  spark frequency in ventricular myocytes.', *The American journal of physiology*. United States, 272(2 Pt 2), pp. H657–68. doi: 10.1152/ajpheart.1997.272.2.H657.

Savio-Galimberti, E. and Knollmann, B. C. (2015) 'Channel activity of cardiac ryanodine receptors (RyR2) determines potency and efficacy of flecainide and R-propafenone against

- arrhythmogenic calcium waves in ventricular cardiomyocytes', *PLoS ONE*, 10(6), pp. 1–15. doi: 10.1371/journal.pone.0131179.
- SCHERF, D. (1947) 'Studies on auricular tachycardia caused by aconitine administration.', *Proceedings of the Society for Experimental Biology and Medicine. Society for Experimental Biology and Medicine (New York, N.Y.)*. United States, 64(2), pp. 233–239. doi: 10.3181/00379727-64-15754.
- Scherr, Johannes, M. H. (2015) 'Reply', *Journal of the American College of Cardiology*, 65(4), pp. 408–409. doi: 10.1016/j.jacc.2014.10.054.
- Schwartz, P. J. *et al.* (1993) 'Diagnostic criteria for the long QT syndrome: An update', *Circulation*, 88(2), pp. 782–784. doi: 10.1161/01.CIR.88.2.782.
- Sedej, S. *et al.* (2010) 'Na<sup>+</sup>-dependent SR Ca<sup>2+</sup> overload induces arrhythmogenic events in mouse cardiomyocytes with a human CPVT mutation', *Cardiovascular Research*, 87(1), pp. 50–59. doi: 10.1093/cvr/cvq007.
- Seidel, M. *et al.* (2015) 'Dantrolene rescues aberrant N-terminus intersubunit interactions in mutant pro-arrhythmic cardiac ryanodine receptors', *Cardiovascular Research*, 105(1), pp. 118–128. doi: 10.1093/cvr/cvu240.
- SELZER, A. and WRAY, H. W. (1964) 'QUINIDINE SYNCOPE. PAROXYSMAL VENTRICULAR FIBRILLATION OCCURRING DURING TREATMENT OF CHRONIC ATRIAL ARRHYTHMIAS.', *Circulation*. United States, 30, pp. 17–26. doi: 10.1161/01.cir.30.1.17.
- Sendfeld, F. *et al.* (2019) 'Experimental models of brugada syndrome', *International Journal of Molecular Sciences*, 20(9). doi: 10.3390/ijms20092123.
- Shah, M., Akar, F. G. and Tomaselli, G. F. (2005) 'Molecular basis of arrhythmias', *Circulation*, 112(16), pp. 2517–2529. doi: 10.1161/CIRCULATIONAHA.104.494476.
- Shan, J. *et al.* (2012) 'Calcium leak through ryanodine receptors leads to atrial fibrillation in 3 mouse models of catecholaminergic polymorphic ventricular tachycardia', *Circulation Research*, 111(6), pp. 708–717. doi: 10.1161/CIRCRESAHA.112.273342.
- Shannon, T. R., Ginsburg, K. S. and Bers, D. M. (2002) 'Quantitative assessment of the SR Ca<sup>2+</sup> leak-load relationship', *Circulation Research*, 91(7), pp. 594–600. doi: 10.1161/01.RES.0000036914.12686.28.
- Sharma, M. R. *et al.* (1998) 'Cryoelectron microscopy and image analysis of the cardiac ryanodine receptor', *Journal of Biological Chemistry*, 273(29), pp. 18429–18434. doi: 10.1074/jbc.273.29.18429.
- Sharma, M. R. *et al.* (2000) 'Three-dimensional structure of ryanodine receptor isoform three in two conformational states as visualized by cryo-electron microscopy', *Journal of Biological Chemistry*, 275(13), pp. 9485–9491. doi: 10.1074/jbc.275.13.9485.
- Sharma, M. R. *et al.* (2006) 'Three-dimensional visualization of FKBP12.6 binding to an open conformation of cardiac ryanodine receptor', *Biophysical Journal*. Elsevier, 90(1), pp. 164–172. doi: 10.1529/biophysj.105.063503.

- Shattock, M. J. *et al.* (2015) 'Na<sup>(+)</sup> /Ca<sup>(2+)</sup> exchange and Na<sup>(+)</sup> /K<sup>(+)</sup> -ATPase in the heart.', *The Journal of physiology*, 593(6), pp. 1361–82. doi: 10.1113/jphysiol.2014.282319.
- Silva, J. and Rudy, Y. (2003) 'Mechanism of Pacemaking in IK1 -Downregulated Myocytes', pp. 261–263. doi: 10.1161/01.RES.0000057996.20414.C6.
- Silva, R. A. D. E. and Frpc, C. (1997) 'George Ralph Mines , Ventricular Fibrillation and the Discovery of the Vulnerable Period \*', *Journal of the American College of Cardiology*. Elsevier Masson SAS, 29(6), pp. 1397–1402. doi: 10.1016/S0735-1097(97)00067-3.
- Silvia G. Priori, Carlo Napolitano, Natascia TisoMirella Memmi, Gabriele Vignati, Raffaella Bloise, Vincenzo Sorrentino, G. A. D. (2001) 'Mutations in the Cardiac Ryanodine Receptor Gene (hRyR2) Underlie Catecholaminergic Polymorphic Ventricular Tachycardia', *Circulation*, 103, pp. 196–200. doi: 10.1007/978-1-4471-4881-4\_31.
- Singh, H. *et al.* (2019) 'Pharmacogenomics in the clinic: Genetic polymorphism contributing to venlafaxine-associated heart failure', *Pharmacogenomics*, 20(17), pp. 1175–1178. doi: 10.2217/pgs-2019-0083.
- De Smedt, R. H. E. *et al.* (2008) 'Decompensation of chronic heart failure associated with pregabalin in a 73-year-old patient with postherpetic neuralgia: A case report', *British Journal of Clinical Pharmacology*, 66(2), pp. 327–328. doi: 10.1111/j.1365-2125.2008.03196.x.
- Song, L. *et al.* (2007) 'Calsequestrin 2 (CASQ2) mutations increase expression of calreticulin and ryanodine receptors, causing catecholaminergic polymorphic ventricular tachycardia', *Journal of Clinical Investigation*, 117(7), pp. 1814–1823. doi: 10.1172/JCI31080.
- Song, Y. *et al.* (2006) 'Blocking late sodium current reduces hydrogen peroxide-induced arrhythmogenic activity and contractile dysfunction.', *The Journal of pharmacology and experimental therapeutics*. United States, 318(1), pp. 214–222. doi: 10.1124/jpet.106.101832.
- Sorensen, A. B., Søndergaard, M. T. and Overgaard, M. T. (2013) 'Calmodulin in a Heartbeat', *FEBS Journal*, 280(21), pp. 5511–5532. doi: 10.1111/febs.12337.
- Spitalieri, P. *et al.* (2018) 'Modelling the pathogenesis of Myotonic Dystrophy type 1 cardiac phenotype through human iPSC-derived cardiomyocytes.', *Journal of molecular and cellular cardiology*. Elsevier Ltd, 118, pp. 95–109. doi: 10.1016/j.yjmcc.2018.03.012.
- Stoetzer, C. *et al.* (2016) 'Differential inhibition of cardiac and neuronal Na<sup>+</sup> channels by the selective serotonin-norepinephrine reuptake inhibitors duloxetine and venlafaxine', *European Journal of Pharmacology*, 783, pp. 1–10. doi: 10.1016/j.ejphar.2016.04.051.
- Suetomi, T. *et al.* (2011) 'Mutation-linked defective interdomain interactions within ryanodine receptor cause aberrant Ca<sup>2+</sup> release leading to catecholaminergic polymorphic ventricular tachycardia', *Circulation*, 124(6), pp. 682–694. doi: 10.1161/CIRCULATIONAHA.111.023259.
- Sumitomo, N. *et al.* (2003) 'Catecholaminergic polymorphic ventricular tachycardia: electrocardiographic characteristics and optimal therapeutic strategies to prevent sudden death.', *Heart (British Cardiac Society)*. England, 89(1), pp. 66–70. doi: 10.1136/heart.89.1.66.

Sun, B. *et al.* (2016) 'The cytoplasmic region of inner helix S6 is an important determinant of cardiac ryanodine receptor channel gating', *Journal of Biological Chemistry*, 291(50), pp. 26024–26034. doi: 10.1074/jbc.M116.758821.

Sun, G. *et al.* (2014) 'Aconitine-induced Ca<sup>2+</sup> overload causes arrhythmia and triggers apoptosis through p38 MAPK signaling pathway in rats', *Toxicology and Applied Pharmacology*. Elsevier Inc., 279(1), pp. 8–22. doi: 10.1016/j.taap.2014.05.005.

Sung, R. J. *et al.* (2006) 'Electrophysiological mechanisms of ventricular arrhythmias in relation to Andersen-Tawil syndrome under conditions of reduced I<sub>K1</sub>: A simulation study', *American Journal of Physiology - Heart and Circulatory Physiology*, 291(6), pp. 2597–2605. doi: 10.1152/ajpheart.00393.2006.

Tadross, M. R., Dick, I. E. and Yue, D. T. (2008) 'Mechanism of Local and Global Ca<sup>2+</sup> Sensing by Calmodulin in Complex with a Ca<sup>2+</sup> Channel', *Cell*, 133(7), pp. 1228–1240. doi: 10.1016/j.cell.2008.05.025.

Takahashi, K. *et al.* (2007) 'Induction of Pluripotent Stem Cells from Adult Human Fibroblasts by Defined Factors', *Cell*, 131(5), pp. 861–872. doi: 10.1016/j.cell.2007.11.019.

Takahashi, K. and Yamanaka, S. (2006) 'Induction of Pluripotent Stem Cells from Mouse Embryonic and Adult Fibroblast Cultures by Defined Factors', *Cell*, 126(4), pp. 663–676. doi: 10.1016/j.cell.2006.07.024.

Taylor, C. P., Angelotti, T. and Fauman, E. (2007) 'Pharmacology and mechanism of action of pregabalin: The calcium channel  $\alpha_2\text{-}\delta$  subunit as a target for antiepileptic drug discovery', *Epilepsy Research*, 73(2), pp. 137–150. doi: 10.1016/j.eplepsyres.2006.09.008.

Terentyev, D. *et al.* (2005) 'Triadin overexpression stimulates excitation-contraction coupling and increases predisposition to cellular arrhythmia in cardiac myocytes', *Circulation Research*, 96(6), pp. 651–658. doi: 10.1161/01.RES.0000160609.98948.25.

Tester, D. J. *et al.* (2005) 'Compendium of cardiac channel mutations in 541 consecutive unrelated patients referred for long QT syndrome genetic testing.', *Heart rhythm*. United States, 2(5), pp. 507–517. doi: 10.1016/j.hrthm.2005.01.020.

Tester, D. J. (2007) 'A mechanism for sudden infant death syndrome (SIDS): Stress-induced leak via ryanodine receptors', *Heart Rhythm*., 4(6), pp. 733–739. doi: 10.1038/jid.2014.371.

Thevenon, D. *et al.* (2003) 'Human skeletal muscle triadin: gene organization and cloning of the major isoform, Trisk 51.', *Biochemical and biophysical research communications*. United States, 303(2), pp. 669–675. doi: 10.1016/s0006-291x(03)00406-6.

Thiene, G., Corrado, D. and Basso, C. (2007) 'Arrhythmogenic right ventricular cardiomyopathy/dysplasia', *Orphanet Journal of Rare Diseases*, 2(1), pp. 1–16. doi: 10.1186/1750-1172-2-45.

Thomson, J. A. *et al.* (2011) 'Chemically defined conditions for human iPS cell derivation and culture', *Nature methods*, 8(5), pp. 424–429. doi: 10.1038/nmeth.1593.Chemically.

- Timerman, A. P. *et al.* (1994) 'The ryanodine receptor from canine heart sarcoplasmic reticulum is associated with a novel FK-506 binding protein', *Biochemical and Biophysical Research Communications*, 198(2), pp. 701–706. doi: 10.1006/bbrc.1994.1101.
- Tiso, N. (2001) 'Identification of mutations in the cardiac ryanodine receptor gene in families affected with arrhythmogenic right ventricular cardiomyopathy type 2 (ARVD2)', *Human Molecular Genetics*, 10(3), pp. 189–194. doi: 10.1093/hmg/10.3.189.
- Tomaselli, G. F. and Zipes, D. P. (2004) 'What causes sudden death in heart failure?', *Circulation Research*, 95(8), pp. 754–763. doi: 10.1161/01.RES.0000145047.14691.db.
- Tong, M. and Jiang, Y. (2015) 'FK506-Binding Proteins and Their Diverse Functions', *Current Molecular Pharmacology*, 9(1), pp. 48–65. doi: 10.2174/1874467208666150519113541.
- Tse, G. (2016) 'Mechanisms of cardiac arrhythmias', *Journal of Arrhythmia*. Elsevier, 32(2), pp. 75–81. doi: 10.1016/j.joa.2015.11.003.
- Tuluc, P. *et al.* (2007) 'Computer modeling of siRNA knockdown effects indicates an essential role of the Ca<sup>2+</sup> channel alpha2delta-1 subunit in cardiac excitation-contraction coupling.', *Proceedings of the National Academy of Sciences of the United States of America*, 104(26), pp. 11091–11096. doi: 10.1073/pnas.0700577104.
- Tung, C. C. *et al.* (2010) 'The amino-terminal disease hotspot of ryanodine receptors forms a cytoplasmic vestibule', *Nature*. Nature Publishing Group, 468(7323), pp. 585–588. doi: 10.1038/nature09471.
- Uchinoumi, H. *et al.* (2010) 'Catecholaminergic polymorphic ventricular tachycardia is caused by mutation-linked defective conformational regulation of the ryanodine receptor', *Circulation Research*, 106(8), pp. 1413–1424. doi: 10.1161/CIRCRESAHA.109.209312.
- Urena, M. *et al.* (2015) 'Arrhythmia burden in elderly patients with severe aortic stenosis as determined by continuous electrocardiographic recording toward a better understanding of arrhythmic events after transcatheter aortic valve replacement', *Circulation*, 131(5), pp. 469–477. doi: 10.1161/CIRCULATIONAHA.114.011929.
- Valdivia, H. H. *et al.* (1995) 'Rapid adaptation of cardiac ryanodine receptors: Modulation by Mg<sup>2+</sup> and phosphorylation', *Science*, 267(5206), pp. 1997–2000. doi: 10.1126/science.7701323.
- Verrier, R. L. *et al.* (2011) 'Microvolt T-wave alternans physiological basis, methods of measurement, and clinical utility--consensus guideline by International Society for Holter and Noninvasive Electrocardiology.', *Journal of the American College of Cardiology*. United States, 58(13), pp. 1309–1324. doi: 10.1016/j.jacc.2011.06.029.
- Viatchenko-Karpinski, S. *et al.* (2004) 'Abnormal Calcium Signaling and Sudden Cardiac Death Associated with Mutation of Calsequestrin', *Circulation Research*, 94(4), pp. 471–477. doi: 10.1161/01.RES.0000115944.10681.EB.
- Vogel, H. J. (1994) 'The Merck Frosst Award Lecture 1994. Calmodulin: a versatile calcium mediator protein.', *Biochemistry and cell biology = Biochimie et biologie cellulaire*. Canada, 72(9–10), pp. 357–376.

- Wang, L. *et al.* (2014) ‘Optical Mapping of Sarcoplasmic Reticulum Ca<sup>2+</sup> in the Intact Heart Ryanodine Receptor Refractoriness During Alternans and Fibrillation’, *Circulation Research*, pp. 1410–1421. doi: 10.1161/CIRCRESAHA.114.302505.
- Wang, S.-Y. and Wang, G. K. (2003) ‘Voltage-gated sodium channels as primary targets of diverse lipid-soluble neurotoxins.’, *Cellular signalling*. England, 15(2), pp. 151–159.
- Wang, Y. Y. *et al.* (2017) ‘RyR2R420Q catecholaminergic polymorphic ventricular tachycardia mutation induces bradycardia by disturbing the coupled clock pacemaker mechanism.’, *JCI insight*, 2(8). doi: 10.1172/jci.insight.91872.
- Wangüemert, F. *et al.* (2015) ‘Clinical and molecular characterization of a cardiac ryanodine receptor founder mutation causing catecholaminergic polymorphic ventricular tachycardia’, *Heart Rhythm*. Elsevier, 12(7), pp. 1636–1643. doi: 10.1016/j.hrthm.2015.03.033.
- Wanner, C., Herzog, C. A. and Turakhia, M. P. (2018) ‘Chronic kidney disease and arrhythmias: highlights from a Kidney Disease: Improving Global Outcomes (KDIGO) Controversies Conference.’, *Kidney international*. United States, 94(2), pp. 231–234. doi: 10.1016/j.kint.2018.05.005.
- Watanabe, H. *et al.* (2011) ‘Flecainide inhibits arrhythmogenic Ca<sup>2+</sup> waves by open state block of ryanodine receptor Ca<sup>2+</sup> release channels and reduction of Ca<sup>2+</sup> spark mass’, *Journal of molecular and cellular cardiology*, 76(2), pp. 1358–1375. doi: 10.1111/j.1365-2958.2010.07165.x.Characterization.
- Wehrens, X. H. T. *et al.* (2002) ‘Novel insights in the congenital long QT syndrome.’, *Annals of internal medicine*. United States, 137(12), pp. 981–992. doi: 10.7326/0003-4819-137-12-200212170-00012.
- Wehrens, X. H. T. *et al.* (2003) ‘FKBP12.6 deficiency and defective calcium release channel (ryanodine receptor) function linked to exercise-induced sudden cardiac death’, *Cell*, 113(7), pp. 829–840. doi: 10.1016/S0092-8674(03)00434-3.
- Wei, H. *et al.* (2018) ‘CRISPR/Cas9 Gene editing of RyR2 in human stem cell-derived cardiomyocytes provides a novel approach in investigating dysfunctional Ca<sup>2+</sup> signaling’, *Cell Calcium*. Elsevier, 73(April), pp. 104–111. doi: 10.1016/j.ceca.2018.04.009.
- Wei, R. *et al.* (2016) ‘Structural insights into Ca<sup>2+</sup>-activated long-range allosteric channel gating of RyR1’, *Cell Research*. Nature Publishing Group, 26(9), pp. 977–994. doi: 10.1038/cr.2016.99.
- Weiss, J. N. *et al.* (2010) ‘Early afterdepolarizations and cardiac arrhythmias’, *Heart Rhythm*, 7(12), pp. 1891–1899. doi: 10.1016/j.hrthm.2010.09.017.
- Van Der Werf, C. *et al.* (2011) ‘Flecainide therapy reduces exercise-induced ventricular arrhythmias in patients with catecholaminergic polymorphic ventricular tachycardia’, *Journal of the American College of Cardiology*. Elsevier Inc., 57(22), pp. 2244–2254. doi: 10.1016/j.jacc.2011.01.026.
- Willis, B. C. *et al.* (2016) ‘Constitutive intracellular Na<sup>+</sup> excess in purkinje cells promotes arrhythmogenesis at lower levels of stress than ventricular myocytes from mice with catecholaminergic polymorphic ventricular tachycardia’, *Circulation*, 133(24), pp. 2348–2359. doi: 10.1161/CIRCULATIONAHA.116.021936.

- Words, K. (2000) 'VENTRICULAR FIBRILLATION : Mechanisms of Initiation and Maintenance', pp. 25–50.
- Xie, L. *et al.* (2019) 'A compound heterozygosity of *Tecrl* gene confirmed in a catecholaminergic polymorphic ventricular tachycardia family', *European Journal of Medical Genetics*. Elsevier, 62(7), p. 103631. doi: 10.1016/j.ejmg.2019.01.018.
- Xie, W. *et al.* (2013) 'Imaging atrial arrhythmic intracellular calcium in intact heart', *Journal of Molecular and Cellular Cardiology*. Elsevier Ltd, 64, pp. 120–123. doi: 10.1016/j.yjmcc.2013.09.003.
- Xu, L., Mann, G. and Meissner, G. (1996) 'Regulation of cardiac Ca<sup>2+</sup> release channel (ryanodine receptor) by Ca<sup>2+</sup>, H<sup>+</sup>, Mg<sup>2+</sup>, and adenine nucleotides under normal and simulated ischemic conditions.', *Circulation research*. United States, 79(6), pp. 1100–1109. doi: 10.1161/01.res.79.6.1100.
- Xu, X. *et al.* (2010) 'Defective calmodulin binding to the cardiac ryanodine receptor plays a key role in CPVT-associated channel dysfunction', *Biochemical and Biophysical Research Communications*. Elsevier Inc., 394(3), pp. 660–666. doi: 10.1016/j.bbrc.2010.03.046.
- Yamaguchi, N. *et al.* (2003) 'Molecular basis of calmodulin binding to cardiac muscle Ca<sup>2+</sup> release channel (ryanodine receptor)', *Journal of Biological Chemistry*, 278(26), pp. 23480–23486. doi: 10.1074/jbc.M301125200.
- Yamamoto, T., El-Hayek, R. and Ikemoto, N. (2000) 'Postulated role of interdomain interaction within the ryanodine receptor in Ca<sup>2+</sup> channel regulation', *Journal of Biological Chemistry*, 275(16), pp. 11618–11625. doi: 10.1074/jbc.275.16.11618.
- Yan, Z. *et al.* (2015) 'Structure of the rabbit ryanodine receptor RyR1 at near-atomic resolution', *Nature*. Nature Publishing Group, 517(7532), pp. 50–55. doi: 10.1038/nature14063.
- Yankelson, L. *et al.* (2014) 'Life-threatening events during endurance sports: Is heat stroke more prevalent than arrhythmic death?', *Journal of the American College of Cardiology*, 64(5), pp. 463–469. doi: 10.1016/j.jacc.2014.05.025.
- Yano, K. and Zarain-Herzberg, A. (1994) 'Sarcoplasmic reticulum calsequestrins: structural and functional properties.', *Molecular and cellular biochemistry*. Netherlands, 135(1), pp. 61–70. doi: 10.1007/bf00925961.
- Yap, K. L. *et al.* (2000) 'Calmodulin target database.', *Journal of structural and functional genomics*. Netherlands, 1(1), pp. 8–14.
- Yardley, J. P. *et al.* (1990) '2-Phenyl-2-(1-hydroxycycloalkyl)ethylamine Derivatives: Synthesis and Antidepressant Activity', *Journal of Medicinal Chemistry*, 33(10), pp. 2899–2905. doi: 10.1021/jm00172a035.
- Yijun Tang, Xixi Tian, Chen, S. R. W. (2012) 'Abnormal Termination of Ca<sup>2+</sup> Release Is a Common Defect of RyR2 Mutations Associated With Cardiomyopathies', *Circ Res.*, 23(1), pp. 1–7. doi: 10.1038/jid.2014.371.

- Yuchi, Z. *et al.* (2015) ‘Crystal structures of ryanodine receptor SPRY1 and tandem-repeat domains reveal a critical FKBP12 binding determinant’, *Nature Communications*. Nature Publishing Group, 6, pp. 1–13. doi: 10.1038/ncomms8947.
- Yuchi, Z. and Van Petegem, F. (2016) ‘Ryanodine receptors under the magnifying lens: Insights and limitations of cryo-electron microscopy and X-ray crystallography studies’, *Cell Calcium*. Elsevier Ltd, 59(5), pp. 209–227. doi: 10.1016/j.ceca.2016.04.003.
- Zalk, R. *et al.* (2015) ‘Structure of a mammalian ryanodine receptor’, *Nature*, 517(7532), pp. 44–49. doi: 10.1038/nature13950.
- Zeng, J. *et al.* (1995) ‘Two components of the delayed rectifier K<sup>+</sup> current in ventricular myocytes of the guinea pig type. Theoretical formulation and their role in repolarization.’, *Circulation research*. United States, 77(1), pp. 140–152. doi: 10.1161/01.res.77.1.140.
- Zhang, J. *et al.* (2009) ‘Functional cardiomyocytes derived from human induced pluripotent stem cells’, *Circulation Research*, 104(4), pp. 30–41. doi: 10.1161/CIRCRESAHA.108.192237.
- Zhang, M. *et al.* (2012) ‘Structural basis for calmodulin as a dynamic calcium sensor’, *Structure*. Elsevier Ltd, 20(5), pp. 911–923. doi: 10.1016/j.str.2012.03.019.
- Zhang, X. *et al.* (2019) ‘Acid Sensitive Ion channels are expressed in human induced pluripotent stem cell-derived cardiomyocytes’, *Stem Cells and Development*, p. scd.2018.0234. doi: 10.1089/scd.2018.0234.
- Zhang, X. H. *et al.* (2013) ‘Ca<sup>2+</sup> signaling in human induced pluripotent stem cell-derived cardiomyocytes (iPSC-CM) from normal and catecholaminergic polymorphic ventricular tachycardia (CPVT)-afflicted subjects’, *Cell Calcium*, 54(2), pp. 57–70. doi: 10.1016/j.ceca.2013.04.004.
- Zhang, Y. *et al.* (2011) ‘Acute atrial arrhythmogenicity and altered Ca<sup>2+</sup> homeostasis in murine RyR2-P2328S hearts’, *Cardiovascular Research*, 89(4), pp. 794–804. doi: 10.1093/cvr/cvq229.
- Zhang, Y. *et al.* (2013) ‘Conduction slowing contributes to spontaneous ventricular arrhythmias in intrinsically active murine RyR2-P2328S hearts’, *Journal of Cardiovascular Electrophysiology*, 24(2), pp. 210–218. doi: 10.1111/jce.12015.
- Zhao, Y.-T. *et al.* (2015a) ‘(RyR2-A4860G) Arrhythmogenesis in a catecholaminergic polymorphic ventricular tachycardia mutation that depresses ryanodine receptor function.’, *Proceedings of the National Academy of Sciences of the United States of America*, 112(13), pp. E1669-77. doi: 10.1073/pnas.1419795112.
- Zhao, Y.-T. *et al.* (2015b) ‘Arrhythmogenesis in a catecholaminergic polymorphic ventricular tachycardia mutation that depresses ryanodine receptor function.’, *Proceedings of the National Academy of Sciences of the United States of America*, 112(13), pp. E1669-77. doi: 10.1073/pnas.1419795112.
- Zhao, Y. T. *et al.* (2017) ‘Sensitized signalling between L-type Ca<sup>2+</sup> channels and ryanodine receptors in the absence or inhibition of FKBP12.6 in cardiomyocytes’, *Cardiovascular research*, 113(3), pp. 332–342. doi: 10.1093/cvr/cvw247.

Zimmer, T., Haufe, V. and Blehschmidt, S. (2014) 'Voltage-gated sodium channels in the mammalian heart', *Global Cardiology Science and Practice*, 2014(4), p. 58. doi: 10.5339/gcsp.2014.58.

Zühlke, R. D. *et al.* (1999) 'Calmodulin supports both inactivation and facilitation of L-type calcium channels.', *Nature*. England, 399(6732), pp. 159–162. doi: 10.1038/20200.

Zühlke, R. D. *et al.* (1999) 'Calmodulin supports both inactivation and facilitation of L-type calcium channels', *Nature*, 399(6732), pp. 159–162. doi: 10.1038/20200.

# Annexes

## **A peculiar variant abolishing ryanodine receptor type2 response to adrenergic stress**

Malorie Blancard<sup>1,2</sup>, Zahia Touat-Hamici<sup>1,2\*</sup>, Yuriana Aguilar-Sanchez<sup>3\*</sup>, **Liheng Yin**<sup>4</sup>, Guy Vaksman<sup>5</sup>, Nathalie Roux-Buisson<sup>6</sup>, Véronique Fressart<sup>7</sup>, Isabelle Denjoy<sup>1,2,8</sup>, Didier Klug<sup>9</sup>, Nathalie Neyroud<sup>1,2</sup>, Josefina Ramos-Franco<sup>3</sup>, Ana Maria Gomez<sup>4</sup>, Pascale Guicheney<sup>1,2</sup>

<sup>1</sup> Inserm, UMRS 1166, Paris, France

<sup>2</sup> Sorbonne University, UPMC Univ Paris 06, Institute of Cardiometabolism and Nutrition (ICAN), Paris, France.

<sup>3</sup> Rush University Medical Center, Dept. Physiology & Biophysics, Chicago, IL, USA

<sup>4</sup> Inserm, UMRS 1180, « Signaling and cardiovascular pathophysiology », Univ. Paris-Sud, Université Paris Saclay, 92296 Châtenay-Malabry, France

<sup>5</sup> Service de cardiologie pédiatrique, Hôpital Privé de la Louvière, Lille, France

<sup>6</sup> Université Joseph Fourier, Grenoble, France

<sup>7</sup> AP-HP, Unité de Cardiogénétique et Myogénétique Paris

<sup>8</sup> AP-HP, Hôpital Bichat, Département de Cardiologie, Centre de Référence des Maladies Cardiaques Héritaires, Paris, France.

<sup>9</sup> Hôpital cardiologique, CHRU de Lille, Lille, France

### **Corresponding author :**

Dr Pascale Guicheney

UMRS 1166, Faculté de médecine Sorbonne Université

91, boulevard de l'Hôpital, 75013 Paris, France.

Phone : +33 1 40 77 98 05

pascale.guicheney@upmc.fr

**Keywords:** Arrhythmia, CPVT, RYR2, calcium, sudden death, risk factors, adrenergic stimulation

**Background and Aims:** Catecholaminergic polymorphic ventricular tachycardia (CPVT) are triggered by exercise or acute emotion in patients with normal resting electrocardiogram. The major disease-causing gene is *RYR2*, encoding the cardiac ryanodine receptor (RyR2). We report a novel *RYR2* mutation in two CPVT families with numerous sudden deaths.

**Methods:** Family members were evaluated by exercise-stress tests, and CPVT genes were sequenced. WT and mutant hRyR2 activity was studied after transfection in HEK293 cells by confocal microscopy and single channel recordings.

**Results:** In a four-generation family, where eight sudden cardiac deaths occurred before the age of 30 years in a context of acute emotion or exercise, we identified a novel *RYR2* missense variant, p.Asp3291Val. All 24 phenotype positive subjects harbored at least one copy of the *RYR2* variant, but many young carriers (10) presented a negative phenotype. Three affected sisters were homozygous for the variant. We identified the same mutation in another CPVT family where two sudden deaths have occurred. The D3291V variant is located in the helical domain 2, outside the CPVT mutation hotspots, and changes a negatively charged amino-acid widely conserved through evolution. D3291V is associated with a normal response to cytosolic Ca<sup>2+</sup>, a reduced response to luminal Ca<sup>2+</sup> and caffeine, and more importantly an absence of normal response to 8-bromo-cAMP and forskolin.

**Conclusions:** Our data support that the D3291V-RyR2 variant is a loss-of-function CPVT mutation inducing a mild dysfunction in basal conditions but is responsible for fatal events through its unresponsiveness to adrenergic stimulation.

## I. Introduction

Catecholaminergic polymorphic ventricular tachycardia (CPVT) is a rare inherited life-threatening disorder characterized by adrenergic induced bi-directional or polymorphic ventricular tachyarrhythmia (PVT) in absence of any detectable structural heart abnormalities (Leenhardt et al., 1995). It occurs in children and adults and causes syncope and sudden cardiac death (SCD). The baseline electrocardiogram (ECG) is usually normal and diagnosis is therefore mainly based on the occurrence of arrhythmias during exercise-stress-testing or Holter monitoring (Priori et al., 2015). When left untreated, CPVT diagnosis carries a high mortality rate, especially in probands (Hayashi et al., 2009; Priori et al., 2002; Werf et al., 2012), and treatment by  $\beta$ -blockers is mandatory. Flecainide should be considered as the first addition to  $\beta$ -blockers when control of arrhythmias is incomplete (Kannankeril et al., 2017; Watanabe et al., 2009).

Missense mutations in *RYR2*, the gene encoding the cardiac ryanodine receptor (RyR2), is the major cause of the dominant form of CPVT with detection of a *RYR2* mutation in 60 to 65% of patients, including a high rate of *de novo* mutations (Laitinen et al., 2001; Medeiros-Domingo et al., 2009; Priori et al., 2001). More recently, several dominant mutations in the calmodulin genes (*CALM1*, *CALM2*, *CALM3*) leading to severe *de novo* or familial CPVT have been discovered (Gomez-Hurtado et al., 2016; Hwang et al., 2014; Jiménez-Jáimez et al., 2016; Makita et al., 2014; Nyegaard et al., 2012). Recessive mutations account for a small fraction of CPVT patients, and have been mainly associated with proteins regulating the RyR2 complex activity, calsequestrin2 (*CASQ2*) and triadin (*TRDN*) (Lahat et al., 2001; Postma et al., 2002; Roux-Buisson et al., 2012).

RyR2, a large homotetrameric channel located in the membrane of the sarcoplasmic reticulum, is the main actor of  $\text{Ca}^{2+}$  release from sarcoplasmic reticulum (SR) into cytosol. The previously reported mutations are mostly located in four specific domains (hotspot) (George et al., 2007; Venetucci et al., 2012). CPVT mutations render RyR2  $\text{Ca}^{2+}$  release channel prone to more spontaneous opening, resulting in more spontaneous  $\text{Ca}^{2+}$  release and propagated  $\text{Ca}^{2+}$  waves that trigger membrane depolarizations, premature ventricular beats (PVB), and polymorphic ventricular tachycardia (PVT) during physical activity or emotional stress (Nyegaard et al., 2012; Watanabe and Knollmann, 2011).

In this study, we reported a new *RYR2* variant, located outside the mutation hotspot, in two CPVT families. One of these families was a four-generation family with homozygous and heterozygous carriers of the variant, where eight family members died suddenly before the age of 30, in a context of acute emotion or exercise. Here, we defined the RyR2's variant  $\text{Ca}^{2+}$  release activity, as well as its response to adrenergic stimulation, at cellular and single channel levels.

## II. Materials and methods

### Patients

In both families, CPVT was suspected because of family history of several sudden deaths during a physical exercise or an emotional stress in young subjects. Clinical evaluation of the patients included a 12-lead ECG, 24h Holter ECGs, exercise-stress test (EST), isoproterenol infusion and echocardiography. Relatives were considered as affected when an exercise-stress test or isoprenaline test showed bi-directional premature ventricular beats (PVBs), bigeminy, bi-directional or polymorphic ventricular tachycardia (PVT) (Piori et al., 2015).

Blood samples were obtained after signed informed consent forms were collected for genetic analyses and upon approval of the local ethics committee of the Saint-Louis Hospital. The study was conducted according to the principles of the Helsinki Declaration.

### Genetic analysis

Genomic DNA was isolated from whole blood using standard protocol. All coding exons of *RYR2* (NM\_001035), *CASQ2* (NM\_001232) and *TRDN* (NM\_006073) were screened by direct sequencing and linkage analysis was performed in family 1 with intragenic or closely linked microsatellites to the *RYR2* locus (D1S2800, D1S2680, D1S204). Several genes (*CASQ2*, *CALM1*, *RYR2*, *TRDN*, *SCN5A*, *KCNQ1*, *DSC2*, *DSG2*, *DSP*, *KCNE1*, *KCNE2*, *KCNH2*, *KCNJ2*, *LMNA*, *NKX2-5*, *PKP2*) implicated in arrhythmias were screened for the proband of family 2 by Multiplex Amplification of coding regions, were analyzed by High-throughput Sequencing and then confirmed by Sanger sequencing. The *RYR2* variant was genotyped by Sanger sequencing in all family members.

### RYR2 cloning and mutagenesis

The plasmid containing the human *RYR2* sequence (**X98330**) tagged with enhanced green fluorescent protein (eGFP) was kindly provided by Dr Spyros Zissimopoulos (UK) (Tunwell, 1996, George, 2003). The 5 mismatches between the **X98330** sequence and the ***RYR2* reference sequence** (NM\_001035.2) were firstly corrected by oligonucleotide directed mutagenesis (QuikChange II Site-Directed mutagenesis Kit, Agilent Technologies): proline 1037 was changed to a leucine, and p.RTMRT at position 2785-2789 was replaced by p.WGWRI. To generate the D3291V variant, a fragment of h*RYR2*, digested by KpnI and FseI, was sub-cloned into pCR<sup>®</sup>-Blunt, and the aspartic acid was replaced by a valine by site-directed mutagenesis. Then the mutated KpnI/FseI fragment of the pCR<sup>®</sup>-Blunt plasmid was amplified by overlapping PCR to be re-inserted into the full-length *RYR2* plasmid using a recombination kit (NEBuilder HiFi DNA Assembly Cloning kit, New England Biolabs, Evry, France).

The GFP-free human *RYR2* plasmid was created for single channel experiments using a recombination kit (NEBuilder HiFi DNA Assembly Cloning kit, New England Biolabs, Evry, France). The GFP sequence was removed from the full-length *RYR2* plasmid by a AfeI/FspAI digestion (leaving a AfeI/FspAI linearized *RYR2* plasmid). This plasmid was then sealed with a GFP-free *RyR2* fragment with overlapping ends to the AfeI/FspAI linearized *RYR2* plasmid.

## Cell culture and transfection

Human embryonic kidney 293 (HEK293) cells were cultured in Dulbecco's Modified Eagle Medium (DMEM) (Life technologies) supplemented with 10% FBS and 1% penicillin-streptomycin. Cell transfection was performed using Lipofectamine 3000 (Life Technologies, Saint-Aubin, France) according to manufacturer's instruction. HEK293 cells were seeded and transfected when 60-70% confluent either with RYR2-WT or RYR2-D3291V plasmids 48h before the different analyses.

## Protein extraction and Western blotting

Cells were seeded in 25 cm<sup>2</sup> dishes and then transfected with 2µg of RYR2-WT or RYR2-D3291V plasmids. Two days after transfection, transfected cells were lysed with a lysis buffer containing 50 mM Tris-HCl (pH 7.5), 150 mM NaCl, 1% Triton X-100, 0.5% sodium deoxycholate, 0.1% SDS and 5 mM EDTA, during one hour at 4°C under gentle stirring, and then centrifuged at 13 200 rpm for 10 min at 4°C. Protein concentration of the cell supernatants was determined using a Pierce™ BCA Protein Assay kit (ThermoScientific, France). Total proteins (20 µg) were separated by 3-8% Tris Acetate polyacrylamide gel electrophoresis and then transferred into a nitrocellulose membrane for 90 min at 35 V. Membranes were saturated with 5% milk-0.1% Tween PBS for 45 min, and then incubated overnight with antibodies against RyR2 (1/1000) (MA3-916, ThermoScientific, France) and α-tubulin (1/2000) (ab4074, Abcam, Cambridge, United Kingdom). Membranes were washed four times in 0.1% Tween-PBS and then incubated with IR-fluorescent secondary antibodies (1/10000) (ThermoScientific, France). Membranes were washed again twice in 0.1% Tween-PBS and twice in PBS before IR-fluorescence imaging. RyR2 and α-tubulin expression was quantified with ImageJ. The expression level of RYR2 was normalized by the transfection efficiency.

## Calcium imaging

For Ca<sup>2+</sup> imaging, HEK293 cells were seeded in 35 mm µ-dish with glass bottom (Ibidi, Clinisciences, France). RYR2-WT or RYR2-D3291V plasmids were transfected using lipofectamine 3000 (280 ng/dish). Two days after transfection, cells were loaded with the fluorescent Ca<sup>2+</sup> dye Fura2-AM (5µM) for 45 min at 37°C, 5% CO<sub>2</sub>. Caffeine (10 mM) was added at the end of each recording to assess the RyR2 functionality. For some experiments, before Fura-2 loading, cells were pretreated with 250 µM of 8-bromo-cAMP (Sigma-Aldrich, France) or 5µM Forskolin (Sigma-Aldrich, France) for 20 min at room temperature. Cells were then perfused with Krebs-Ringer-Hepes (KRH) buffer (125mM NaCl, 25mM HEPES, 5mM KCl, 1.2mM MgCl<sub>2</sub>, 6mM glucose, pH 7.4) containing different Ca<sup>2+</sup> concentrations (0.1-2 mM) at room temperature. To test caffeine sensitivity and to assess the stored Ca<sup>2+</sup>, caffeine at 0.1 or 10 mM were added at the beginning of the recording. Ca<sup>2+</sup> oscillations were assessed using a fluorescent Nikon Eclipse Ti-U microscope. The fluorescence was recorded at excitation wavelengths of 340 and 380 nm and at emission wavelength of 510 nm for 3 minutes. The F340/F380 ratio was determined for each region of interest (ROI) and only cells responding to caffeine were analyzed.

### Single channel analysis

Single-channel studies were carried out with crude microsomes obtained from HEK293 cells transfected with RyR2-WT or RyR2-D3291V plasmids. Lipid planar bilayers were made of a mixture of phosphatidylethanolamine, phosphatidylserine, and phosphatidylcholine in a 5:4:1 ratio (50 mg/ml in decane) (Avanti Polar Lipids Inc, USA). Microsomes were incorporated into the lipid bilayers formed across a 100- $\mu$ m hole in a thin teflon partition separating two aqueous compartments where the cytosolic compartment (cis chamber) was virtually grounded and filled with a HEPES–Tris solution (250 mM/118 mM) at pH 7.4. Microsomes were added to the cis chamber. The luminal compartment (trans chamber) was filled with HEPES–Ca<sup>2+</sup> (250 mM/50 mM) at pH 7.4, and the voltage was applied in this compartment. Immediately upon observing single-channel activity, we replaced the solutions to establish the specific test conditions. Ca<sup>2+</sup>-buffer solutions (BAPTA and 5-5'-dibromo-BAPTA, Thermo Fisher Scientific, USA) were prepared using MaxChelator. Membrane voltage was controlled using an Axopatch 200B (Molecular Devices LLC, USA). The current signal was digitized at 20 kHz through a Digidata 1322A interface (Molecular Devices LLC, USA) and subsequently filtered at 2 kHz, unless specified otherwise. Data acquisition and analysis were carried out using *pClamp* software (Molecular Devices LLC, USA).

### Statistical analysis

Cellular data and single channels results are expressed as mean  $\pm$  SEM unless otherwise stated. Results for fitting histograms and the Hill equation are given as the mean  $\pm$  SD. Statistical tests (unpaired student's *t*-test, ANOVA) were performed with OriginPro Software (OriginLab, USA). A *p*-value of 0.05 was considered significant.

## III. Results

### Clinical phenotype and genetic analysis

#### *Family 1*

Family 1 is a four-generation family originating from the North of France in which eight sudden death occurred during a physical or an emotional stress, before the age of 30 (Figure 1A, Table 1). The grand-parents were first cousins. The proband III.13 had a first syncope at the age of 10 and experienced an aborted sudden cardiac death at the age of 14 in a context of emotion and moderate hypokalemia (3.2 mmol/l). Relatives underwent clinical evaluations including a 12-lead ECG, echocardiography, 24h Holter ECGs, and exercise-stress test or isoprenaline test. All ECG were normal at rest and echocardiograms showed no structural abnormalities. Most of the family members were treated by nadolol, when bidirectional ventricular tachycardia or PVT was detected during clinical evaluation. It should be noted that there are relatively few living symptomatic subjects compared to the high number of sudden deaths (Table 1).

When CPVT was diagnosed in the proband after her cardiac arrest, “classical CPVT” exons of *RYR2* and all coding exons of *CASQ2* and *TRDN*, were first screened but no variant was found. Then linkage analysis with microsatellite markers was performed, which showed cosegregation of the *RYR2* locus with the affected phenotype (Suppl Figure 1). Hence, all *RYR2*

exons were screened and a new variant was identified in exon 68, c.9872A>T, leading to a change of an aspartate to a valine at position 3291. This variant, p.Asn3291Val (D3291V), was absent in all databases (Genome Aggregation Database gnomAD). It was first considered as a polymorphism by the diagnostic laboratories, as it was located outside of the four CPVT mutation hotspots.

In accordance with the microsatellite haplotypes, the variant was found at the homozygous state in three sisters of the second generation (II.1, II.2, II.5), and in all the other phenotype-positive members at the heterozygous state. Surprisingly, one of the three sisters (II.5) never had syncope but her exercise-stress test was stopped because of too many bidirectional PVBs. The sister II.1 had several syncopes during exercise and an isoprenaline test showed bidirectional PVBs and a short VT. The last homozygous sister II.2 had syncope at 18 during exercise and her exercise-stress test revealed PVT. Two siblings died suddenly in a context of physical activity at 24 (II.3) and 17 (II.17) while a brother (II.4), who was heterozygous carrier and had coronary disease, died during the night at the age of 54 years. The eight children of the three homozygous sisters were all obligate heterozygous carriers. One of them died while swimming at the age of 22 years. The grand-mother (I.2) had several children from a second marriage, one of them died at 54 and one affected daughter (II.11) lost her two sons when they were 20 and 15 while swimming and biking, respectively.

Most of the phenotype-negative members of generations II and III did not carry the variant, except four of them (III.6, III.18, III.23 and III.26), who were heterozygous carriers with a negative exercise-stress tests at the ages of 32, 21, 29 and 49, respectively. Two girls (III.5, III.14) had a negative exercise stress-test at first examinations at 11 and 16, but developed bigeminy during exercise-stress test later at the ages of 21 and 27. In the fourth generation, only 2 of the 14 young carriers have a positive phenotype, IV.3 who had bigeminy at exercise-stress test even after nadolol (80 mg) and IV.13 who presented an auriculo-ventricular block (AV block) and bradycardia at birth, and ventricular salvoe on Holter recording at the age of 2 (Figure 2).

### *Family 2*

Proband III.2 had syncopes at 20 and 25 and an exercise-stress test performed under  $\beta$ -blocker revealed many PVBs and ventricular bigeminism originating from right ventricular outflow track (RVOT) which disappeared during recovery but no typical bidirectional PVT. MRI, echocardiography were normal and an implanted Reveal did not record any abnormality. Her mother (II.1) died suddenly at age 45 in a context of emotion, attending the funeral of a friend, and her brother (III.1) at 8 years while swimming. The proband's DNA was screened on a genetic testing panel for cardiac diseases and the only variant found as potentially pathogenic was p.Asp3291Val in RyR2 at the heterozygous state. The maternal grand-mother (I.2) was positive for this variant and remained asymptomatic all her life. Nevertheless, a 24-hour Holter recording performed at the age of 80 revealed many PVBs and bigeminism. The mother (II.1) was thus an obligate carrier of the variant.

The 2 families originate from the same region in the North of France and they probably share a common ancestor as they harbor the same mutated haplotype (Suppl Figure 2).

### Localization and conservation of the RyR2 p.D3291V variant

The negatively charged aspartate at position 3291 is located in the second part of the helical domain 2 (HD2), where no pathogenic mutation has been reported (Figure 3A). It presents a high conservation level among vertebrate RyR2, as well as in RyR1 and RyR3, even in an aquatic vertebrate such as the spotted gar or *Lepisosteus Oculatus*. In these species, the whole area is well conserved with two negatively charged residues next to one another (aspartate-glutamate: DE). D3291 is also conserved in a number of invertebrates, such as flies. It is replaced by a negatively charged glutamate in *Caenorhabditis elegans* (Figure 3B).

In contrast to RyR1, the C-terminal part of HD2 in RyR2 could not be assessed for structural crystallography since number of armadillo repeats in this domain were invisible (Peng et al., 2016). This domain is implicated in the conformational changes characterized by the outward tilt of the four S6 segments inducing the dilatation of the central pore (Peng et al., 2016).

### Blunted adrenergic response of D3291V-RyR2 channels

To study the D3291V-RyR2 effect on channel activity, HEK293 cells were transfected with eGFP-WT-hRYR2 or eGFP-D3291V-hRYR2 plasmids. Forty-eight hours after, WT or D3291V-RyR2 expressing cells, loaded with Fura2-AM, were challenged with increasing  $\text{Ca}^{2+}$  concentrations (0.1 to 1 mM) and the spontaneous  $\text{Ca}^{2+}$  release was recorded. In basal condition, the percentage of oscillating cells and the number of oscillations per minute occurred to be similar between the two cell types suggesting that the mutant channel has a normal sensitivity to cytosolic  $\text{Ca}^{2+}$  (Figure 4A, 4B, squares, dotted lines). The expression level of WT-RyR2 and D3291V-RyR2 channels were also similar as shown by Western blots (WT: 100% vs D3291V:  $99.53 \pm 9.93\%$ ,  $n=12$ , Suppl Figure 3).

As the cardiac arrests were triggered by adrenergic discharges, WT-RyR2 or D3291V-RyR2 transfected cells were challenged by 250  $\mu\text{M}$  8-Bromo-cyclic AMP (cAMP) or 5  $\mu\text{M}$  forskolin to mimic this condition (Figure 4A, 4B Fig 3). As expected, at 0.5 mM  $\text{Ca}^{2+}$ , cAMP treatment induced a higher percent of oscillating WT-RyR2 cells compared to untreated cells (WT + cAMP =  $42.30\% \pm 2.84$ , WT =  $30.71\% \pm 1.89$ ,  $p=0.008$ ) (Figure 4A, black triangles and line). The treatment also induced significant increases in the number of oscillations per WT cells compared to untreated ones at 0.5, 1 and 2 mM  $\text{Ca}^{2+}$  (WT + cAMP =  $0.63 \pm 0.019$  vs WT =  $0.45 \pm 0.011$ ,  $p<0.001$ ;  $0.73 \pm 0.025$  vs  $0.50 \pm 0.01$ ,  $p<0.001$ ;  $0.87 \pm 0.03$  vs  $0.73 \pm 0.02$ ,  $p<0.001$ , respectively) (Figure 4B, black triangles and line).

In contrast, the same treatments of D3291V-RyR2 cells did not change the percentage of oscillating cells, nor the number of oscillations per minute at any  $\text{Ca}^{2+}$  concentration. Finally, cAMP treatment revealed significant differences between WT-RyR2 and D3291V-RyR2 cells both for the fractions of oscillating cells at 0.5 mM  $\text{Ca}^{2+}$  (WT + cAMP =  $42.30\% \pm 2.84$  vs D3291V + cAMP =  $28.65\% \pm 4.08$ ,  $p = 0.017$ ) and the frequencies of oscillations (WT + cAMP =  $0.87 \pm 0.03$  vs D3291V + cAMP:  $0.75 \pm 0.02$ ,  $p<0.001$ ) (Figure 4B, red triangles and lines). Similar results were obtained with 5  $\mu\text{M}$  forskolin (Suppl Figure 4). Our results suggested that the variant D3291V abolishes the channel response to adrenergic stimulation.

### Loss of luminal sensitivity of D3291V-RyR2 single channel

To test channel  $\text{Ca}^{2+}$  conductance, single WT-RyR2 and D3291V-RyR2 were incorporated into planar lipid bilayers and recorded using  $\text{Ca}^{2+}$  as charge carrier (Suppl Figure 5A). Under this condition, we compared the current-voltage relationships of WT-RyR2 and D3291V-RyR2 channels (Suppl Figure 5B). We found that the slope conductances ( $104 \pm 10$  pS for WT and  $102 \pm 12$  pS for D3291V) and the extrapolated reversal potentials ( $-30$  mV) were similar, suggesting that the D3291V variant does not alter RyR2  $\text{Ca}^{2+}$  conductance (Suppl Figure 5B). Furthermore, the identity of the HEK293-expressed RyR2 channels was confirmed by their sensitivity to the selective antagonist ryanodol (Suppl Figure 5C-D).

We examined the sensitivity of WT-RyR2 and D3291V-RyR2 channel open probability ( $P_o$ ) to cytosolic and luminal  $\text{Ca}^{2+}$ , to determine if the variant alters RyR2  $\text{Ca}^{2+}$  regulation. Figure 5A illustrates the effect of cytosolic free  $[\text{Ca}^{2+}]$  on channel activity and Figure 5C compares the  $P_o$ -cytosolic  $[\text{Ca}^{2+}]$  relationships. WT-RyR2 and D3291V-RyR2 channels were both maximally active ( $P_o=0.9$ ) at 20-30  $\mu\text{M}$  and had similar cytosolic  $\text{Ca}^{2+}$   $\text{EC}_{50}$ 's ( $438$  nM  $\pm$  75 for WT vs  $320$  nM  $\pm$  41 for D3291V). These cytosolic  $\text{Ca}^{2+}$  sensitivity data were collected at a high luminal  $\text{Ca}^{2+}$  level. Figure 5B illustrates the action of luminal free  $[\text{Ca}^{2+}]$  on channel activity and Figure 5D compares the  $P_o$ -luminal  $[\text{Ca}^{2+}]$  relationships with 5  $\mu\text{M}$  cytosolic  $\text{Ca}^{2+}$  present. As luminal  $[\text{Ca}^{2+}]$  decreased, the  $P_o$  of D3291V-RyR2 channels decreased to a significantly lower level compared to WT-RyR2 channels. These results indicated that the loss of a negative charge at the position 3291 site alters the luminal  $\text{Ca}^{2+}$  regulation of the RyR2 channel.

### Caffeine response of the D3291V-RyR2 channels

To investigate the intracellular  $\text{Ca}^{2+}$  release in response to caffeine, WT-RyR2 or D3291V-RyR2 transfected cells treated or not by 250 $\mu\text{M}$  of cAMP were challenged with either 0.1 mM or 10 mM caffeine. Surprisingly, the amplitudes of  $\text{Ca}^{2+}$  release after addition of 0.1 or 10 mM caffeine were significantly decreased in D3291V-RyR2 expressing cells, treated or not by cAMP, in comparison with WT-RyR2 expressing cells (Figure 5E). For instance, the amplitude of  $\text{Ca}^{2+}$  release in presence of 10 mM caffeine was  $0.36 \pm 0.005$  for WT-RyR2 cells,  $0.28 \pm 0.005$  for D3291V-RyR2 cells ( $p < 0.001$ ),  $0.42 \pm 0.005$  for WT + cAMP cells and  $0.39 \pm 0.006$  for D3291V + cAMP cells (Figure 6A). The caffeine effect was also evaluated at the single channel level but no significant difference was observed between WT-RyR2 and D3291V-RyR2 channels (Figure 5F).

## IV. Discussion

In this study, we identified a novel *RYR2* variant, p.Asp3291Val, segregating with the CPVT phenotype in two families. To our knowledge, it is the first report of a RyR2 variant identified at the heterozygous and homozygous states. Unlike most of CPVT mutations inducing a hyperexcitability of the RyR2 channels, this variant induces a loss of function, as we observed a loss of luminal  $\text{Ca}^{2+}$  sensitivity and a blunted response to adrenergic stimulation.

### Clinical characterization of the two families

CPVT is a rare arrhythmia which can lead to sudden death in a context of emotion or physical stress in patients without any structural abnormalities. Up to 30% of the patients experience SCD as an initial presentation, and up to half experience cardiac arrest by 20 to 30 years of age (Leenhardt 1995, Swan 1999, Baucé 2002). Here, we reported two families affected by CPVT. In family 1, the proband who is a heterozygous carrier, had an aborted sudden death at the age of 14 while her three homozygous aunts presented few or no syncope. Several young patients died suddenly in a context of exercise or acute emotion and were obligate heterozygous carriers. The stress test of family 2's proband (II.2) revealed many PVBs and ventricular bigeminy but no typical bidirectional PVT. The presence of bidirectional or PVT represents an obvious indication for CPVT diagnosis but it remains a rare observation (Sy et al., 2011). Several studies reported that some CPVT patients who presented a SCD always had a normal Holter and a negative stress test (Hayashi et al., 2009; Sy et al., 2011). The presence of homozygous living patients suggested that the variant is not too severe by itself, and the severity of phenotype in some heterozygous patients could be explained by additional modifier genes for sudden death (Schwartz et al., 2018).

### **Identification of a novel *RYR2* variant in two families**

The D3291V variant was identified for the first time at the homozygous state, but some compound heterozygous carriers have already been described (Milting et al., 2006; Paech et al., 2014; Postma et al., 2005).

This variant is located outside the four domains where most of the CPVT mutations have been identified (George et al., 2007). Some CPVT variants of unknown significance (p.G2866del, p.R3190Q, p.G3037D) located in the proximity of our variant, have been reported (Atik et al., 2018; Broendberg et al., 2017). The variant p.Asn3308Ser was the only one for which a functional analysis was performed (Marjamaa et al., 2009). Single channel analysis revealed a normal sensitivity to cytosolic  $Ca^{2+}$  but its luminal sensitivity has not been tested. This variant is more frequent in the Finnish population (MAF = 0.26%) than in others and it was reported as benign variant.

The D3291V variant involves a highly conserved negatively charged residue among the hRyR homologs and RyR proteins from other animal species, thus reinforcing the hypothesis that this variant is associated with functional change in the hRyR2 gene product. A substitution affecting the corresponding asparagine residue in RyR1, p.D3330G, has been described in a patient with central core disease (CDD), a neuromuscular disorder (Amburgey et al., 2013). This patient was a compound heterozygous carrier of two RYR1 mutations, D3330G and G4897D (Amburgey et al., 2013).

### **Functional study of the D3291V-RyR2 channel**

We performed  $Ca^{2+}$  imaging to assess the D3291V-RyR2 pathogenicity. We recorded channel activity by measuring the fraction of oscillating cells and the number of oscillations per minute. Unlike most of the CPVT mutations expressed in HEK293 cells, we did not identify any difference between the WT-RyR2 and D3291V-RyR2 transfected cells under basal conditions (Jiang et al., 2010; Thomas et al., 2004). As the symptomatic expression of CPVT is triggered

by adrenergic stimulation, we challenged the transfected cells with cAMP or forskolin. The D3291V-RyR2 cells showed no significant response when treated with cAMP unlike the WT-RyR2 cells. This suggests that the D3291V variant prevents the normal response of the RyR2 channel to an adrenergic stimulation. Interestingly, Wangüemert and coworkers also reported a RyR2 variant, p.G357S, with a normal activity in basal conditions in transfected HEK293 cells, but an enhanced channel activity under forskolin to mimic stress conditions (Wangüemert et al., 2015). The cAMP is a well-known second messenger that activates the protein kinase A (PKA) in response to an adrenergic stimulation and RyR2 channels are known to be one of the PKA targets. Three phosphorylation sites (S2030, S2808 and S2814) have been implicated in the regulation of the RyR2 adrenergic response but the main RyR2 phosphorylation site of PKA is still not well defined (Meissner, 2017).

Single channel recordings showed that the D3291V variant did not alter the channel  $\text{Ca}^{2+}$  conductance. We examined the sensitivity of D3291V-RyR2 channel  $P_o$  to cytosolic and luminal  $\text{Ca}^{2+}$  and identified a reduced D3291V-RyR2 response to luminal  $\text{Ca}^{2+}$  activation. At present, RyR2 luminal  $\text{Ca}^{2+}$  regulation mechanisms is a matter of debate. One proposed mechanism involves direct  $\text{Ca}^{2+}$  binding on a luminal activation site (Laver, 2007) whereas another involves luminal  $\text{Ca}^{2+}$  passing through opened RyR2 and acting at cytosolic  $\text{Ca}^{2+}$  binding sites of the same channel (Fill and Copello, 2002; Györke and Györke, 1998; Porta et al., 2011). A third proposed mechanism relies on  $\text{Ca}^{2+}$  binding to luminal proteins such as calsequestrin 2 which are closely associated with RyR2, but this complex is absent in HEK293 cells and in single channel experiments (Györke and Terentyev, 2008). However, our single-channel data suggested that the intra-SR  $\text{Ca}^{2+}$  sensitivity is reduced in the D3291V mutant. Because the 3291 residue is located in the cytoplasmic portion, and our data is taken in isolated RyR2 channels, the second mechanism is the most likely. However, an alteration of the tertiary structure by the D3291V mutation modifying the exposure of a putative luminal  $\text{Ca}^{2+}$  binding site cannot be excluded.

The measure of the caffeine response showed a reduced  $\text{Ca}^{2+}$  release in D3291V cells compared to WT cells in untreated and cAMP treated cells. This could be explained by a lower caffeine sensitivity, a lower  $\text{Ca}^{2+}$  luminal sensitivity and/or a lower SR  $\text{Ca}^{2+}$  load. In order to identify the underlying molecular mechanism, we assessed the effect of caffeine on WT-RyR2 and D3291V-RyR2 single channels. Data revealed a similar caffeine sensitivity for the WT and D3291V-RyR2 channels. The loss in caffeine sensitivity cannot be totally excluded as single channel experiments were carried out with “high SR load” where, accordingly to our results on luminal  $\text{Ca}^{2+}$ -dependency, there were no significant differences above 1 mM  $\text{Ca}^{2+}$  concentration, between WT-RyR2 and D3291V-RyR2. Thus, it is possible that any caffeine sensitivity alteration, between WT and the mutant, could be masked at high  $\text{Ca}^{2+}$  luminal concentrations.

In summary, we identified a new CPVT variant with a loss of  $\text{Ca}^{2+}$  luminal sensitivity and more importantly a blunted response to adrenergic stimulation. A loss-of-function RyR2 variant was recently identified in a patient with idiopathic ventricular fibrillation associated with short-coupled torsade de pointes (Fujii et al., 2017). Moreover, two loss-of-function RyR2 CPVT mutations localized in the pore region, where a lot of gain-of-function *RYR2* CPVT mutations were have been found, were recently reported (Roston et al., 2017; Zhao et al., 2015). The

first loss-of-function *RyR2* mutation, p.A4860G, revealed a loss in luminal  $\text{Ca}^{2+}$  activation (Jiang et al., 2007). The authors hypothesized that these hypoactive channels left, at each  $\text{Ca}^{2+}$  release event through *calcium-induced calcium release* (CICR), a small quantity of  $\text{Ca}^{2+}$  in the SR. As the CICR occurred, this residual quantity of  $\text{Ca}^{2+}$  would increase. Once the threshold activation of these hypoactive RyR2 channels was reached, these channels would release  $\text{Ca}^{2+}$  and induced EADs (Zhao et al., 2015). A similar mechanism could occur with the D3291V channels in cardiac myocytes. In presence of an adrenergic stimulation, the increased  $\text{Ca}^{2+}$  current  $I_{\text{Ca,L}}$  and the phospholamban phosphorylation will lead to an increased SR  $\text{Ca}^{2+}$  store. We can hypothesize that the hypoactive D3291V-RyR2 channels will not be able to regulate the  $\text{Ca}^{2+}$  store level. The  $\text{Ca}^{2+}$  could accumulate in the SR and reach the threshold of D3291V-RyR2 activation releasing a high level of  $\text{Ca}^{2+}$  during diastole which could lead to NCX activation and the consequent membrane depolarization being able to trigger an extra action potential leading to arrhythmias.

To conclude, the mechanism underlying the D3291V variant effects could rely on a conformational change or a phosphorylation state alteration. Performing the same experiments in a more physiological model such as cardiac cells could improve our understanding of the mechanism.

## Legends of figures

### Figure 1: Pedigrees of the two families

Arrows indicate the probands, squares and circles indicate the men and the females respectively, and slashes indicate deceased individuals. For family 1, only deceased and living genotyped individuals were shown for generations I, II and III, and for generation IV only the D3291V carriers were indicated, 13 healthy genotype negative carriers were excluded for gain of space.

### Figure 2 Abnormal ECGs during exercise-stress tests in D3291V heterozygous carriers

A. Exercise-stress test performed in an asymptomatic untreated subject (III.20) after genetic diagnosis at the age of 17 showing bigeminism, bi-directional doublets, and ventricular tachycardia at 125W. B. Polymorphic ventricular tachycardia at exercise-stress test in a 44-year-old subject treated by 80 mg of nadolol (III.2). Her daughter (IV.3) developed also PVT under 80 mg of nadolol. C. Holter recording of an untreated child (IV.13) at the age of 2 with auriculo-ventricular block and bi-directional ventricular doublets at 110 bpm.

### Figure 3. Localisation of the D3291V- RyR2 variant

A. The D3291V variant is located in HD2 outside the 4 mutation hotspots (red double arrows) where CPVT mutations are mostly found. B. Sequence alignment of RyR orthologues. The Uniprot accession numbers are the following: Homo sapiens (RyR1 P21817, RyR2 Q92736, RyR3 Q15413), Sus scrofa (RyR2 F1RHM3), Oryctolagus cuniculus (RyR2 P30957), Rattus norvegicus (RyR1 BOLPN4), Gallus gallus (RyR2 AOA1D5PAZ1), Xenopus tropicalis (RyR1 F7E4CO), Lepisosteus oculatus (RyR2 W5NIQ4, RyR1 W5NAB3, RyR3 W5N4D0), Drosophila melanogaster (RyR Q24498), Musca domestica (RyR A0A1I8MDA8), Caenorhabditis elegans (I2HAA6\_CAEEL, unc-68). Sequence alignment was done at <http://www.ebi.ac.uk/Tools/msa/clustalo/>.

### Figure 4. Functional study of D3291V-RyR2 variant.

A. Percentages of oscillating WT-RyR2 (n=29 dishes) and D3291V-RyR2 (n=23 dishes) cells at different concentrations of Ca<sup>2+</sup> (0.1-1 mM) under basal conditions or challenged by 250 μM cAMP. WT: black squares, WT + cAMP: black triangles, D3291V: red squares, D3291V + cAMP: red triangles. B. Number of oscillations per minute of WT-RyR2 (n=300 cells) or D3291V-RyR2 cells (n=265 cells) at different Ca<sup>2+</sup> concentrations (0.1-2 mM) under basal condition or challenged by 250 μM cAMP. WT compared to WT+ cAMP or forskolin: \*p<0.05; \*\*p<0.01; \*\*\*p<0.001. WT+cAMP compared to D3291V+cAMP #p<0.05; ##p<0.01; ###p<0.001.

### Figure 5. Cytosolic and luminal Ca<sup>2+</sup> regulation and caffeine response of the D3291V-RyR2 channels

A. Single-channel recordings from WT-RyR2 (black) and D3291V-RyR2 (red) recorded at a membrane holding potential of 0 mV at three cytosolic free Ca<sup>2+</sup> concentrations. Open events are upward deflections from zero current level (blue dotted line, c). The cytosolic solution contained 120 mM Tris/250 mM HEPES (pH 7.4) and the cytosolic Ca<sup>2+</sup> levels adjusted with 0.2 mM BAPTA and 1 mM Dibromo-BAPTA in *Cis*, and 50 mM CaOH<sub>2</sub>/250 mM HEPES (pH 7.4) in *Trans*. B. Single-channel recordings from WT-RyR2 (black) and D3291V-RyR2 (red) in

symmetrical conditions of 250mM CsCH<sub>3</sub>O<sub>3</sub>S, 20mM HEPES, pH 7.4 and the desired luminal Ca<sup>2+</sup> levels adjusted with 1mM BAPTA on *Trans* and 5 μM free [Ca<sup>2+</sup>] on *Cis* taken at +20 mV holding potential. **C.** Open probability of WT-RyR2 (black squares) and D3291V-RyR2 (red circles) obtained, under the same conditions as in A, and challenged with increasing free [Ca<sup>2+</sup>] in *Cis*. The sigmoidal curves resulted from the fitting using a Hill function:  $y = V_{max} * x^n / (k^n + x^n)$  where  $V_{max}$  is the max velocity,  $k$  is Michaelis constant, and  $n$  is the number of cooperative sites. At the same concentrations of free Ca<sup>2+</sup>, open probability of WT-RyR2 and D3291V-RyR2 channels were not significantly different. (ANOVA, one-way analysis at  $p < 0.05$ ). The EC<sub>50</sub>'s for the WT-RyR2 and D3291V-RyR2 were  $438 \pm 75$  nM ( $n = 2-7$ ) and  $320 \pm 41$  nM ( $n = 3-5$ ), respectively. **D.** Open probabilities of WT-RyR2 (black squares) and D3291V-RyR2 (red circles) obtained under the same conditions as in C, and challenged with increasing free [Ca<sup>2+</sup>] in *Trans*. The open probabilities of WT-RyR2 and D3291V-RyR2 channels were significantly different at low luminal concentrations of free Ca<sup>2+</sup> (ANOVA one-way test at  $p < 0.05$ ). Currents traces were filtered at 800 Hz. **E.** Normalized amplitudes of caffeine response of WT-RyR2 ( $n = 674$  cells) or D3291V-RyR2 ( $n = 469$  cells) HEK293 cells under basal conditions or challenged by 250 μM cAMP. Data shown are means  $\pm$  SEM (\*\* $p < 0.001$ ). **F.** Effects of caffeine on channel open probability of the WT-RyR2 (black squares) and D3291V-RyR2 single channels (red circles) defined at 100 nM cytosolic free [Ca<sup>2+</sup>] and 50 mM luminal Ca<sup>2+</sup>, and at 0mV. Caffeine data points are the means  $\pm$  SE ( $n = 5-7$ ).

- Amburgey, K., Bailey, A., Hwang, J.H., Tarnopolsky, M.A., Bonnemann, C.G., Medne, L., Mathews, K.D., Collins, J., Daube, J.R., Wellman, G.P., et al. (2013). Genotype-phenotype correlations in recessive RYR1-related myopathies. *Orphanet J. Rare Dis.* *8*, 117.
- Atik, S.U., Alp, F.E., Dedeoğlu, R., Koka, A., Öztunç, F., and Eroğlu, A.G. (2018). A rare cause of sudden cardiac arrest: Catecholaminergic polymorphic ventricular tachycardia. *Turk. Arch. Pediatr. Pediatri Arş.* *53*, 124–128.
- Broendberg, A.K., Nielsen, J.C., Bjerre, J., Pedersen, L.N., Kristensen, J., Henriksen, F.L., Bundgaard, H., and Jensen, H.K. (2017). Nationwide experience of catecholaminergic polymorphic ventricular tachycardia caused by RyR2 mutations. *Heart* *103*, 901–909.
- Fill, M., and Copello, J.A. (2002). Ryanodine receptor calcium release channels. *Physiol. Rev.* *82*, 893–922.
- Fujii, Y., Itoh, H., Ohno, S., Murayama, T., Kurebayashi, N., Aoki, H., Blancard, M., Nakagawa, Y., Yamamoto, S., Matsui, Y., et al. (2017). A type 2 ryanodine receptor variant associated with reduced Ca<sup>2+</sup> release and short-coupled torsades de pointes ventricular arrhythmia. *Heart Rhythm* *14*, 98–107.
- George, C.H. (2003). Ryanodine Receptor Mutations Associated With Stress-Induced Ventricular Tachycardia Mediate Increased Calcium Release in Stimulated Cardiomyocytes. *Circ. Res.* *93*, 531–540.
- George, C.H., Jundi, H., Thomas, N.L., Fry, D.L., and Lai, F.A. (2007). Ryanodine receptors and ventricular arrhythmias: Emerging trends in mutations, mechanisms and therapies. *J. Mol. Cell. Cardiol.* *42*, 34–50.
- Gomez-Hurtado, N., Boczek, N.J., Kryshtal, D.O., Johnson, C.N., Sun, J., Nitu, F.R., Cornea, R.L., Chazin, W.J., Calvert, M.L., Tester, D.J., et al. (2016). Novel CPVT-Associated Calmodulin Mutation in CALM3 (CALM3-A103V) Activates Arrhythmogenic Ca Waves and Sparks. *Circ. Arrhythm. Electrophysiol.* *9*.
- Györke, I., and Györke, S. (1998). Regulation of the cardiac ryanodine receptor channel by luminal Ca<sup>2+</sup> involves luminal Ca<sup>2+</sup> sensing sites. *Biophys. J.* *75*, 2801–2810.
- Györke, S., and Terentyev, D. (2008). Modulation of ryanodine receptor by luminal calcium and accessory proteins in health and cardiac disease. *Cardiovasc. Res.* *77*, 245–255.

Hayashi, M., Denjoy, I., Extramiana, F., Maltret, A., Buisson, N.R., Lupoglazoff, J.-M., Klug, D., Hayashi, M., Takatsuki, S., Villain, E., et al. (2009). Incidence and Risk Factors of Arrhythmic Events in Catecholaminergic Polymorphic Ventricular Tachycardia. *Circulation* *119*, 2426–2434.

Hwang, H.S., Nitu, F.R., Yang, Y., Walweel, K., Pereira, L., Johnson, C.N., Faggioni, M., Chazin, W.J., Laver, D., George, A.L., et al. (2014). Divergent regulation of ryanodine receptor 2 calcium release channels by arrhythmogenic human calmodulin missense mutants. *Circ. Res.* *114*, 1114–1124.

Jiang, D., Chen, W., Wang, R., Zhang, L., and Chen, S.R.W. (2007). Loss of luminal Ca<sup>2+</sup> activation in the cardiac ryanodine receptor is associated with ventricular fibrillation and sudden death. *Proc. Natl. Acad. Sci. U. S. A.* *104*, 18309–18314.

Jiang, D., Jones, P.P., Davis, D.R., Gow, R., Green, M.S., Birnie, D.H., Chen, S.R.W., and Gollob, M.H. (2010). Characterization of a novel mutation in the cardiac ryanodine receptor that results in catecholaminergic polymorphic ventricular tachycardia. *Channels Austin Tex* *4*, 302–310.

Jiménez-Jáimez, J., Palomino Doza, J., Ortega, Á., Macías-Ruiz, R., Perin, F., Rodríguez-Vázquez del Rey, M.M., Ortiz-Genga, M., Monserrat, L., Barriales-Villa, R., Blanca, E., et al. (2016). Calmodulin 2 Mutation N98S Is Associated with Unexplained Cardiac Arrest in Infants Due to Low Clinical Penetrance Electrical Disorders. *PloS One* *11*, e0153851.

Kannankeril, P.J., Moore, J.P., Cerrone, M., Priori, S.G., Kertesz, N.J., Ro, P.S., Batra, A.S., Kaufman, E.S., Fairbrother, D.L., Saarel, E.V., et al. (2017). Efficacy of Flecainide in the Treatment of Catecholaminergic Polymorphic Ventricular Tachycardia: A Randomized Clinical Trial. *JAMA Cardiol.* *2*, 759–766.

Lahat, H., Pras, E., Olender, T., Avidan, N., Ben-Asher, E., Man, O., Levy-Nissenbaum, E., Khoury, A., Lorber, A., Goldman, B., et al. (2001). A Missense Mutation in a Highly Conserved Region of CASQ2 Is Associated with Autosomal Recessive Catecholamine-Induced Polymorphic Ventricular Tachycardia in Bedouin Families from Israel. *Am. J. Hum. Genet.* *69*, 1378–1384.

Laitinen, P.J., Brown, K.M., Piippo, K., Swan, H., Devaney, J.M., Brahmbhatt, B., Donarum, E.A., Marino, M., Tiso, N., Viitasalo, M., et al. (2001). Mutations of the Cardiac Ryanodine Receptor (RyR2) Gene in Familial Polymorphic Ventricular Tachycardia. *Circulation* *103*, 485–490.

Laver, D.R. (2007). Ca<sup>2+</sup> Stores Regulate Ryanodine Receptor Ca<sup>2+</sup> Release Channels via Luminal and Cytosolic Ca<sup>2+</sup> Sites. *Biophys. J.* *92*, 3541–3555.

Leenhardt, A., Lucet, V., Denjoy, I., Grau, F., Ngoc, D.D., and Coumel, P. (1995). Catecholaminergic Polymorphic Ventricular Tachycardia in Children. *Circulation* *91*, 1512–1519.

Makita, N., Yagihara, N., Crotti, L., Johnson, C.N., Beckmann, B.-M., Roh, M.S., Shigemizu, D., Lichtner, P., Ishikawa, T., Aiba, T., et al. (2014). Novel calmodulin mutations associated with congenital arrhythmia susceptibility. *Circ. Cardiovasc. Genet.* *7*, 466–474.

Marjamaa, A., Laitinen-Forsblom, P., Lahtinen, A.M., Viitasalo, M., Toivonen, L., Kontula, K., and Swan, H. (2009). Search for cardiac calcium cycling gene mutations in familial ventricular arrhythmias resembling catecholaminergic polymorphic ventricular tachycardia. *BMC Med. Genet.* *10*, 12.

Medeiros-Domingo, A., Bhuiyan, Z.A., Tester, D.J., Hofman, N., Bikker, H., van Tintelen, J.P., Mannens, M.M.A., Wilde, A.A.M., and Ackerman, M.J. (2009). Comprehensive Open Reading Frame Mutational Analysis of the RYR2-Encoded Ryanodine Receptor/Calcium Channel in Patients Diagnosed Previously with Either Catecholaminergic Polymorphic Ventricular Tachycardia or Genotype Negative, Exercise-Induced Long QT Syndrome. *J. Am. Coll. Cardiol.* *54*, 2065–2074.

Meissner, G. (2017). The structural basis of ryanodine receptor ion channel function. *J. Gen. Physiol.* *149*, 1065–1089.

Milting, H., Lukas, N., Klauke, B., Körfer, R., Perrot, A., Osterziel, K.-J., Vogt, J., Peters, S., Thieleczek, R., and Varsányi, M. (2006). Composite polymorphisms in the ryanodine receptor 2 gene associated with arrhythmogenic right ventricular cardiomyopathy. *Cardiovasc. Res.* *71*, 496–505.

Nyegaard, M., Overgaard, M.T., Søndergaard, M.T., Vranas, M., Behr, E.R., Hildebrandt, L.L., Lund, J., Hedley, P.L., Camm, A.J., Wettrell, G., et al. (2012). Mutations in Calmodulin Cause Ventricular Tachycardia and Sudden Cardiac Death. *Am. J. Hum. Genet.* *91*, 703–712.

Paech, C., Gebauer, R.A., Karstedt, J., Marschall, C., Bollmann, A., and Husser, D. (2014). Ryanodine Receptor Mutations Presenting as Idiopathic Ventricular Fibrillation: A Report on Two Novel Familial Compound Mutations, c.6224T>C and c.13781A>G, With the Clinical Presentation of Idiopathic Ventricular Fibrillation. *Pediatr. Cardiol.* *35*, 1437–1441.

Peng, W., Shen, H., Wu, J., Guo, W., Pan, X., Wang, R., Chen, S.R.W., and Yan, N. (2016). Structural basis for the gating mechanism of the type 2 ryanodine receptor RyR2. *Science* *354*, aah5324.

Porta, M., Zima, A.V., Nani, A., Diaz-Sylvester, P.L., Copello, J.A., Ramos-Franco, J., Blatter, L.A., and Fill, M. (2011). Single ryanodine receptor channel basis of caffeine's action on Ca<sup>2+</sup> sparks. *Biophys. J.* *100*, 931–938.

Postma, A., Denjoy, I., Kamblock, J., Alders, M., Lupoglazoff, J., Vaksman, G., Dubosq-Bidot, L., Sebillon, P., Mannens, M., Guicheney, P., et al. (2005). Catecholaminergic polymorphic ventricular tachycardia: RYR2 mutations, bradycardia, and follow up of the patients. *J. Med. Genet.* *42*, 863–870.

Postma, A.V., Denjoy, I., Hoorntje, T.M., Lupoglazoff, J.-M., Costa, A.D., Sebillon, P., Mannens, M.M.A.M., Wilde, A.A.M., and Guicheney, P. (2002). Absence of Calsequestrin 2 Causes Severe Forms of Catecholaminergic Polymorphic Ventricular Tachycardia. *Circ. Res.* *91*, e21–e26.

Priori, S.G., Napolitano, C., Tiso, N., Memmi, M., Vignati, G., Bloise, R., Sorrentino, V., and Danieli, G.A. (2001). Mutations in the Cardiac Ryanodine Receptor Gene (hRyR2) Underlie Catecholaminergic Polymorphic Ventricular Tachycardia. *Circulation* *103*, 196–200.

Priori, S.G., Napolitano, C., Memmi, M., Colombi, B., Drago, F., Gasparini, M., DeSimone, L., Coltorti, F., Bloise, R., Keegan, R., et al. (2002). Clinical and Molecular Characterization of Patients With Catecholaminergic Polymorphic Ventricular Tachycardia. *Circulation* *106*, 69–74.

Priori, S.G., Blomström-Lundqvist, C., Mazzanti, A., Blom, N., Borggrefe, M., Camm, J., Elliott, P.M., Fitzsimons, D., Hatala, R., Hindricks, G., et al. (2015). 2015 ESC Guidelines for the management of patients with ventricular arrhythmias and the prevention of sudden cardiac death The Task Force for the Management of Patients with Ventricular Arrhythmias and the Prevention of Sudden Cardiac Death of the European Society of Cardiology (ESC) Endorsed by: Association for European Paediatric and Congenital Cardiology (AEPC). *Eur. Heart J.* *36*, 2793–2867.

Roston, T.M., Guo, W., Krahn, A.D., Wang, R., Van Petegem, F., Sanatani, S., Chen, S.R.W., and Lehman, A. (2017). A novel RYR2 loss-of-function mutation (I4855M) is associated with left ventricular non-compaction and atypical catecholaminergic polymorphic ventricular tachycardia. *J. Electrocardiol.* *50*, 227–233.

Roux-Buisson, N., Cacheux, M., Fourest-Lieuvin, A., Fauconnier, J., Brocard, J., Denjoy, I., Durand, P., Guicheney, P., Kyndt, F., Leenhardt, A., et al. (2012). Absence of triadin, a protein of the calcium release complex, is responsible for cardiac arrhythmia with sudden death in human. *Hum. Mol. Genet.* *21*, 2759–2767.

Schwartz, P.J., Crotti, L., and George, A.L. (2018). Modifier genes for sudden cardiac death. *Eur. Heart J.*

Sy, R.W., Gollob, M.H., Klein, G.J., Yee, R., Skanes, A.C., Gula, L.J., Leong-Sit, P., Gow, R.M., Green, M.S., Birnie, D.H., et al. (2011). Arrhythmia characterization and long-term outcomes in catecholaminergic polymorphic ventricular tachycardia. *Heart Rhythm* 8, 864–871.

Thomas, N.L., George, C.H., and Lai, F.A. (2004). Functional heterogeneity of ryanodine receptor mutations associated with sudden cardiac death. *Cardiovasc. Res.* 64, 52–60.

Venetucci, L., Denegri, M., Napolitano, C., and Priori, S.G. (2012). Inherited calcium channelopathies in the pathophysiology of arrhythmias. *Nat. Rev. Cardiol.* 9, 561.

Wangüemert, F., Bosch Calero, C., Pérez, C., Campuzano, O., Beltran-Alvarez, P., Scornik, F.S., Iglesias, A., Berne, P., Allegue, C., Ruiz Hernandez, P.M., et al. (2015). Clinical and molecular characterization of a cardiac ryanodine receptor founder mutation causing catecholaminergic polymorphic ventricular tachycardia. *Heart Rhythm* 12, 1636–1643.

Watanabe, H., and Knollmann, B.C. (2011). Mechanism underlying catecholaminergic polymorphic ventricular tachycardia and approaches to therapy. *J. Electrocardiol.* 44, 650–655.

Watanabe, H., Chopra, N., Laver, D., Hwang, H.S., Davies, S.S., Roach, D.E., Duff, H.J., Roden, D.M., Wilde, A.A.M., and Knollmann, B.C. (2009). Flecainide prevents catecholaminergic polymorphic ventricular tachycardia in mice and humans. *Nat. Med.* 15, 380–383.

Werf, C. van der, Nederend, I., Hofman, N., Geloven, N. van, Ebink, C., Frohn-Mulder, I.M.E., Alings, A.M.W., Bosker, H.A., Bracke, F.A., Heuvel, F. van den, et al. (2012). Familial Evaluation in Catecholaminergic Polymorphic Ventricular Tachycardia. *Circ. Arrhythm. Electrophysiol.* 5, 748–756.

Zhao, Y.-T., Valdivia, C.R., Gurrola, G.B., Powers, P.P., Willis, B.C., Moss, R.L., Jalife, J., and Valdivia, H.H. (2015). Arrhythmogenesis in a catecholaminergic polymorphic ventricular tachycardia mutation that depresses ryanodine receptor function. *Proc. Natl. Acad. Sci. U. S. A.* 112, E1669–E1677.

Figure 1.

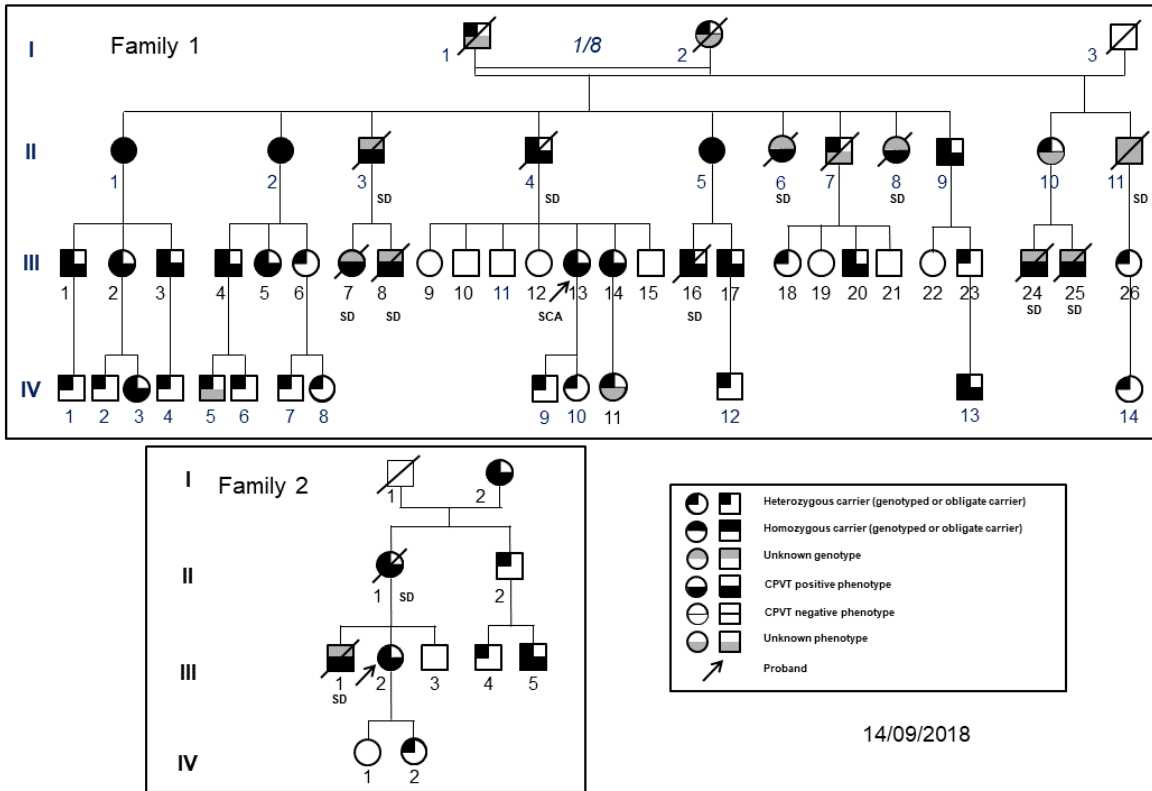


Figure 2.

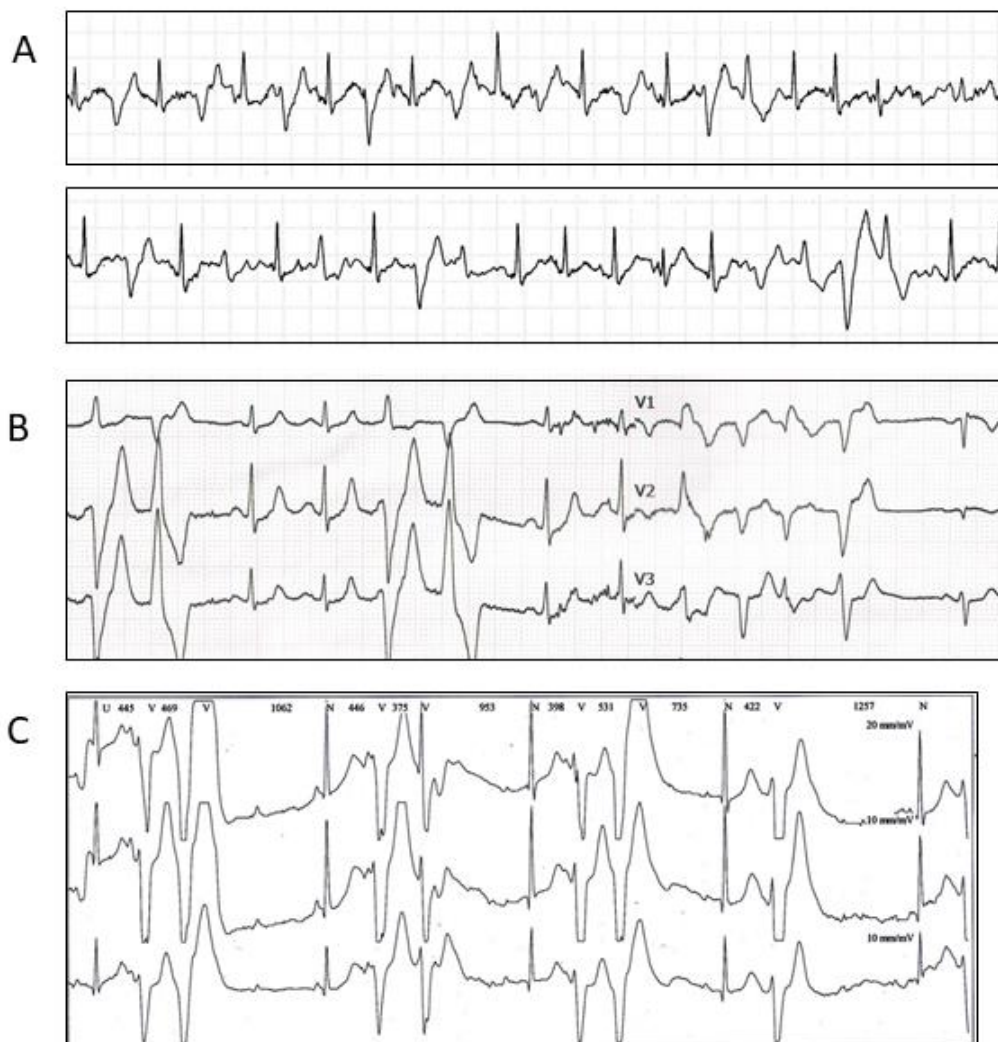


Figure 3.

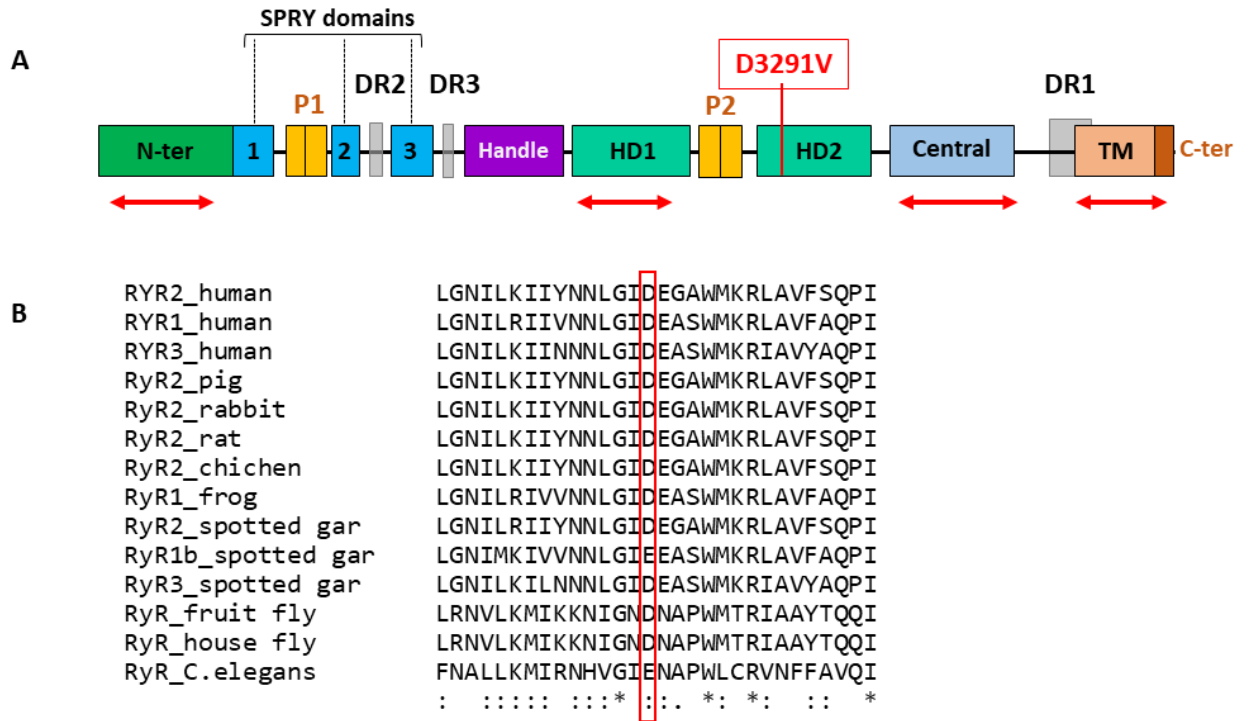


Figure 4.

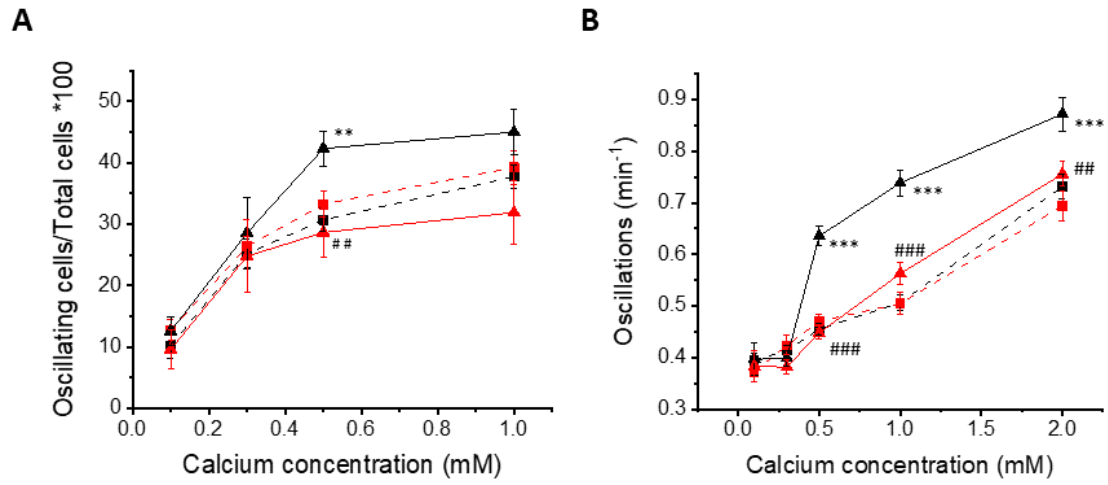
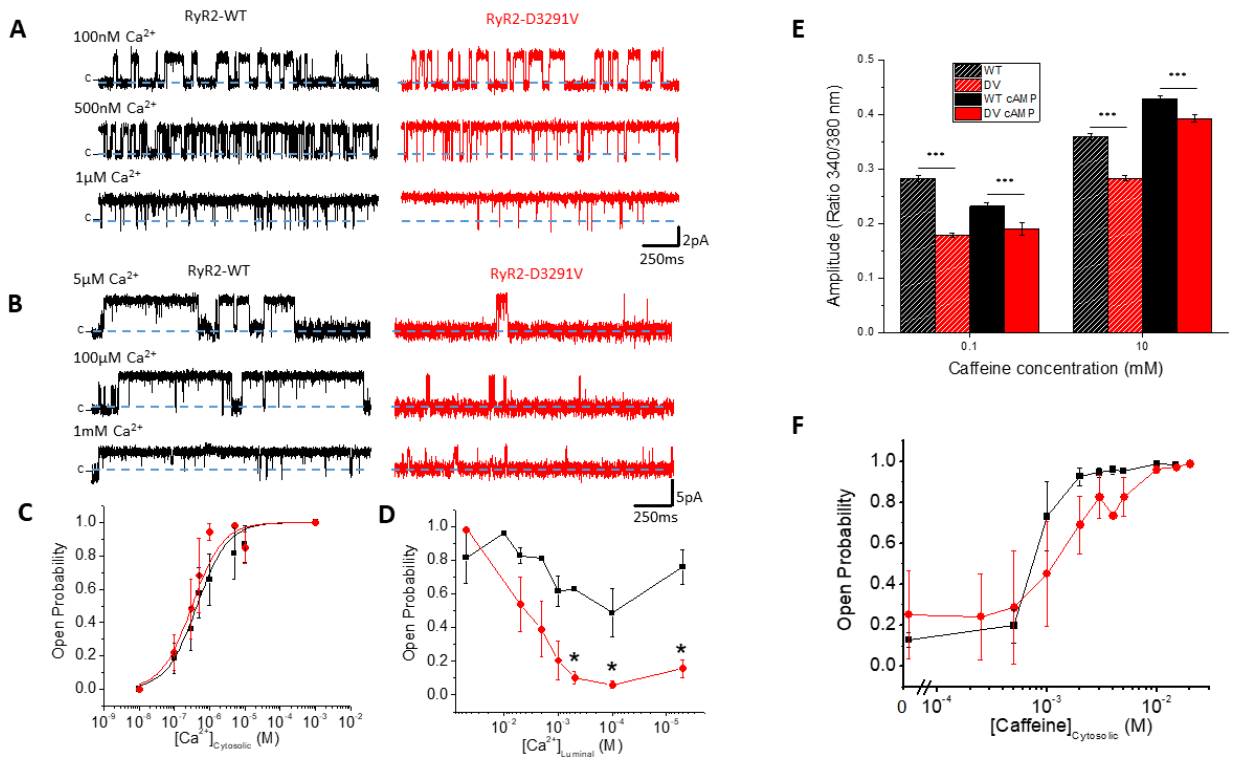
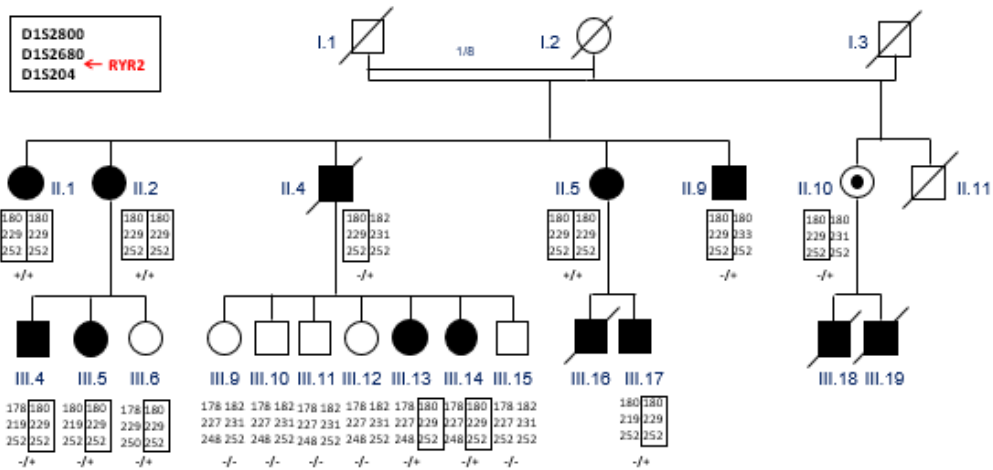


Figure 5.



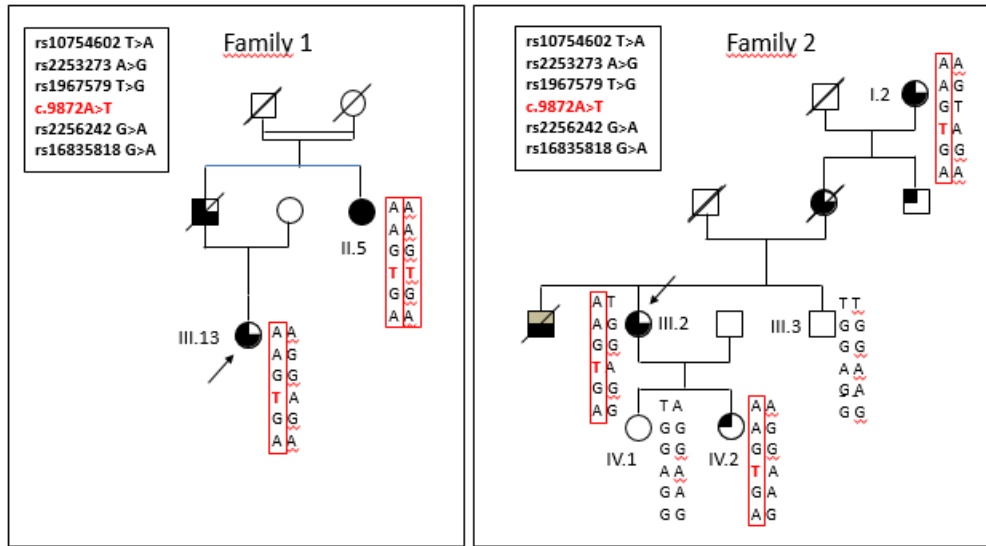
## Supplemental figures

Supplemental figure 1. Microsatellite analysis showing the cosegregation of the *RYR2* locus with the affected phenotype.



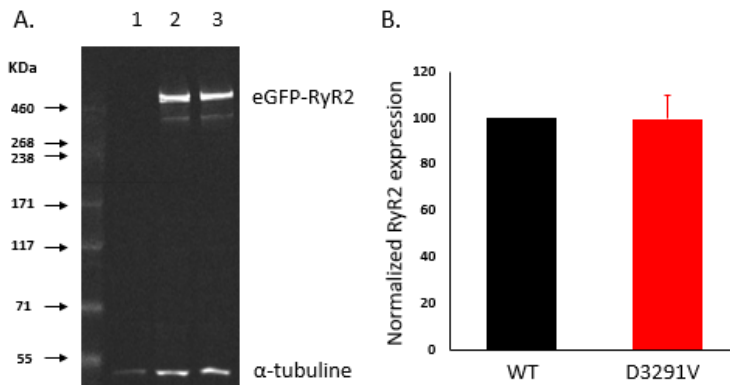
Informative microsatellites closely linked to the *RYR2* locus (D1S2800, D1S2680, *RYR2*, D1S204) were genotyped in affected and unaffected individuals in Family 1.

**Supplemental figure 2. Founder effect in the two families.**



Five polymorphisms (rs10754602, rs2253273, rs1967579, rs2256242, rs16835818) flanking the D3291V variant (c.9872A>T) were genotyped in some individuals of families 1 and 2. The probands are shown by an arrow. All affected subjects harbored the same mutated haplotype in the two families.

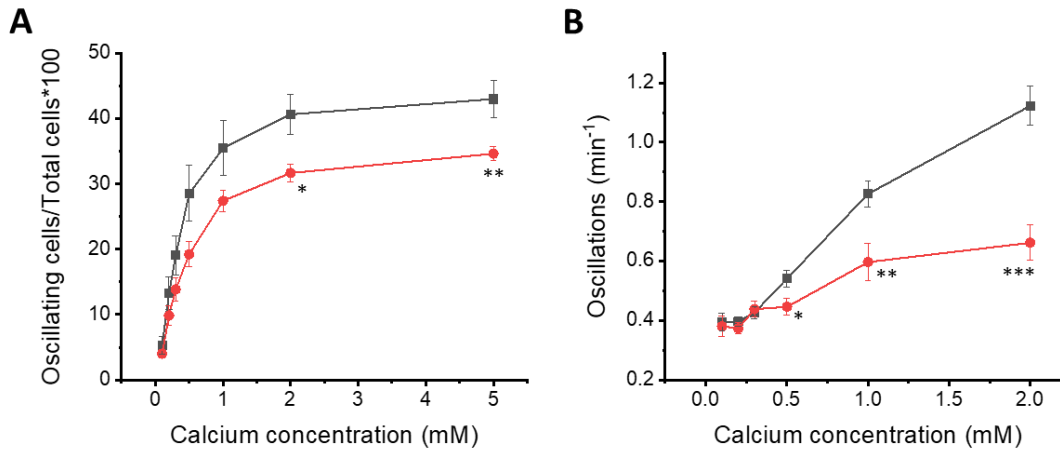
**Supplemental figure 3. Expression levels of RyR2-WT and RyR2-D3291V.**



**A.** Representative western blot of total proteins extracted from HEK293 cells transfected with RYR2-WT or RYR2-D3291V plasmids (n=12). **B.** Western blot quantification of RyR2 expression

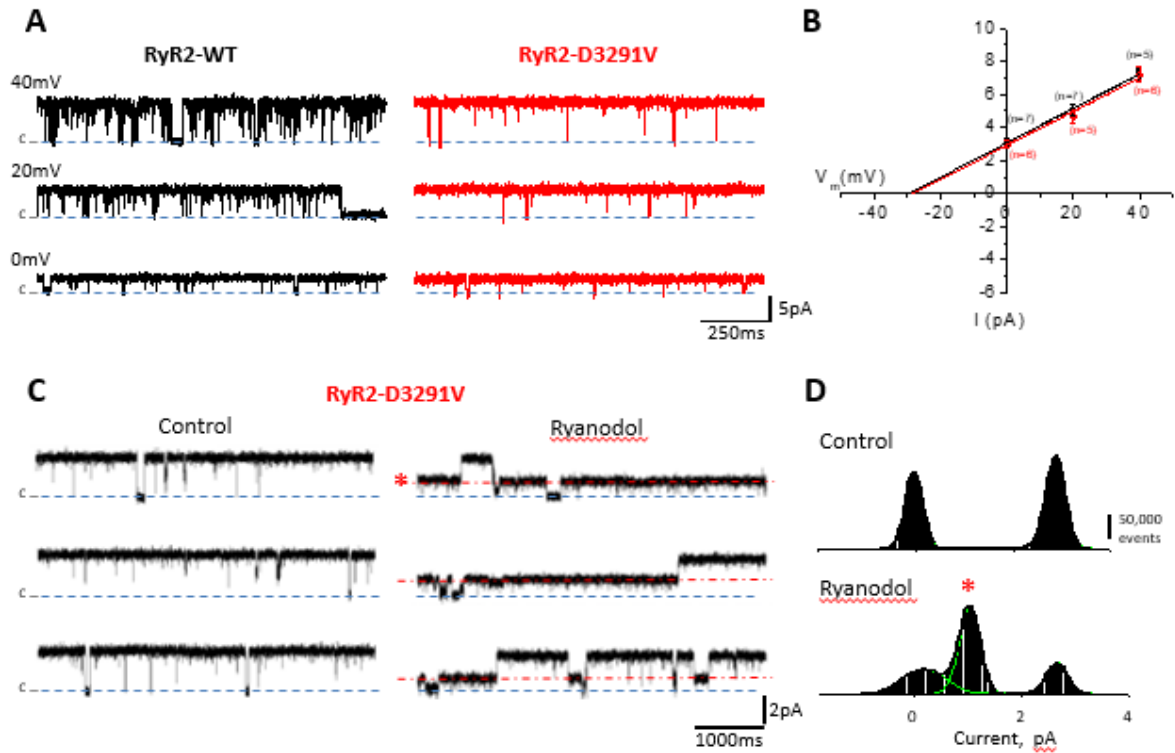
normalized to  $\alpha$ -tubuline expression. 1: Non transfected cells, 2: HEK293 cells transfected with cDNA WT-RyR2, 3: HEK293 cells transfected with cDNA D3291V-RyR2.

**Supplemental figure 4. Effect of forskolin on RyR2-D3291V channel activity.**



A. Percentages of oscillating WT-RyR2 (n=29 dishes) (black squares) and D3291V-RyR2 (n=23 dishes) (red circles) cells at different concentrations of Ca<sup>2+</sup> (0.1-1 mM) challenged by 5 $\mu$ M forskolin. B. Number of oscillations per minute of WT-RyR2 (n=300 cells) (black squares) or D3291V-RyR2 cells (n=265 cells) (red circles) at different Ca<sup>2+</sup> concentrations (0.1-2 mM) under basal condition or challenged by 5 $\mu$ M forskolin. \* $p$ <0.05; \*\* $p$ <0.01; \*\*\* $p$ <0.001.

**Supplemental figure 5. The RyR2-D3291V variant does not alter the ion channel conductance.**



**A.** Single-channel recordings from WT-RyR2 (top left) and D3291V-RyR2 (top right) at different membrane holding potentials. Open events are shown as upward deflections from marked zero current level (closed state) indicated by the blue dashed line to the right of each trace. Data were recorded in presence of 120 mM Tris/250 mM HEPES (pH 7.4) and 10  $\mu$ M free  $\text{Ca}^{2+}$  in *Cis*, and 50 mM  $\text{CaOH}_2$ /250 mM HEPES (pH 7.4) in *Trans*.  $\text{Ca}^{2+}$  (the charge carrier) was moving in the lumen-to-cytosol direction. **B.** Current-voltage relationships for WT-RyR2 (black squares) and D3291V-RyR2 (red circles) channels, obtained from single-channel experiments under the same conditions as in A. Slope conductances were  $104 \pm 10$  pS and  $102 \pm 12$  pS for the WT-RyR2 and D3291V-RyR2, respectively. **C.** Single-channel traces from D3291V-RyR2 were obtained at 0 mV, with the same solutions used in A. Control conditions (bottom left) show complete transitions to the open state, but in the presence of 25  $\mu$ M ryanodol (bottom right) the transition to a subconductance state was favored (red asterisk). **D.** Corresponding all-points amplitude histograms from D3291V-RyR2 single-channel recorded in C. The two populations of events

indicate the closed and open states of the D3291V-RyR2 at 10  $\mu\text{M}$  free  $[\text{Ca}^{2+}]$  on *Cis*. Ryanodol addition (bottom histogram) created a new population of events that represents the subconductance state marked by a red asterisk. Current traces were filtered at 800 Hz.

**Titre :** titre (en français) : Impacte des mutations du RyR2 (R420Q) liées à la tachycardie ventriculaire polymorphe sur la fonciton du cardiomyocyte.

**Mots clés :** CPVT, RyR2, KI souris, hiPSC-CM, antiarythmique effet

**Résumé :** La tachycardie ventriculaire polymorphe catécholergique (CPVT) est une arythmie génétique létale qui se manifeste par une syncope ou une mort subite chez les enfants et les jeunes adultes dans des conditions de stress sans anomalie structurelle cardiaque évidente. Une nouvelle mutation CPVT située sur la partie N terminale RyR2 a été identifiée dans une famille espagnole (RyR2<sup>R420Q</sup>). Ici, nous avons utilisé un modèle de souris KI exprimant le canal RyR2<sup>R420Q</sup> et des cardiomyocytes différencié de cellules souches pluripotentes induites (hiPS-CM) générées à partir de deux patients frères (l'un avec mutation, l'autre sans mutation utilisé comme témoin). L'analyse des cardiomyocytes ventriculaires exprimant le RyR2<sup>R420Q</sup> humain et de souris étudiées par imagerie Ca<sup>2+</sup> confocale montre une augmentati-

on des libérations de Ca<sup>2+</sup> spontanée durant la diastole (visualisé par les Sparks Ca<sup>2+</sup>), une libération fractionnelle plus élevée et une fréquence de vagues Ca<sup>2+</sup> proarythmogènes augmentée après stimulation à l'isoprotérénol. L'analyse électrophysiologique, étudiée en enregistrant les potentiels d'action (AP) en utilisant les techniques de micro-électrodes sur les hiPSC-CM et de patch-clamp sur les cellules ventriculaires de souris KI, a montré des post-dépolarisations retardées dépendants du Ca<sup>2+</sup> (DAD). Nous avons ensuite étudié l'effet antiarythmique potentiel de la venlafaxine et de la prégabaline. Nous avons constaté que ces deux médicaments atténuaient les événements arythmogènes de libération du Ca<sup>2+</sup> induits par l'ISO.

**Title :** Titre (en anglais) Impact of the catecholaminergic polymorphic ventricular tachycardia (CPVT) mutation RyR2<sup>R420Q</sup> on cell function.

**Keywords :** CPVT, RyR2, KI mouse, hiPSC-CM, antiarrhythmic effect

**Abstract:** Catecholaminergic polymorphic ventricular tachycardia (CPVT) is a lethal genetic arrhythmia that manifests by syncope or sudden death in children and young adults under stress conditions without obvious cardiac structural abnormality. A novel CPVT mutation located on RyR2 N terminal portion has been identified in a Spanish family (RyR2<sup>R420Q</sup>). Here we used a KI mice model expressing the RyR2<sup>R420Q</sup> channel, and differentiated cardiomyocytes from induced pluripotent stem cells (hiPS-CM) generated from two brother patients (one with mutation, the other without mutation used as control). Confocal Ca<sup>2+</sup> imaging analysis showed that human and mouse RyR2<sup>R420Q</sup> expressing ventricular

cardiomyocytes have higher occurrence of Ca<sup>2+</sup> sparks, enhanced fractional release, and significantly more proarrhythmogenic Ca<sup>2+</sup> waves after isoproterenol (ISO) stimulation. The action potential (AP) analysis, recorded using the micro-electrode technique in hiPSC-CMs and patch-clamp in KI mouse ventricular cells showed Ca<sup>2+</sup>-dependent delayed after depolarizations (DADs). We then studied the potential antiarrhythmic effect of venlafaxine and pregabalin, two drugs among other medications that have been prescribed to one family carrier member and devoted of CPVT symptoms. We found that both of those drugs blunted ISO induced arrhythmogenic events.